# The Pleura

1

Chad D. Strange, Jitesh Ahuja, Saadia A. Faiz, Horiana B. Grosu, William C. Harding, Keerthana Keshava, Carlos A. Jimenez, Vickie R. Shannon, Patricia M. de Groot, Mylene T. Truong, and Cesar A. Moran

## Introduction

Pleural disease is often a mirror of intrathoracic and systemic diseases caused by an extensive list of neoplastic and nonneoplastic conditions. Both neoplastic and nonneoplastic pleural diseases can present with similar clinical features. Nonneoplastic disorders of the pleura may result from a variety of infectious as well as drug- and trauma-related causes. Many of these conditions when persistent or severe, may lead to encasement of the lung by a thick fibrous layer, known as fibrous pleuritis. The management and prognoses of these diverse conditions vary greatly. Thus, accurate diagnosis of pleural diseases is critical.

Primary pleural disease owing to a myriad of inflammatory and neoplastic pleural disorders is less common, but nonetheless relevant due to its potential to cause devastating respiratory compromise. Moreover, many of the benign tumors of the pleura closely mimic malignant disease in their radiographic and histologic appearance. Thus, early recognition and management are critical components to the successful outcomes of primary pleural disorders. In this chapter, we will discuss the clinical, radiographic, and pathologic correlates of the spectrum of primary and secondary diseases of the pleura. The intent of this multidisciplinary approach is to provide a detailed overview and update of diseases of the pleura that can be directly applied to clinical practice and to stimulate basic research investigations in areas where there are unanswered questions. We begin with a brief discussion of pleural anatomy and radiology concepts as critical background information to understanding pleural disease. This is followed by detailed descriptions of benign and malignant neoplastic and inflammatory disorders affecting the pleura. Pleural effusions are often the first manifestation of many of the diseases affecting the pleura and we end the chapter with a discussion of the pathogenesis, diagnosis, and management of pleural effusions, which will hopefully provide the reader with a more complete understanding of this complex disease.

C. D. Strange · J. Ahuja · P. M. de Groot (✉) · M. T. Truong
Department of Thoracic Imaging, The University of Texas MD Anderson Cancer Center, Houston, TX, USA
e-mail: cdstrange@mdanderson.org; jahuja@mdanderson.org; pdegroot@mdanderson.org; mtruong@mdanderson.org

S. A. Faiz · C. A. Jimenez · V. R. Shannon
Department of Pulmonary Medicine, The University of Texas MD Anderson Cancer Center, Houston, TX, USA
e-mail: cajimenez@mdanderson.org; vshannon@mdanderson.org

H. B. Grosu
Department of Pulmonary Medicine, MD Anderson Cancer Center, Houston, TX, USA

W. C. Harding
Pulmonary Medicine, Critical Care Medicine and Sleep Medicine, McGovern Medical School at University of Texas Science Center, Houston, TX, USA

K. Keshava
Interventional Pulmonology, Department of Pulmonary, Critical Care and Sleep Medicine, New York Presbyterian Brooklyn Methodist Hospital, New York, NY, USA

C. A. Moran
Department of Pathology, The University of Texas MD Anderson Cancer Center, Houston, TX, USA
e-mail: cesarmoran@mdanderson.org

## Pleural Anatomy

During early embryogenesis, the coelomic cavity is partitioned into three distinct spaces (pleura, pericardial, and peritoneal). Lung buds invaginate the coelomic cavity, which folds on itself to form the visceral and parietal pleura. In humans, the visceral and parietal pleura merge at the left and right hila, separating the thorax into two noncontiguous spaces. The surface of the pleural membranes is composed of a monolayer of mesothelial cells. The visceral pleura lines the lungs and interlobar fissures while the parietal pleura covers the thoracic wall and diaphragm and is subdivided into the costal, diaphragmatic, mediastinal, and cervical pleura [1, 2]. Under normal conditions, the visceral and parietal pleurae are separated by 10–20 mL of a lubricating, glycoprotein-rich pleural



C. A. Moran et al. (eds.), *The Thorax*, https://doi.org/10.1007/978-3-031-21040-2_1

fluid, which is secreted by the mesothelial lining cells [3]. This fluid reduces friction by lubricating the pleural space, thereby facilitating normal lung movements during respiration. Production and absorption of pleural fluid primarily occurs at the level of the parietal pleura. Fluid homeostasis reflects a balance of hydrostatic and oncotic pressure differences between the systemic and pulmonary circulations and the pleural space.

The pleural space is equipped with an extensive network of lymphatic vessels that line the parietal pleura and play a critical role in pleural fluid homeostasis. This lymphatic network supplies the costal, diaphragmatic, and mediastinal surfaces of the parietal pleura and is lined by specialized openings between mesothelial cells known as stomata. Excess fluid derived from the lung via the visceral pleura is absorbed through the parietal stomata into underlying lymphatic lacunae, which ultimately empty into larger lymphatic vessels. Lymphatic drainage along with oncotic and hydrostatic pressures maintain the delicate balance of fluid within the pleural space; disturbances in any one of these systems can lead to abnormal accumulation of pleural fluid [4]. Thus, excess production, diminished resorption, or a combination of these two factors substantially overwhelms the ability of lymphatic vessels to resorb fluid resulting in clinically significant effusions [5]. The pleural fluid is bland, with a low protein content of approximately 1.5 g/dL and comprised predominantly of mesothelial cells, macrophages, and lymphocytes. The visceral pleura receives innervation from the pulmonary plexus, which is a network of nerves that originate from the sympathetic trunk and vagus nerve. As such it can detect stretch, but is insensitive to pain, temperature, and touch. The parietal pleura is innervated by sensory fibers of the phrenic nerve at its diaphragmatic portion and the intercostal nerves elsewhere. The vascular supply of the visceral pleura is provided by pulmonary and bronchial arteries, while the parietal pleura receives its vascular supply from the systemic circulation [1, 4].

Histologically, distinction between visceral and parietal pleura is not possible, as both of these serosal surfaces are lined by similar type of epithelium. The mesothelial lining is composed of low cuboidal type of epithelium. However examination of large sections of tissue may permit visualization of visceral pleura overlying the lung parenchym (Fig. 1.1a, b), while histological sections from the parietal pleura will demonstrate epithelium (mesothelium) lining adipose tissue (Fig. 1.2).

Both neoplastic and nonneoplastic pleural diseases can present with similar clinical features. Nonneoplastic disorders of the pleura may result from a variety of infectious as well as drug- and trauma-related causes. Many of these conditions when persistent or severe, may lead to encasement of the lung by a thick fibrous layer, known as fibrous pleuritis. The management and prognoses of these diverse conditions vary greatly. So, accurate diagnosis of pleural diseases is critical.

## General Radiology Concepts

Imaging plays a crucial role in the diagnosis and management of patients with pleural diseases. Modalities of imaging include chest radiography, computed tomography (CT), magnetic resonance imaging (MRI), ultrasound (US), and F-18 fluorodeoxyglucose (FDG) positron emission tomog-

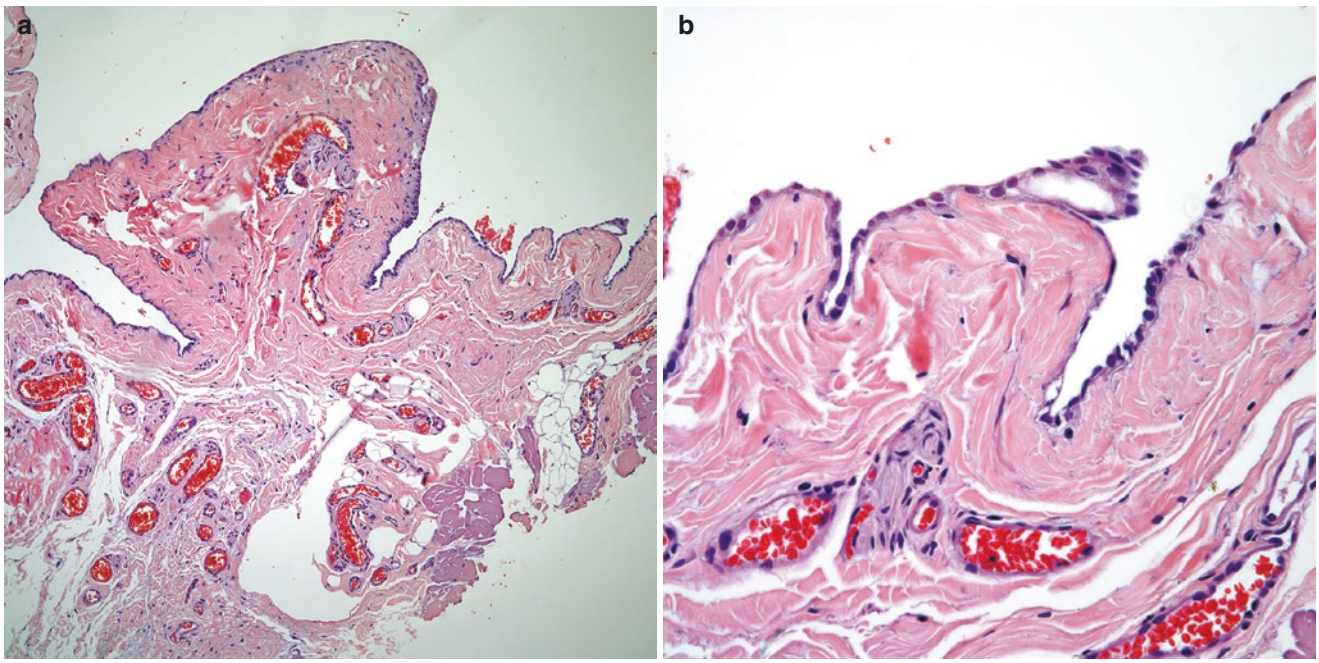


**Fig. 1.1** (**a**) Low power view of a section from the visceral pleura, note the presence of fibroadipose tissue lined by epithelium; (**b**) closer view of the epithelium composed of low cuboidal cells

raphy/computed tomography (PET/CT). Chest radiography remains the initial imaging modality for the evaluation of pleural diseases but it may be normal or may not be able to differentiate benign from malignant conditions. Various cross-sectional imaging modalities are available for further evaluation and characterization of pleural diseases. Thoracic ultrasound is easily available and widely used for detection and characterization of pleural fluid and guidance of thoracentesis and pleural biopsies. CT is the mainstay imaging modality for primary assessment of pleural diseases and exhibits high sensitivity for identification of pleural diseases and in differentiating benign and malignant pleural processes. MRI and PET/CT play important roles in further evaluation and can provide additional staging and prognostic information.

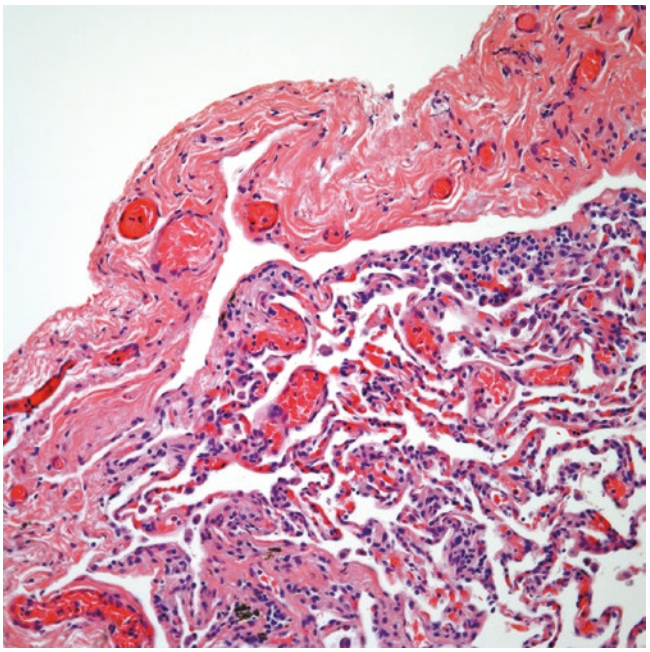

**Fig. 1.2** Histological sections showing visceral pleura overlying the lung parenchyma

Cancer cells show on FDG-PET/CT, increased uptake of glucose due to an overexpression of glucose transporter proteins and increased rate of glycolysis. A glucose analogue, F-18 fluorodeoxyglucose (FDG) undergoes the same uptake as glucose. However, following phosphorylation by hexokinase, FDG is unable to enter intracellular glycolytic pathways due to a downregulation of phosphatase and is sequestered in cancer cells. The most common semiquantitative method of evaluating malignancies using FDG-PET is the standardized uptake value (SUV) calculated as a ratio of tissue radiotracer concentration (mCi/ml) and injected dose (mCi) at the time of data acquisition divided by body weight (g). It should be noted that inflammatory conditions, such as talc pleurodesis, can also cause FDG activity in the pleural space (Fig. 1.3a, b).

Imaging features to differentiate pleural lesions from peripheral pulmonary and extrapleural tumors are important.

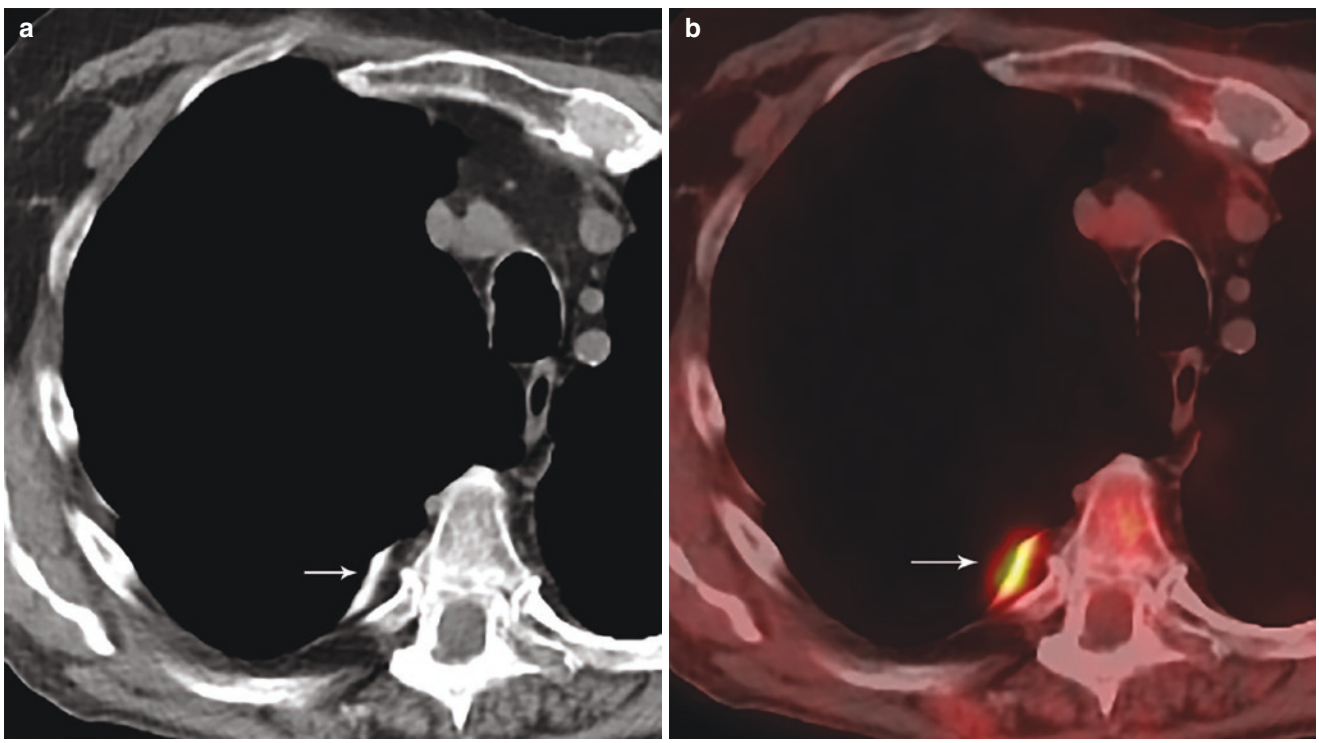


**Fig. 1.3** (**a**) Non-contrast axial CT shows high attenuation material in the posterior right pleural space (arrow) consistent with talc pleurodesis. (**b**) axial PET/CT shows increased radiotracer uptake in the talc deposits

**Fig. 1.4** Contrast-enhanced axial CT shows the left lower lobe mass abuts the posterior pleura and forms acute angles (black arrows) with the chest wall. The angles that a lesion forms with the chest wall are useful to differentiate lung lesions (acute angles) from pleural lesions (obtuse angles)

Tumors arising within the periphery of the lungs form acute angles with the chest wall, are centered within the lungs, and are perfused by pulmonary vessels (Fig. 1.4). Pleural tumors have more obtuse angles with the chest wall and displace the pulmonary parenchyma and vessels inward and the extrapleural fat outward (Fig. 1.5a–c). Typically pleural tumors do not cause adjacent osseous erosive change. Additionally, pleural tumors often demonstrate an "incomplete border sign" on radiographs where only one margin of the tumor (the margin abutting the pulmonary parenchyma) is radiographically identified. Extrapleural tumors arise from the extrapleural fat, muscles, ribs, or neurovascular bundles and will displace extrapleural fat inward [1].

Imaging in general cannot absolutely distinguish between benign and malignant pleural processes; however, there are certain characteristics that favor a malignant etiology. On chest radiographs, nodular or circumferential pleural thickening, especially if greater than 1 cm in thickness, involvement of the mediastinal pleura, and larger effusions suggest malignancy. CT and MRI findings that suggest malignancy include pleural nodularity, pleural rind, involvement of the mediastinal pleura, and invasion of adjacent structures (Fig. 1.6a, b). FDG uptake in areas of pleural thickening or nodularity, hypermetabolic pleural effusions, hypermetabolic adenopathy, and evidence of hypermetabolic distant metastasis on PET/CT are highly suggestive of malignancy [6–11].

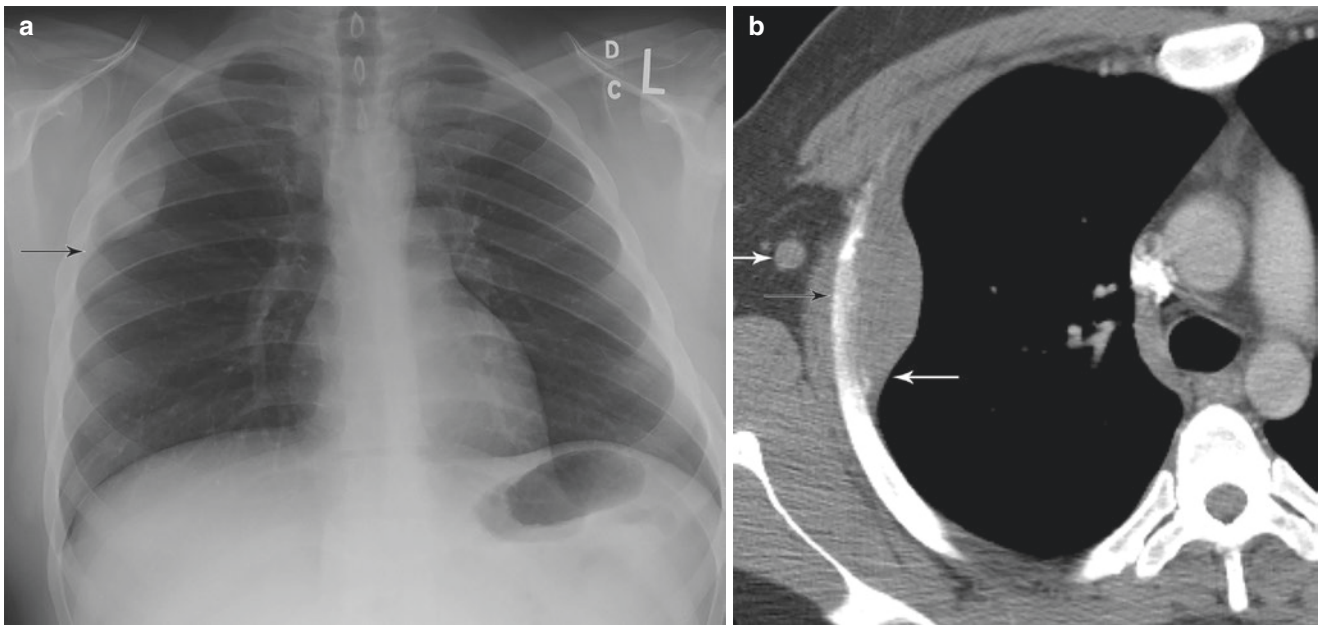


**Fig. 1.5** (**a**) Frontal chest radiograph shows the right pleural metastasis forms obtuse angles (arrow) with the chest wall. In contrast, lung lesions that abut the pleura form acute angles with the chest wall; (**b**) contrast-enhanced axial CT shows the right pleural metastasis forms obtuse angles with the chest wall (long white arrow) and is associated with erosive and sclerotic changes in the adjacent rib (black arrow). Note small right axillary nodal metastasis (short white arrow); (**c**) contrast-enhanced axial CT shows the right pleural metastasis displaces the lung parenchyma and bronchopulmonary vessels inward (arrow)

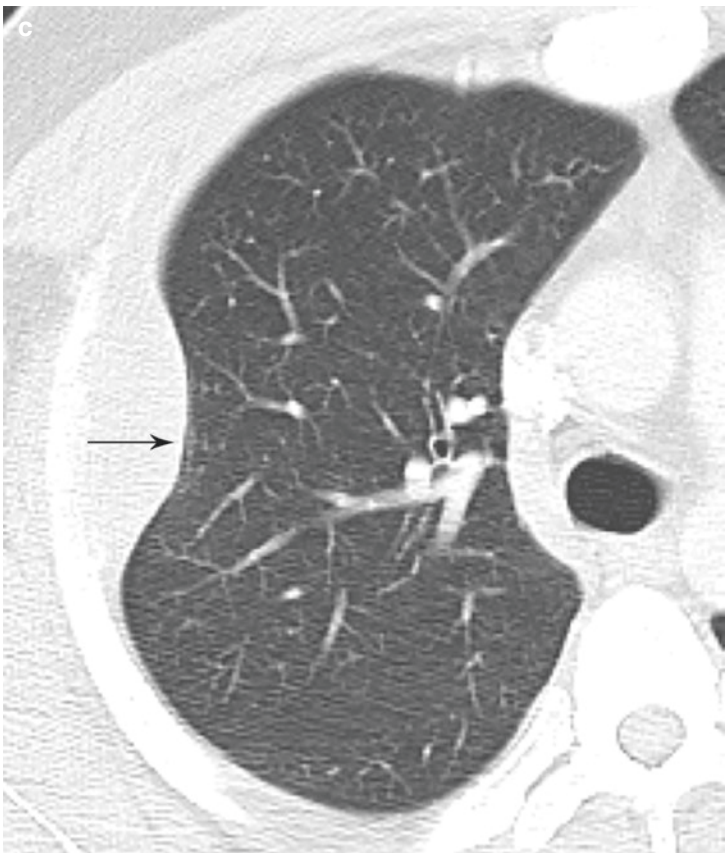


**Fig. 1.5** (continued)

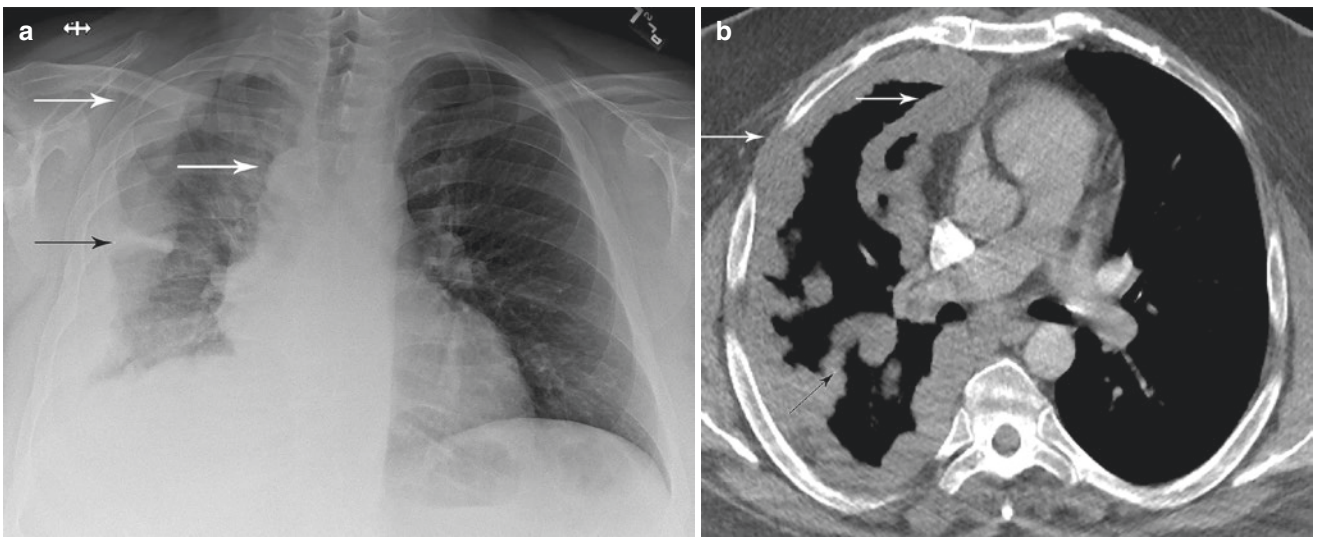


**Fig. 1.6** (**a**) Frontal chest radiograph shows the features of malignant pleural disease, with a right nodular pleural rind of tumor encasing the right lung (white arrows). There is involvement of the minor fissure (black arrow); (**b**) contrast-enhanced axial CT shows nodular configuration, circumferential distribution (white arrows) with extension into the major fissure (black arrow), and pleural thickness greater than 1 cm

## Nonneoplastic

### Fibrous and Fibrinous Pleuritis

Fibrous pleuritis, also referred to as pleural fibrosis, fibrothorax, fibrous pleurisy, fibrosing pleuritis, and dry pleurisy, is an uncommon disorder. The physiologic mechanisms underlying the development of fibrous pleuritis are not well understood; however, disordered fibrin turnover associated with pleural injury and repair are central events in its pathogenesis. Fibrous pleuritis most commonly occurs as a complication of hemothorax or empyema caused by bacterial, mycobacterial, or fungal processes (Fig. 1.7a–c). However, a variety of other inflammatory and infiltrative pleural processes may underlie the development of this disorder (Table 1.1). Metastatic disease and other infiltrative immunologic disorders, such as rheumatoid arthritis or sarcoidosis, may produce pleural effusions with varying degrees of pleural fibrosis. Underlying thoracic conditions, such as pneumothorax, improperly drained hemothorax, chest trauma, uremia, lung transplantation, and prior coronary artery bypass surgery also predispose to fibrous pleuritis. Drug-induced pleural effusions have been well described; however, medication-associated fibrous pleuritis is less commonly observed. Other causes include systemic fibrosing diseases that involve the pleura, such as nephrogenic systemic fibrosis and immunoglobulin G4 (IgG-4)-related sclerosing disease [12]. Idiopathic and isolated familial cases of pleural fibrosis have been reported [13].

The integrity of the mesothelial cell and its response to any one of these inciting events dictate whether normal healing or pleural fibrosis occurs after injury. Mesothelial cells initiate and orchestrate inflammatory and exudative reactions via the release of cytokines, chemokines, oxidants, and

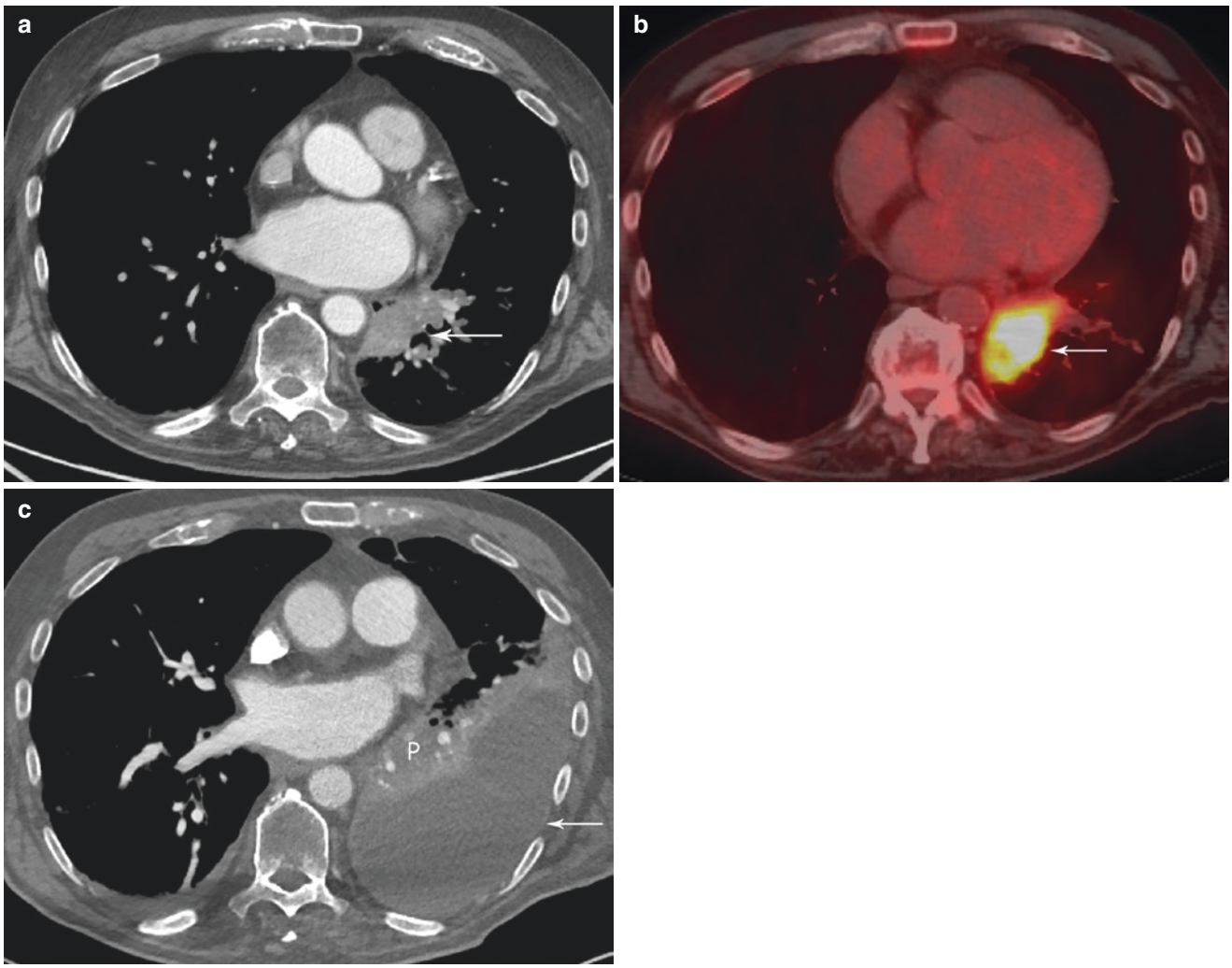


**Fig. 1.7** (**a**) Contrast-enhanced axial CT shows left lower lobe mass-like consolidation (arrow); (**b**) axial FDG-PET/CT shows increased FDG uptake in the consolidation suspicious for malignancy (arrow); (**c**) contrast-enhanced axial CT 2 months later shows persistence of the organizing pneumonia (P) and moderate left pleural effusion with pleural thickening consistent with empyema (arrow)

**Table 1.1** Common causes of fibrous pleuritis

| |
|---|
| Diffuse pleural thickening with/without calcification |
| Pleural infections |
| *Bacterial* (Staphylococcus aureus, Streptococcus pneumonia, Tuberculosis, enteric gram-negative bacilli, Actinomycetes, Nocardia) |
| *Fungal* (*pneumocystis jirovecii, Coccidioides, histoplasma)* |
| Mineral dust exposure |
| Asbestos |
| Silica |
| Drug reactions |
| Ergot derivatives, methysergide, ergoline, bromocriptine, pergolide, cabergoline nicergoline) |
| Antibiotics (tetracycline, nitrofurantoin) |
| Anti-arrhythmics (amiodarone) |
| Chemotherapeutic agents (cyclophosphamide, bleomycin, procarbazine) |
| Uremia |
| Hemothorax |
| Trauma-related |
| Iatrogenic |
| Tumor-related (primary pleural tumors, primary bronchogenic carcinoma, metastatic pleural disease) |
| Connective tissue diseases |
| Rheumatoid arthritis |
| Systemic lupus erythematosus |
| Wegener's granulomatosis |
| IgG4-related |
| Trauma |
| Localized pleural thickening |
| Pleural plaques |
| Apical pleural plaques |
| Mineral dust related (Asbestos, silica) |
| Hemothorax |
| Organized empyema |
| Cardiac surgery (coronary artery bypass graft) |
| Connective tissue diseases |
| Rheumatoid arthritis |
| Systemic lupus erythematosus |
| Wegener's granulomatosis |
| Drug-induced |
| Ergot derivatives, methysergide, ergoline, bromocriptine, pergolide, cabergoline nicergoline) |
| Antibiotics (tetracycline, nitrofurantoin) |
| Anti-arrhythmics (amiodarone) |
| Chemotherapeutic agents (cyclophosphamide, bleomycin, procarbazine) |
| IgG4-related |
| Pleuroparenchymal fibroelastosis |

proteases [14]. With persistent and/or severe inflammatory injury, the pleural space may become focally or diffusely obliterated due to the formation of dense fibrous adhesions. Acute fibrinous pleuritis is potentially reversible. With continued fibrin deposition, irreversible fibrous pleuritis associated with trapped lung may ensue. The propensity for some insults to the pleura to cause irreversible pleural fibrosis while others trigger reversible fibrinous pleuritis with complete resolution is not well understood.

Fibrothorax represents the most severe form of fibrous pleuritis in which progressive fibrosis of the visceral and parietal pleural surfaces leads to pleural adhesion. The dense pleural peel disallows lung expansion, resulting in trapped lung. Trapped lung implies chronicity of a remote inciting inflammatory event, unassociated with active disease and resulting in restrictive physiology that is usually irreversible. Associated pleural effusions are commonly small to moderate in size and transudative. Lung entrapment is also associated with a restrictive defect; however, entrapment typically arises from an active inflammatory process or malignancy and is potentially reversible. Pleural effusions in this setting are usually exudates. Therapeutic pleural drainage in either case results in a post-procedure pneumothorax, also known as pneumothorax ex-vacuo, which signifies the inability of the lung to reexpand into the evacuated pleural space. Distinguishing pneumothorax ex-vacuo from pneumothorax due to breach of the pleural membrane is crucial in directing appropriate therapy. Pleural manometry during pleural drainage procedures may be helpful in assessing abnormal lung expansion. Abnormal lung expansion is signified by a sharp decline in pleural pressure with minimal fluid drainage and may be accompanied by pleuritic chest pain [15–18]. Fibrothorax may be associated with mild to moderate restrictive pattern on pulmonary function testing. With extensive disease, particularly in cases of bilateral fibrothorax, hypercapnic respiratory failure associated with a severe restrictive defect may develop and necessitate noninvasive ventilation.

## Histological Features

Histologically, one can separate fibrous pleuritis from fibrinous pleuritis, as the former lacks the presence of a fibrinous exudate. Clinical correlation is paramount to determine the etiology of the histologic findings.

- *Fibrous pleuritis/pleurisy:* The histological hallmark of this process is the presence of a thickened pleura with minimal inflammatory and conspicuous fibroblastic components (Fig. 1.8a, b). In focal areas, the spindle cell fibroblastic component appears to dissect sections of hyalinized pleura. However, it is important to highlight that such process although may present as thickened pleura, does not invade adjacent adipose tissue or skeletal muscle. Those latter features are commonly associated with mesothelioma, which with these particular features would make it suspicious for desmoplastic mesothelioma (see below discussion on mesothelioma). In some other cases, the process may show more cellular component in the form of prominent spindle cell fibroblastic proliferation admixed with vascular structures and minimal inflammatory cells, namely, lymphocytes and plasma cells (Fig. 1.9a, b). Very likely due to the inflammatory insult, the cellular proliferation may become more reactive

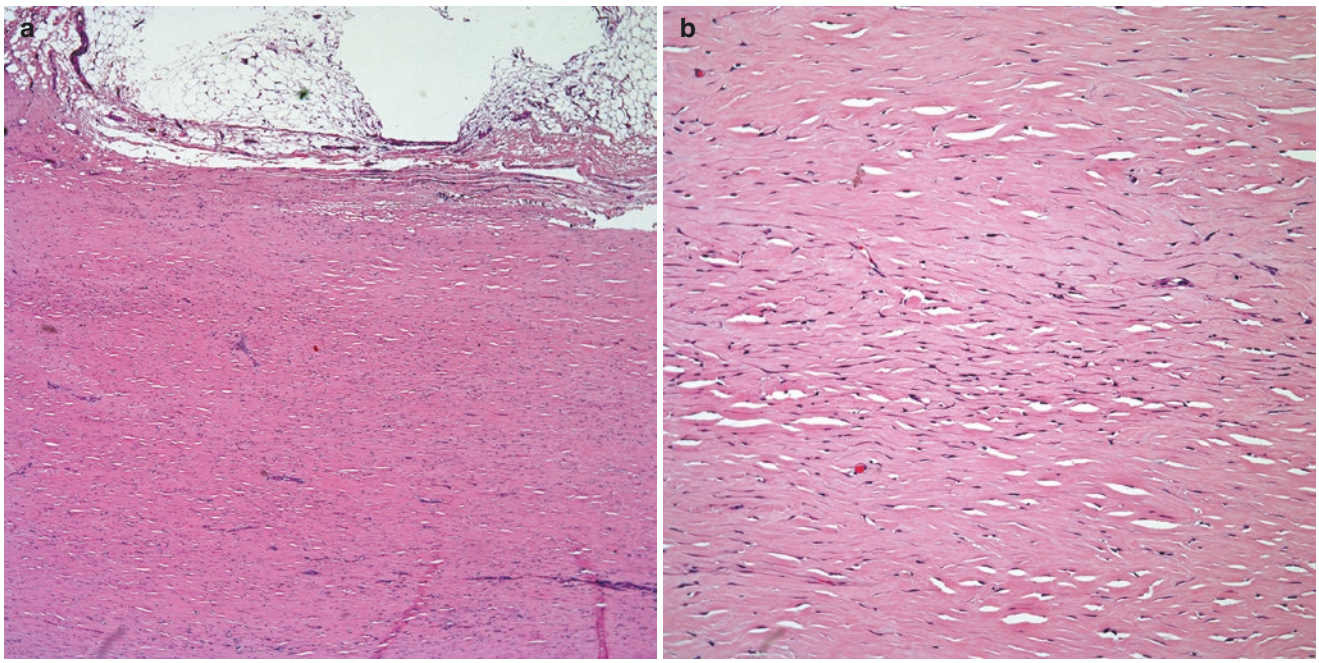


**Fig. 1.8** (**a**) Low power view of fibrous pleuritis, note the presence of uninvolved adipose tissue, (**b**) higher magnification showing only focal areas of spindle cellular proliferation

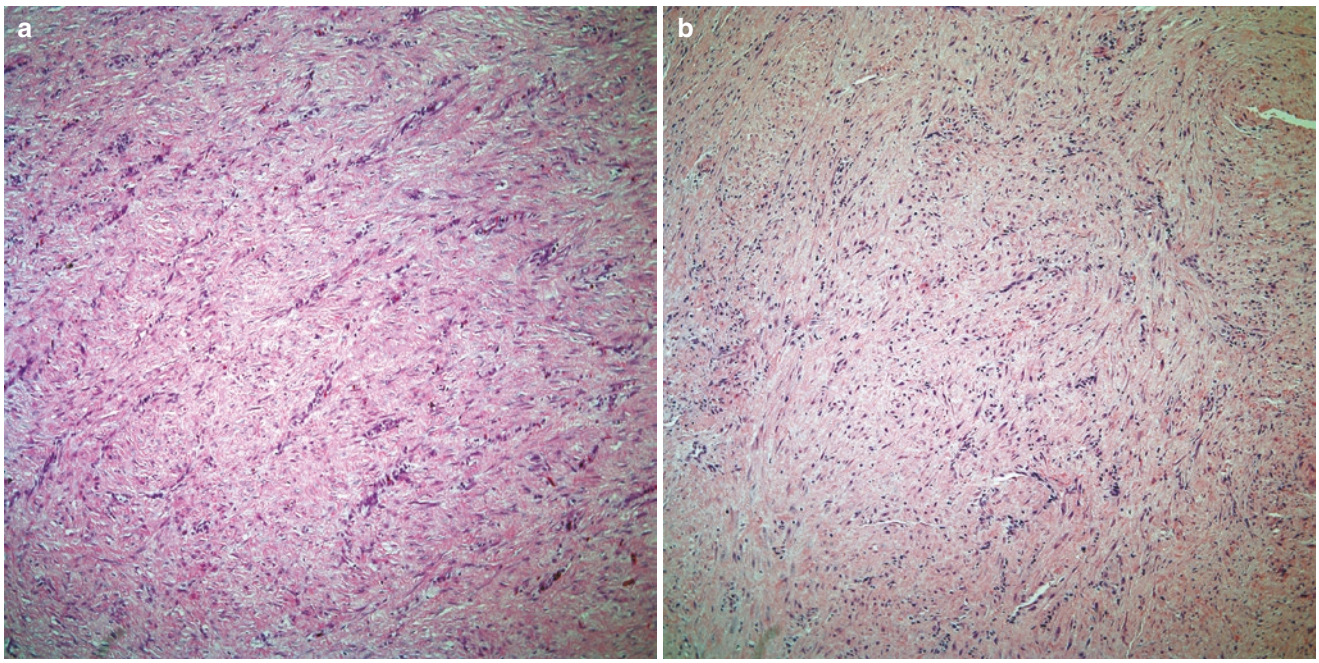


**Fig. 1.9** (**a**) Dense fibrocollagen admixed with vessels and fibroblastic cells, (**b**) fibrous pleuritis showing more cellularity admixed with dilated vessels and minimal inflammatory response

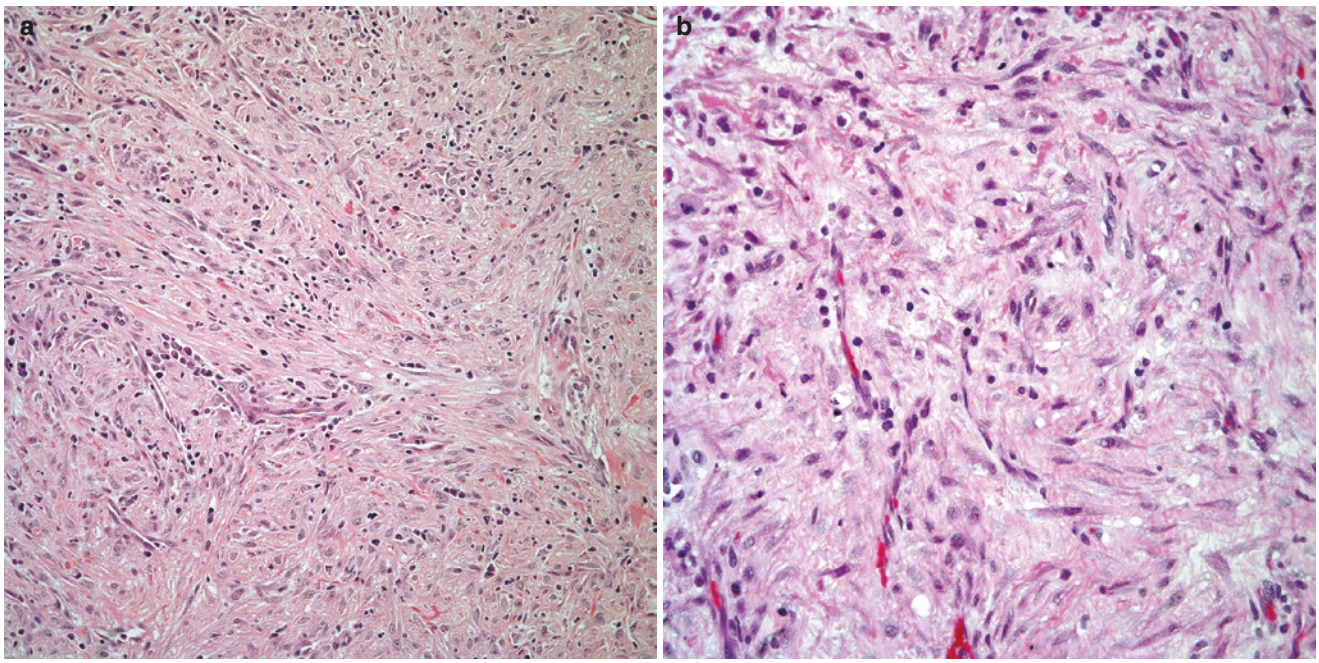


**Fig. 1.10** (**a**) Cellular fibrous pleuritis with minimal inflammatory response, (**b**) fibrous pleuritis with cellular atypia

owing to inflammation, which results in atypical mesothelial proliferation showing larger cells with round to oval nuclei and in some cells with prominent nucleoli (Fig. 1.10a, b). In some cases, mitotic figures may also be present. The use of immunohistochemical studies in these cases has limited value, as reactive mesothelial cells will show positive staining for the common markers used for mesothelioma, such as keratin, keratin 5/6, and/or calretinin. In unusual cases in which the biopsy specimen is limited, the use of molecular studies such as p16 by fluorescence in situ hybridization (FISH) may aid in the diagnosis as the presence of a homozygous deletion will be more compatible with mesothelioma (see discussion of mesothelioma below).

- *Fibrinous pleuritis:* As the term implies, the presence of fibrinous exudates that may be admixed with acute and chronic inflammatory cells are the hallmark for this process (Figs. 1.11a–c). Frequently, the use of histochemical stains (AFB and GMS) to rule out the possibility of microorganisms is commonly requested. However, the use of tissue cultures is also helpful in identifying organisms.
- *Xanthomatous pleuritis:* The inflammatory component in this process is based on the marked presence of foamy histiocytes (Fig. 1.12a, b) with minimal inflammatory reaction and the absence of fibrinous exudates. Commonly, this type of process occurs as a reaction to drug therapy or radiation [19].
- *Eosinophilic pleuritis:* This process has been linked to pneumothorax, infections, and adverse drug reactions [20–22]. It is more commonly seen in adult individuals. Eosinophilic pleuritis is characterized histologically by the presence of sheets of eosinophils admixed with other inflammatory cells and occasionally giant cells (Fig. 1.13a–c).

## Pleural Infections

The prevalence of fibrous pleuritis varies broadly with the specific inciting organism. The gamut of infectious processes that can seed the pleural surface is vast and theoretically any organism, whether bacterial or fungal, can be the leading cause of the infection. Bacterial or tuberculous pneumonia is the most common infectious cause of fibrous pleuritis, which typically occurs as a sequela of empyema, lung abscess, or aspiration. Staphylococcus aureus, streptococcus pneumoniae, and enteric gram-negative bacilli are the principal organisms implicated in the general population, while infections caused by Actinomycetes and Nocardia are primarily implicated in the setting of aspiration and immunocompromised states, respectively [23, 24]. Tuberculous pleuritis is the most common extrapulmonary manifestation of tuberculosis, with sequelae of residual pleural fibrosis occurring in 20–50% of patients [25–28]. Most of these patients have mild disease. Associated dyspnea and functional restric-

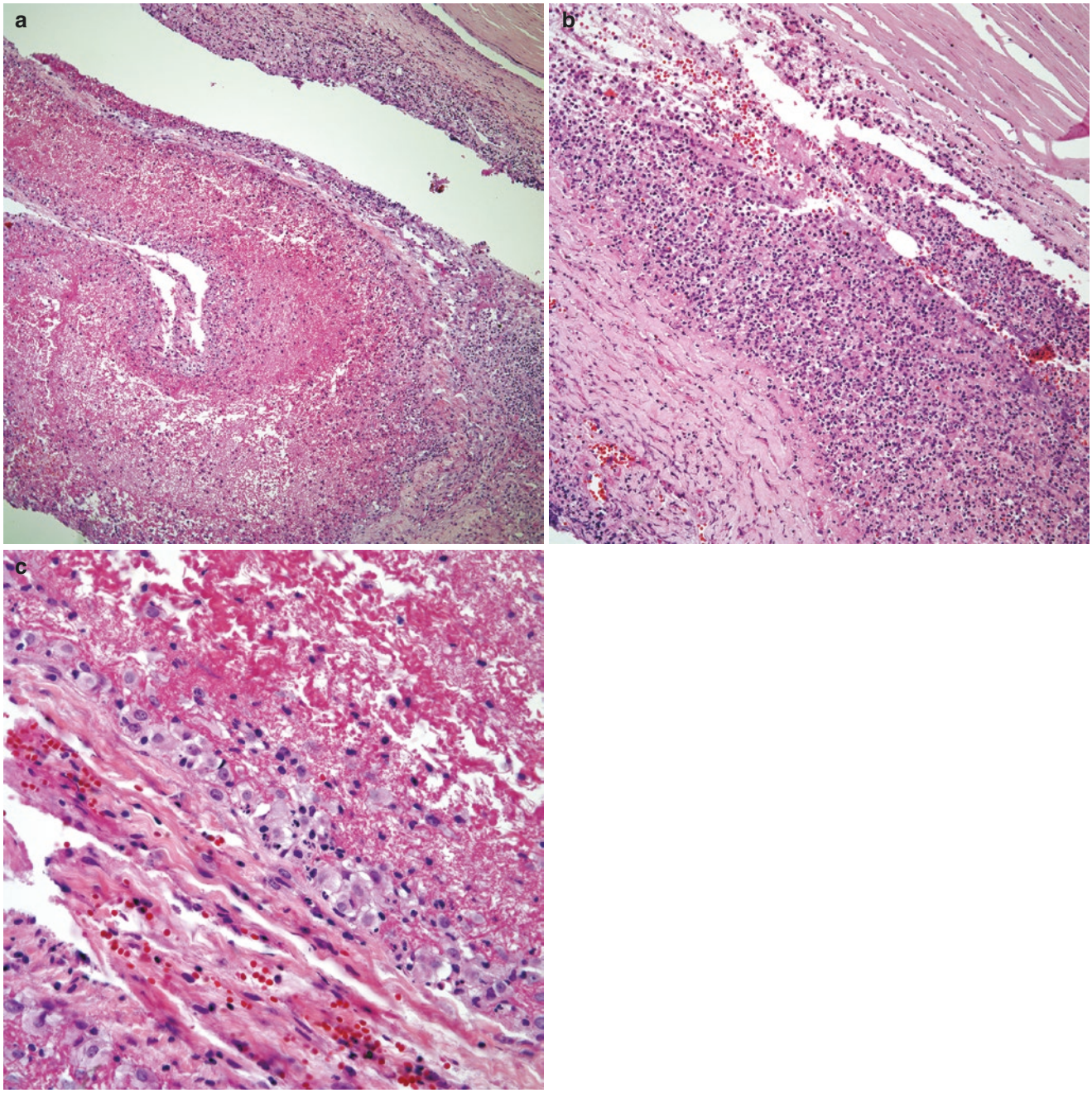


**Fig. 1.11** (**a**) Low power view of fibrinous pleuritis. Note the presence of fibrinous exudate, (**b**) fibrinous exudate with areas of acute and chronic inflammation, (**c**) closer view of fibrinous pleuritis showing the fibrinous exudate and hyperplastic mesothelial cells

tive physiology are seen in only 10% [21–24, 29–32]. The development of post tuberculous pleural fibrosis does not appear to correlate with clinical symptoms, or with the size and microbiologic characteristics of the preceding pleural fluid [31]. Neither early drainage of the pleural effusion nor systemic corticosteroids has been shown to be of definitive clinical benefit in limiting the subsequent development of pleural fibrosis [26, 33–35]. Tuberculous pleuritis may clinically and radiographically mimic pleural neoplasms [28, 36].

The prevalence of fibrous pleuritis owing to fungal empyemas varies with geographic distribution and immunocompromised states. For example, the ubiquitous environmental

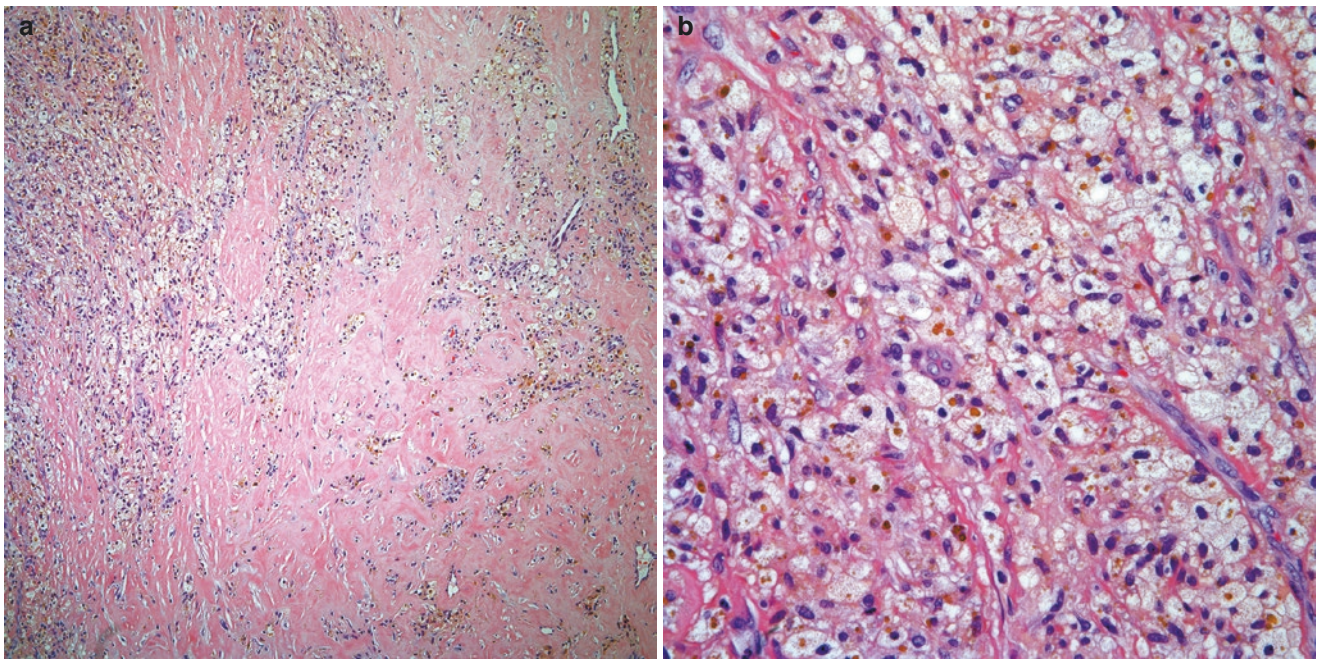


**Fig. 1.12** (**a**) Low power view of Xanthomatous pleuritis, note the diffuse presence of histiocytes with minimal inflammatory response, (**b**) higher magnification showing foamy histiocytes admixed with mesothelial cells

fungi, Pneumocystis jirovecii, may contribute to fibrous pleuritis among immunocompromised patients with empyema while patients residing in endemic areas for coccidioidomycosis (Southwestern United States) or histoplasmosis (Ohio River Valley) may develop fibrinous pleuritis as a sequela of empyema associated with these specific infectious organisms.

### Histopathological Features

Evaluation of pleural fluid cultures may potentially provide invaluable information and guide specific treatment. Pleural biopsies may offer additional information. The basic histochemical stains used will depend largely on the histological features present in the biopsy. Light microscopic examination typically demonstrates an acute inflammatory reaction in which inflammatory cells are embedded in a fibrinous exudate (Fig. 1.14a–d). The predominant cells are polymorphonuclear cells admixed with plasma cells and lymphocytes. Bacterial cultures and histochemical stains, such as Gram's may be of aid in attempting to demonstrate the presence of bacterial organisms. In addition to an inflammatory exudate, granulomatous inflammation, characterized by the presence of slightly nodular architecture with the presence of numerous multinucleated giant cells admixed with other inflammatory cells, predominantly histiocytes can be found (Fig. 1.14a–d). Other inflammatory cells that may be present include lymphocytes, plasma cells, and eosinophils. In such cases the use of silver stains such as Gomori Methenamine Silver (GMS) can identify fungal organisms (Fig. 1.14e). The use of histochemical stains for acid fast bacteria (AFB) is important to properly exclude the possibility of mycobacterial infection [36].

## Uremia

Pleural abnormalities of uremia, including fibrinous pleuritis have been observed in up to 20% of patients at autopsy [37]. The mechanism of uremic fibrous pleuritis has not been established, however, abnormal filtration forces and lymphatic absorption across subpleural surfaces have been implicated [38]. Pleural disease in this setting ranges from subclinical pleural thickening to severe dyspnea associated with pleural deposition of a gelatinous material and formation of a thick pleural peel. Uremic fibrosing pleuritis typically develops several years after initiation of dialysis. Pleural thickening may initially respond to dialysis, or wax and wane spontaneously [39]. Optimal therapies, including the therapeutic

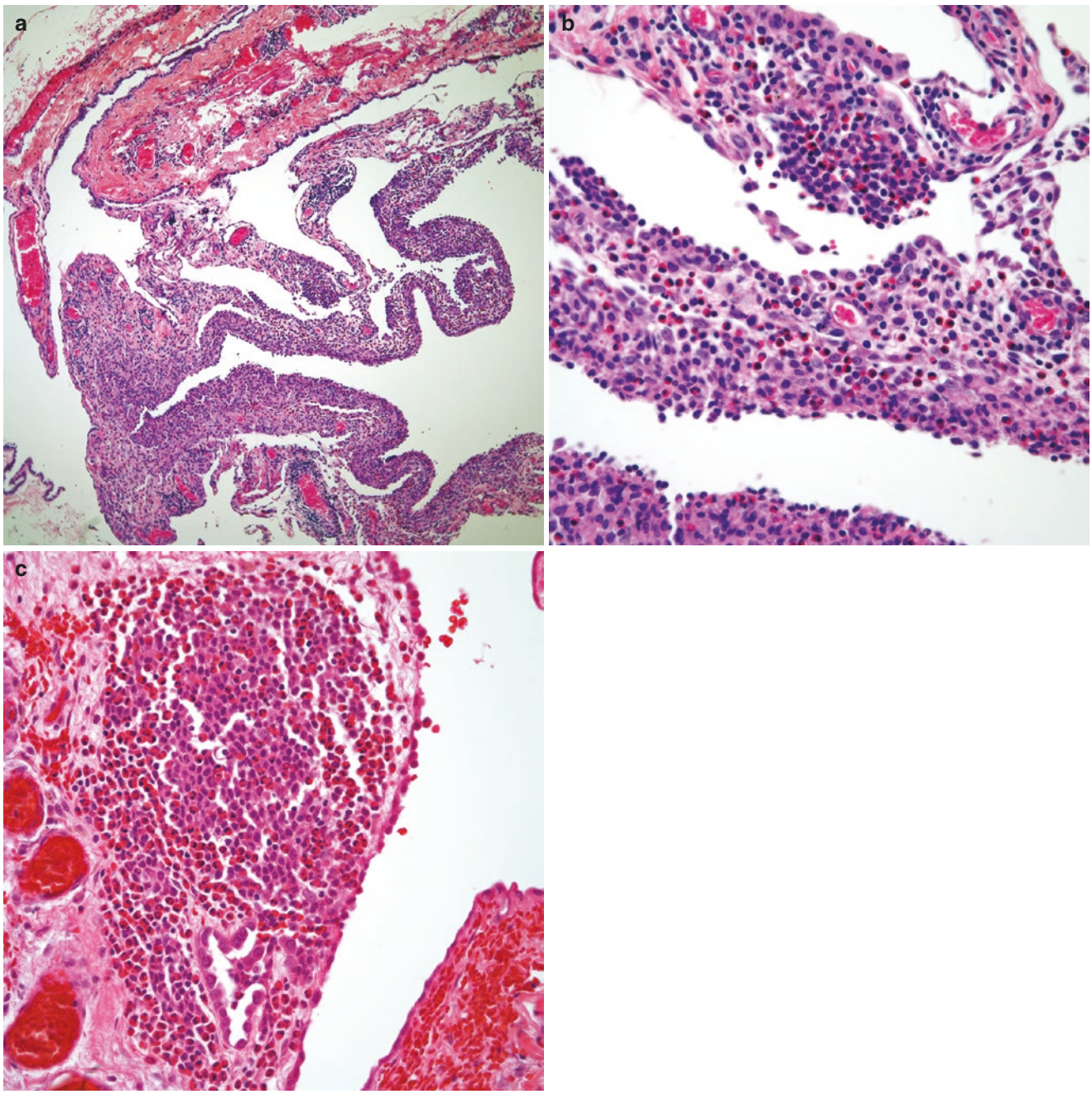


**Fig. 1.13** (**a**) Low power view of strip of pleura with inflammatory cells, (**b**) higher magnification shows sheets of eosinophils, (**c**) eosinophilic pleuritis with areas of mesothelial hyperplasia

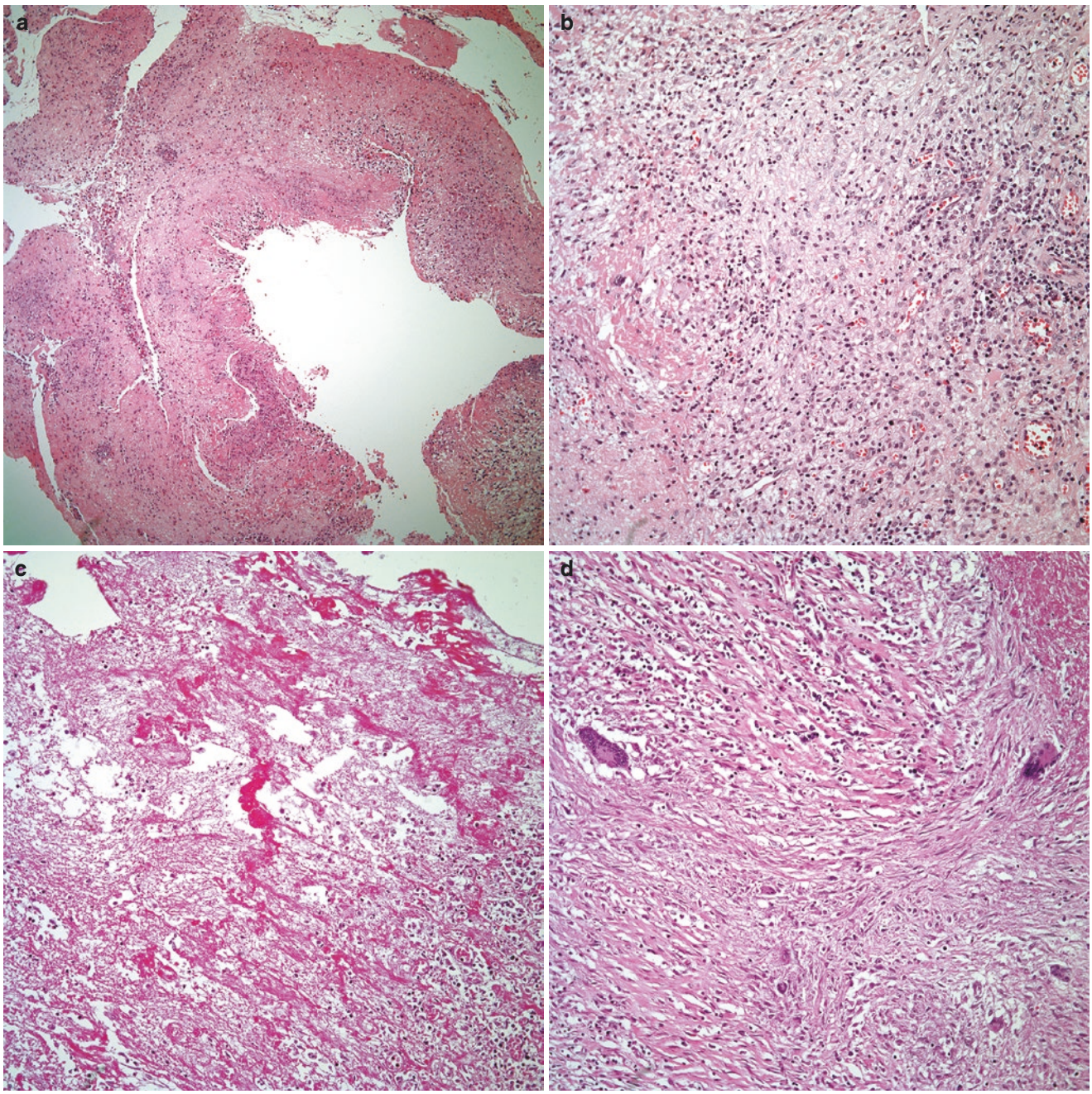


**Fig. 1.14** (**a**) Low power view of acute pleuritis; (**b**) higher magnification showing the presence of an inflammatory reaction composed predominantly of histiocytes; (**c**) predominantly fibrinous exudate in fibrinous pleruritis; (**d**) pleuritis showing numerous multinucleated giant cells with inflammatory reaction; (**e**) GMS stain showing numerous fungal organisms

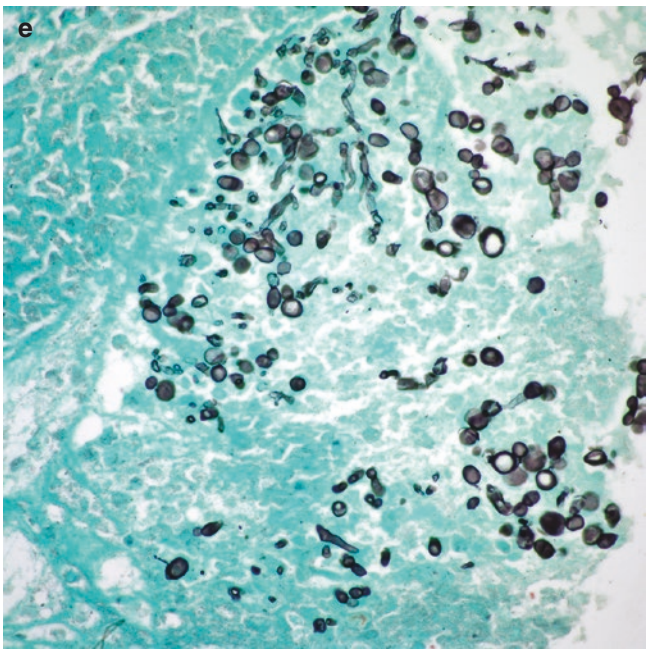


**Fig. 1.14** (continued)

benefit of systemic corticosteroids, are not well defined. As pleural deposition progresses, irreversible restrictive physiology requiring surgical decortication may occur.

## Hemothorax

Hemothorax, or the accumulation of blood into the pleural space, has been reported most frequently after trauma to the chest or in association with iatrogenic causes (Fig. 1.15a, b). Primary or metastatic pleural tumors, bleeding diatheses, anticoagulation, pleural endometriosis, arteriovenous malformations, and vascular rupture are other attributable causes. Fibrothorax associated with trapped lung is a rare late complication of hemothorax. Early and complete chest tube drainage of the hemothorax is generally recommended to mitigate the complications of fibrothorax. Operative therapies, including video-assisted thoracoscopic surgery (VATS), are generally reserved for hemodynamically unstable patients with more than 1000 ml of blood drainage from the initial thoracotomy or brisk ongoing blood losses of more than 100–200 ml/h [40, 41]. Decortication may alleviate fibrothorax and trapped lung; however, operative risk is substantial.

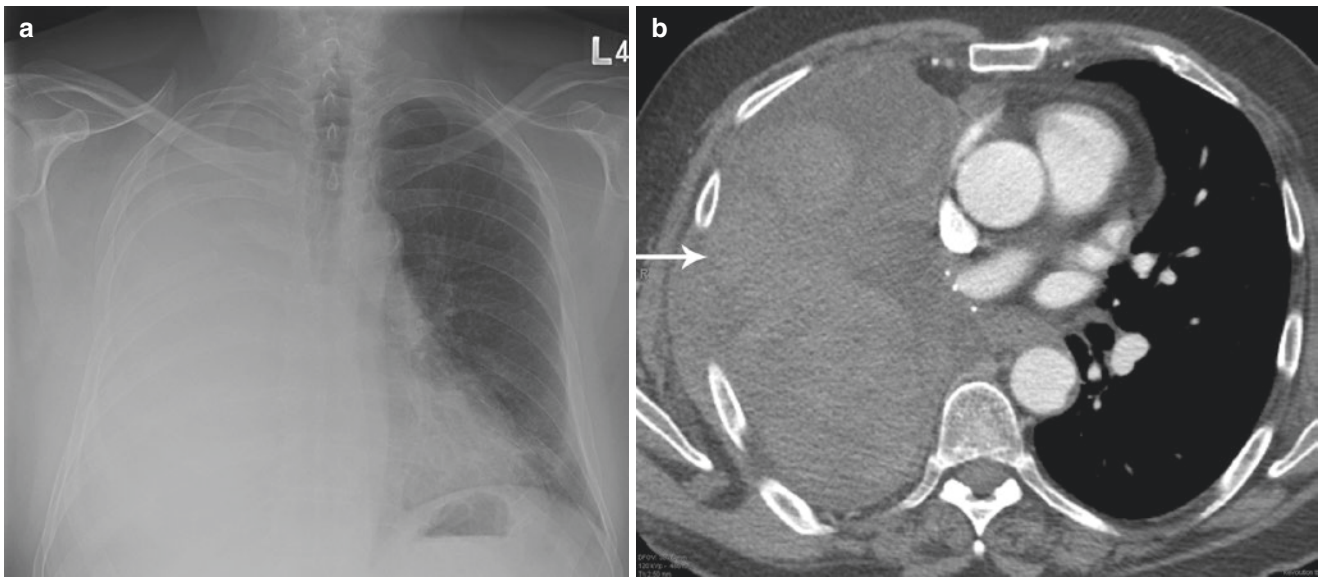


**Fig. 1.15** (**a**) Frontal chest radiograph shows complete opacification of the right hemithorax; (**b**) contrast-enhanced axial CT shows heterogeneous attenuation in the right pleural fluid in the pneumonectomy space consistent with blood products (arrow)

### Coronary Artery Bypass Surgery

Pleural effusions occur throughout the perioperative and postoperative period following a variety of cardiac surgeries, including coronary artery bypass grafting (CABG). Diagnostic thoracentesis should be performed for patients with large symptomatic pleural effusions or fever after CABG surgery. Early effusions may spontaneously resolve, while late effusions may persist 6 or more months after the surgery. Many of the early pleural effusions post CABG may be directly attributable to pleural injury during surgery. Persistent late effusions, however, have been ascribed to lymphatic damage, and/or immune mechanisms [42–44]. Over time, these lymphocyte-predominant exudates are replaced with fibrin deposition and subsequent trapped lung. In patients with advanced disease, significant dyspnea associated with a severe restrictive defect often requires surgical decortication [45].

### Apical Pleural Plaques

Localized visceral pleural plaques may exist as apical caps or nodular histiocytic hyperplasia. Apical caps exist morphologically as unilateral or bilateral fibroelastic scars involving the lung apex. These benign lesions are typically identified as asymptomatic findings on chest radiographs. Bilateral lesions may be asymmetric. The pathogenesis of apical caps is not completely understood. The apical segments of the upper and lower lobes are subject to intrinsic physiologic under-perfusion, causing chronic low-grade local ischemia. This ischemia coupled with chronic low-grade inflammation is the proposed mechanism, although the pathogenesis remains unproven. The scars typically remain stable, although minimal enlargement occurring over years has been reported. The prevalence of apical caps increase with age, occurring in 64% of patients over the age of 66 years in one study [46]. There is no sex predilection and no predilection for either side.

On light microscopy, apical caps are characterized by the presence of subpleural fibroelastosis or fibrosis with or without the presence of entrapped alveoli and scattered inflammatory cells (Fig. 1.16a, b). Occasionally, alveolar entrapment may have features that are similar histologically to adenocarcinoma.

### Pneumoconiosis

Pneumoconiosis caused by significant exposure to asbestos and silica are well known causes of pleural fibrosis. Asbestos-related pleural fibrosis may exist as pleural plaques or diffuse pleural fibrosis. These two clinically distinct entities may overlap; however, the presence of pleural plaques does not imply or predict the development of asbestosis. Pleural plaques arise along the parietal surface of the pleura and are most commonly distributed along the lateral and posterior walls of the lower half of the thorax, sparing the costophrenic angles. Diaphragmatic, mediastinal, pericardial distribution is also seen.

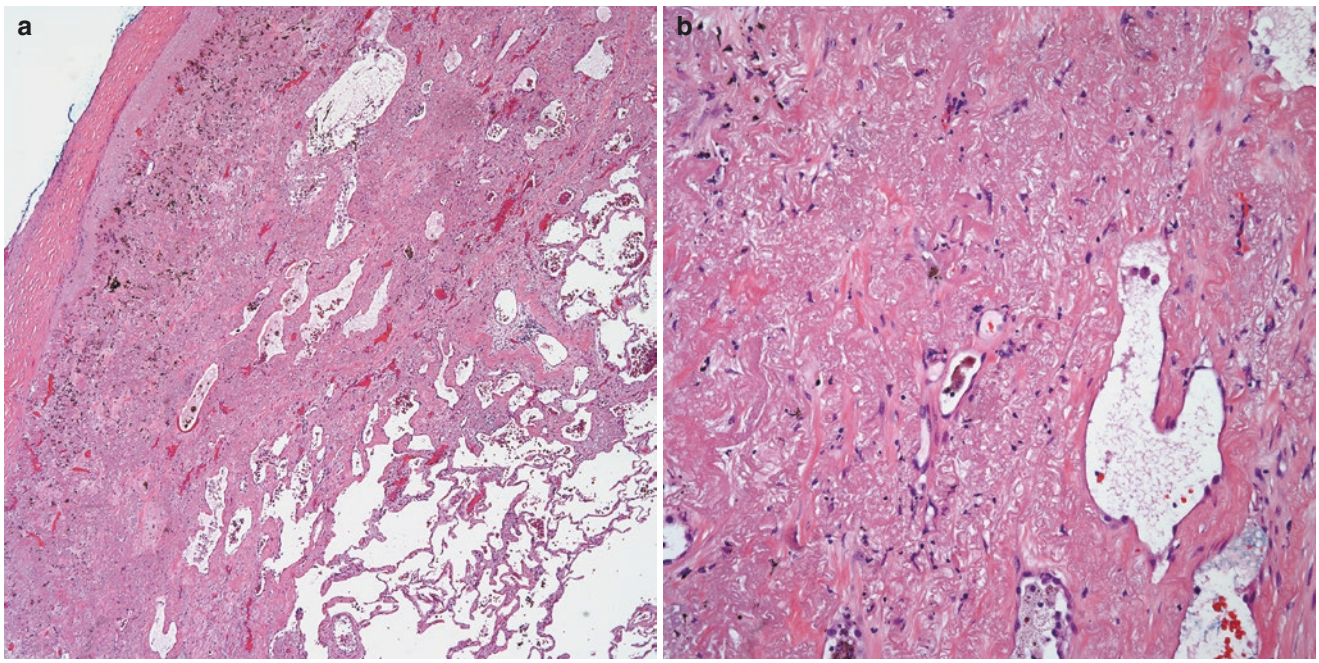


**Fig. 1.16** (**a**) Low power view of an apical cap showing subpleural fibroelastotic changes, (**b**) higher magnification showing low cellularity and dilated vessels

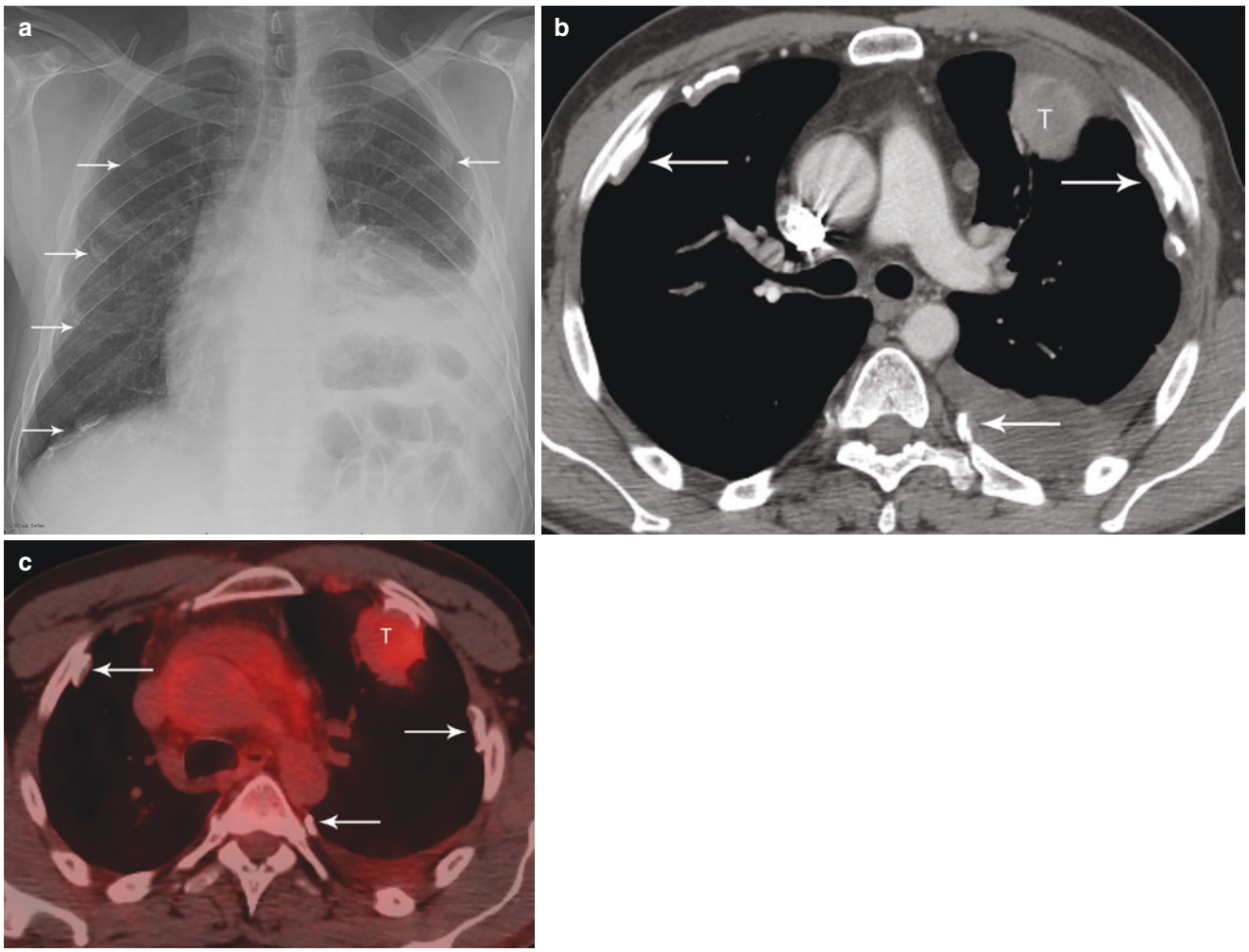


**Fig. 1.17** (**a**) Frontal chest radiograph shows bilateral curvilinear areas of calcification consistent with pleural plaques due to asbestos exposure. A moderate left pleural effusion is present; (**b**) contrast-enhanced axial CT chest shows the left upper lobe lung cancer (T) and bilateral calcified pleural plaques (arrows) with a left pleural effusion; (**c**) axial FDG-PET/CT shows the left upper lobe primary tumor is hypermetabolic. Calcified pleural plaques (arrows) due to prior exposure to asbestos are not FDG avid on PET

Calcified bilateral lesions are virtually pathognomonic of significant prior asbestos exposure (Fig. 1.17a–c). Pleural plaques typically develop 20–30 years after initial asbestos exposure and are frequently incidental findings on chest radiographs in asymptomatic patients [46–48]. The mechanism of pleural plaque formation has not been definitively elucidated, however penetration of inhaled asbestos fibers through the visceral pleura, which incites an inflammatory reaction along the parietal pleura has been proposed. In contrast to asbestos-related pleural plaques, asbestos-associated diffuse pleural thickening involves the visceral pleura, frequently distributes over the costophrenic angles, and may be accompanied by fibrotic parenchymal disease. Patients typically present with dyspnea on exertion associated with a restrictive physiology and reduced diffusing capacity on lung function testing [49–51].

The presence of hyalinzed fibroconnective tissue with minimal inflammatory reaction is a hallmark of asbestos-related pleural plaques (Fig. 1.18a–c). Despite significant asbestos exposure, ferruginous bodies on pleural sections are rare findings, which more often occur in alveolated lung parenchyma.

Treatment options for asbestos-related diffuse pleural disease are very limited. In the absence of significant pulmonary fibrosis, decortication may be considered, although surgical outcomes have been mixed.

Silica-associated fibrous pleuritis occurs in 18–58% of exposed persons. In addition to the traditional mining industry, occupational exposure to silica has been reported in a variety of workplaces, including sandblasting, stone masonry, semiprecious stone manufacturing, electrical cable industries, hydraulic fracturing industries, and construction. Acute, accelerated, and chronic forms of silicosis exist, occurring within weeks to 5 years, less than 10 years, and more than 10 years after significant silica exposure, respectively. Patients commonly present with progressive dyspnea and dry cough in association with recalcitrant, diffuse pleu-

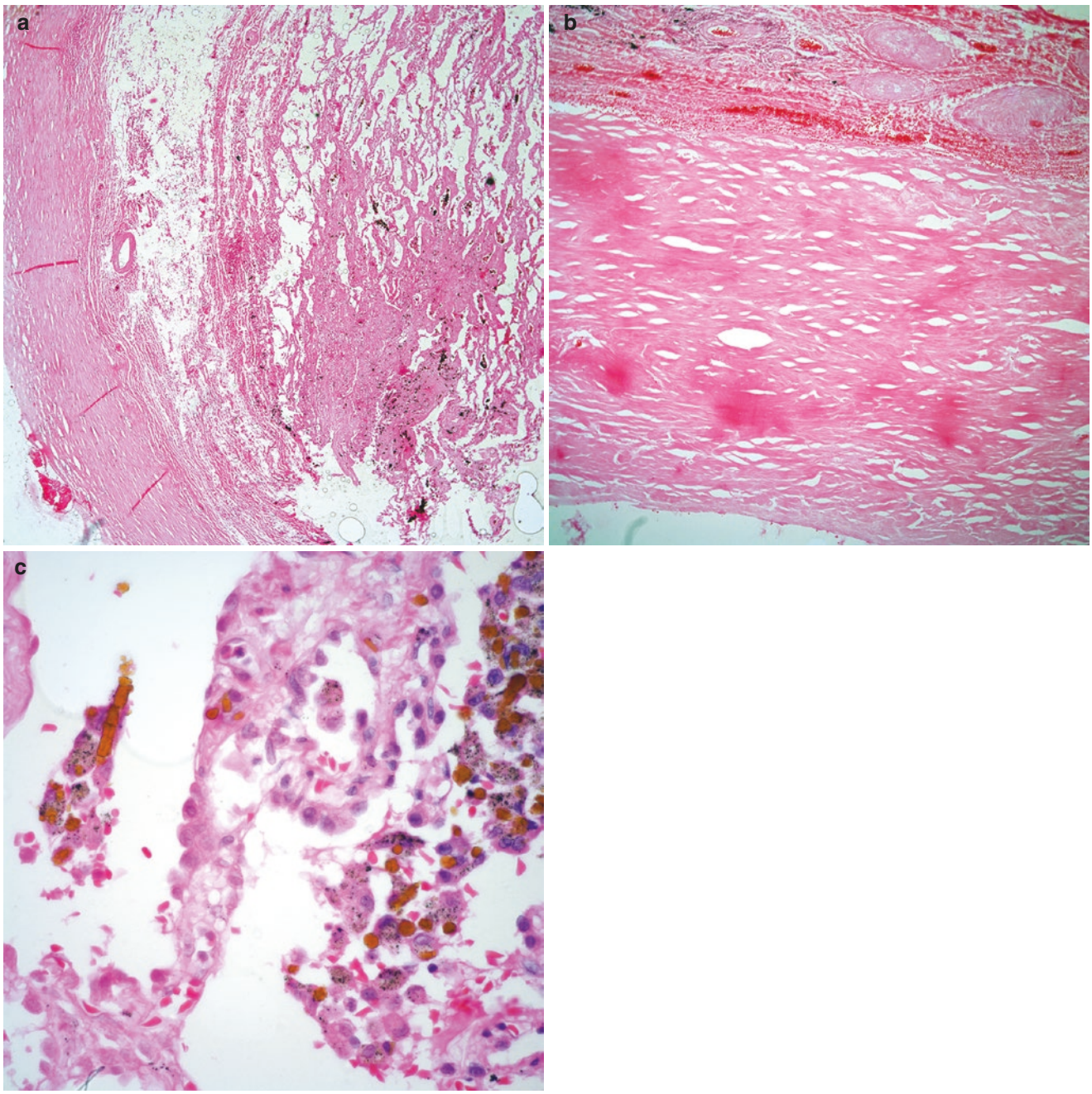


**Fig. 1.18** (**a**) Low power view of a thick pleural surface overlying lung parenchyma; (**b**) higher magnification of the pleura showing extensive hyalinization with minimal inflammation; (**c**) alveolated lung parenchyma showing numerous ferruginous bodies

ral fibrosis and upper-lobe predominant fibrotic parenchymal disease, known as progressive massive fibrosis (PMF) [52, 53]. The diagnostic workup relies on chest CT imaging and pulmonary function testing coupled with a compatible history of silica dust exposure.

Mixed inflammatory reaction composed of histiocytes and lymphocytes with fibrosis and the presence of dust-like dark silica particles are noted on histological sections of the pleura (Fig. 1.19a, b). Silica particles are best detected with polarized light or by X-ray diffraction analysis.

Superimposed bacterial infection, in particular, mycobacterial disease, is a well-known complication of silicosis with PMF and should be suspected in patients with fever and other constitutional symptoms, worsening respiratory impairment, hemoptysis, and cavitation in regions of PMF on chest imaging studies. Chronic necrotizing aspergillosis, chronic bronchitis, autoimmune diseases, and lung cancer are other associated conditions [54]. Treatment is primarily supportive. Avoidance of further exposure to respirable silica and tobacco products may help to slow disease progression. A role for glucocorti-

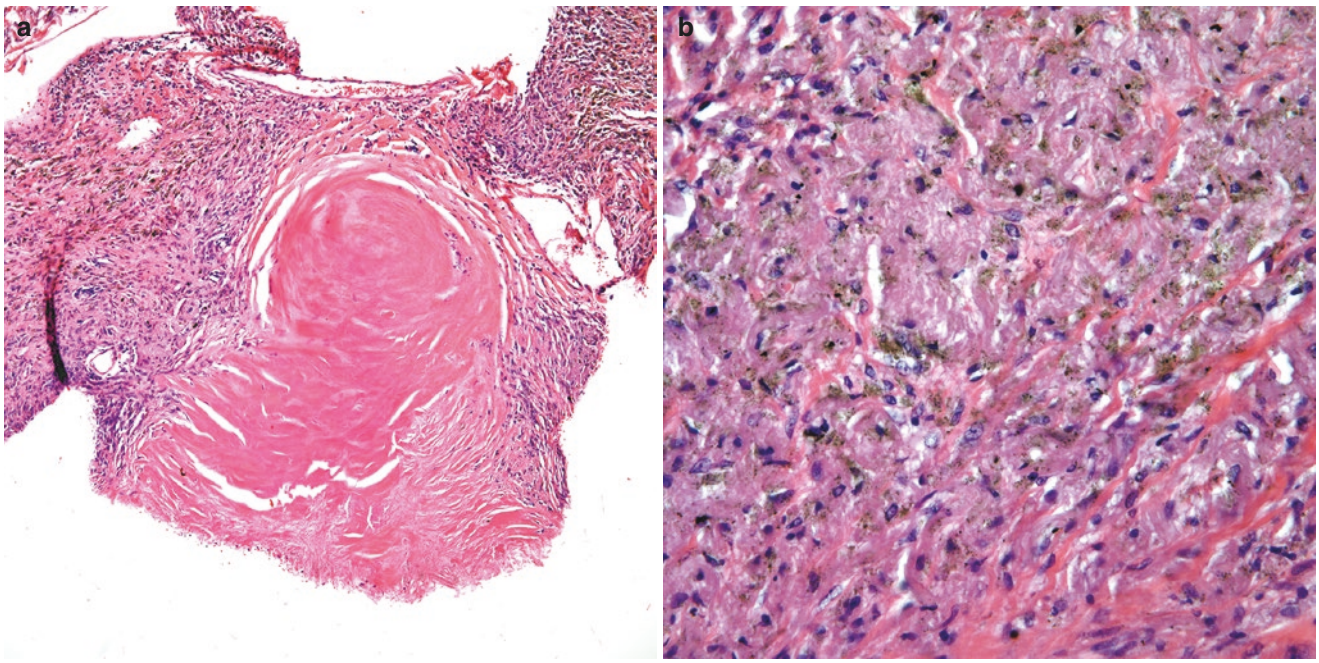


**Fig. 1.19** (**a**) Low power view of a hyalinized nodule in the pleural surface associated with mixed inflammatory reaction; (**b**) higher magnification of the inflammatory reaction showing the presence of histiocytes and dark particles (silica), which is best visualized by polarizing microscopy

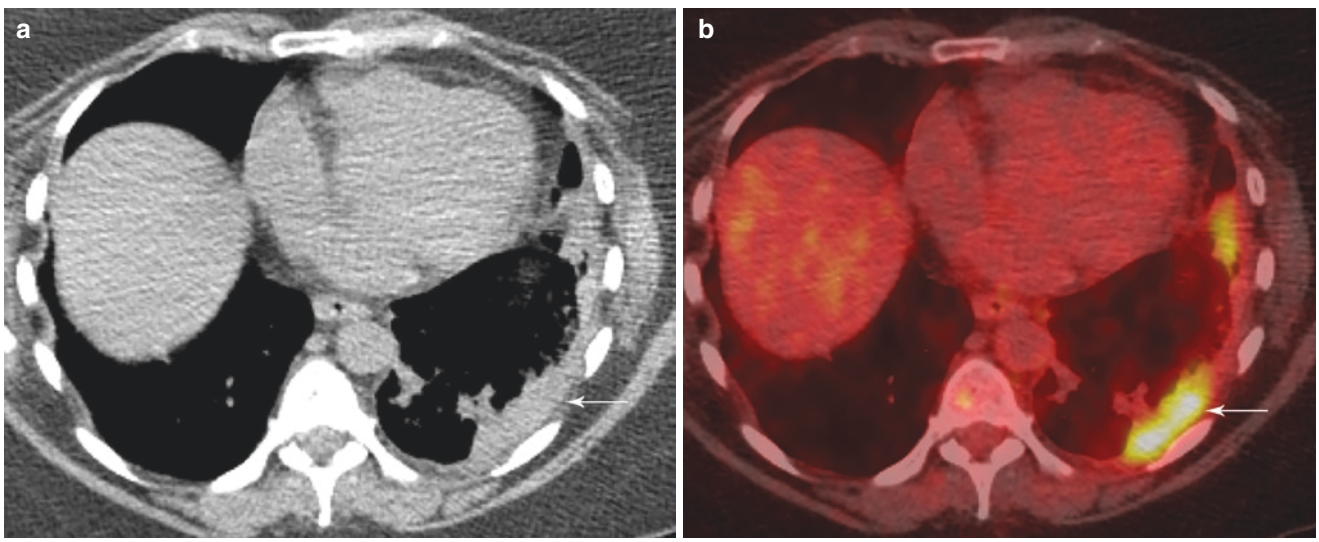


**Fig. 1.20** (**a**) Non-contrast axial CT shows left posterior pleural thickening (arrow); (**b**) axial FDG-PET/CT shows intense FDG avidity of the left pleural thickening (arrow)

coids in the management of acute and chronic forms of silicosis has not been fully established. Successful lung transplantation has been reported in patients with advanced disease [54–56].

## Connective Tissue Diseases

Pleural pathologic findings associated with systemic connective tissue diseases (CTD), such as rheumatoid arthritis, systemic lupus erythematosus, and granulomatosis with polyangiitis, may vary from small fibrous plaques to extensive reactive fibrosis. Fibrous pleuritis may presage the clinical diagnosis of primary CTDs or, alternatively, develop in the context of established disease [57, 58]. Among the CTDs, pleural involvement in association with rheumatoid arthritis is most common, occurring in up to 50% of patients (Fig. 1.20a, b). Concomitant interstitial lung disease is reported in 30% of patients. Significant pleural fibrosis may lead to restrictive lung physiology and trapped lung. Systemic and intrapleural steroids have been

used with variable success. The effect of disease modifying antirheumatic drugs in mitigating rheumatoid fibrous pleuritis is unknown.

## Drug-Induced Fibrous Pleuritis

Drug reactions are common causes of pleural effusions; however drug-induced pleural thickening and pleural fibrosis are less commonly observed. Ergot-derived dopamine agonists used to treat migraine headaches, including methylsergide and ergoline were among the earliest reports of drug-related pleural fibrosis. Other ergots such as bromocriptine, pergolide, cabergoline, and nicergoline, which are used in the treatment of Parkinson's disease, have also been implicated. Fibrous pleuritis has been reported in 2–4% of ergot-treated patients and may occur in isolation or accompanied by fibrosis of other organ systems, including the mediastinum, pericardium, retroperitoneum, and cardiac valves [59–64]. Pleural disease typically develops within the first 6 months following initiation of the drug and is signaled by dyspnea and pleuritic pain associated with bilateral pleural thickening along the lateral and bibasilar aspects of the thorax. Late fibrosis, occurring many years after drug exposure, has also been described. Thus vigilance throughout the treatment period must be maintained. Cessation of the drug halts disease progression in most cases, though complete resolution is rare.

Other classes of drugs that have been implicated in the development of fibrous pleuritis include antibiotics (tetracycline, nitrofurantoin), anti-arrhythmics (amiodarone), and chemotherapeutic agents (cyclophosphamide, bleomycin, procarbazine) [65–69]. Antecedent pleural effusions with or without associated parenchymal disease is reported in most cases, however isolated fibrous pleuritis may also occur, particularly following amiodarone exposure [67].

## IgG4-Related Fibrous Pleuritis

Tissue infiltration by immunoglobulin G4 positive plasma cells is known to cause systemic fibroinflammatory injury to diverse tissues, including the pleura. This multisystem disorder most often occurs in middle-aged men. Pleural manifestations of IgG4-related disease include fibrous pleuritis, pleural mass, and effusions (Fig. 1.21a, b). Fibrous pleuritis typically occurs in the context of other organ system disease, such as pancreatitis, sialadenitis, or hepatitis, but has been increasingly identified without other organ involvement. The diagnosis should be made in the context of clinical, radiological, and histological correlations.

Histologically, sections of the pleura show areas of pleural thickening with fibrosis admixed with an inflammatory reaction composed predominantly of plasma cells (Fig. 1.22a, b).

Immunohistochemical stains to determine the presence of IgG4 will light up most of the plasma cells present with the inflammatory reaction. The presence of more than 10 IgG4-positive plasma cells per high-power field and an IgG4/IgG-positive plasma cell ratio of more than 40% is suggestive of IgG4-related pleural disease. Close monitoring is reasonable in asymptomatic patients with isolated pleural effusions. Systemic corticosteroids are recommended for patients with multi-organ disease and/or fibrous pleuritis. Treatment delays may result in irreversible pleural fibrosis and other organ dysfunction [70–72].

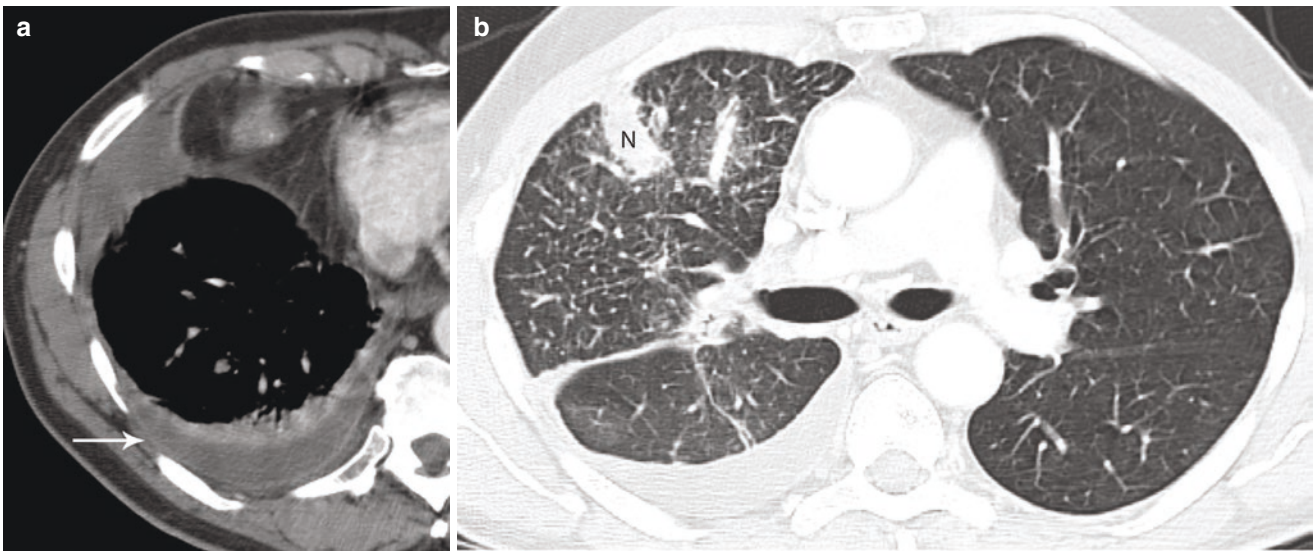


**Fig. 1.21** (**a**) Contrast-enhanced axial CT shows right pleural thickening with a small right pleural effusion; (**b**) contrast-enhanced axial CT shows interlobular septal thickening and an irregular 2 cm right upper lobe solid nodule (N)

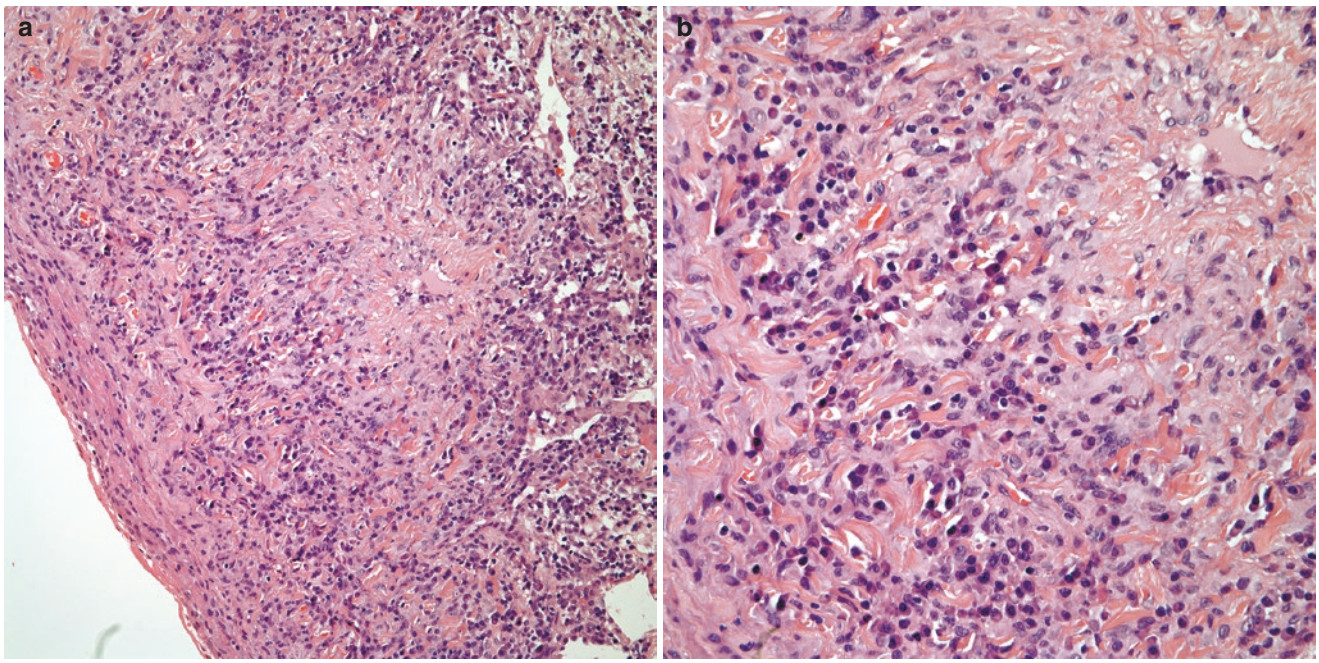


**Fig. 1.22** (**a**) Low power view showing a thickened pleural surface with inflammatory reaction; (**b**) higher magnification shows the presence of discrete areas of fibrosis admixed with numerous plasma cells

## Pleuroparenchymal Fibroelastosis

Pleuroparenchymal fibroelastosis (PPFE) is a rare type of interstitial pneumonia in which there is upper-lobe predominant fibrosis involving the visceral pleura and elastin-rich fibroelastotic changes that are most conspicuous in the subpleural lung parenchyma of the upper lobes (Fig. 1.23a, b). Most cases are considered idiopathic, although secondary forms of PPFE associated with autoimmunity (scleroderma, rheumatoid arthritis, inflammatory bowel disease), infections (Aspergillus, nontuberculous mycobacteria), and hematopoietic stem cell transplantation have been described [73, 74]. Patients typically present between 40 and 70 years of age. Dyspnea, dry cough, weight loss, and recurrent infections associated with worsening volume loss of the upper lobes typically progress slowly over years. Rarely, PPFE may take an inexorably progressive course that culminates in platythorax and irreversible respiratory failure with early death [75, 76] The diagnosis is predicated on the exclusion of competing conditions associated with upper lobe disease, including sarcoidosis, hypersensitivity pneumonitis, atypical nontuberculous mycobacterial infection, pneumoconiosis, malignancy, apical pleural cap, and post–lung injury remodeling. Coexisting usual interstitial pneumonia (UIP) and idiopathic pulmonary fibrosis (IPF) have been reported in some cases [77, 78]. The diagnosis is suggested by CT findings of intense upper-lobe predominant pleural fibrosis, pronounced parenchymal fibroelastosis, and sparing of the lung away from the pleura. These observations help to distinguish PPFE from other interstitial lung diseases.

On imaging, fibrous and fibrinous pleuritis are usually seen as diffuse pleural thickening. Benign pleural thickening typically manifests as a continuous process more than 5 cm wide, 8 cm in craniocaudal extent, and 3 mm thick, all of which are best measured on CT [79]. The costal and paravertebral regions are most commonly involved; the mediastinal pleura are rarely affected. The appearance of benign pleural thickening is similar regardless of the cause. However, certain associated features on CT may give clues as to the etiology. Pleural calcification, volume loss, thickened extra-pleural fat layer, and associated parenchymal abnormality may favor prior empyema (particularly tuberculosis), whereas pleural calcification with rib deformity and normal lung parenchyma would indicate previous traumatic hemothorax (Fig. 1.24a–c). Talc pleurodesis on CT typically demonstrates high attenuation talc material in the pleura and increased soft tissue visceral pleural thickening [80].

## Mesothelial Hyperplasia

Mesothelial hyperplasia, also referred to as benign reactive mesothelial hyperplasia (RMH), may cause pleural effusions and pleural thickening and occurs in a variety of clinical settings [81]. Histologically, the hallmark of this benign condition is a dense proliferation of mesothelial cells, which must be distinguished from malignant mesothelioma. Patients with mesothelial hyperplasia are typically asymptomatic and no specific treatment is required.

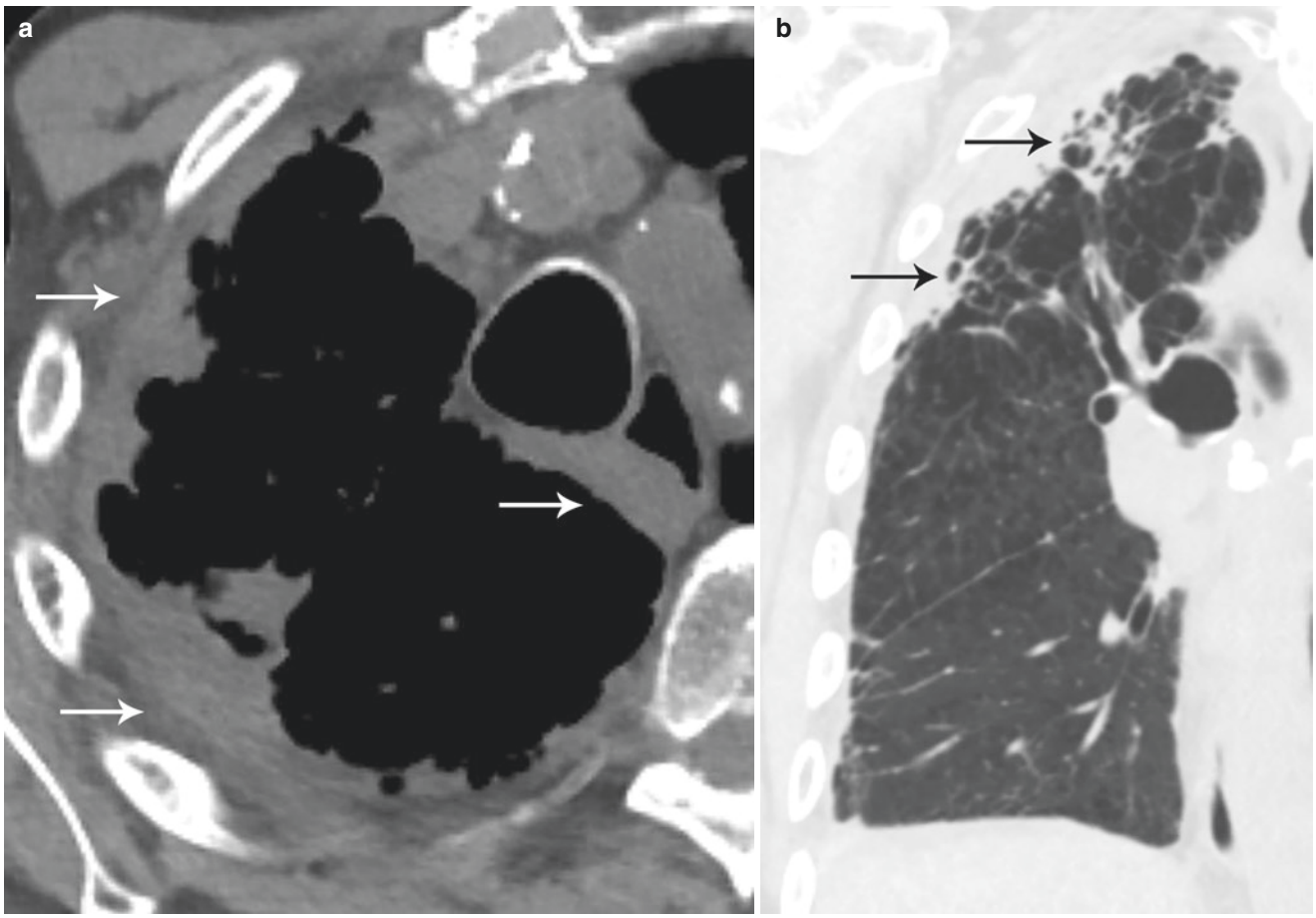


**Fig. 1.23** (**a**) Non-contrast axial CT shows the right pleural thickening (arrows) in the upper thorax; (**b**) non-contrast coronal CT shows reticulonodular lung fibrosis in the subpleural distribution (arrows) typical of PPFE. Note lung emphysematous changes

A critical difficulty lies in differentiating benign RMH from malignant disease, which is fraught with a spectrum of diagnostic challenges. The diagnostic gold standard is based on the histopatholgical assessment of the lesion. Biopsy specimens should be large enough to permit examination of mesothelial cell proliferation as well as assessment of adjacent tissue landmarks, such as skeletal muscle and adipose tissue. Infiltration of mesothelial cells into adipose tissue or the skeletal muscle is a key criterium for the diagnosis of mesothelioma. Tissue biopsies of 1 mm in size or less may not include key landmarks that allow definitive diagnosis of malignant pleural mesothelioma (MPM). Florid mesothelial proliferation without infiltration into adipose tissue and/or muscle is indicative of mesothelial hyperplasia rather than malignant mesothelioma. Common immunohistochemical markers such as keratin 5/6 and calretinin are positive in reactive as well as in malignant mesothelial proliferations. Thus, immunohistochemical stains are of minimal benefit in distinguishing malignant versus hyperplastic pleural proliferation. The tumor suppressors, p16 (cyclin-dependent kinase 2A, CNDK2A) and breast cancer-1-associated protein (BAP-1) are two of the most frequently mutated genes in MPM pathogenesis and have been identified as potentially useful molecular markers in distinguishing benign reactive hyperplasia from malignant disease. However, a small percentage of true malignant mesotheliomas may not demonstrate homozygous deletion of p16 as assessed by fluorescent in situ hybridization (FISH). Retention of BAP1 expression on immunohistochemistry suggests reactive changes, whileloss of BAP1 staining, may suggest the possibility of mesothelioma in situ [82–87].

## Pleural Endometriosis

Ectopic endometrial tissue, or endometriosis, is believed to affect 6–10% of reproductive-age women. Nearly 50% of these women are infertile [88]. Endometriosis of non-reproductive organs most often occurs within the thoracic cavity where it may involve the lung parenchyma, diaphragm, and pleural surfaces. Intrathoracic endometriosis produces a range of clinical and radiological manifestations, collectively referred to as thoracic endometriosis syndrome (TES) that includes catamenial pneumothorax, hemothorax,

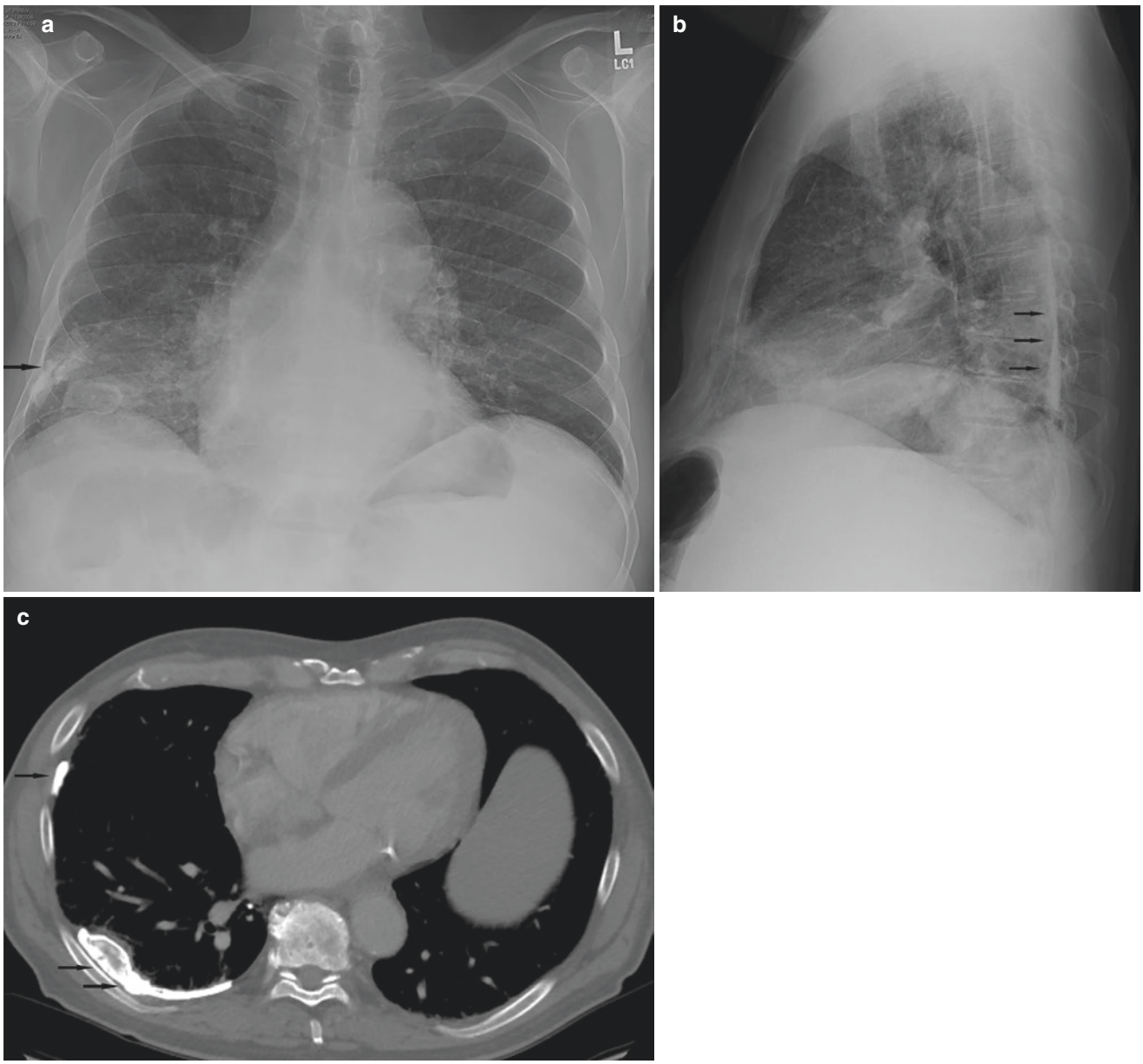


**Fig. 1.24** (**a**, **b**) Frontal and lateral chest radiographs show coarse calcifications are seen in the right pleural space in the lower thorax (arrows); (**c**) contrast-enhanced axial CT shows densely calcified pleural rind along the posterior and lateral aspect (arrows) with volume loss in the right hemithorax due to prior history of tuberculous empyema

hemoptysis, and pulmonary nodules, catamenial chest pain, endometriosis-related pleural effusion, and diaphragmatic hernia (Fig. 1.25a, b). Catamenial pneumothorax and catamenial hemothorax are the most common manifestations of pleural TES, occurring in 74% and 14% of all patients, respectively [89–91]. Catamenial hemoptysis occurs in 7% of patients, and is usually mild. Pulmonary nodules may be seen in 6% of patients and have no predilection for laterality [92]. Although TES may occur in isolation, 50–84% of patients have extensive pelvic disease, which may predate TES by 5–7 years [93]. Thus, the absence of an association with pelvic endometriosis does not exclude TES. The pathogenesis of TES is not completely understood. Retrograde movement of endometrial cells into the peritoneum with subsequent implantation of cells on the lung, diaphragmatic, and pleural surface is the most widely held theory. Other hypotheses include coelomic metaplasia, lymphatic or hematogenous embolization [94]. The constellation of symptoms appears to be temporally related to menstruation and largely correlates with the anatomic location of endometrial cells. For example, presenting symptoms of pleural TES include catamenial pneumothorax, pleuritic chest pain, chest

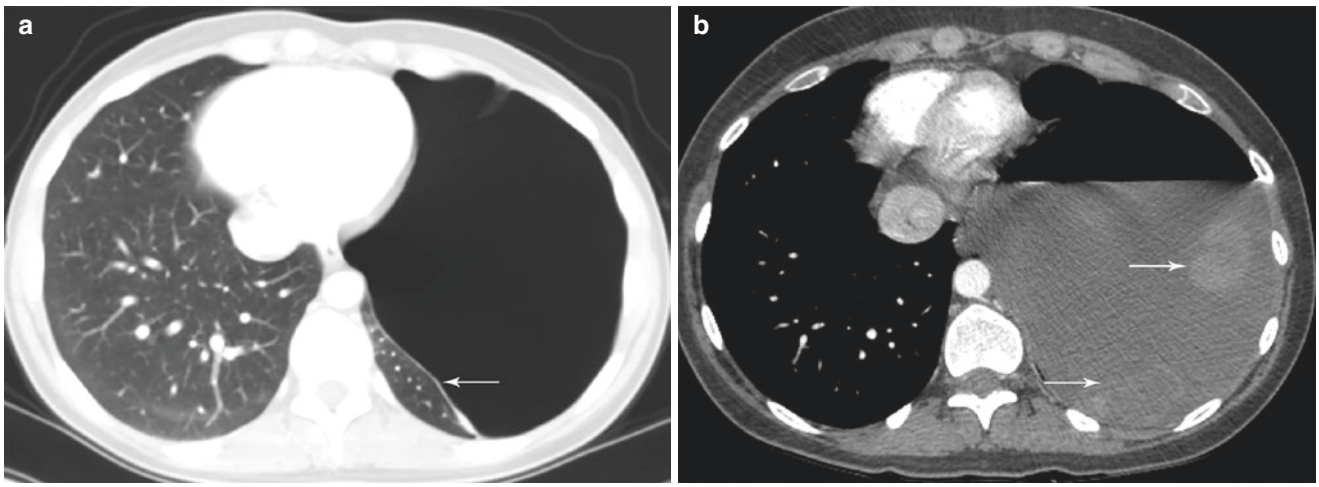


**Fig. 1.25** (**a**) Contrast-enhanced axial CT 7 years previously shows large left pneumothorax with mass effect compressing the left lung (arrow); (**b**) contrast-enhanced axial CT shows large left pleural effusion. The two foci of heterogeneous attenuation (arrows) within the left pleural effusion are consistent with blood clots

and shoulder pain, or referred pain to the periscapular region or neck. Signs and symptoms are predominantly right-sided, although rare cases of left-sided and bilateral disease have been reported [95]. Patients with catamenial pneumothorax or catamenial hemothorax typically present with cough, shortness of breath, and pleuritic chest pain within 48–72 h of the onset of menstruation, however, a temporal association with menstruation is not always recognized [91]. Thus, a high level of clinical suspicion is essential to ensure a timely diagnosis. TES should be considered in any ovulating woman with spontaneous pneumothorax or hemothorax.

Imaging findings are usually nonspecific but may be helpful to rule out other diagnoses and to map the endometrial lesions for surgery, if feasible. Chest radiographs may reveal pleural effusion, pneumothorax, or pleural nodules, but they are often normal [96]. Ultrasound of the chest may show echogenic nodules on the pleural surface with pleural effusion or hemothorax. On CT, small soft-tissue pleural nodules representing endometrial implants may be seen along with pneumothorax and hemothorax. These nodules tend to demonstrate homogeneous enhancement after administration of intravenous contrast. MR imaging is said to be more accurate than CT in the detection of pleural endometriosis. Similar to pelvic endometriosis, pleural endometriosis may show different signal intensities on T1 and T2 images, depending on the stage of the lesion. However, a pleural lesion exhibiting homogeneous high signal intensity on T1- and T2-weighted images is highly suggestive of pleural endometriosis. Thoracic CT or MR imaging in patients suspected of thoracic endometriosis should be performed during menstruation to maximize diagnostic sensitivity [96, 97]. Video-assisted thoracoscopy is the method of choice for direct demonstration of nodular or plaque-like endometrial deposits that are usually <1 cm in size. More than 60% of affected patients require thoracoscopy or thoracotomy as part of diagnostic evaluation of suspected thoracic endometriosis, and these procedures are frequently needed to establish the correct diagnosis [98].

Well-documented cases of either ectopic endometrial tissue, endometriomas, or endometriosis and deciduosis of the pleura and lung have been recorded in the literature [99–102]. In cases in which endometriosis presents as a pulmonary mass, the lesion may show cystic and hemorrhagic areas and measured up to 3 cm in size. Histologically, pleuropulmonary endometriosis is characterized by the presence of endometrial glands lined by cuboidal, columnar, or pseudostratified epithelium with round to oval nuclei and inconspicuous nucleoli, scant cytoplasm, which could be light eosinophilic or clear. Mitotic activity is present. The glandular proliferation is embedded in a fibrocollagenous stroma containing abundant inflammatory cells, mainly plasma cells (Fig. 1.26a–i). A proliferation of small arterioles may also be present. In some cases, the histological features are those of a prominent decidual reaction characterized by a light eosinophilic glassy stroma containing elongated cells with small nuclei and absent nucleoli (Fig. 1.27a–c).

By immunohistochemistry, the glandular proliferation may show positive staining for keratin, keratin 7, CEA, and Her-2neu, while the stromal cells will show positive staining for estrogen and progesterone receptors and WT-1 (Fig. 1.26g–i).

Chest tube drainage and hormonal therapies are the mainstay of treatments for catamenial pneumothorax and hemothorax. Surgical management of catamenial hemothorax, including video-assisted thoracoscopic surgery remains controversial. The indications for surgical resection are failure of hormonal therapy, intolerable adverse effects from medication, or symptom recurrence after cessation of medical treatment.

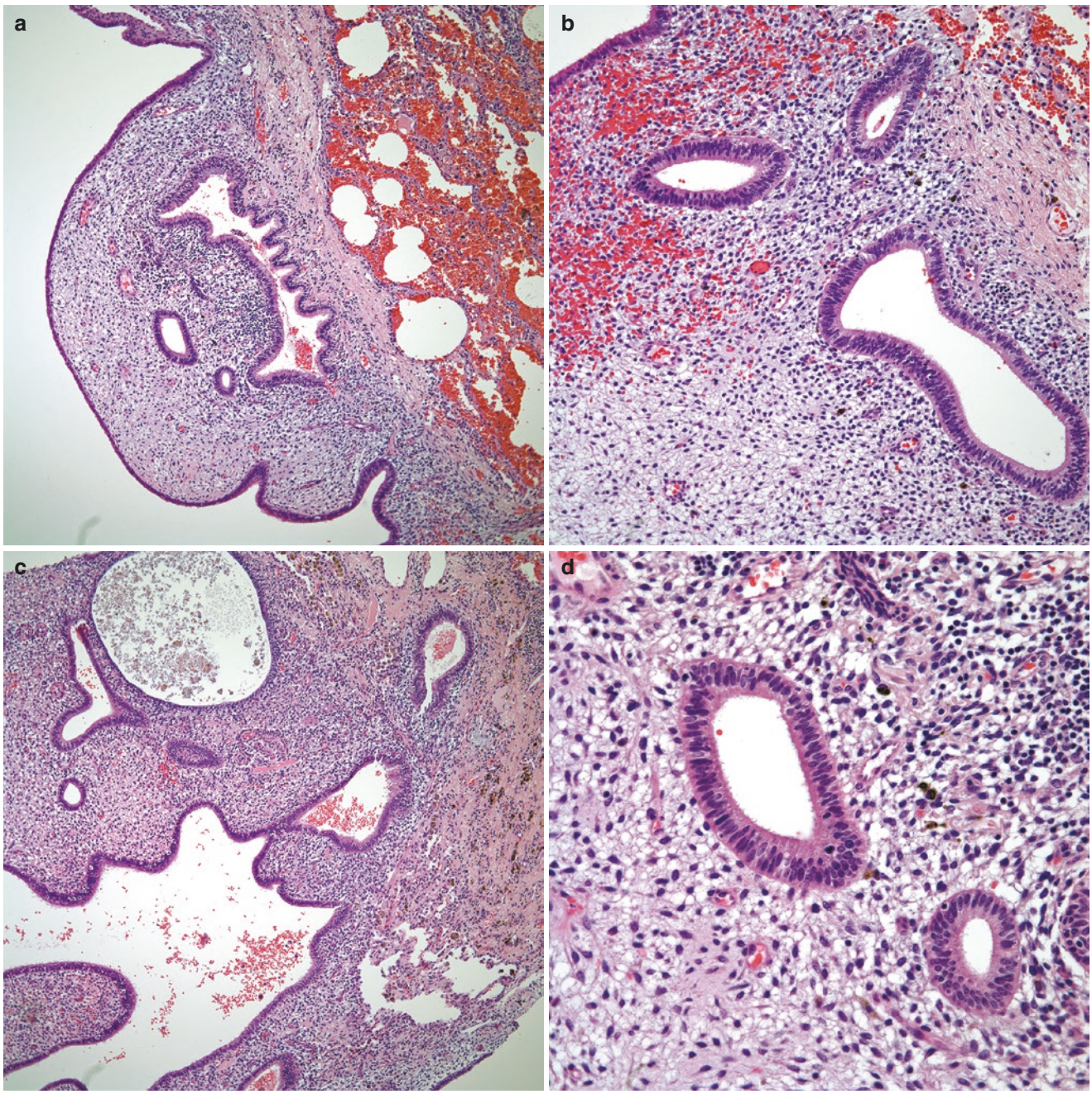


**Fig. 1.26** (**a**) Low power view of a pleural endometriosis. Note the presence of uninvolved lung parenchyma; (**b**) closer view of the glandular proliferation showing glands of different sizes; (**c**) pleural endometriosis with cystic changes; (**d**) endometriosis showing glands with mitotic activity; (**e**) glandular proliferation embedded in an edematous stroma with small vessels proliferation; (**f**) Pleural endometriosis showing elongated gland embedded in a cellular stroma; (**g**) immunohistochemical stain for estrogen receptor showing strong nuclear staining in stromal cells; (**h**) immunohistochemical stain for WT-1 showing strong nuclear staining in stromal cells; (**i**) immunohistochemical stain for keratin outlines the glandular epithelial component

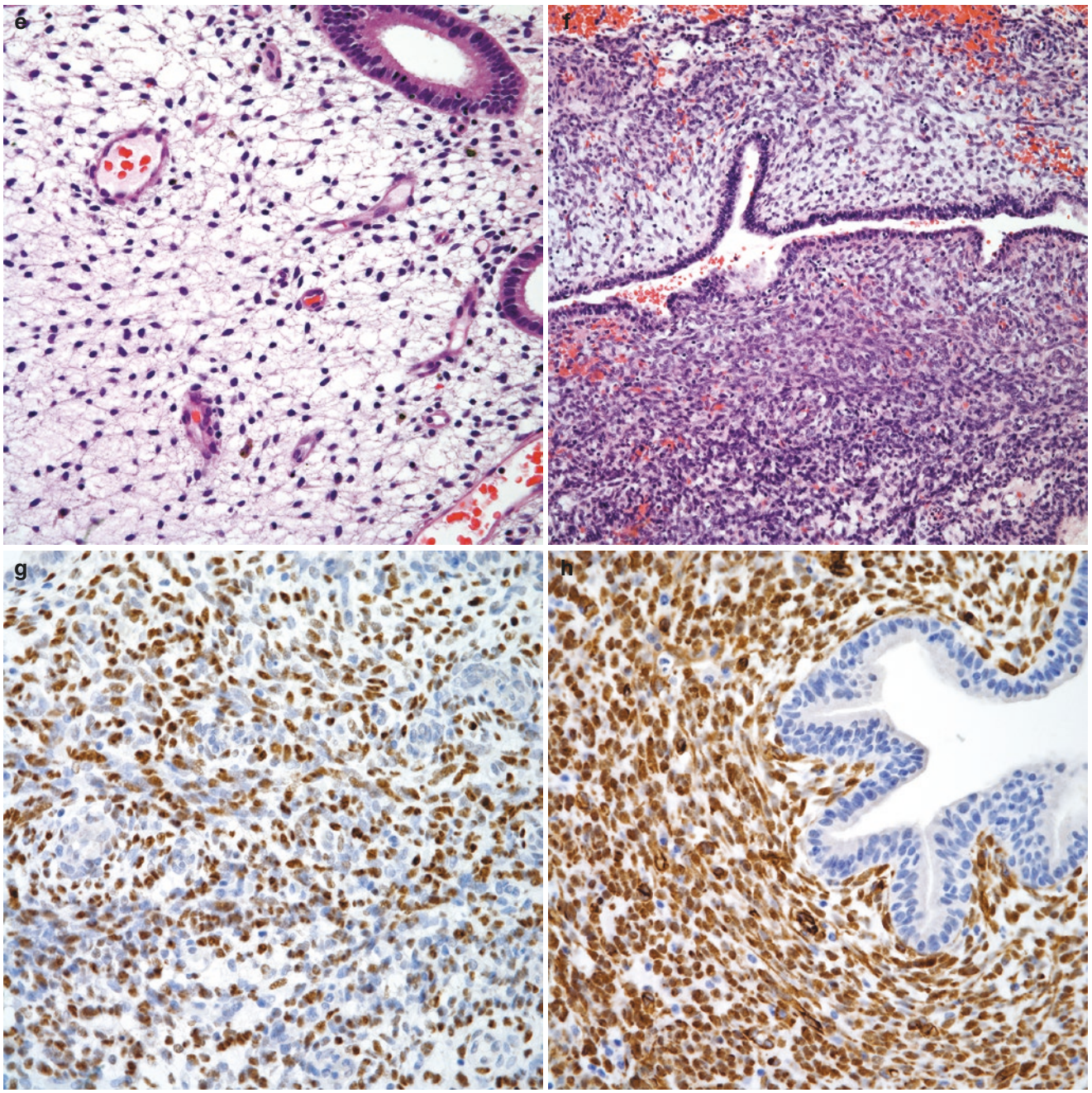


**Fig. 1.26** (continued)

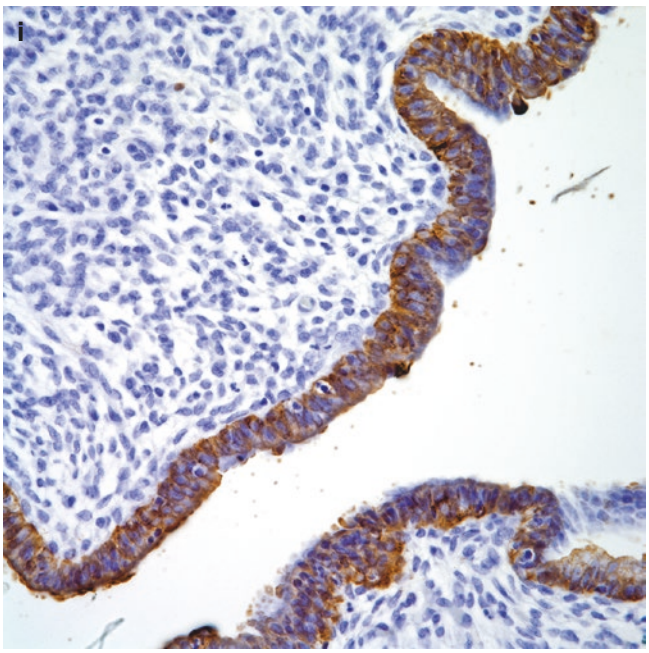


**Fig. 1.26** (continued)

### Adenomatoid Tumor

Adenomatoid tumors are benign solitary lesions of mesothelial origin. These rare tumors typically present as nonspecific nodules ranging from 0.5 to 2.5 cm on CT imaging and are most often found incidentally during surgery [103]. The tumors predominantly localize to the male and female genital tract. Extragenital presentations have been reported in the heart, adrenal glands, mesentery, lymph nodes, and pleura [104]. Adenomatoid tumors of the pleura may affect the visceral or parietal layers and mimic malignant pleural lesions [105]. The epidemiology and risk factors of these lesions are unknown. Correlation of the clinical, diagnostic imaging, and pathology findings leads to a correct diagnosis.

Adenomatoid tumors are usually small nodules ranging from 0.5 to 2.5 cm incidentally found during surgery [103]. Radiology is nonspecific and adenomatoid tumors present as a pleural nodule on chest radiograph or CT.

Histologically, the cellular proliferation is arranged in sheets or cords of medium size cells dissecting fibroconnective tissue. The cells are of medium size with eosinophilic cytoplasm, round to oval nuclei, and inconspicuous nucleoli. In some areas the cells may exhibit a signet-ring cell like appearance. Mitotic activity is not present and areas of necrosis and hemorrhage are generally absent (Fig. 1.28a–d). By immunohistochemistry [106] adenomatoid tumors may share similar immunophenotype as mesotheliomas. Both tumors may share positive staining for keratin, calretinin, and keratin 5/6. Also, both tumors show negative staining with carcinomatous epitopes including CEA, CD15, B72.3, and TTF-1. In addition, it is important to highlight that some mesotheliomas have also been described as having an "adenomatoid growth pattern" [106]. Thus, it is essential that the diagnosis of mesothelioma is correlated with the imaging. In difficult cases where the imaging is not available and the histology and immunohistochemistry is not definitive, molecular studies may be attempted, as adenomatoid tumors are negative for homozygous deletion using p16 FISH [107–115].

## Neoplastic

### Malignant Mesothelioma

Malignant mesothelioma (MM) is a neoplasm that arises from mesothelial cells lining body cavities, including the pleura, pericardium, peritoneum, and tunica vaginalis [116]. Malignant pleural mesothelioma (MPM) is the most common form, occurring in 70–90% of all malignant mesotheliomas. MPMs are most often attributable to asbestos exposure, however the relationship between asbestos and MPM varies greatly with gender, asbestos fiber type, occupation, and industry. The frequency of asbestos fiber subtypes varies with specific geographic and occupational environments. Mesothelioma risk is highest following exposure to the more harmful crocidolite asbestos fibers. However, chrysotile is more widely commercially used, and thus, accounts for the majority of cases of asbestos-induced mesothelioma. Occupational exposure to asbestos accounts for 85–90% of all MPMs in men in North America and Europe. By contrast, direct occupational exposure to asbestos accounts for only 40% of all female MPMs, which are more often attributed to para-occupational and domestic asbestos exposures as well as spontaneous causes [117]. Induction of MPM has also been reported following exposure to non-asbestos fibers, including fluoro-edenite and erionite [118–121]. Convincing evidence links the development of MPM to radiation exposure from multiple sources, including therapeutic thoracic radiation, radioactive thorium dioxide contrast medium (thorotrast), and atomic energy/nuclear industries [122–125]. An inherited predisposition for MPM has been recently linked to germline alterations in BRCA-associated protein 1 gene (BAP-1) expression [126].

The overall incidence of MPM is approximately 1 in 100,000 in the United States and 1–3 in 100,000 in the majority of European countries. Although a trend toward leveling off of the incidence of asbestos-related MPM has been noted in recent years in Western countries, in developing countries where restrictions on the industrial use of asbestos are much more relaxed, the incidence continues to climb. Due to the long latency period of approximately 20–40 years between asbestos exposure and disease, patients are typically older at presentation, with a median age of 63 years. The incidence of MPM is three to fourfold higher in men, reflecting the his-

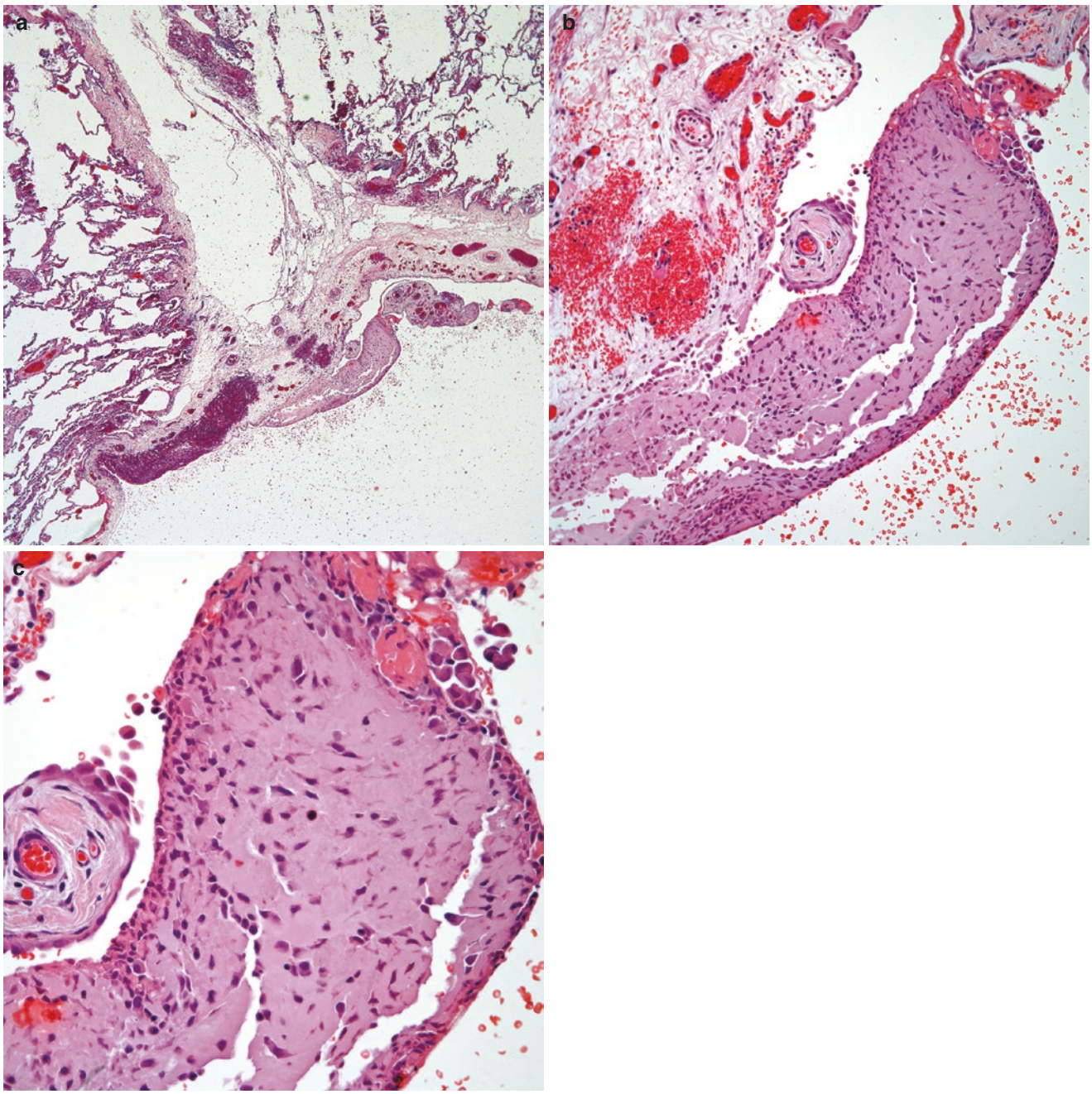


**Fig. 1.27** (**a**) Low power view of pleural deciduosis, note the presence of a pleural nodule; (**b**) small pleural nodule composed of decidualized cells; (**c**) higher magnification showing decidualized stroma and scant elongated cells without atypia or mitotic activity

torical male preponderance in at-risk occupations [127, 128]. Gradually, progressive symptoms of dyspnea, chest wall pain, and/or pleurisy herald the onset of disease [129, 130]. Most patients have a high burden of disease at the time of presentation due to late-onset symptom development. Occasionally, asymptomatic patients are diagnosed at an earlier stage on chest imaging performed for other purposes. The disease is typically confined to the ipsilateral pleura. However, patients may infrequently present with distant metastases to spleen, liver, thyroid, or brain [131].

A detailed occupational history coupled with imaging and tissue acquisition is the mainstay of the diagnostic workup. Plain chest radiography is not sufficiently sensitive for definitive diagnosis and staging, which requires computed tomography with contrast enhancement. PET/CT imaging may help to direct biopsies by identifying FDG-avid sites [132, 133]. Adequate tissue is essential for definitive histological analysis. Immunohistochemical investigations of tumor biomarkers can also be performed on tissue samples, which may help to distinguish malignant mesothelioma from other malignant

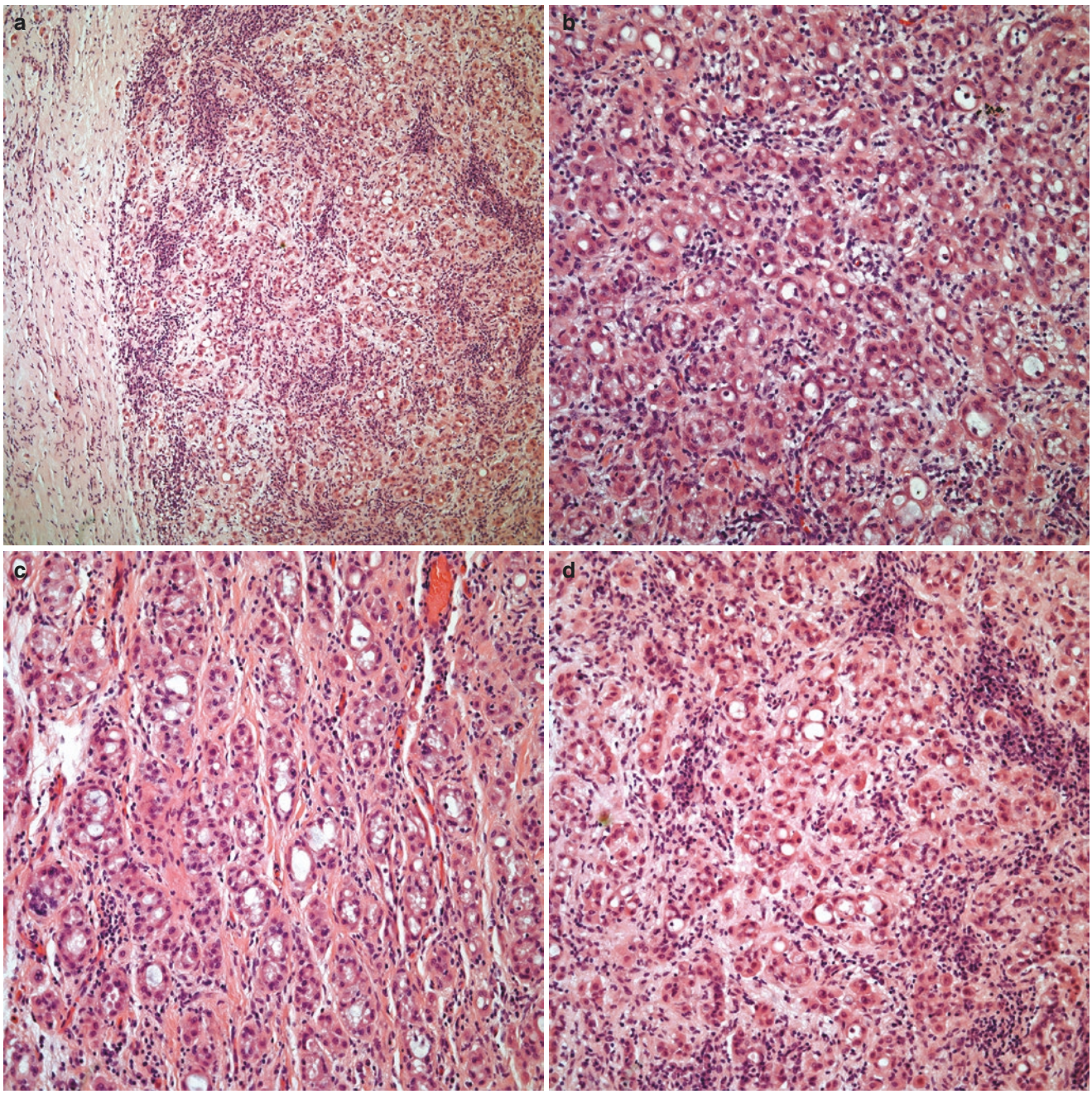


**Fig. 1.28** (**a**) Low power of an adenomatoid tumor of the pleura, (**b**) tumor cells forming small nests, (**c**) adenomatoid tumor showing cords of tumor cells, (**d**) adenomatoid tumor with areas of inflammatory reaction

processes, such as metastatic diseases to the pleura and from benign, reactive mesothelial proliferations. Tissue obtained from blind core needle biopsies is often insufficient to establish the diagnosis. Surgical biopsies obtained from thoracoscopy or video-assisted thoracic surgery (VATs) are preferred modalities for tissue acquisition. Disease stage according to the tumor-node-metastases (TNM) staging system has been validated by the International Mesothelioma Interest Group (IMIG). This staging system is an important MPM prognosticator and preferred system for mesothelioma staging [129, 134, 135].

Tumor stage and histology are the most important prognosticators, with advanced stage, sarcomatoid, and biphasic MPM histologies conferring a worse prognosis. In addition to tumor stage, male gender, poor performance status, older age, pure sarcomatoid histology, elevated white count above 15,000/μL, and platelet count greater than 400,000/μL are unfavorable prognostic factors [112–115]. These prognosticators have been incorporated into scoring systems which not only inform treatment outcomes, but also facilitate personalized management strategies [136, 137].

In untreated patients with advanced-stage disease, the overall prognosis remains poor with a median survival of 4–13 months. Surgery, radiation therapy, and systemic chemotherapy, given as a single therapeutic modality or in combination, have only shown marginal survival benefit (6–18 months) regardless of the therapeutic approach [110].

Treatment planning requires a multidisciplinary team of experts in medical oncology, radiation oncology, and surgery after histologic diagnosis, determination of histologic subtype and mediastinal staging have been established. Operative management, including extrapleural pneumonectomy (EPP) or pleurectomy with decortication (P/D) is reserved for patients with good performance status, no medical contraindications to surgery, and anatomically resectable tumors. EPP entails en bloc resection of the ipsilateral visceral and parietal pleurae, pericardium, lung, and diaphragm. P/D only involves parietal and visceral pleurectomy, sparing resection of the diaphragmatic muscle and lungs. Although no randomized trials exist, P/D has been associated with less perioperative morbidity and mortality, with a comparable overall survival to EPP in retrospective analyses [138]. The goals of surgery are to achieve macroscopic complete resection (MCR) with curative intent in selected patients or palliative surgical cytoreduction in others when MCR is not deemed to be feasible [111]. Significant differences in overall survival rates have been demonstrated among patients undergoing surgery for curative versus palliative intent (median survival 18 versus 12 months) and with treatment plans that included curative-intent surgery combined with nonsurgical modalities such as chemotherapy, radiation therapy, or both (median survival 20 versus 11 months) [111, 139].

Nonsurgical candidates may be eligible for symptom-directed therapy and/or chemotherapy. Standard chemotherapy is typically given as a platinum-based doublet plus pemetrexed with or without a vascular endothelial growth factor (VEGF) inhibitor. Chemotherapy may be given in the neoadjuvant setting or following definitive surgery. Knowledge that the tumor microenvironment in MPM may be modulated to promote antitumor response has fueled ongoing investigations of immunotherapy as a component of multimodality therapy for MPM [110, 114, 140]. Dyspnea and pain associated with tumor burden or large pleural effusions are common sequelae of MPM. Thoracentesis as an initial approach may provide significant symptom palliation; however, these effusions are often rapidly recurrent and require more definitive strategies, such as placement of a tunneled intrapleural catheter or attempted pleurodesis. The latter requires complete drainage of the pleural effusion by tube thoracostomy or video thoracoscopy. If lung reexpansion is confirmed, an intrapleural sclerosing agent (most commonly asbestos-free talc) may be administered, which is either insufflated as a powder or instilled via chest tube as a slurry [141, 142]. The presence of a thick pleural rind or bulky tumor in the pleural space may limit lung reexpansion, thereby precluding successful pleurodesis. MPM has a tendency to travel along biopsy and catheter tracts [143]. Considerations for radiation to the chest wall to prevent tumor seeding at the site of instrumentation (chest drains, thoracoscopy, video-assisted thoracoscopic surgery biopsies, and open surgical biopsies) are a source of considerable controversy and generally not recommended. This guideline is based on a summation of data that suggested no significant difference with or without prophylactic radiation [144–147].

### Radiography

Chest radiographs are often the initial imaging modality to suggest MPM. Unilateral pleural effusions are the most common finding, seen in 30–80% of patients. Pleural thickening is seen in 60% of patients followed by pleural masses in 45–60% [148]. Intrathoracic adenopathy is suggested by abnormal mediastinal or hilar contours and abnormal thickening of lines and stripes. Foci of calcification or ossification can be seen if there is cartilaginous or osseous differentiation. Finally, if there is encasement of the lung and/or invasion of the chest wall, radiographs may demonstrate hemithorax volume loss, elevation of the diaphragm, narrowing of intercostal spaces, and ipsilateral mediastinal shift [149].

### Computed Tomography

Tumor characteristics, such as extent of the primary tumor, presence of intrathoracic adenopathy, local invasion of the mediastinum, diaphragm or chest wall, and the presence of extrathoracic spread can be discerned with chest computed tomography CT), which is the imaging modality of choice for the evaluation of MPM. Unilateral pleural effusions (74%) and nodular pleural thickening (92%) are the most common CT findings in MPM (Figs. 1.29 and 1.30a, b)

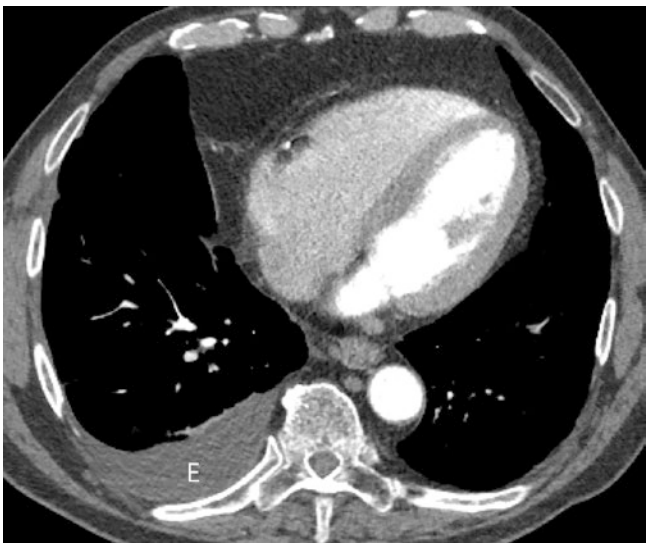


**Fig. 1.29** Contrast-enhanced axial CT, which demonstrates a small right pleural effusion (E), a common presenting finding in malignant pleural mesothelioma

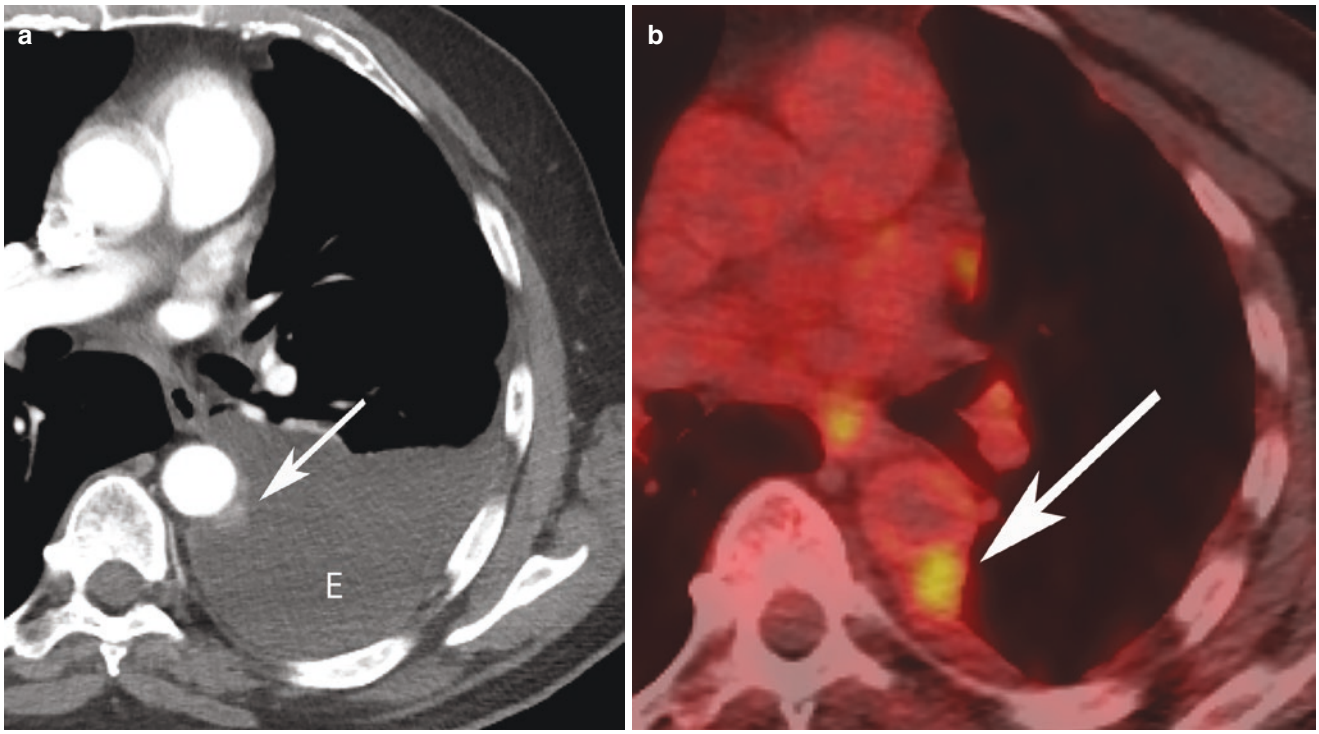


**Fig. 1.30** (**a**) Contrast-enhanced axial CT demonstrates a moderate left pleural effusion (E) with a small area of nodular pleural thickening (arrow) adjacent to the descending thoracic aorta; (**b**) axial FDG-PET/CT performed after thoracentesis demonstrates increased FDG uptake in the pleural nodule (arrow)

[150]. In particular, when the pleura is greater than 1 cm in thickness, nodular, and circumferential, MPM should be considered [151]. Classically, MPM demonstrates circumferential nodular pleural thickening, which encases the lung, creating the often described "rind-like" appearance with extension along the diaphragmatic surface and into the fissures (Fig. 1.31a, b) [135]. Although calcification is unusual, punctate or large calcifications can be seen in the setting of cartilaginous or osseous differentiation. This is to be distinguished from more linear areas of calcification that are commonly associated with benign pleural plaques in the setting of benign asbestos-related pleural disease [152].

CT is often adequate to determine areas of local tumor invasion in MPM, which commonly include the chest wall, mediastinum, pericardium, and the diaphragm (Fig. 1.32a, b). Chest wall invasion manifests as loss of the normal extrapleural fat plane, invasion of intercostal muscles, rib displacement, and osseous destructive changes. Mediastinal involvement is suggested when normal fat and tissue planes are lost and the trachea or esophagus is encased by more than 50% [153]. Pericardial invasion can result in pericardial effusion, pericardial thickening, and pericardial nodularity or masses. While difficult to differentiate, pericardial involvement can be transmural or nontransmural. The preservation of epicardial fat suggests nontransmural involvement while tumor extension to the inner surface of the pericardium or into the myocardium suggests transmural invasion. Similarly, evaluation of transdiaphragmatic extension with CT is difficult. Generally, if a fat plane is preserved between the undersurface of the diaphragm and the adjacent abdominal organ, disease confined to the thoracic cavity is considered [149]. Laparoscopy and peritoneal lavage are used to evaluate for peritoneal spread and can identify implants along the undersurface of the diaphragm and in the peritoneal cavity that are undetected on imaging [143].

CT is the primary imaging method to evaluate intrathoracic nodal involvement. CT with intravenous contrast administration can detect enlarged thoracic lymph nodes. Mediastinal (subcarinal, paraesophageal, and paraaortic) and hilar nodes are considered abnormal with a short axis CT measurement of 1 cm or larger. While internal mammary chain, extrapleural, and retrocrural lymph nodes have no set upper limit size criteria, their presence is generally considered abnormal. Knowledge of lymphatic drainage patterns of diseases involving the diaphragm and pleura are helpful in the detection of nodal metastases. The anterior and lateral diaphragms are drained by the internal mammary chain and anterior peridiaphragmatic nodes while the posterior diaphragm is drained by the paraaortic and posterior mediastinal nodes. The visceral pleural lymphatics follow the same drainage pattern as the lungs. The parietal pleural lymphatic drainage system is different. The anterior parietal pleura is drained by the internal mammary chain and peridiaphragmatic nodes while the posterior parietal pleura is drained by the extrapleural/intercostal lymph nodes. The anterior and lateral chest wall is drained by

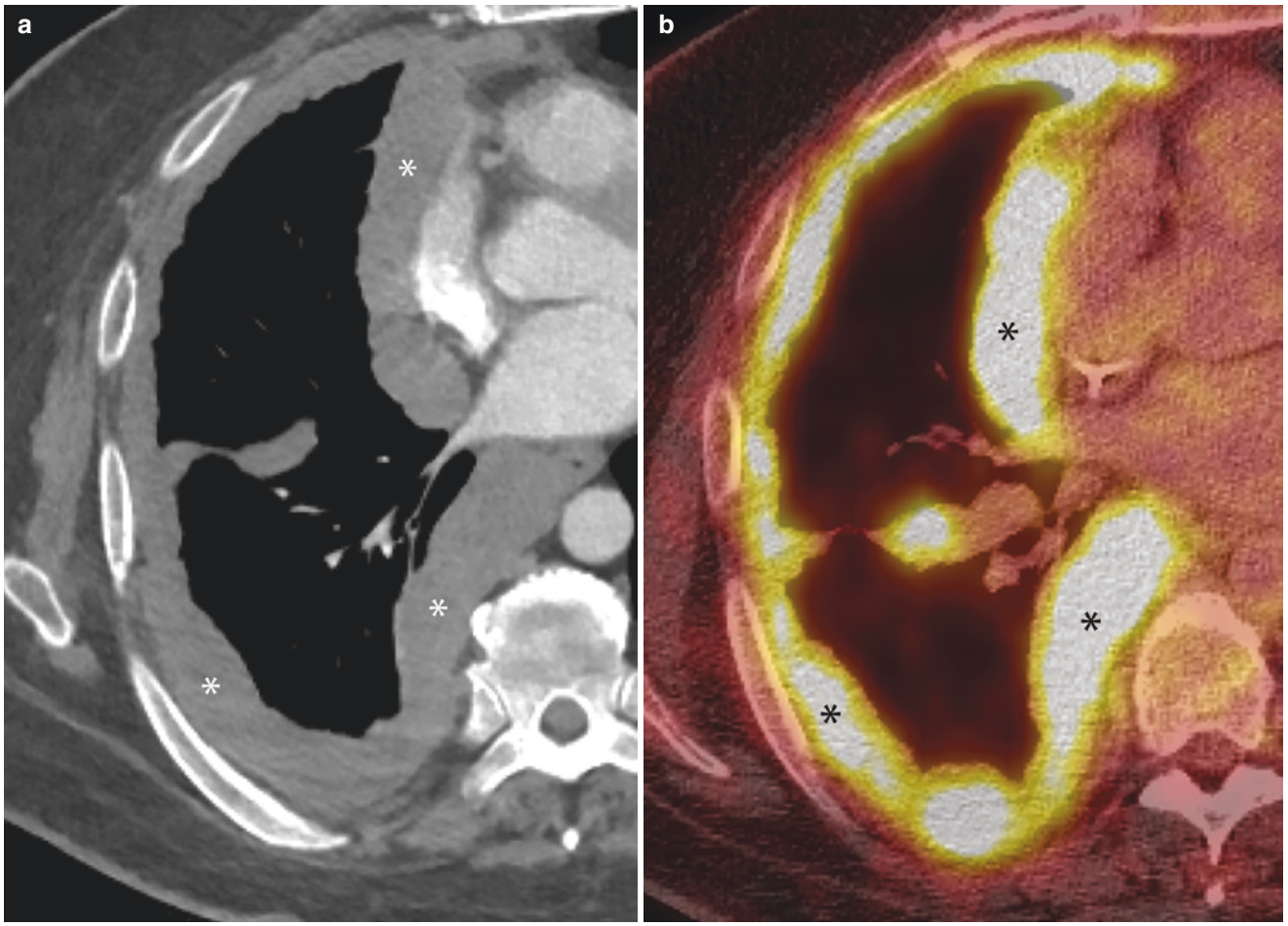


**Fig. 1.31** (**a**) Contrast-enhanced axial CT demonstrates circumferential "rind-like" pleural thickening and nodularity (*) in the right hemithorax, (**b**) axial FDG PET/CT shows increased FDG uptake (*) in the right circumferential nodular pleural thickening consistent with malignant pleural mesothelioma

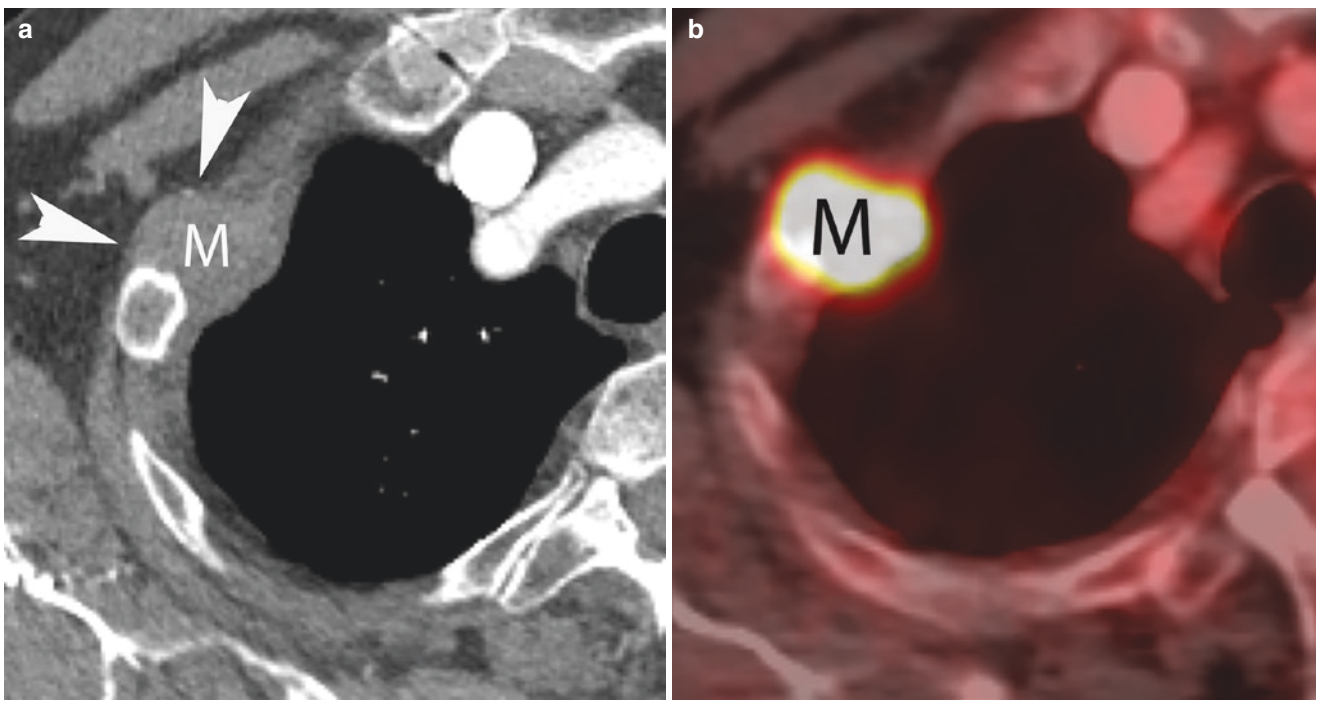


**Fig. 1.32** (**a**) Contrast-enhanced axial CT demonstrates a pleural mass (M) in the right upper thorax invading the chest wall (arrowheads), (**b**) Axial FDG PET/CT shows marked FDG uptake on PET/CT

the anterior or pectoral nodes, while the posterior chest wall is drained by the axillary nodes [154, 155].

Finally, CT often will demonstrate intrathoracic and extrathoracic metastatic disease such as ipsilateral or contralateral pulmonary nodules and masses, lymphangitic spread of tumor, and distant metastatic sites including solid organs and osseous structures.

### Magnetic Resonance Imaging

CT is generally adequate for evaluation of local invasion, lymphadenopathy, and metastatic disease; however, in certain situations, MRI adds value. MRI is superior to CT for the detection of chest wall, mediastinal, and diaphragmatic invasion, particularly when post contrast T1 sequences with fat suppression are utilized.

Additional advantages of MRI exist. MRI avoids the use of ionizing radiation. Given the superior soft tissue contrast of MRI as compared to CT, nonenhanced studies can well demonstrate pleural pathology in patients who cannot tolerate intravenous contrast due to allergy or diminished renal function. MRI has been shown to be superior to CT for the evaluation of pleural fluid using T2-weighted imaging sequences [156]. MRI shows better interobserver agreement in assessing pleural effusion and pleural thickening in MPM [157]. Tumor neovascularization has been documented in MPM. Parametric images based on dynamic contrast-enhanced MRI demonstrate not only the extent of pleural lesions but also the heterogeneity of tumoral vascularization. It is suggested that pharmacokinetic parameters of pleural enhancement may predict therapeutic response [158]. Finally, there are certain clinical scenarios where the greater contrast and spatial resolution of MRI can more precisely detect early invasion of the endothoracic fascia, chest wall (Fig. 1.33) mediastinum, pericardium, and diaphragm, which aids in determining surgical resectability.

On MRI, MPM can present as a unilateral pleural effusion that is hyperintense on T2-weighted images with mixed signal intensity seen in more complex or hemorrhagic effusions. Areas of pleural thickening and nodularity are typically isointense to mildly hyperintense compared to adjacent muscle on T1-weighted images and moderately hyperintense compared to muscle on T2-weighted images [149]. Areas of pleural nodularity and thickening demonstrate heterogeneous to avid enhancement after the administration of gadolinium-based contrast agents.

There are additional roles for MRI beyond anatomic imaging. MRI studies have shown that the apparent diffusion coefficient (ADC) of epithelioid subtype of MPM is higher than the ADC of the sarcomatoid subtype, suggesting that MRI can be used as a surrogate biomarker for MPM [159]. Another study has described a new sign in diffusion-weighted imaging called "pleural pointillism" that is potentially useful in diagnosis and guidance for pleural biopsies [160].

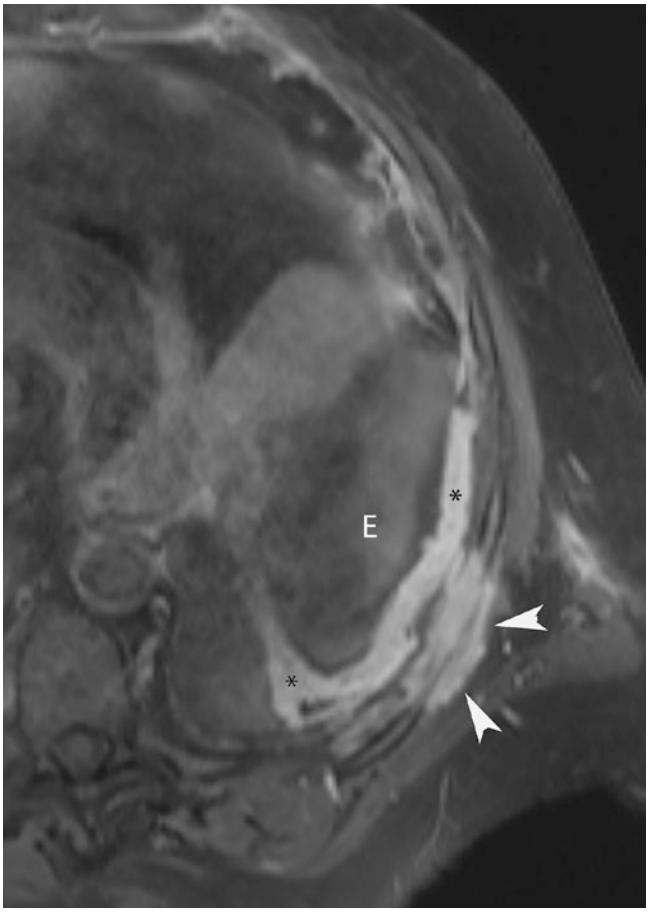


**Fig. 1.33** Contrast-enhanced axial T1 fat saturation MRI image with nodular enhancing pleural thickening (*) and a malignant pleural effusion (E). Areas of abnormal enhancing soft tissue extend into the chest wall (arrowheads) consistent with chest wall invasion of malignant pleural mesothelioma. MRI is superior to CT in the evaluation of chest wall invasion

### PET/CT

FDG PET/CT plays an important role in the diagnosis and staging of MPM because it combines the metabolic information obtained by the uptake of the radiopharmaceutical F-18 fluorodeoxyglucose with the anatomic information provided by CT. FDG uptake, as measured by the standardized uptake value (SUV), can help distinguish between common benign pleural thickening and MPM. As expected, FDG uptake in MPM is significantly higher than benign pleural disease [161]. Pleural thickening, pleural nodularity, malignant pleural effusions, malignant lymphadenopathy, and metastasis associated with MPM demonstrate markedly elevated SUV. FDG PET/CT can often better demonstrate more subtle malignant intrathoracic and extrathoracic lymphadenopathy as well as metastatic disease compared to CT and other imaging modalities (Fig. 1.34). Overall, PET/CT is the modality of choice to detect occult metastasis when other imaging modalities are negative.

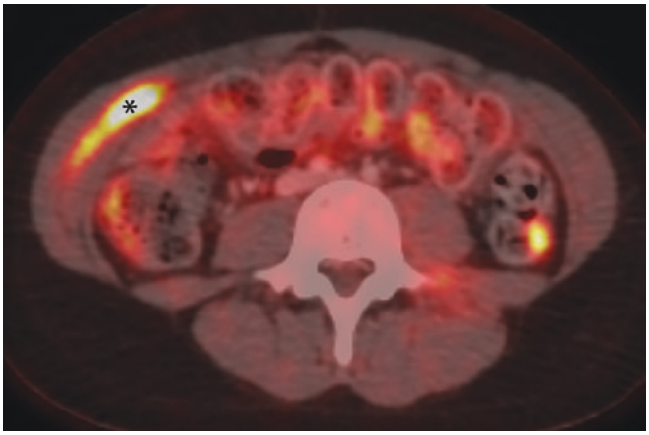

**Fig. 1.34** Axial image from a staging FDG PET/CT demonstrates focal increased FDG uptake in the right rectus abdominis musculature (*) consistent with a soft tissue metastasis from malignant pleural mesothelioma. This metastatic lesion was not detected on CT, demonstrating the strength of PET/CT in the detection of distant metastasis in the staging of MPM

There are additional benefits of PET/CT compared to CT and MRI. PET/CT has been shown to be more accurate than CT, MRI, and PET alone in the staging of MPM. For stage II and III disease, PET/CT accuracy is 1.0, compared with 0.77 in stage II and 0.75 in stage III for CT and 0.86 in stage II and 0.83 in stage III for MRI [162].

PET/CT can be used for image-guided and surgical biopsy planning by helping to target the most metabolically active and most anatomically accessible locations for tumor sampling. Additionally, the degree of FDG uptake, as measured by SUV, has been associated with time to tumor progression and survival. Finally, the metabolic information provided by PET/CT is beneficial in evaluating response to treatment and detection of recurrent disease.

### Ultrasound

While the role of ultrasound in the anatomic evaluation of MPM is limited due to technical difficulties related to artifact from the ribs, it can be used in the setting of image-guided thoracentesis for cytological evaluation as well as for image-guided biopsies of the pleura.

### Limitations of Routine Imaging

There are several limitations when imaging MPM. Given the unusual growth pattern of MPM along the pleural and fissural surfaces, determining the longest measurement of the tumor is often quite difficult for all imaging modalities. CT is particularly limited given the pleural tumor, chest wall musculature, and associated complex pleural fluid collections often have very similar attenuation coefficients, precluding differentiation and delineation of the tumor. Other limitations of CT are the use of ionizing radiation and the necessity of intravenous contrast agents, which are problematic in patients with iodinated contrast allergies and diminished renal function. Limitations to MRI generally relate to cost, availability, and long scan times. Limitations of PET/CT are most notable when patients have had prior pleurodesis as this can result in false positive pleural findings. While some of these issues can be partially overcome, it remains that clinical or radiologic staging often does not accurately predict pathologic stage or prognosis [163]. In regard to these limitations, there is well-documented high interobserver variability [129].

### Therapy Response Assessment

There has been a steady evolution of the criteria for evaluating response to therapy in MPM over the last two decades. The original Response Evaluation Criteria in Solid Tumors (RECIST) guidelines were released in 2000 [164]. Up to ten total lesions, with no more than five in a single organ, were measured in longest unidimensional diameter in the original RECIST criteria. It was soon recognized, however, that these criteria were not suitable in MPM due to the parietal growth pattern of ill-defined pleural thickening and the absence of a well circumscribed measurable mass [165]. This led to the advent of the modified RECIST (mRECIST) criteria that were specifically formulated for MPM [135]. In the mRECIST, tumor thickness perpendicular to the chest wall is utilized instead of the longest unidimensional diameter as this is difficult to measure and reproduce in MPM. These perpendicular measurements are obtained in two positions at three separate levels with the sum of these six measurements defining the pleural unidimensional measurements. In 2009 RECIST was updated to version 1.1 with the revised modified RECIST (mRECIST 1.1) for MPM following in 2018 [166]. RECIST 1.1 decreased the total number of summed lesions to five, with no more than two per organ and added lymph nodes into the measurements. Since growth patterns of MPM limit evaluation of distinct single anatomic lesions, the mRECIST 1.1 focuses on selecting specific measurable sites that can be reliably and reproducibly measured irrespective of how many distinct anatomic lesions these measurement sites represent. The mRECIST 1.1 additionally defines numerous technical issues about measurable disease, including which lesions are measurable, measurement sites, non-pleural disease, measurable lymph nodes, and accommodation for bilateral pleural disease [167]. The mRECIST 1.1 is used to determine complete response (the disappearance of all pleural and non-pleural disease), partial response (decrease of at least 30% in summed measurements), progressive disease (increase of at least 20% in summed measurements), or stable disease (between partial response and progression of disease) [167].

## Volumetric and Future Imaging of MPM

In view of these limitations, there has been greater focus on new imaging paradigms in MPM. In particular, the focus has been on quantitative tumor measurements, most notably tumor volume analysis. As early as 1998, Pass et al. demonstrated correlation of MPM tumor volume manually derived from CT with T stage, N stage, prognosis, and time to recurrence [168]. Over the next several years, numerous studies evaluated different aspects of MPM tumor volume analysis. In 2011, Frauenfelder et al. found that tumor volume more reliably measured response to chemotherapy than RECIST [169]. In the largest single center study to date in 2012, Gill et al. reported that preoperative tumor volumes were related to survival and went so far as to recommend tumor volume analysis in patients undergoing extrapleural pneumonectomy [170]. A follow-up prospective multicenter feasibility study by Gill et al. in 2016 again demonstrated that tumor volume analysis in MPM correlated with T stage, N stage, and survival and, due to improvements in segmentation software was technically feasible in routine practice [171]. In addition to CT-derived tumor volumes, PET/CT can be used to calculate the volume of metabolically active tumor, which has also been strongly associated with survival [172, 173]. Taken together, tumor volume analysis in MPM has been shown to be superior to TNM, RECIST, and mRECIST for staging and assessment of therapy response and is now technically feasible with available software programs.

## Staging

The 8th edition of the Tumor, Node, Metastasis staging classification (TNM 8), the most recent staging guidelines for MPM, was released in 2018, with only minor changes from the 7th edition (Tables 1.2 and 1.3) [174]. Because of the unconventional growth pattern of MPM along pleural and fissural surfaces, assessment of tumor size is difficult and is not part of the staging classification. MPM generally presents as pleural nodules that coalesce rather than the more conventional concentrically enlarging tumor. The tumor (T) descriptor is, therefore, based on location and degree of invasion, not on tumor size. It should be noted, however, that the gold standard for evaluation of invasion is pathologic, not radiologic. The most recent TNM classification for MPM is given below:

T descriptors: progressive degrees of soft tissue invasion:

- T1 tumors involve the ipsilateral parietal pleura (including mediastinal and diaphragmatic) with or without involvement of the visceral pleura.
- T2 tumors involve each of the ipsilateral pleura (parietal, mediastinal, diaphragmatic, and visceral) with involvement of at least one of the following: confluent

**Table 1.2** TNM 8th edition staging system for malignant pleural mesothelioma

| |
|---|
| *T—Primary tumor* |
| T1 |
| Tumor involving ipsilateral parietal pleura (including mediastinal and diaphragmatic pleura) with or without involvement of visceral pleura |
| T2 |
| Tumor involving each ipsilateral pleural surfaces (parietal, mediastinal, diaphragmatic, and visceral pleura) with at least one of the following features: |
| • Involvement of diaphragmatic muscle |
| • Confluent visceral pleural tumor (including fissures) |
| • Invasion of lung parenchyma |
| T3 |
| Tumor involving all of ipsilateral pleural surfaces with at least one of the following: |
| • Invasion of endothoracic fascia |
| • Extension into mediastinal fat |
| • Solitary, completely resectable focus invading soft tissues of chest wall |
| • Nontransmural involvement of pericardium |
| T4 |
| Tumor involving all of ipsilateral pleural surfaces with at least one of the following: |
| • Diffuse or multifocal invasion of soft tissues of the chest wall |
| • Any rib involvement |
| • Invasion of the peritoneum through the diaphragm |
| • Direct extension to contralateral pleura |
| • Invasion of any mediastinal organ |
| • Invasion of spine or brachial plexus |
| • Transmural invasion of pericardium (with or without pericardial effusion), or myocardium invasion |
| *N—Lymph nodes* |
| NX regional lymph nodes not assessable |
| N0 no regional lymph node metastases |
| N1 metastases in ipsilateral bronchopulmonary or hilar or mediastinal lymph nodes (including internal mammary, peridiaphragmatic, pericardial, or intercostal lymph nodes) |
| N2 metastases in contralateral bronchopulmonary, hilar, or mediastinal lymph nodes, or ipsilateral or contralateral supraclavicular lymph nodes |
| *M—Metastases* |
| MX distant metastases not assessable |
| M0 no distant metastases |
| M1 evidence of distant metastases |

**Table 1.3** Stage grouping of malignant pleural mesothelioma by TNM 8th edition

| Stage | Description |
|---|---|
| 1A | T1 N0 M0 |
| | T2–T3 N0 M0 |
| II | T1–T2 N1 M0 |
| IIIA | T3 N1 M0 |
| IIIB | T1–T3 N2 M0 |
| | T4 N0–N2 M0 |
| IV | Any T any N M1 |

visceral tumor including fissures, involvement of the diaphragmatic muscle, or invasion of the lung parenchyma.
- T3 tumors involve all of the ipsilateral pleural surfaces with at least one of the following: invasion of the endothoracic fascia, extension into the mediastinal fat, solitary resectable focus of invasion in the chest wall, or nontransmural involvement of the pericardium.
- T4 tumors involve all of the ipsilateral pleural surfaces with at least one of the following: diffuse or multifocal invasion of soft tissues of the chest wall, any rib involvement, invasion of the peritoneum through the diaphragm, invasion of any mediastinal organ, direct extension to the contralateral pleura, invasion of the spine or brachial plexus, or transmural pericardium (with or without pericardial effusion) or myocardial involvement.

N descriptor: Nodal metastases

- N1 nodes include ipsilateral bronchopulmonary, hilar, or mediastinal lymph nodes as well as internal mammary, peridiaphragmatic, pericardial, or intercostal lymph nodes.
- N2 nodes include contralateral bronchopulmonary, hilar, or mediastinal nodes as well as ipsilateral or contralateral supraclavicular nodes.

M descriptor: metastatic disease

- M0 denotes the absence of metastatic disease.
- M1 signifies distant metastasis.

### Pathological Features

Evaluation of pleural tissue is essential for the diagnosis of mesothelioma, the sample of a few millimeters of tissue may not show the entire growth pattern that one can observe in resected specimens, mainly those obtained by extrapleural pneumonectomy (EPP). In a review of 56 cases treated by EPP, Arrossi et al. correlated the histopathologic classification of the initial biopsy and the EPP [175]. The authors identified that there is significant disagreement between those two modalities that can be as high as 45%. Therefore, even though it is highly important to obtain tissue for final diagnosis, the histological classification of these tumors may vary depending on the available material. In addition, mesothelioma is one of the tumors, which historically has undergone extensive scrutiny by different means, ranging from morphology, histochemistry, electron microscopy, immunohistochemistry, and currently molecular analysis [176]. Therefore, we consider that the appropriate approach to the diagnosis of mesothelioma requires strict global interpretation of clinical-radiological-pathological features, which can be summarized as follows:

- *Clinical information*—Mainly that of asbestos exposure, or other more relevant clinical information that can be correlated.
- *Radiological information*—As has been stated above.
- *Tissue interpretation*—Preferably a biopsy that contains points of references such as the presence of adipose tissue or skeletal muscle.
  - Histopathological interpretation.
  - Immunohistochemical phenotype.
  - Molecular analysis—(if needed).

#### Macroscopic Features

EPP as a surgical option in cases of mesothelioma has provided a wealth of knowledge regarding the different histopathological growth patterns that can be seen in these tumors. More importantly, it provides information in terms of the extent of disease as one can macroscopically determine the extent of pleural involvement, pleural thickening, diaphragmatic, pericardial, or pulmonary invasion. In essence, EPP constitutes a pneumonectomy specimen containing parietal and visceral pleura, pericardium, and diaphragm, as well as hilar lymph nodes. The depiction of an EPP is presented in Fig. 1.35a–e. However, it is also important to highlight that even though the vast majority of mesotheliomas involved the pleura in a diffuse manner, cases of "localized" mesotheliomas have been presented in the literature [177].

#### Microscopic Features

Even though mesotheliomas have been traditionally separated in three different categories—Epitheioid, Sarcomatoid, and Bipahsic (epethilioid/sarcomatoid), the wealth of different histological growth patterns that can be seen in mesotheliomas is extensive. However, before addressing the different growth pattern of mesothelioma, it is important to start with the concept of "malignant mesothelioma in situ."

## Malignant Mesothelioma In Situ

The concept of mesothelioma in situ dates back a couple of decades ago. In 1998, Henderson et al. reviewed more than 1500 cases of mesothelioma from different institutions in Australia and outline criteria for the distinction between reactive hyperplasia and malignant mesothelioma including the in situ tumor [84]. However, it is important to note that such presentation was done at the time in which immunohistochemistry was not as developed as it is today and also

the molecular diagnosis on mesothelioma were not available. Nevertheless, several important parameters were presented as criteria in the diagnosis of *mesothelioma* in situ.

- Mesothelioma in situ should be considered only when unequivocal invasion is identified.
- The diagnosis of pure mesothelioma in situ should not be made in patients not exposed to asbestos.

Even though the concept had been presented in the literature, in practice the concept became more an academic exercise due to the criteria exposed. In 2018, Churg et al. alluding to the "lack" of morphological criteria for the diagnosis of in situ mesothelioma, presented two cases that the authors conceptualized as "true" in situ mesotheliomas [178]. In one patient the biopsy was from the pleura while in the second patient the biopsy was from the peritoneum. In both cases BRCA-1 associated protein 1 (BAP1) was lost (negative nuclear staining by immunohistochemistry) while CDKN2A (p16) FISH analysis showed homozygous deletion in 3.8% of cells in one case and 10% in the second case. Based on those results, the authors concluded that the cases presented correspond to mesothelioma in situ. More recently, Churg et al. presented a study of ten cases (nine pleural and one peritoneal) in which the authors further stated the concept of mesothelioma in situ by showing biopsies in which the surface mesothelial lining was composed of a single layer of cells with loss of BAP1 (negative nuclear staining by immunohistochemistry) [87]. Interestingly CDKN2A was deleted in only one of eight cases analyzed. In addition, seven patients developed invasive mesothelioma in a period of time ranging from 12 to 92 months while in three other patients invasive disease had not developed after 12, 57, and 120 months. The authors further recommended performing BAP1 on any case with history of recurrent effusions, regardless of the histological features of the surface mesothelium. Essentially, based on those studies, the diagnosis of mesothelioma in situ has been relegated to the use of BAP1 (negative nuclear staining) by immunohistochemistry in the context of the clinical setting.

## Invasive Malignant Mesothelioma

Different studies of mesotheliomas have provided important information not only from the morphological aspects of the tumor but also from the immunohistochemical profiles that these tumors may show. Often the studies

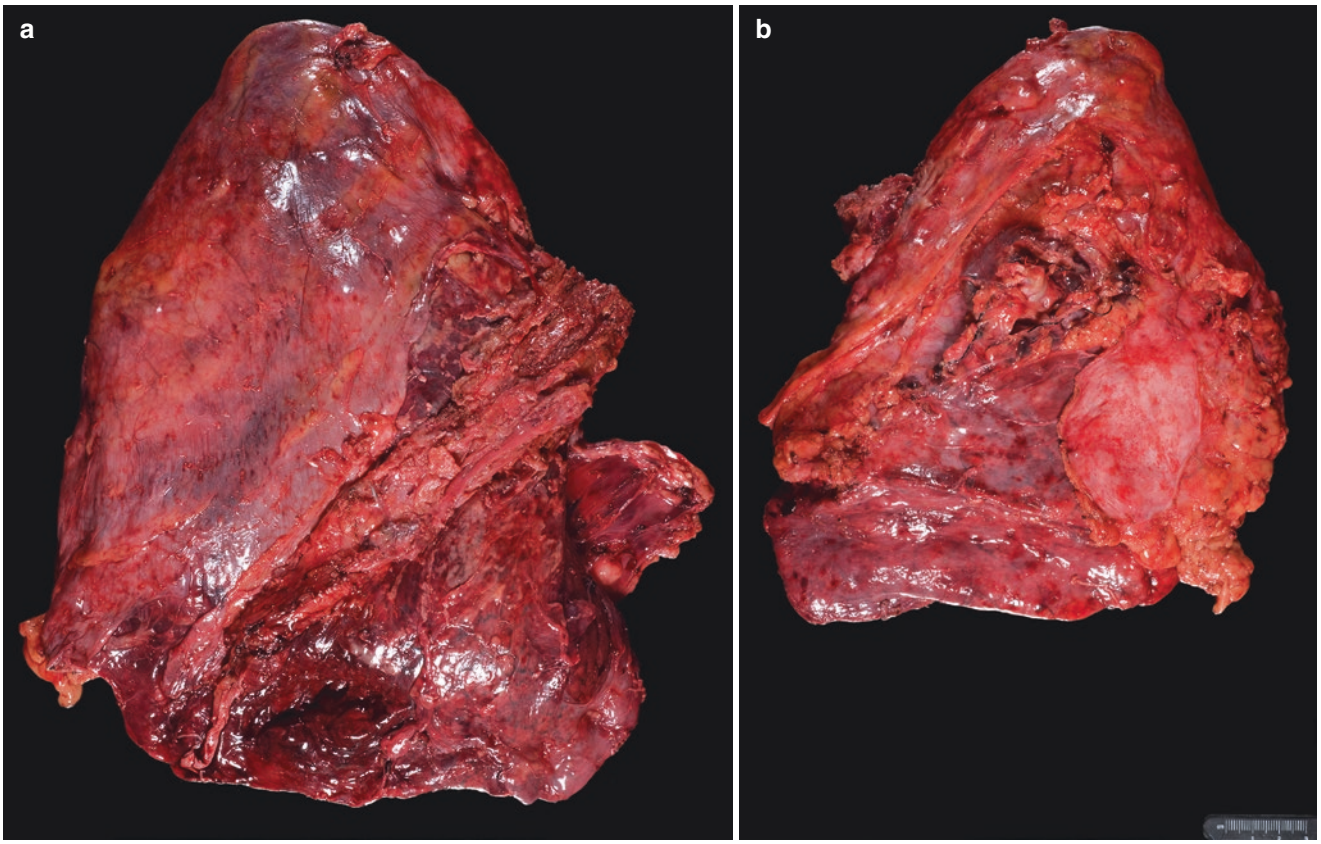


**Fig. 1.35** (**a**) Extrapleural pneumonectomy specimen (EPP), (**b**) EPP showing important anatomical structures—lung, pleura, pericardium, and diaphragm, (**c**) EPP showing thickening of the pleura, (**d**) closer view of thickened pleura, which in addition shows small nodules, (**e**) cross-section of the EPP showing invasion of the tumor into both pleuras, pulmonary fissure, pericardium, and superficial invasion of the diaphragm

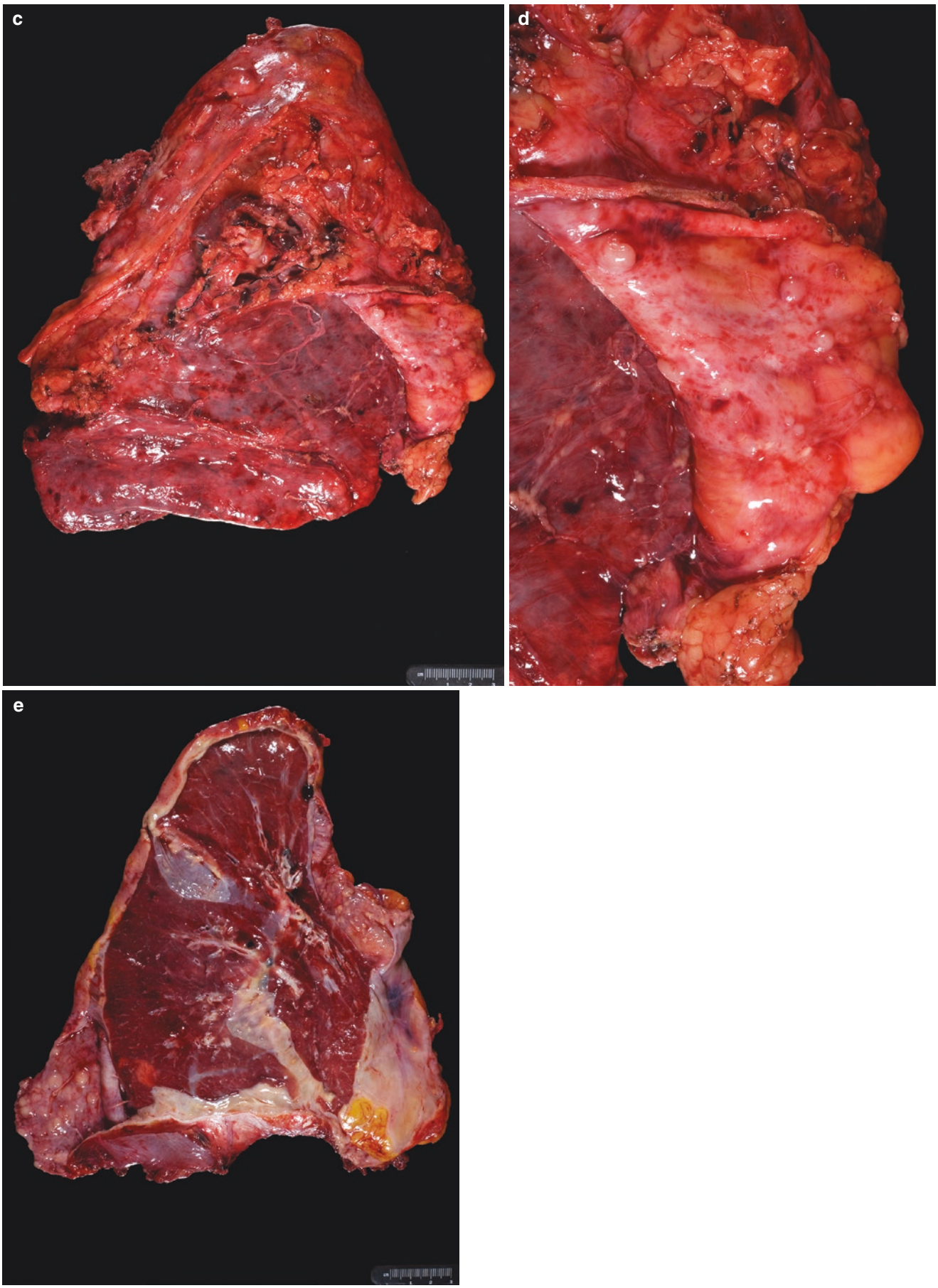


**Fig. 1.35** (continued)

are comparative studies to separate pleural involvement by adenocarcinoma from mesothelioma, which on morphological ground may show somewhat similar features, while in other reports the emphasis has been on specific morphological features that may be unusual in these tumors [179–191].

However, traditionally mesotheliomas have been divided into three specific groups with several distinct subgroups:

- *Epithelioid.*
  - *Tubulopapillary*: This may represent the most common growth pattern, which characteristically show the presence of papillae and tubular structures formed by medium size cells with eosinophilic cytoplasm, round to oval nuclei, and conspicuous nucleoli. The tumor is fairly uniform and does not show marked nuclear atypia or mitotic activity (Fig. 1.36a–f).

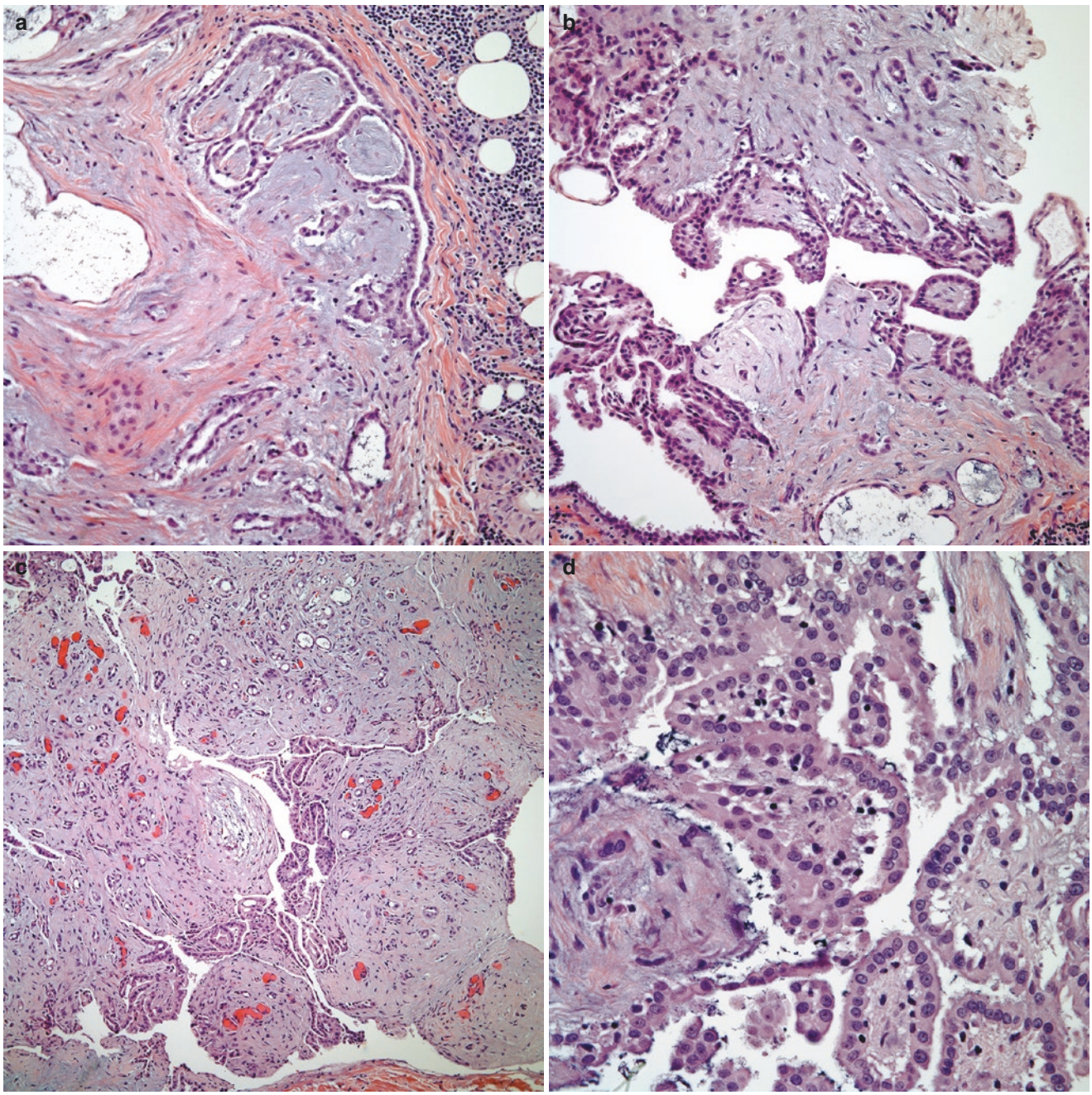


**Fig. 1.36** (**a**) Malignant mesothelioma showing tubular structures; (**b**) combined tubular and papillary structures; (**c**) malignant cells dissecting fibroconnective tissue; (**d**) higher magnification shows lack of nuclear atypia and mitotic activity in tumor cells; (**e**) low power view of a predominantly papillary mesothelioma; (**f**) higher magnification of the pseudopapillary structures are lined by mesothelium

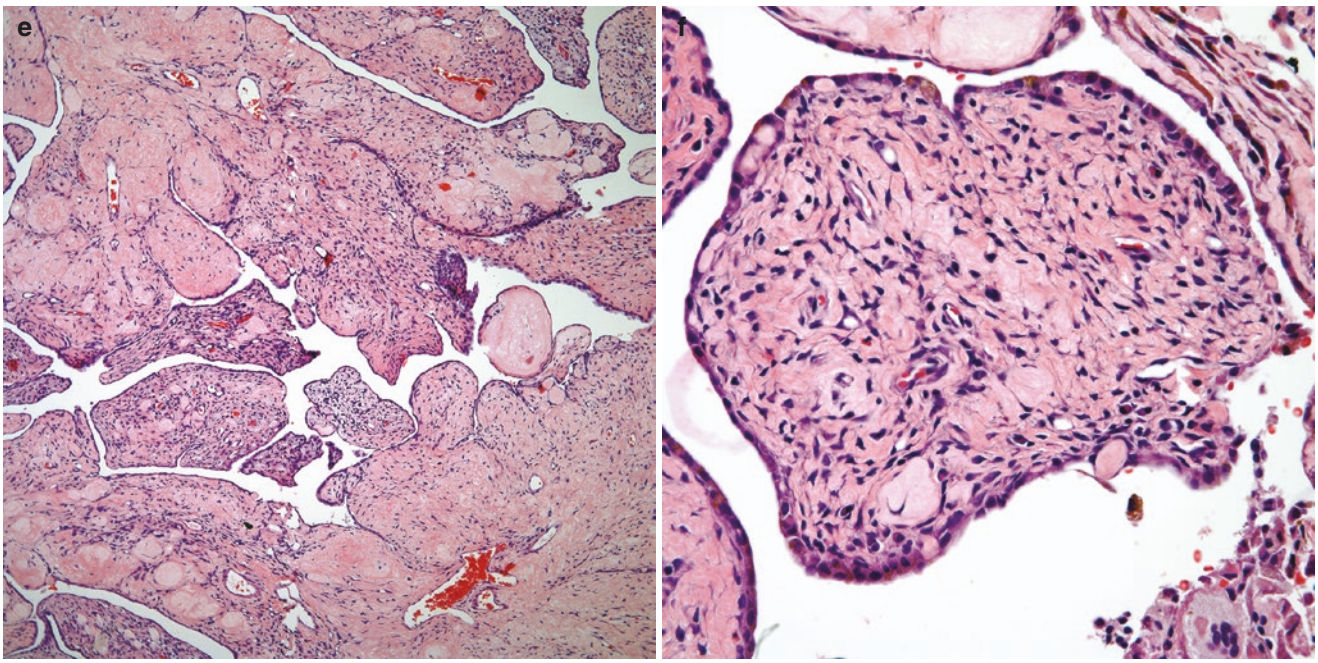


**Fig. 1.36** (continued)

- *Adenomatoid*: As its name implies the features are similar to those seen in adenomatoid tumors, namely, the presence of cords or nest of medium size cells with bland histological appearance, in some areas with signet-ring-cell-like areas but lacking cytological atypia and mitotic activity (Fig. 1.37a–d).
- *Deciduoid*: The tumor shows sheets of medium size neoplastic cells with eosinophilic cytoplasm and showing features similar to those seen in deciduoid cyclic endometrial changes with deciduoid reaction (Fig. 1.38a–c).
- *Clear cell*: As its name implies and contrary to the other growth pattern of mesothelioma, this tumor shows sheets of malignant cells with clear cytoplasm, oval nuclei, and conspicuous nucleoli with a discrete vascular network. The tumor does not show marked nuclear atypia or mitotic activity (Fig. 1.39a–d).
- *Glandular*: This growth pattern is the one that most closely resembles adenocarcinoma. The tumor shows well-formed glandular structures; however, marked cytologic atypia and increased mitotic activity is not commonly seen in this glandular proliferation (Fig. 1.40a–c).
- *Myxoid/mucoid*: In this growth pattern the neoplastic cells are embedded in pools of mucoid material (Fig. 1.41a–c).
- *Rhabdoid*: The neoplastic cells in these cases have ample cytoplasm and nuclei displaced toward the periphery of the cells, which imparts a "rhabdoid" appearance (Fig. 1.42a, b).
- *Cartilaginous and osseous differentiation*: These tumors may pose significant problem in the interpretation, mainly in small biopsies due to the presence of bone or cartilage (Fig. 1.43a–c).

• *Sarcomatoid*: This pattern is less common and represents no more than 20% of all mesotheliomas. There appear to be two distinct subgroups of this particular variant:

- *Fibrosarcoma or MFH-like:* The growth pattern shows similar features as the fibrosarcoma of soft tissues, characteristically showing spindle cell proliferation with subtle herringbone pattern with scant or moderate amounts of eosinophilic cytoplasm, elongated nuclei, and inconspicuous nucleoli. In other cases, the tumor shows spindle to oval cells with more eosinophiic cytoplasm imparting a more "histiocytic" appearance. Cellular atypia and mitotic activity are easily identifiable in these tumors (Fig. 1.44a–f).

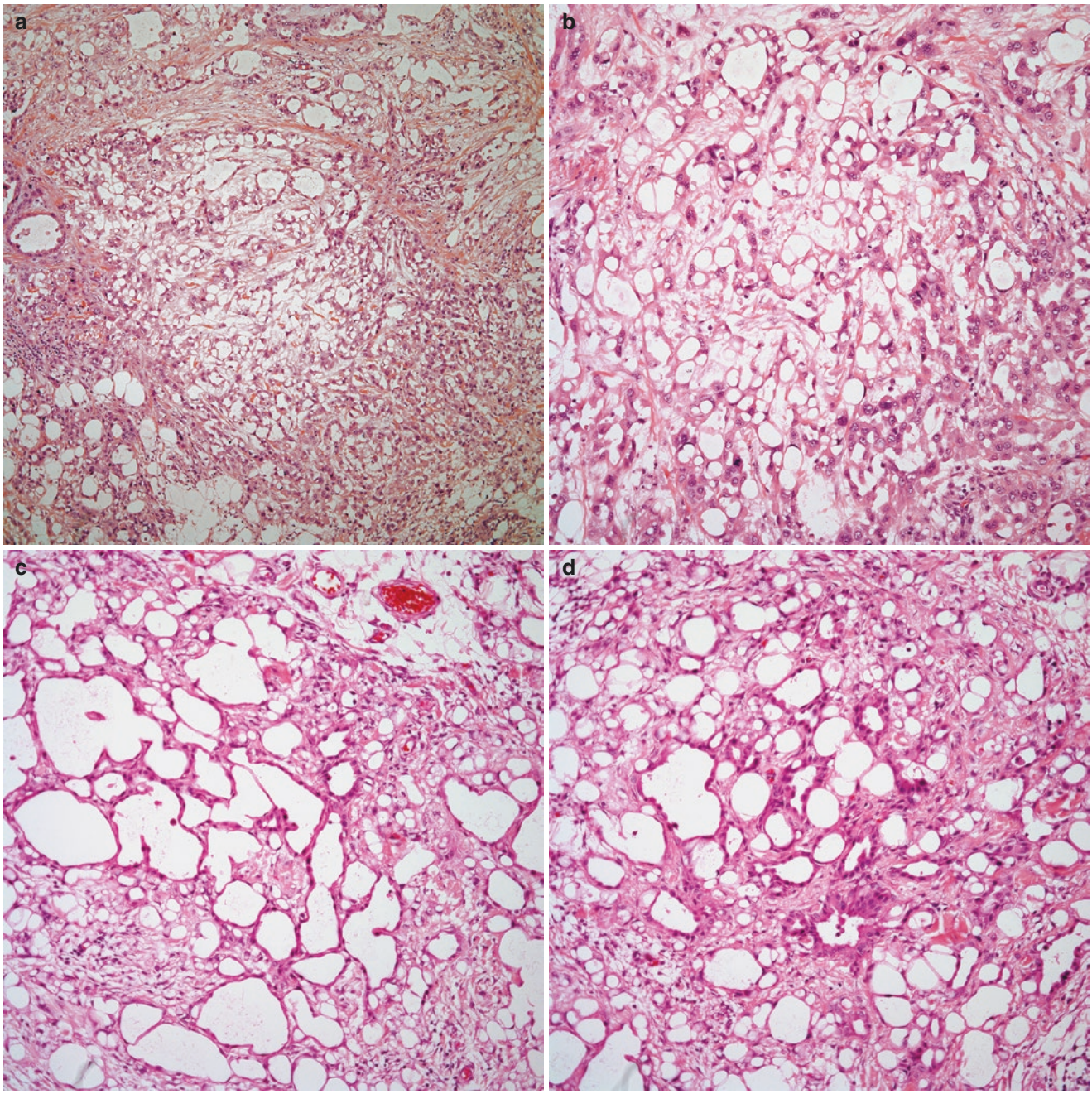


**Fig. 1.37** (**a**) Low power view of a malignant mesothelioma with adenomatoid features, (**b**) adenomatoid mesothelioma showing nest and small glandular structures, mitotic activity is present, (**c**) adenomatoid mesothelioma showing cystic and solid areas; (**d**) higher magnification showing cords and nest of neoplastic cells

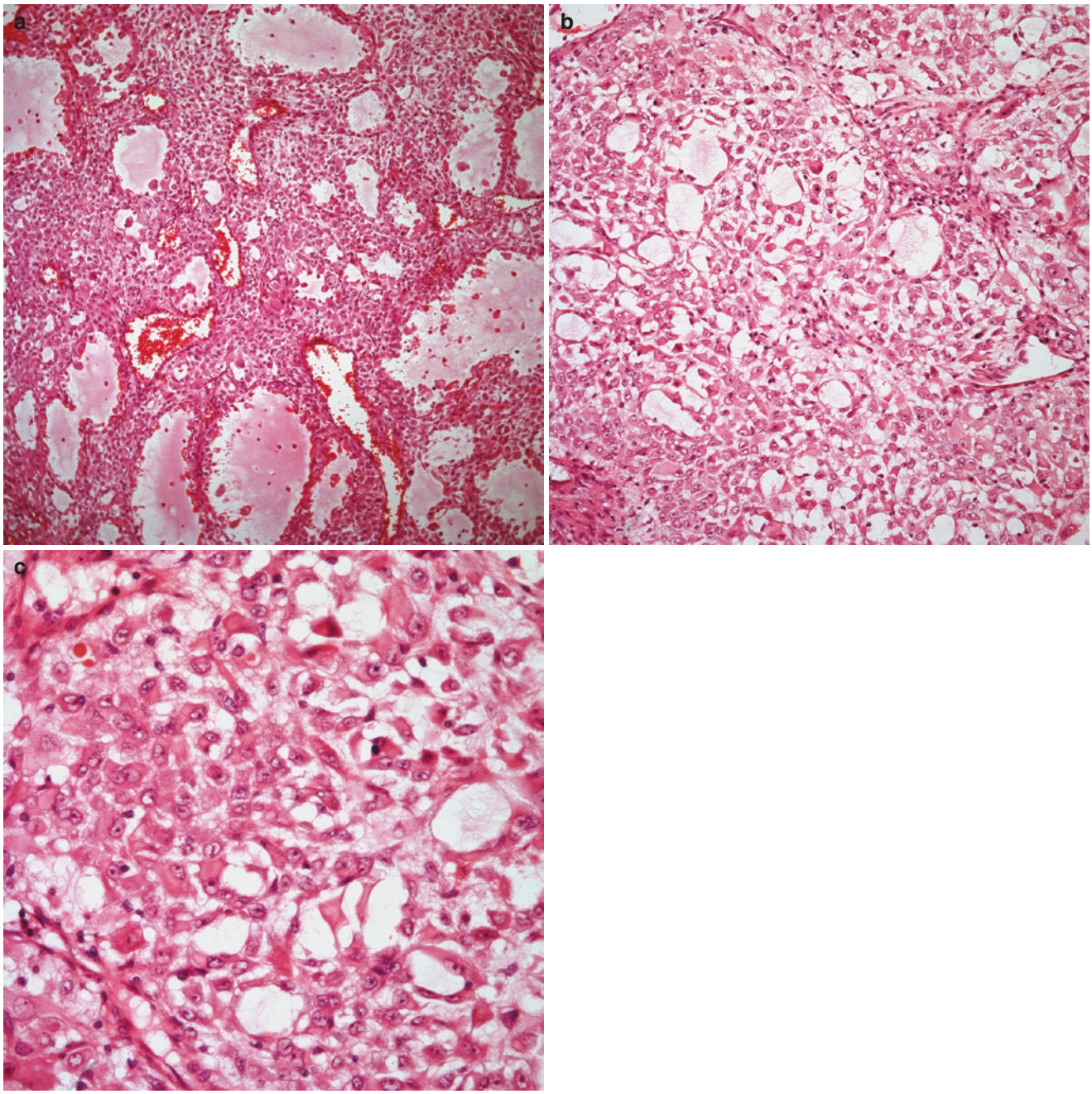


**Fig. 1.38** (**a**) Low power view of a deciduoid mesothelioma showing a subtle alveolar pattern admixed with sheets of tumor cells, (**b**) tumor cell showing decidualized features, (**c**) high power view showing cells with moderate amounts of eosinophiic cytoplasm, round to oval nuclei, and prominent nucleoli

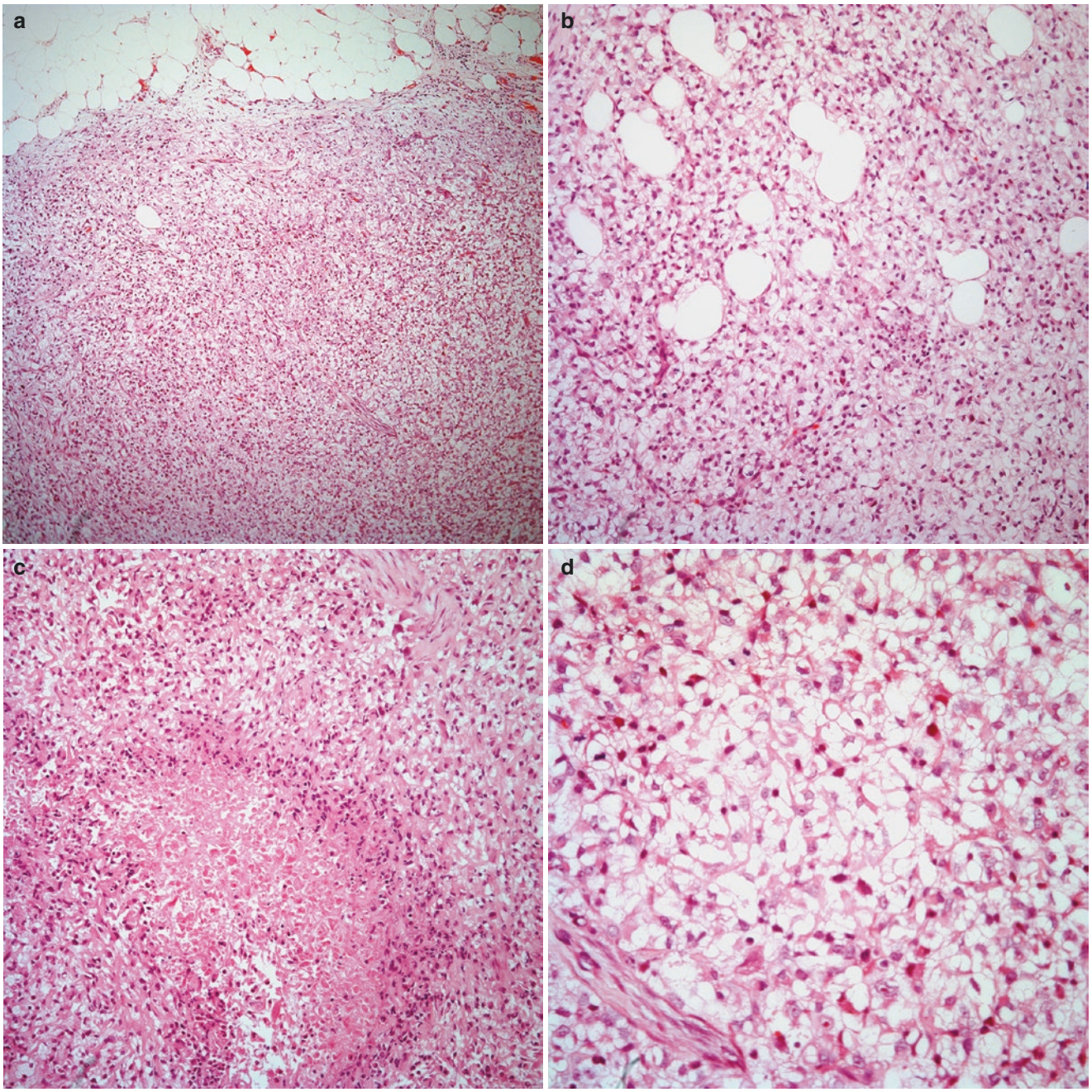


**Fig. 1.39** (**a**) Low power view of a clear cell mesothelioma showing tumor cells infiltrating adipose tissue, (**b**) tumor cells with distinct clear cytoplasm. (**c**) focal areas of necrosis, (**d**) sheets of neoplastic cells with clear cytoplasm and mild nuclear atypical with absence of mitotic activity

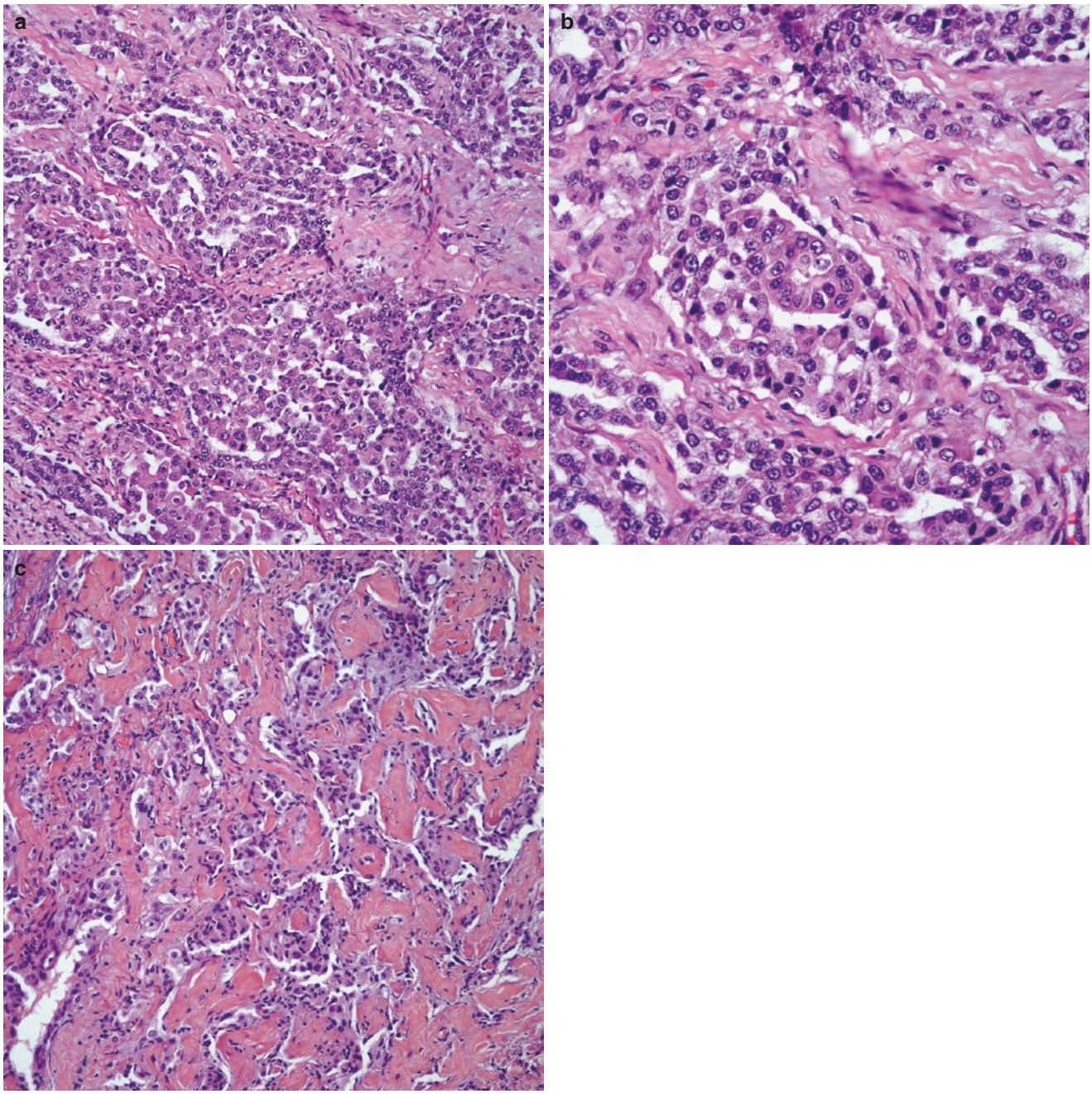


**Fig. 1.40** (**a**) Malignant mesothelioma showing more glandular pattern, (**b**) closer magnification showing small glandular structures, mitotic activity is present, (**c**) poorly defined glands dissecting fibroconnective tissue

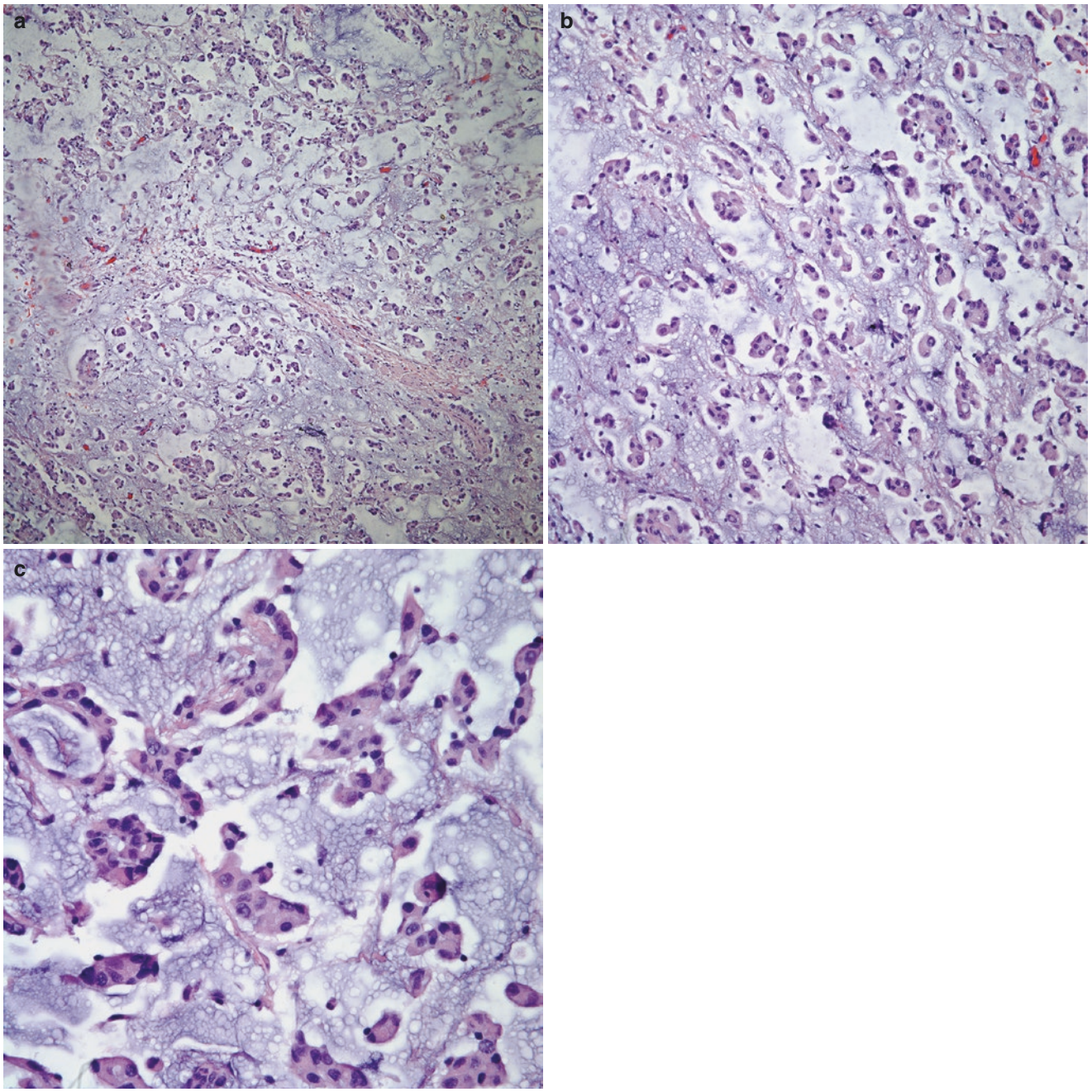


**Fig. 1.41** (**a**) Low power view of a mesothelioma showing extensive mucoid component, (**b**) neoplastic mesothelial cells floating in mucoid material, (**c**) closer magnification showing neoplastic cells admixed with mucoid material

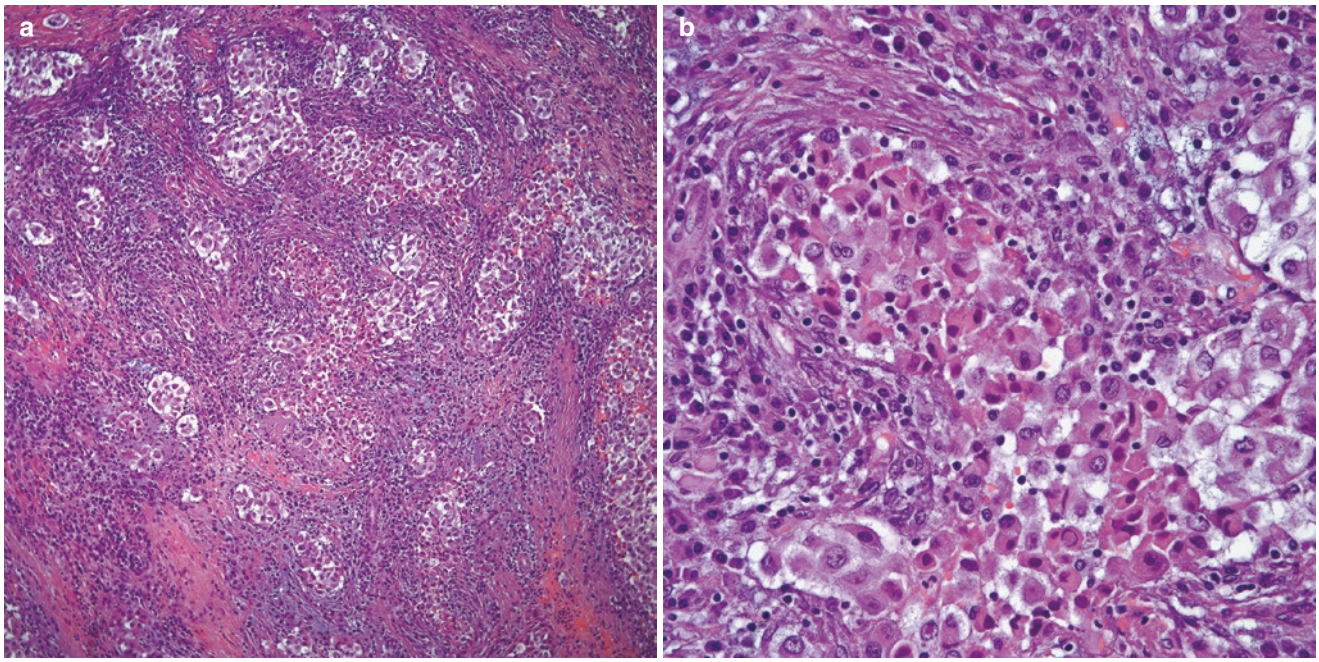


**Fig. 1.42** (**a**) Malignant mesothelioma with prominent rhabdoid features, (**b**) closer view of the tumor showing cells with ample eosinophilic cytoplasm and nuclei displaced toward the periphery imparting a "rhabdoid" appearance

  - *Desmoplastic:* Characteristically the tumor shows marked areas of collagenization with a discrete bland spindle cell proliferation dissecting the bundles of fibrocollagen (Fig. 1.45a, b). Due to the bland appearance of the tumor, specific criteria have been developed for its diagnosis [192, 193]:
    Invasion of chest wall.
    Foci of bland necrosis.
    Frank sarcomatoid foci.
    Distant metastasis.
  - *Lymphohistiocytoid:* The tumor shows sheets of epithelioid cells ranging from oval to spindle associated with a prominent lymphoid-histiocytic component (Fig. 1.46a–d).
- *Biphasic (epithelioid/sarcomatoid):* As its name implies, the tumor is characterized by an admixture of epithelioid and sarcomatoid components (Fig. 1.47a, b).

## Immunohistochemical Features

Over the years, mesothelioma is one tumor that has been extensively studied by immunohistochemical means. However, in practice, the use of immunohistochemical stains often depends on the growth pattern that the tumor may show. Therefore, tumors with spindle cell morphology are likely to be evaluated with a panel of immunohistochemistry to rule out a true sarcoma, while those with an epithelioid growth pattern will be analyzed with a panel of immunohistochemical stains that may also include other epitopes more specific for different tumors. Therefore, if the tumor shows epithelioid morphology, the panels may include the following:

- Positive markers.
  - Keratin 5/6, calretinin, D2–40 (Fig. 1.48a–d), and BAP-1 (negative nuclear staining).
  - Other markers that may show positive staining but are not specific include: GATA3, BerEp4, EMA, keratin cocktail, WT1, thrombomodulin. MOC-31 may show focal positive staining in a few cases (Fig. 1.49a–e).
- Negative markers (Carcinomatous epitopes):
  - CEA, B72.3, CD-15 (Leu M1), TTF-1, Napsin A, MOC-31.

In cases of sarcomatoid growth pattern, the panel of immunohistochemistry may change to include markers that are specific for spindle cell sarcoma.

## Molecular Analysis

The use of FISH analysis, namely, CDKN2A is commonly used in the diagnosis of mesotheliomas and coupled with BAP1 immunohistochemistry, plays an important role in the diagnosis of these tumors [194–204]. However, it is important to highlight the variation in detection rates and sensi-

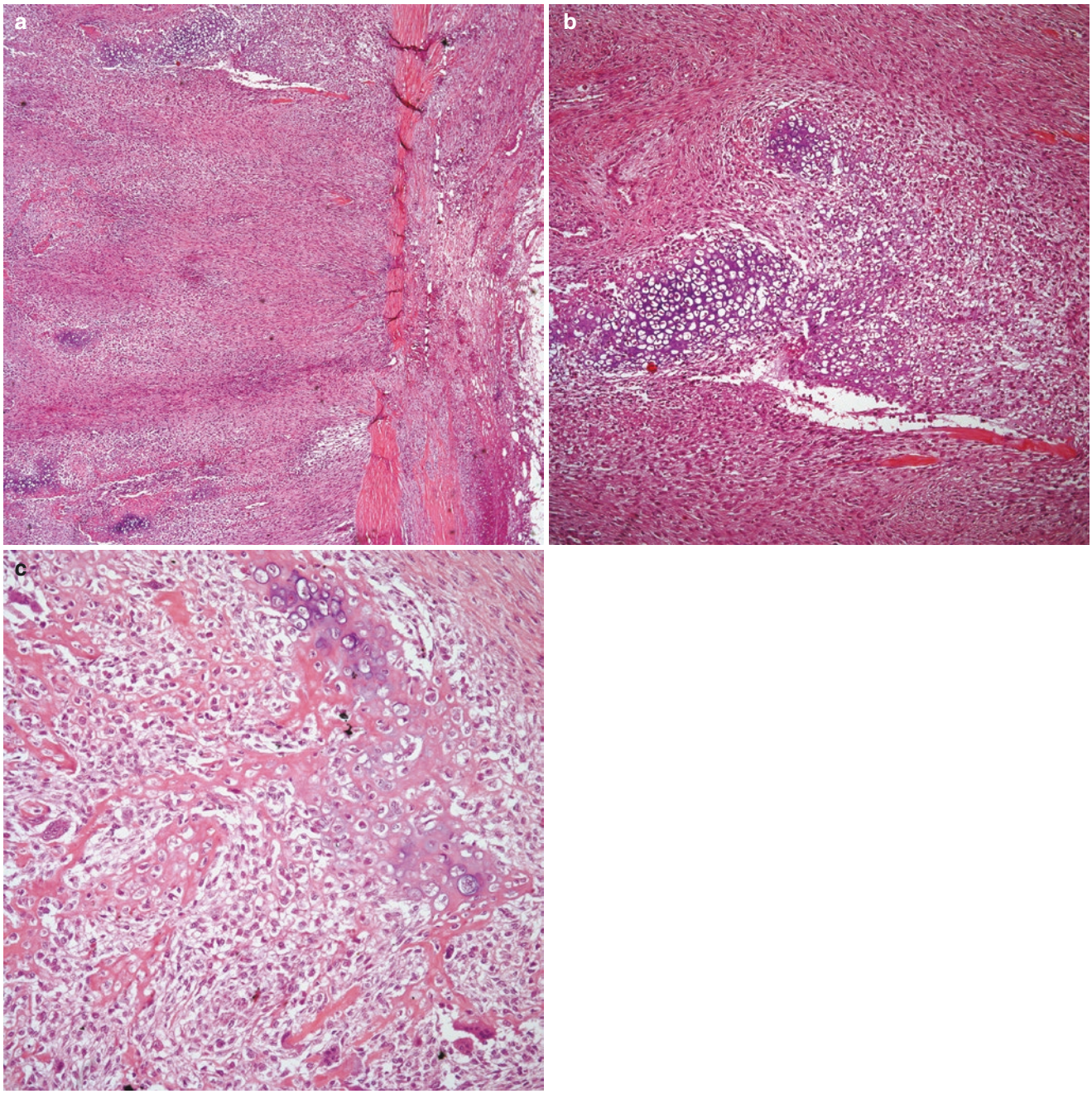


**Fig. 1.43** (**a**) Low power view of a mesothelioma showing focal areas of cartilaginous differentiation, (**b**) mesothelioma with areas of cartilaginous change merging with epithelioid cells, (**c**) mesothelioma showing cartilaginous and osseous differentiation

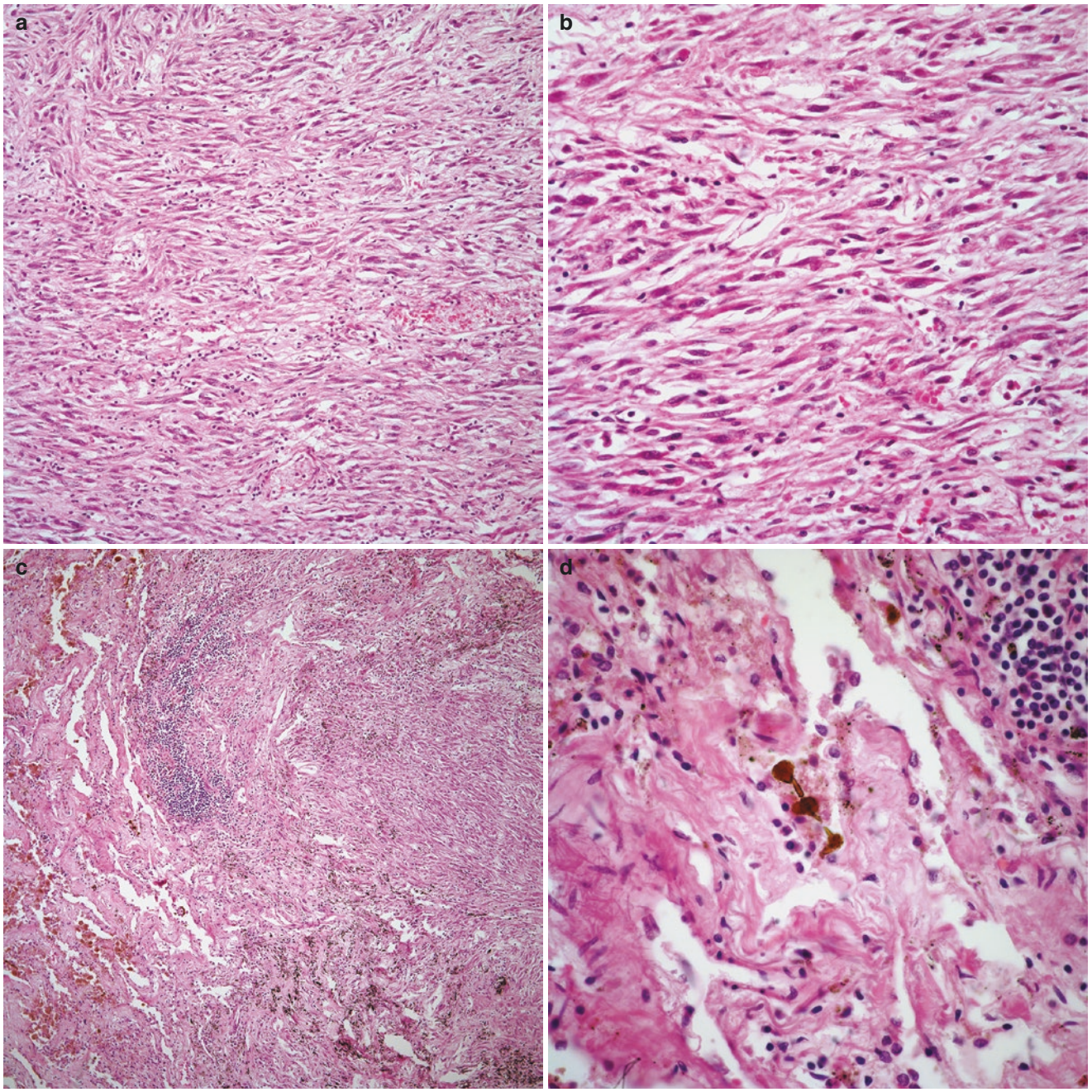


**Fig. 1.44** (**a**) Sarcomatoid mesothelioma showing characteristic spindle cell proliferation—fibrosarcoma-like, (**b**) closer magnification showing spindle cell with elongated nuclei and inconspicuous nucleoli, (**c**) tumor infiltrating lung parenchyma with associated asbestos bodies in the lung parenchyma, (**d**) higher magnification of a ferruginous body, (**e**) sarcomatoid mesothelioma with MFH-like areas, necrosis, and mitotic activity, (**f**) closer magnification showing marked cellular atypia

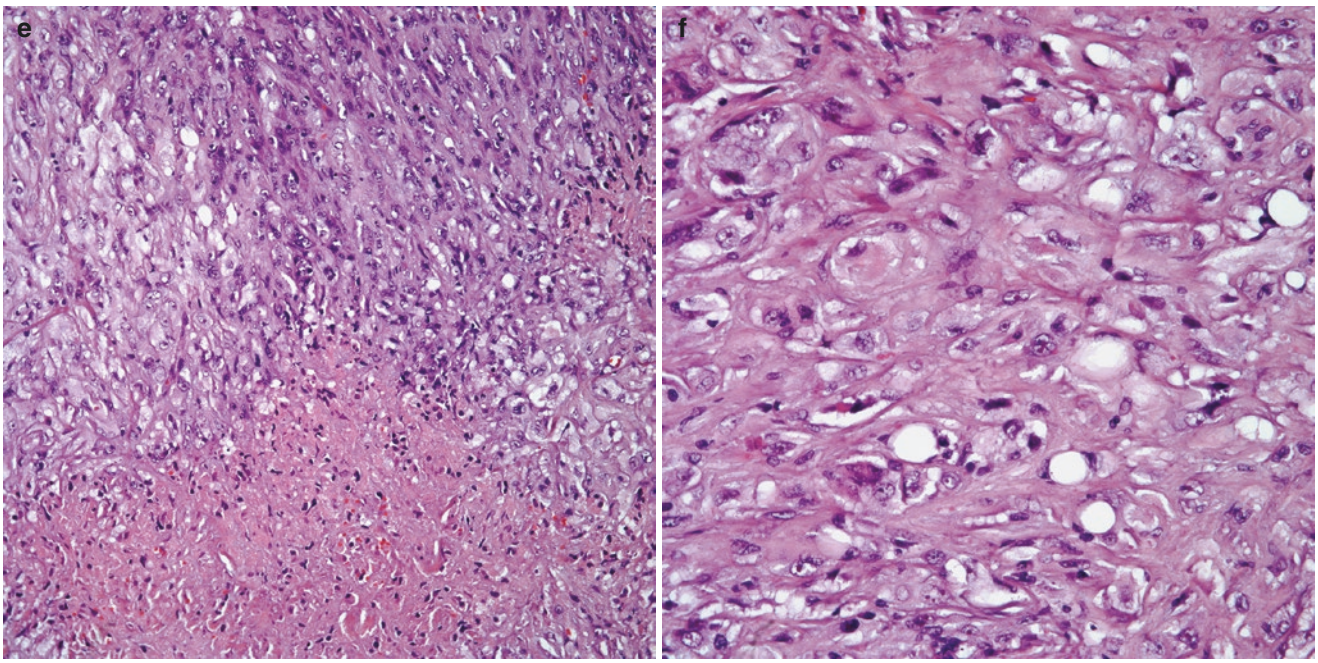


**Fig. 1.44** (continued)

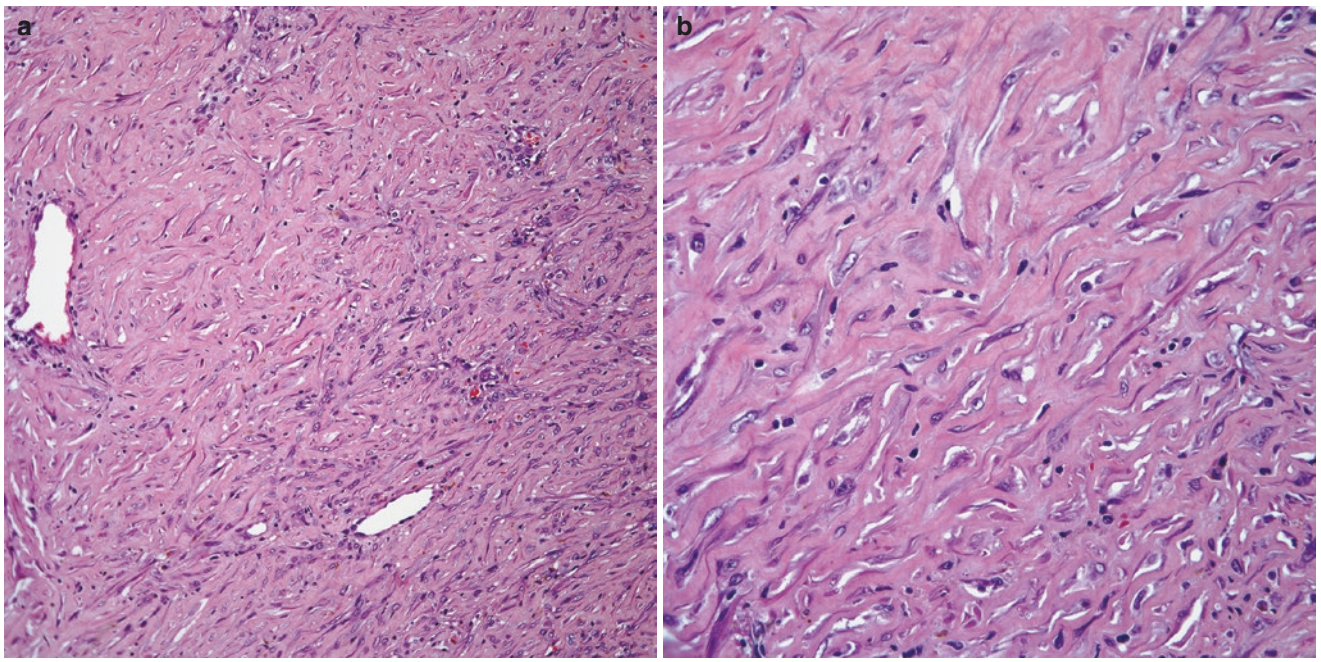


**Fig. 1.45** (**a**) Desmoplastic mesothelioma showing spindle cells dissecting fibrocollagen; (**b**) higher magnification showing bland spindle cell proliferation

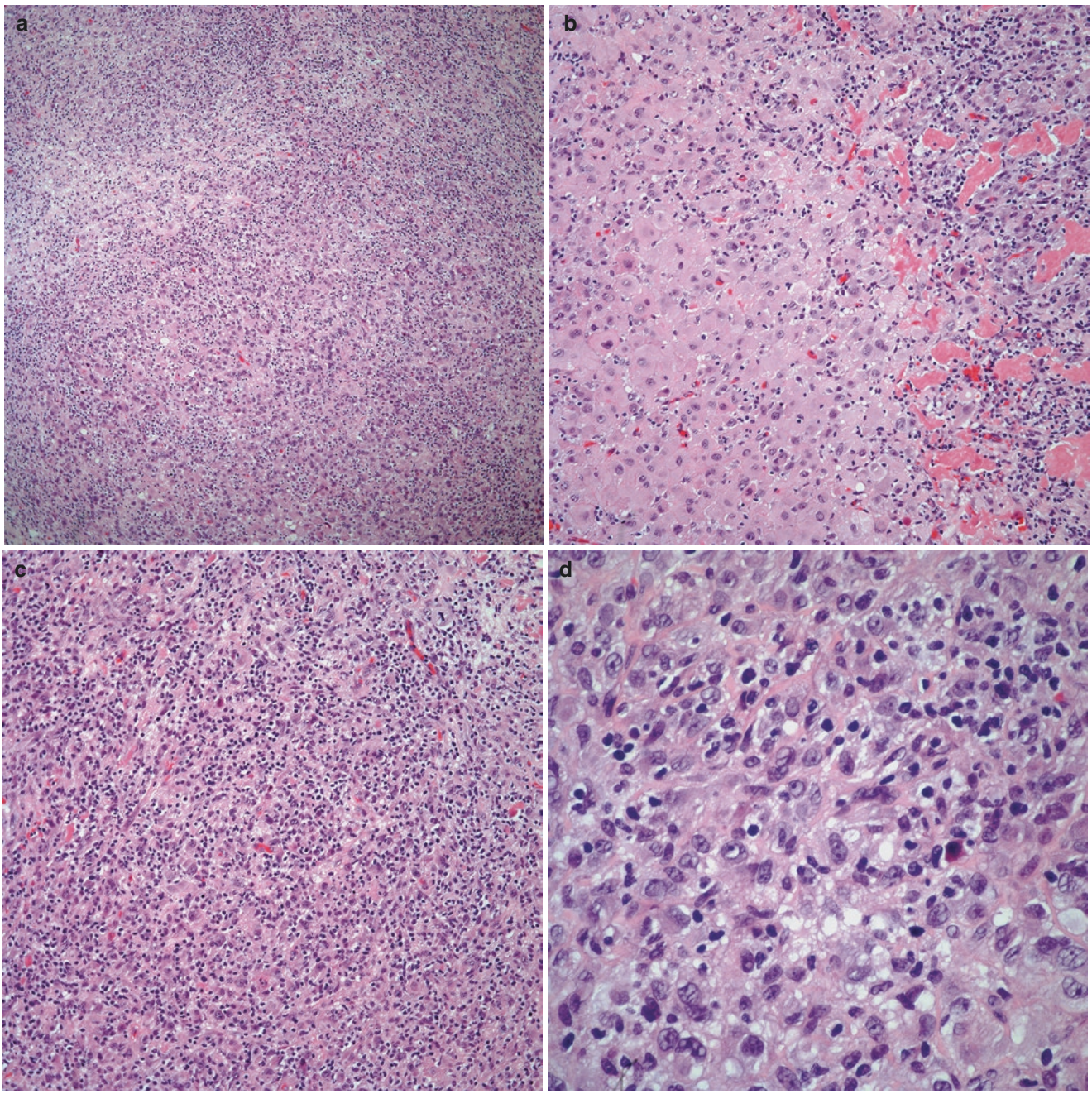


**Fig. 1.46** (**a**) Low power view of a lymphohistiocytoid mesothelioma showing a mixed population of lymphocytes and epithelioid cells, (**b**) neoplastic cells with more ample cytoplasm and histiocytoid appearance, (**c**) dual population of inflammatory cell (lymphocytes) and neoplastic epithelioid cells, (**d**) higher magnification showing cell with moderate amounts of eosinophilic cytoplasm, oval nuclei, and nucleoli admixed with lymphocytes

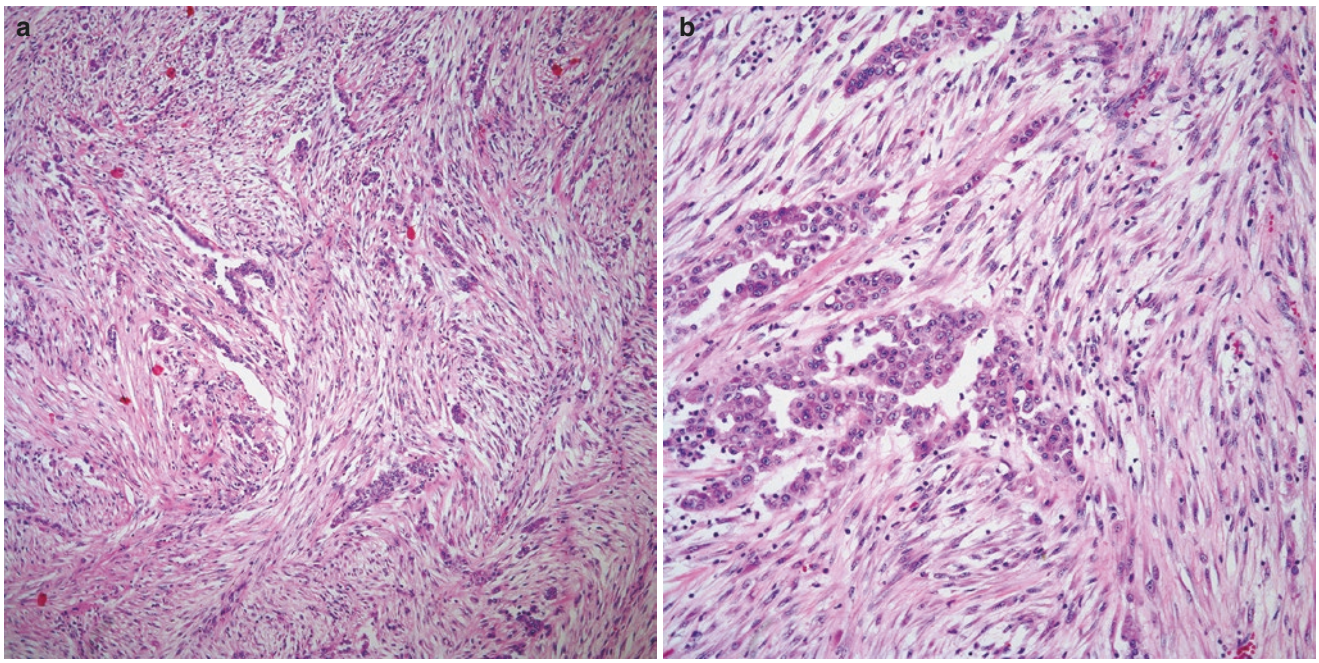


**Fig. 1.47** (**a**) Biphasic mesothelioma showing spindle cell and epithelioid cell components, (**b**) higher magnification showing both components

tivities that have been reported using this methodology. In addition, the detection of the homozygous deletion that commonly correlates with mesothelioma also varies, based on the morphology, which in cases of sarcomatoid mesothelioma has been reported as 90% or 100%. In addition, the reported cut-off of cell showing homozygous deletion varies from different studies and ranges from 10% to 20% deletion. In our experience with sarcomatoid mesotheliomas [205, 206], we determined our cut-off at 2.7% and analyzed 53 cases of such tumor identifying that 41 out of 53 cases showed homozygous deletion, while only 49 of 53 cases show BAP1 loss. When BAP1 and p16 FISH results were compared, only 29 of 53 cases showed BAP1 loss and p16 homozygous deletion. Based on the results published in the literature and in our own experience, we consider that the final diagnosis of mesothelioma needs to be seen in a global interpretation of the clinical, radiological, morphological, immunohistochemical, and, molecular findings.

## Pseudomesotheliomatous Adenocarcinoma

Pseudomesotheliomatous carcinoma (PMC) of the lung was first reported approximately 50 years ago. These rare manifestations of adenocarcinoma represent a unique subtype of epithelial neoplasm involving the pleura with clinical, radiologic, and histologic features that mimic MPM [207, 208]. Diffuse thickening of the visceral and/or parietal pleural with minimal lung invasion are hallmarks of the disease. Most frequently, PMC has been reported as variants of peripheral bronchogenic carcinomas, although a variety of cancers of non-bronchogenic origin, including primary pleural sarcomas, thymic epithelial tumors and lymphomas, and metastatic diseases arising from renal cell carcinomas and pancreatic carcinomas have also been described. A role for asbestos as a driver in PMC has been suggested, but remains uncertain. PMC is primarily a disease of male smokers [209]. Patients typically present with progressive cough, chest pain, and weight loss in the sixth decade of life. Diffuse pleural thickening, pleural effusion, and pleural plaques with inconspicuous lung involvement, similar to MPM, may be seen on CT or MRI imaging of the chest. The pleural lesions are FDG-avid on PET/CT. Tissue analysis is required in all cases to establish the diagnosis and distinguish PMC from MPM. Although the reported prognosis is poor, with a median survival of only 8 months [207, 210–216], targeted therapy and molecular genotyping in PMC have shown encouraging results.

As expected, imaging findings of PMC closely mimic findings in MPM. On routine radiographs, predominantly unilateral pleural effusions with or without pleural thicken-

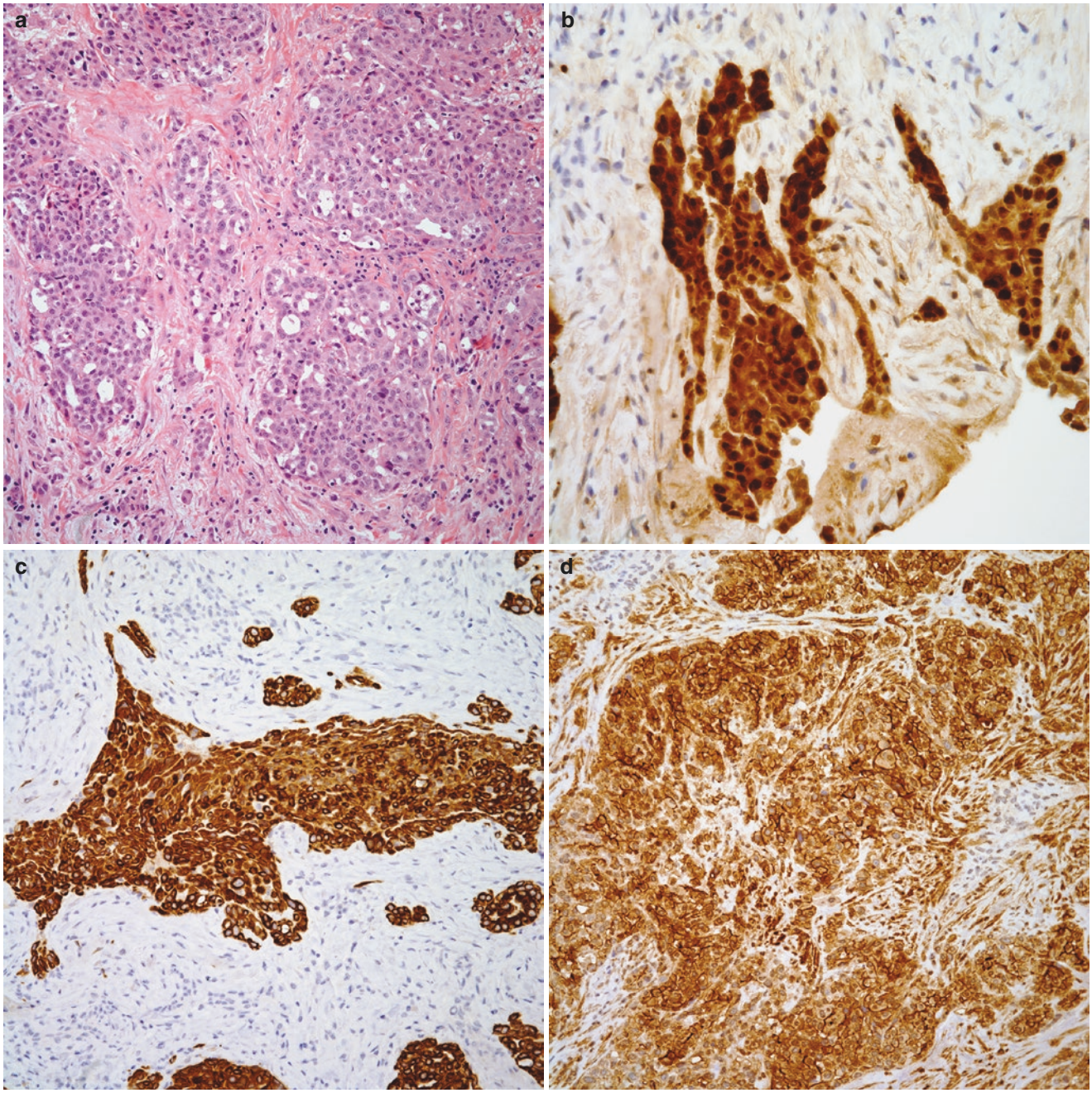


**Fig. 1.48** (**a**) Malignant mesothelioma, epithelioid type (H&E stained section), (**b**) immunohistochemical stain for Calretinin showing positive nuclear and cytoplasmic stain in tumor cells, (**c**) immunohistochemical stain for keratin 5/6 showing positive staining in tumor cells, (**d**) immunohistochemical stain showing positive staining for D2–40 in tumor cells

ing or pleural nodularity can be seen. Contrast-enhanced CT demonstrates simple or complex pleural effusions as well as enhancing pleural thickening or nodularity (Fig. 1.50a, b). In the limited reports available, malignant effusions and nodularity associated with PMC are FDG avid on PET/CT. PMC is known to metastasize to thoracic and extrathoracic regions, such as mediastinal and hilar lymph nodes, pericardium, chest wall, liver, adrenals, spleen, and vertebra. Spread to the brain, kidneys, and peritoneum is reported less commonly [214].

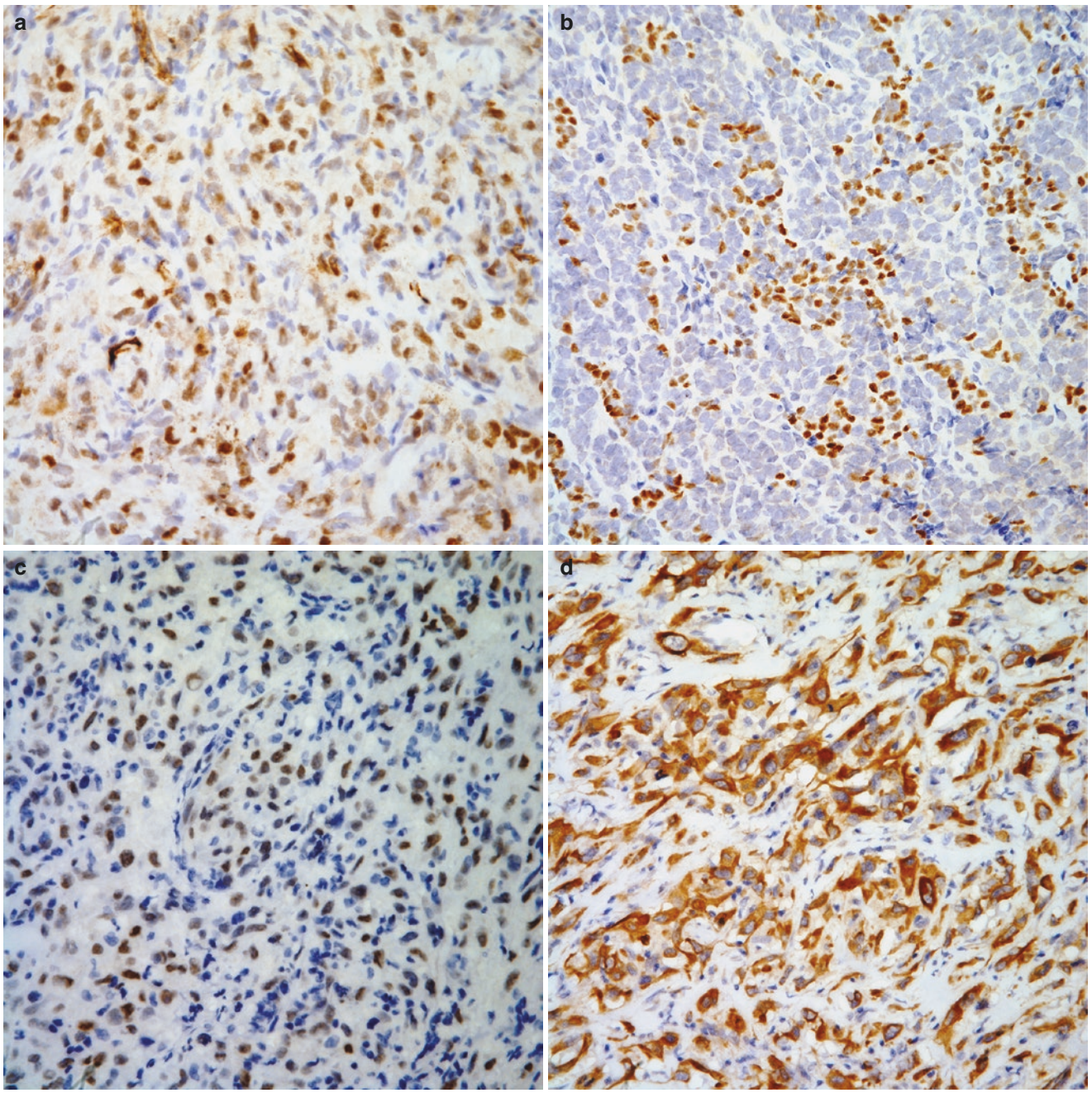


**Fig. 1.49** (**a**) Immunohistochemical stain for WT-1 showing positive nuclear staining in tumor cells, (**b**) immunohistochemical stain for p40 showing numerous cells with positive nuclear staining, (**c**) immunohistochemical stain for GATA3 showing positive nuclear staining in tumor cells, (**d**) immunohistochemical stain for broad spectrum kertatin showing positive staining in tumor cells, and (**e**) immunohistochemical stain for keratin-7 showing strong positive staining in tumor cells

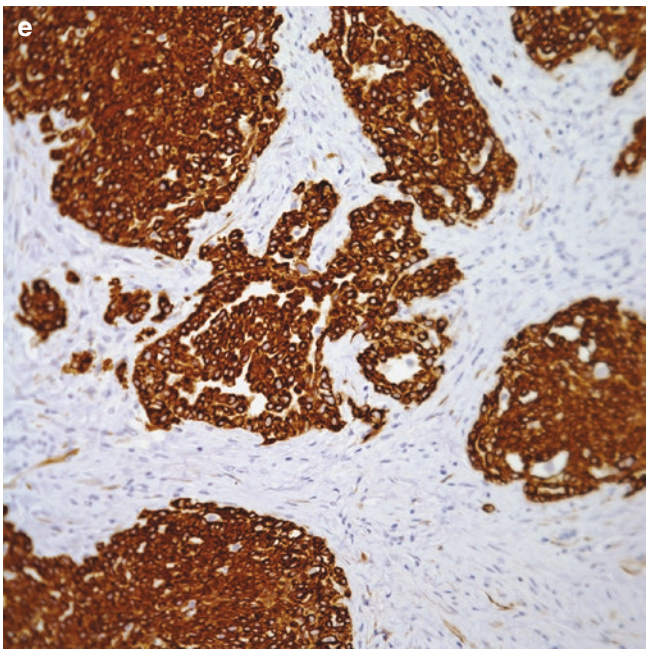


**Fig. 1.49** (continued)

## Pathological Features

As its name implies, this entity represents an adenocarcinoma with diffuse pleural thickening in a manner similar to pleural mesothelioma.

### Macroscopic Features

The tumor characteristically shows diffuse pleural thickening (Fig. 1.51) and often it is possible to observe a small tumor nodule in the periphery of the lung parenchyma.

### Microscopic Features

The tumor characteristically shows a glandular proliferation embedded in fibroconnective tissue (Fig. 1.52a–d). The gland may show the presence of mucin production while in some other cases the tumor may be of the non-mucinous type. The glands are arranged in a haphazard pattern containing cells with nuclear atypia and mitotic activity. Essentially, the features of this tumor are those of an adenocarcinoma that may range from a well to a poorly differentiated tumor.

### Immunohistochemical Features

Because the majority of these neoplasms are of the adenocarcinoma type of lung origin, the use of pneumocytic immuno-

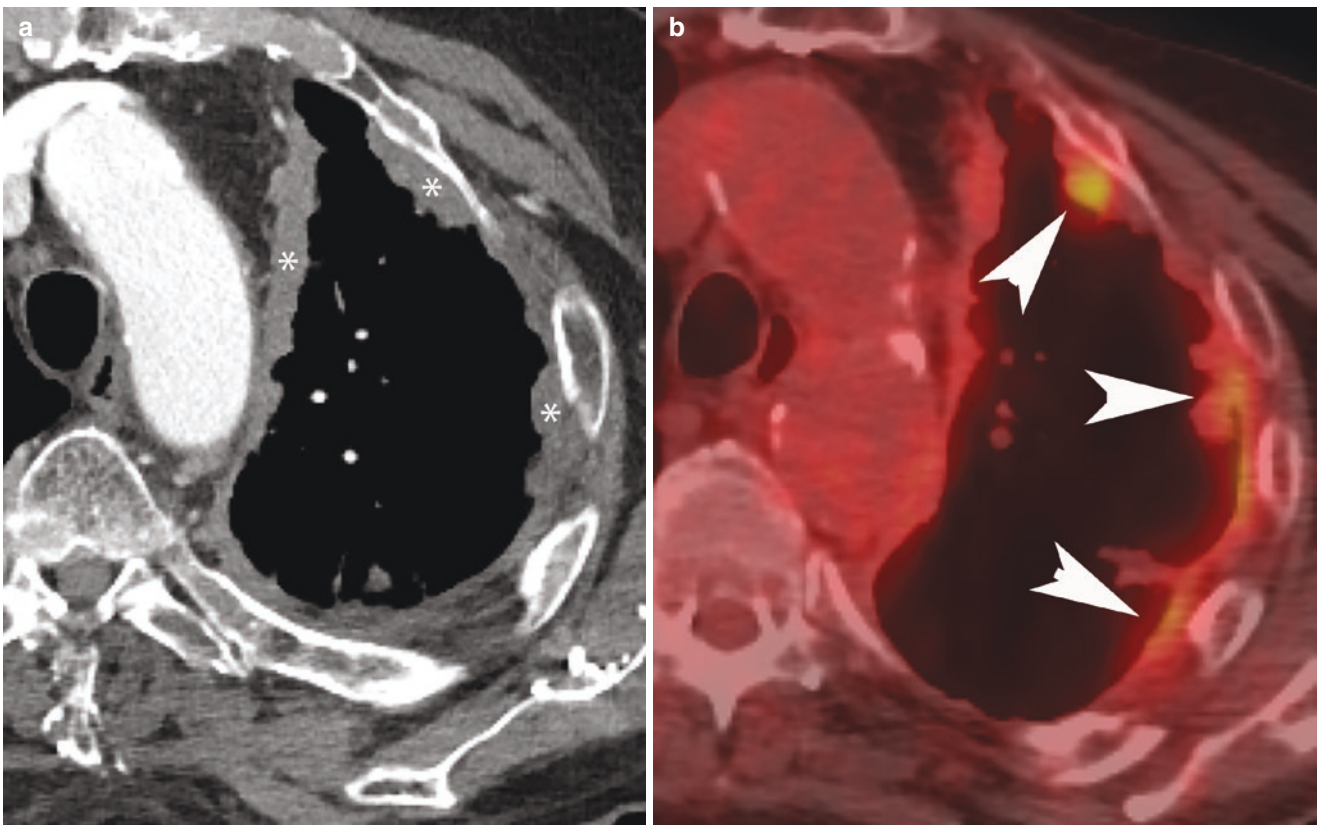


**Fig. 1.50** (**a**) Contrast-enhanced axial CT with left circumferential nodular pleural thickening (*), similar to that seen in mesothelioma, (**b**) axial FDG PET/CT demonstrates increased FDG uptake in the pleural tumor (arrowheads)

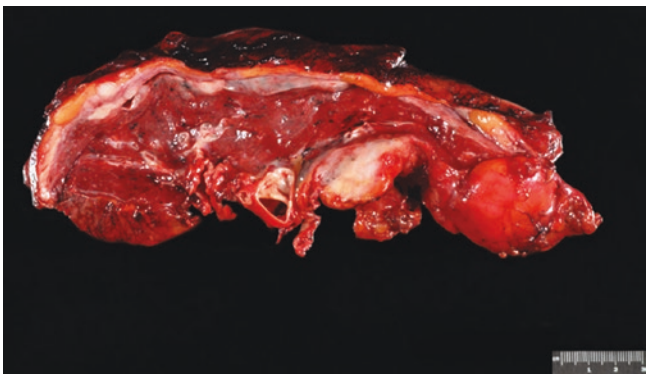

**Fig. 1.51** Pseudomesotheliomatous adenocarcinoma showing diffuse pleural thickening mimicing mesothelioma

histochemical markers is commonly used. Markers such as TTF-1 and Napsin (Fig. 1.53) will provide good information as to the origin of the tumor, while other more generic markers such as CEA (Carcinoembryonic antigen), CD-15 (LeuM1), B72.3, are carcinomatous epitopes that are commonly seen positive in adenocarcinomas without specific origin.

## Pleural Thymoma

Thymomas are epithelial neoplasms of the thymic gland. During embryonic development, the thymus originates from the third and fourth pharyngeal pouches and gradually moves to the anterior mediastinum. Therefore, 96% of the thymic epithelial tumors occur in the anterior mediastinum [217]. Thymomas occurring outside the anterior mediastinum are considered ectopic. Ectopic thymoma is rare, accounting for only 2–4% of total thymomas [218]. Ectopic thymoma is thought to originate from thymic tissue displaced during embryologic development. Another hypothesis suggests that ectopic thymoma derives from stem cells [219]. Ectopic thymoma has been reported in the neck, lung, pleura, thyroid, pericardium, and posterior mediastinum. The lungs and pleura are the second most common sites for ectopic thymoma after the neck [218, 219]. Thymomas originating from the pleura are extremely rare, and very few cases are described in the literature; in contradistinction thymomas originating from the mediastinum and spreading along the pleura are more common. A testament to the unusual occurrence of pleural thymomas is that the largest series reported is of only eight such cases [220].

Both ectopic thymomas and primary pleural thymomas show a female predominance. Myasthenia gravis has been reported in approximately one-third of cases of primary pleural thymoma, but is a very rare complication of ectopic thymomas [221]. Presenting symptoms of ectopic thymomas are often nonspecific and can include dyspnea, fever, and weight loss. The mean age at diagnosis is 55 years. Most cases present as diffuse pleural tumors encasing the lungs, clinically and radiologically mimicing malignant mesothelioma or metastatic pleural disease [220]. Occasionally, the tumors may be well-circumscribed pleural lesions and difficult to differentiate from solitary fibrous tumor on imaging [219, 222].

The diagnosis of ectopic thymomas can be extremely challenging due to their nonspecific clinical and radiological presentation. Fine needle aspiration and core needle biopsy are minimally invasive techniques commonly employed in the initial diagnostic workup of these lesions. Small tissue samples and histopathological heterogeneity of thymomas are common sources for confusion with more common neoplastic or nonneoplastic processes. Therefore, larger tissue samples provided by surgical resection are often required for accurate diagnosis [220]. Complete surgical resection is the treatment of choice for ectopic thymomas. Surgery should be attempted in all patients who are deemed operable irrespective of tumor site. Radiation and/or chemotherapy are treatment options in cases that are considered inoperable, show invasion of local structures, or are incompletely resected [220, 222].

### Pathological Features

#### Macroscopic Features

For tumors in which there is diffuse pleural involvement, the tumor may show the features that are commonly associated with pleural mesothelioma—pleural thickening. However, when the tumor is localized, the tumor may present as a pleural-based mass. In those cases, the tumor may vary in size but rarely more than 10 cm in greatest diameter. Rarely the tumor will show areas of hemorrhage or necrosis.

#### Histological Features

The histological features of pleural thymomas are similar to thymomas when they occur in the mediastinal compartment. The tumor may show either a spindle cell proliferation with sprinkle lymphocytes (spindle cell thymoma) or the tumor may show variable amount of lymphocytes and epithelial cells (Fig. 1.54a, b). The tumor grows along the pleural surface in a manner mimicking mesothelioma. However, it is important to highlight that the diagnosis of pleural thymoma rests on the specific criteria that the patients must not have an anterior mediastinal tumor. Otherwise, the tumor would be interpreted as an invasive thymoma with pleural dissemination.

#### Immunohistochemmical Features

The use of immunohistochemical markers in the diagnosis of thymoma is rather limited. In cases of spindle cell thymoma, the tumor will show positive staining for broad-spectrum keratin, keratin 5/6, p63, and p40 while negative for EMA (epithelial membrane antigen). Sporadic cases may show positive staining for TTF1, calretinin, and Bcl-2. On the other hand, those tumors with lymphocytic component in addition to the epithelial markers previously mentioned in spindle cell thymomas may also show positive staining for CD45 (lymphoid marker) and for CD3 and TdT (T-cell markers).

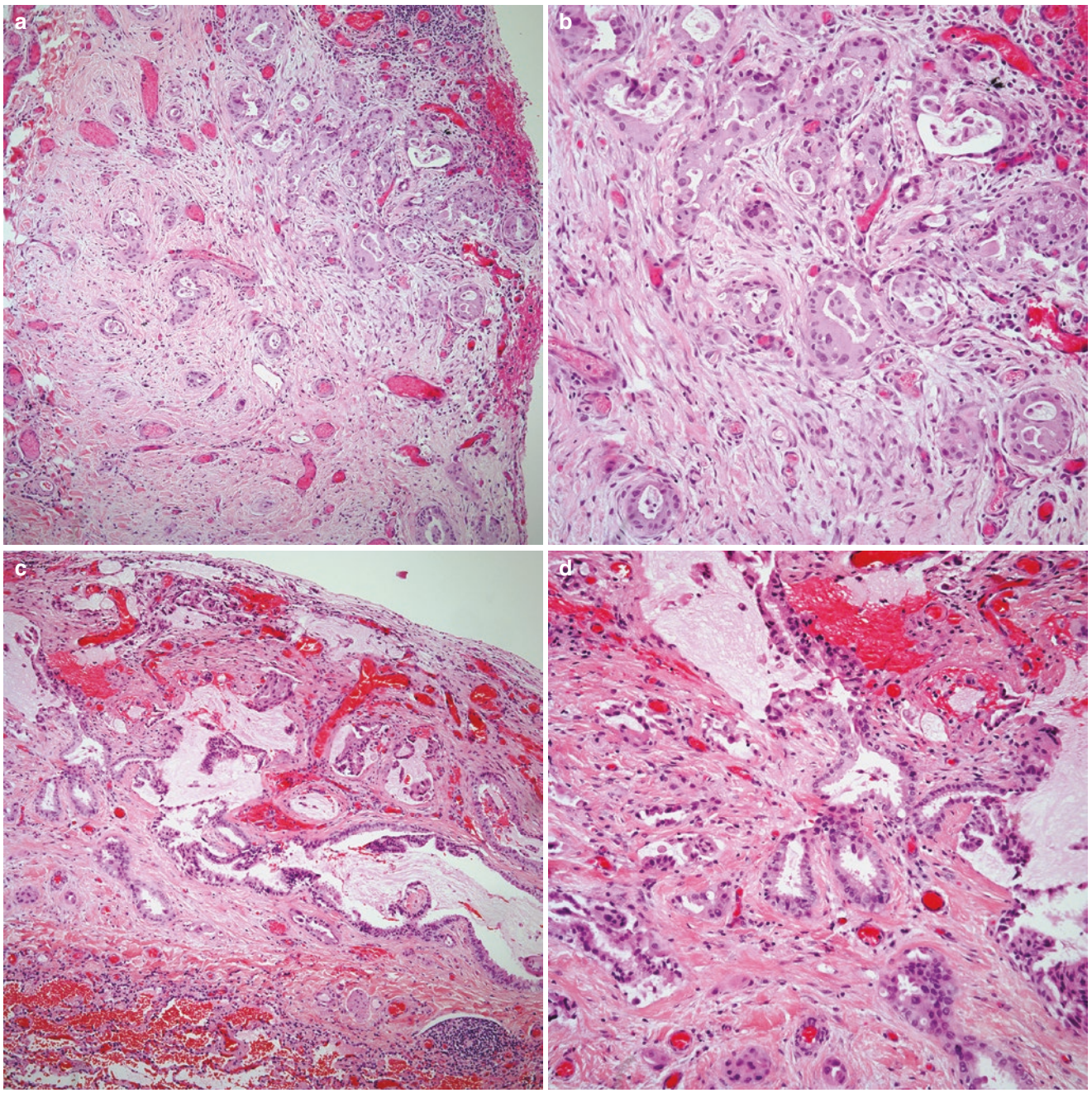


**Fig. 1.52** (**a**) Pseudomesotheliomatous adenocarcinoma showing the conventional glandular proliferation, (**b**) higher magnification of the malignant glands embedded in fibrocollagenous stroma, (**c**) Pseudomesotheliomatous adenocarcinoma in which the tumor shows mucinous changes; note the distribution of the tumor along pleural surface and the rim of uninvolved peripheral lung parenchyma, (**d**) higher magnification of the mucinous adenocarcinoma

## Primary Salivary Gland Type Tumors of the Pleura

These neoplasms have ubiquitous distribution and although they are more common in the head and neck area, similar tumors have been described in the mediastinum and as primary intrapulmonary neoplasms. However, the occurrence of these tumors in the pleura is rare and of this family of tumors, only two of these tumors have been described as presenting as pleural tumors. These tumors are: Mucoepidermoid carcinoma and Epithelial-Myoepithelial carcinoma. Needless to say, the interpretation of those tumors as primary pleural neoplasms, requires that the patients do not have a previous history of head and neck surgery, history of salivary gland type tumor in any other anatomical area, and that the tumors does not have an intrapulmonary component.

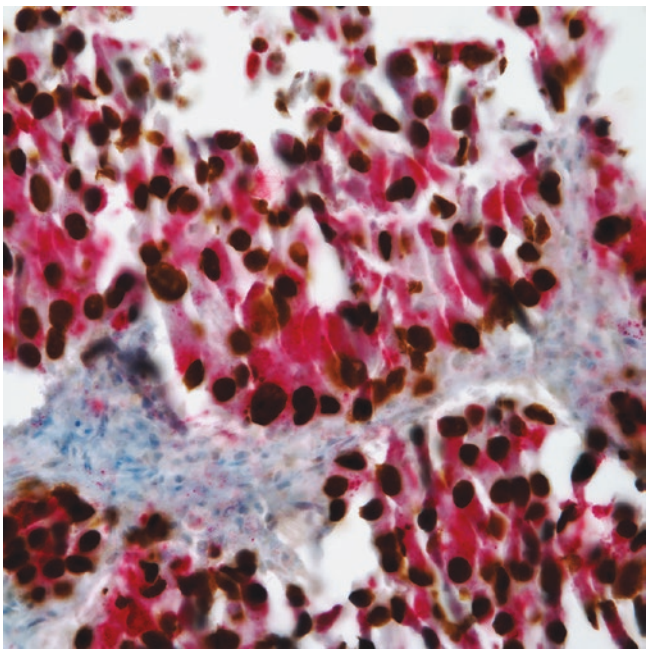

**Fig. 1.53** Dual immunohistochemical stain for TTF1/Napsin, where the nuclear positive staining is TTF-1 while the cytoplasmic stain is Napsin; both stains are commonly seen positive in adenocarcinomas of lung origin

### Mucoepidermoid Carcinoma (MEC)

In the cases reported of MEC, the tumor appears to present as a pleural-based tumor on diagnostic imaging without involvement of the lung parenchyma [223]. Clinically, patients may present with chest pain and dyspnea. The histopathological features of these tumors are similar to those described in the salivary glands. The tumor shows the presence of an epidermoid component composed of medium size cells with eosinophilic cytoplasm, round to oval nuclei and nucleoli. The tumor characteristically does not show areas of keratinization. Admixed with this epidermoid component, there is the presence of mucous producing cells the so-called mucocytes [224] (Fig. 1.55a–c). In the cases described, the tumors have been of the low grade type of malignancy, thus, increased mitotic activity, necrosis, and hemorrhage have not been part of the tumor. By immunohistochemistry, the tumor cells may show positive staining for p63, p40, keratin 5/6, broad-spectrum keratin, and epithelial membrane antigen. Currently, the use of molecular studies such as MAML may help in difficult cases in which the histology may not be representative. Due to the limited number of cases reported, it is very difficult to determine the outcome of these patients; however, since the tumors described have been of the low grade, it is possible that surgical resection is the treatment

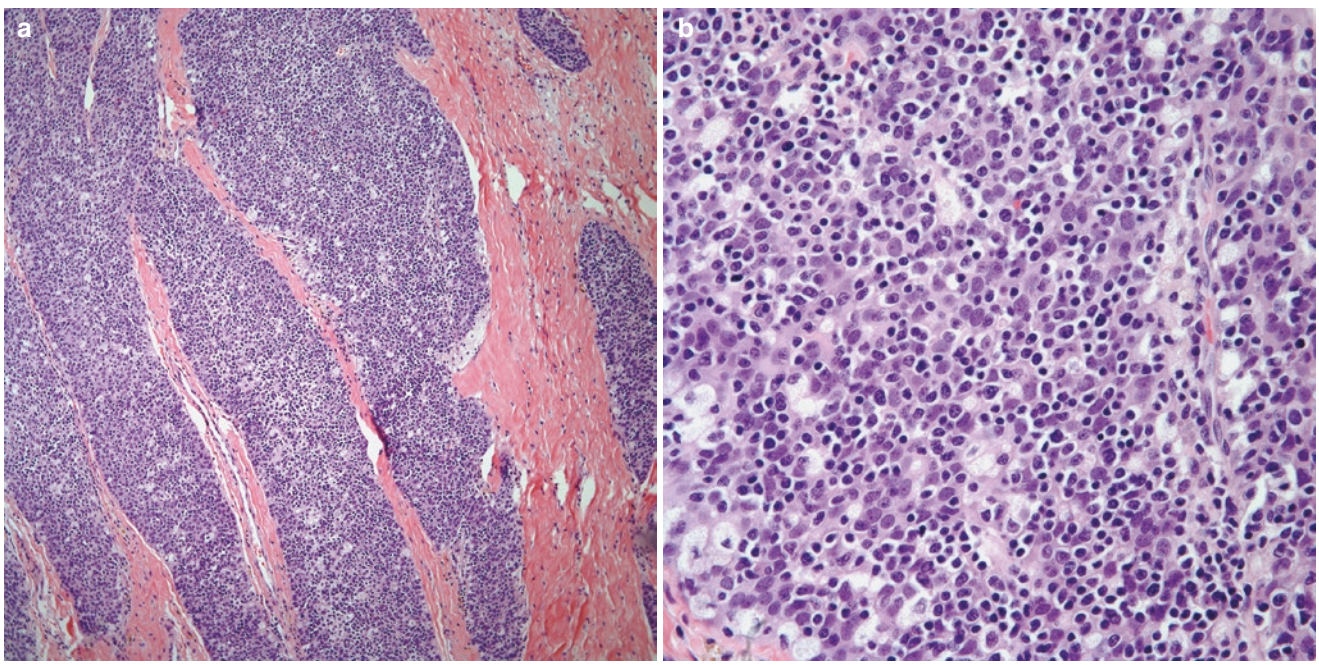


**Fig. 1.54** (**a**) Low power view of a pleural-based thymoma, (**b**) higher magnification showing the conventional biphasic cellular proliferation of epithelial cells admixed with lymphocytes

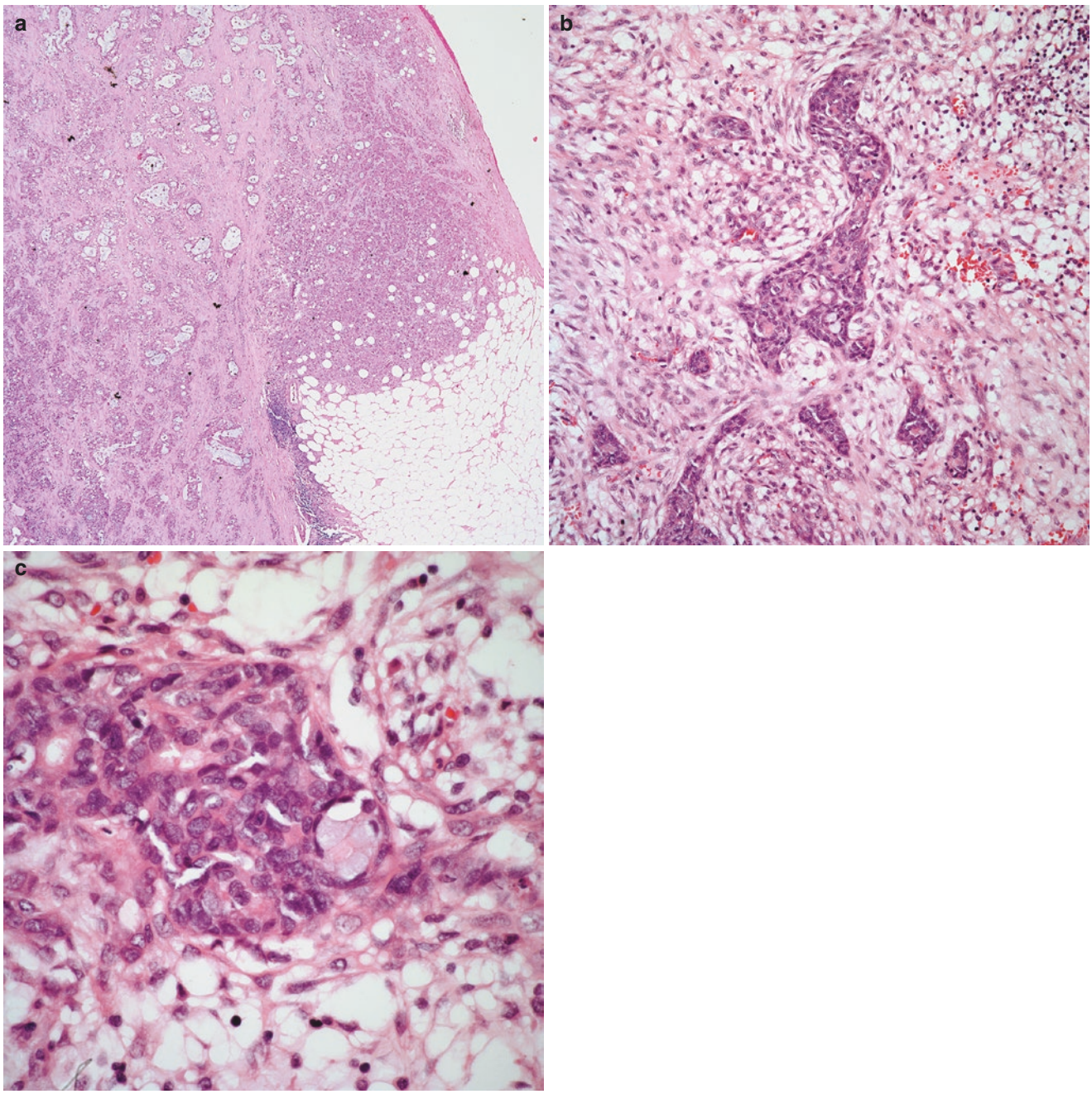


**Fig. 1.55** (**a**) Low power view of a pleural MEC infiltrating adipose tissue, (**b**) pleural MEC with epidermoid component, (**c**) pleural MEC showing the epidermoid component admixed with mucous secreting cells

of choice and that the clinical follow-up be similar to those tumors in the lung or salivary glands.

### Epithelial-Myoepithelial Carcinoma

Similar to MEC, this tumor is more common in the salivary glands but it has also been described in the mediastinum and in the lung. The occurrence of this tumor as a pleural-based neoplasm is rare [225]. The symptomatology of these patients is nonspecific and by diagnostic imaging the tumor presents as a pleural-based neoplasm. Histologically, the tumor shows similar features as their counterparts in the lung or salivary glands. Essentially, the tumor is composed of a glandular proliferation in the form of ducts or tubules that shows two layers of cells—inner layer (epithelial) and an outer layer with clear cells features (myoepithelial) (Fig. 1.56a, b). By immunohistochemistry, the tumor will show myoepithelial differentiation that can be highlighted by positive staining for keratin, S-100 protein, and smooth muscle actin. Similar to pleural MEC, the number of cases reported is too small to provide meaningful clinical outcome.

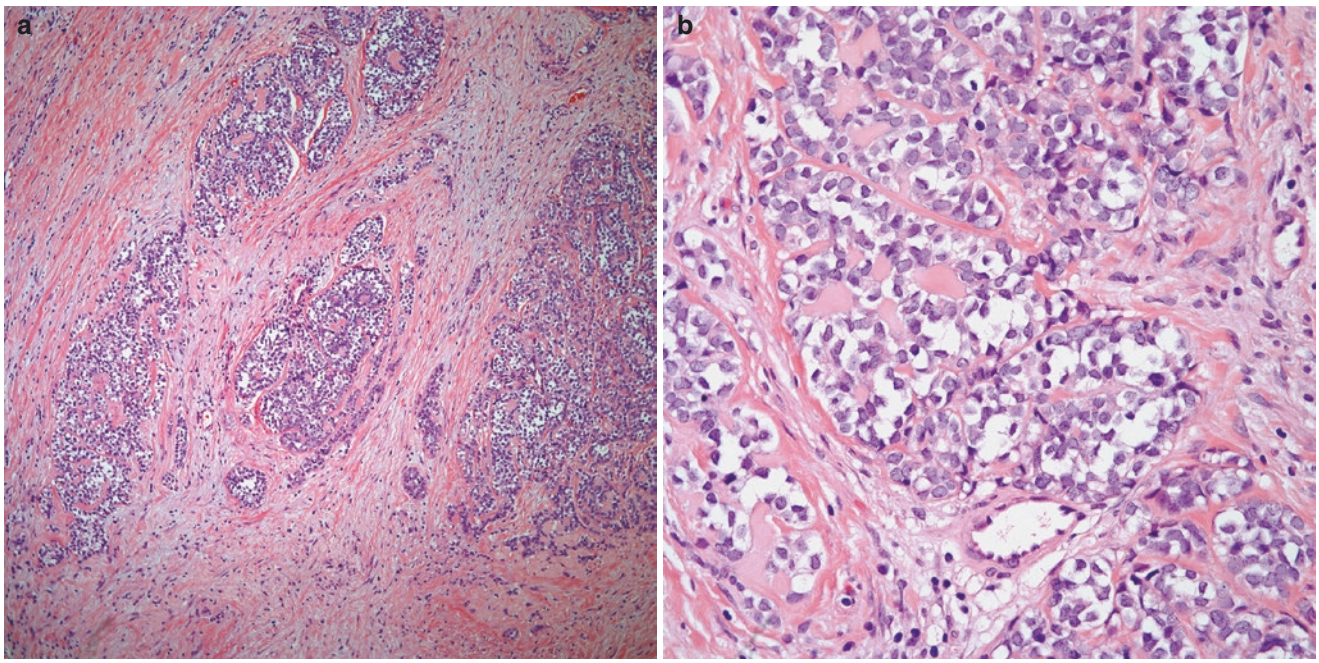


**Fig. 1.56** (**a**) Low power view of a pleural epithelial-myoepithelial carcinoma showing a cellular proliferation with clear cytoplasmic features, (**b**) closer view at the glandular component showing clear cell (myoepithelial) cells

## Solitary Fibrous Tumor

Solitary fibrous tumors (SFTs) are neoplasms of fibroblastic mesenchymal origin that were historically recognized as pleural tumors, but are now known to occur at every anatomical site, albeit with a peculiar predilection for body cavities, including the pleura [226]. Although SFTs are classified as benign, they may be locally aggressive and exhibit potential for malignant transformation [227]. A variety of names have been used to describe these tumors, including hemangiopericytoma, benign mesothelioma, solitary fibrous mesothelioma, and pleural fibroma. With the evolution of our understanding of the histopathologic characteristics of these tumors, the different names have been subsumed under the term "SFT." SFTs arising from the pleura account for less than 5% of primary pleural tumors, with an estimated frequency of 2.8 per 100,000 individuals [228–231].

SFTs are most common in the fifth to seventh decades but may occur at any age. Men and women are affected with equal frequency [232, 233]. There is no known association with environmental exposure to radiation, tobacco, asbestos, or other toxicants, and no known inherited predisposing risk factors [232]. Approximately 40–60% of patients have nonspecific pulmonary symptoms of cough, shortness of breath, or chest pain caused by mass effect on adjacent intrathoracic structures [229, 234]. A sensation of a mass moving within the chest has also been described [235, 236]. Alternatively, the lesions may present with an indolent course associated with slowly enlarging painless masses in asymptomatic individuals [226]. Rarely, hemoptysis and obstructive pneumonitis may occur as a result of airway obstruction. Metastases can cause a wide variety of extrathoracic manifestations [229]. As many as 20% of pleuropulmonary SFTs may be associated with paraneoplastic syndromes. Doege-Potter syndrome has been described, characterized by intractable paraneoplastic hypoglycemia due to tumor secretion of insulin-like growth factor 2 [236, 237]. Secondary hypertrophic osteoarthropathy may also occur and is signaled by a triad of digital clubbing, hypertrophic skin changes, and periosteal bone changes [229, 237–240].

Large amounts of tissue obtained from complete resection of the lesion are required for adequate histopathologic evaluation. Fine needle aspiration biopsies are often insufficiently cellular and are not recommended for diagnosis. In most cases, core biopsy provides adequate material to establish a diagnosis of SFT, but the limited sampling provided by this diagnostic technique may not accurately demonstrate the histologic evidence indicative of high-risk aggressive behavior.

In light of the potential for recurrence or malignant transformation, complete surgical resection is recommended [241]. The efficacy of radiotherapy and conventional chemotherapeutic agents in this setting is limited. Associated paraneoplastic syndromes may completely resolve following complete surgical resection. Prognosis is generally favorable. Pedunculated and benign tumors are less likely

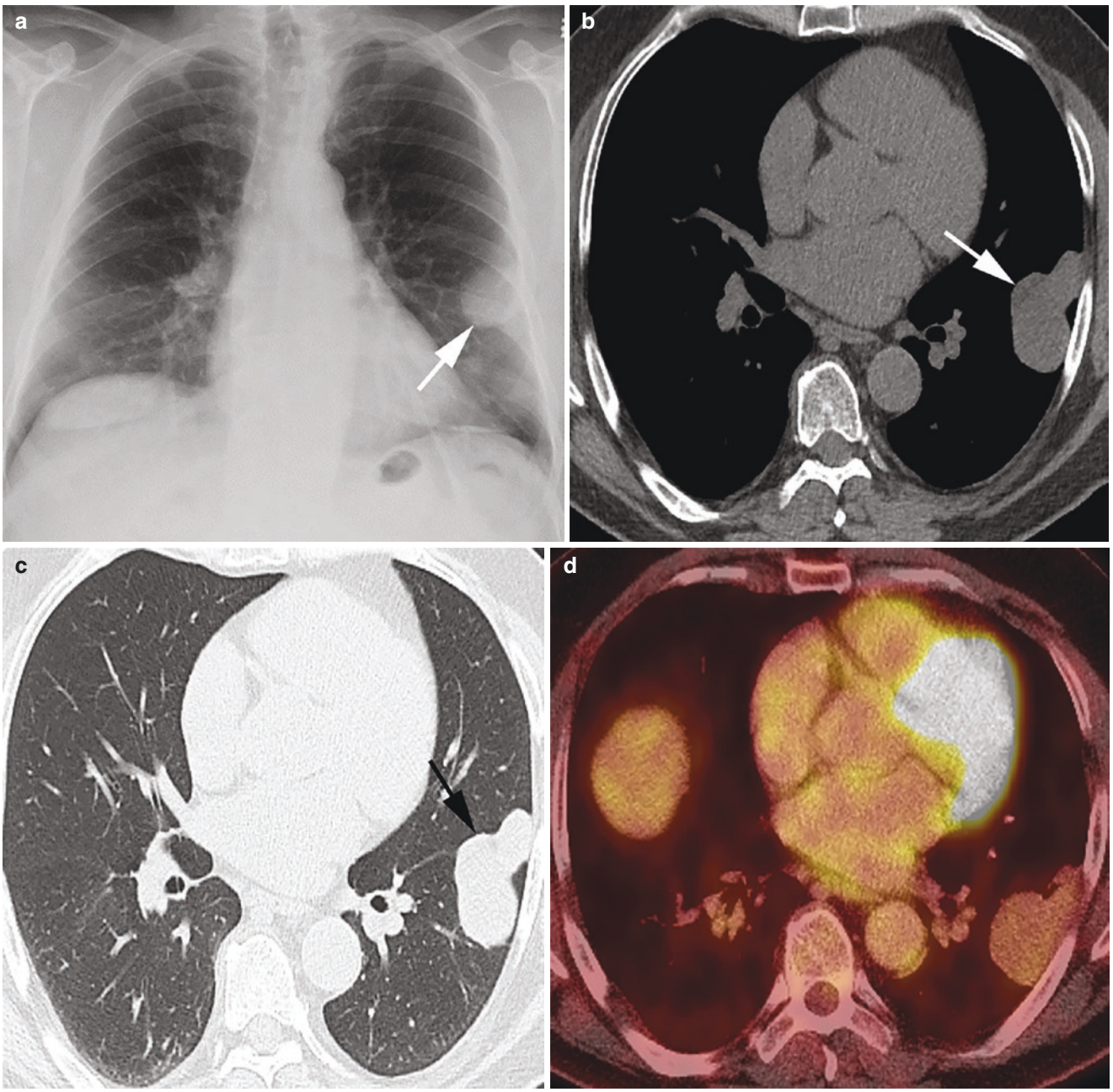


**Fig. 1.57** (**a**) Frontal chest radiograph shows well-defined mass in the left lower hemithorax abutting the lateral pleura (arrow), (**b**, **c**) axial CT in soft tissue and lung windows show homogeneous soft tissue mass (arrow) in the left lower hemithorax along the left major fissure, (**d**) axial FDG PET/CT shows the left pleural mass is not FDG-avid

to recur; however, routine imaging surveillance with annual chest radiographs is recommended, as there is a high risk of local recurrence following resection of a malignant sessile SFT [233]. For postoperative surveillance of malignant SFT, biannual CT follow-up has been suggested for the first 2 years followed by annual CT examinations thereafter [226–240, 242].

SFT of the pleura usually appears as well-defined, rounded, or oval-shaped opacities on chest radiography (Fig. 1.57a–d). Pedunculated tumors have been reported to show a change in shape with change in patient position [243]. CT appearance can vary depending upon the size of the tumor. Small tumors usually have a semilunar shape, form obtuse angles with the pleura, and demonstrate homogeneous enhancement [244]. Medium to large tumors tend to be more ovoid, form acute angles with the pleura, and show heterogeneous enhancement with central areas of low attenuation that correspond to necrosis and/or myxoid degeneration. Prominent intratumoral blood vessels can be seen with large tumors (Fig. 1.58a–c) [245–247]. SFT can cause mass effect

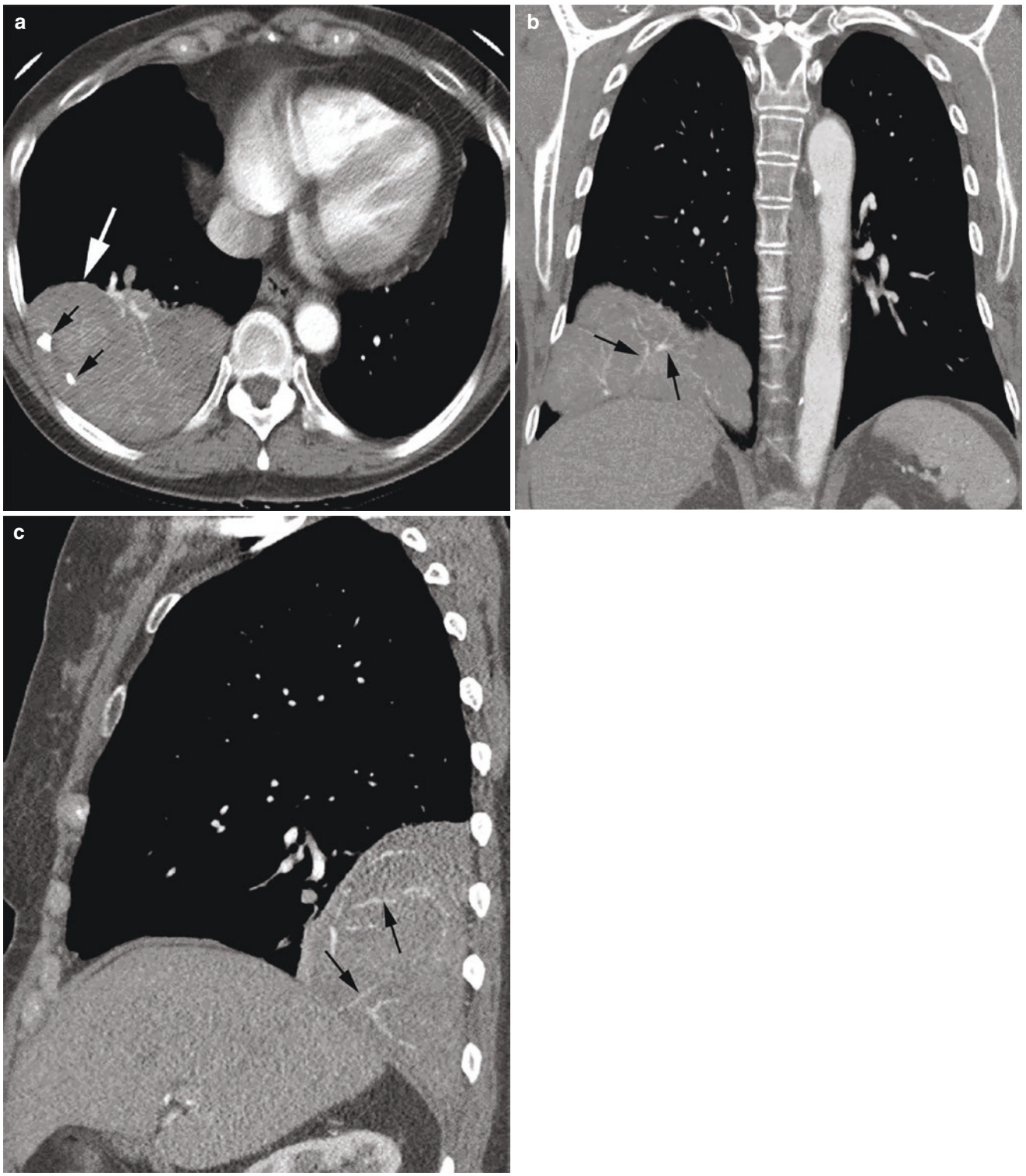


**Fig. 1.58** (**a**) Axial CT shows peripheral soft tissue mass (big arrow) in the right lower hemithorax with foci of calcification (small arrows), (**b**, **c**) coronal and sagittal CT reformations show prominent vessels within the mass (arrows)

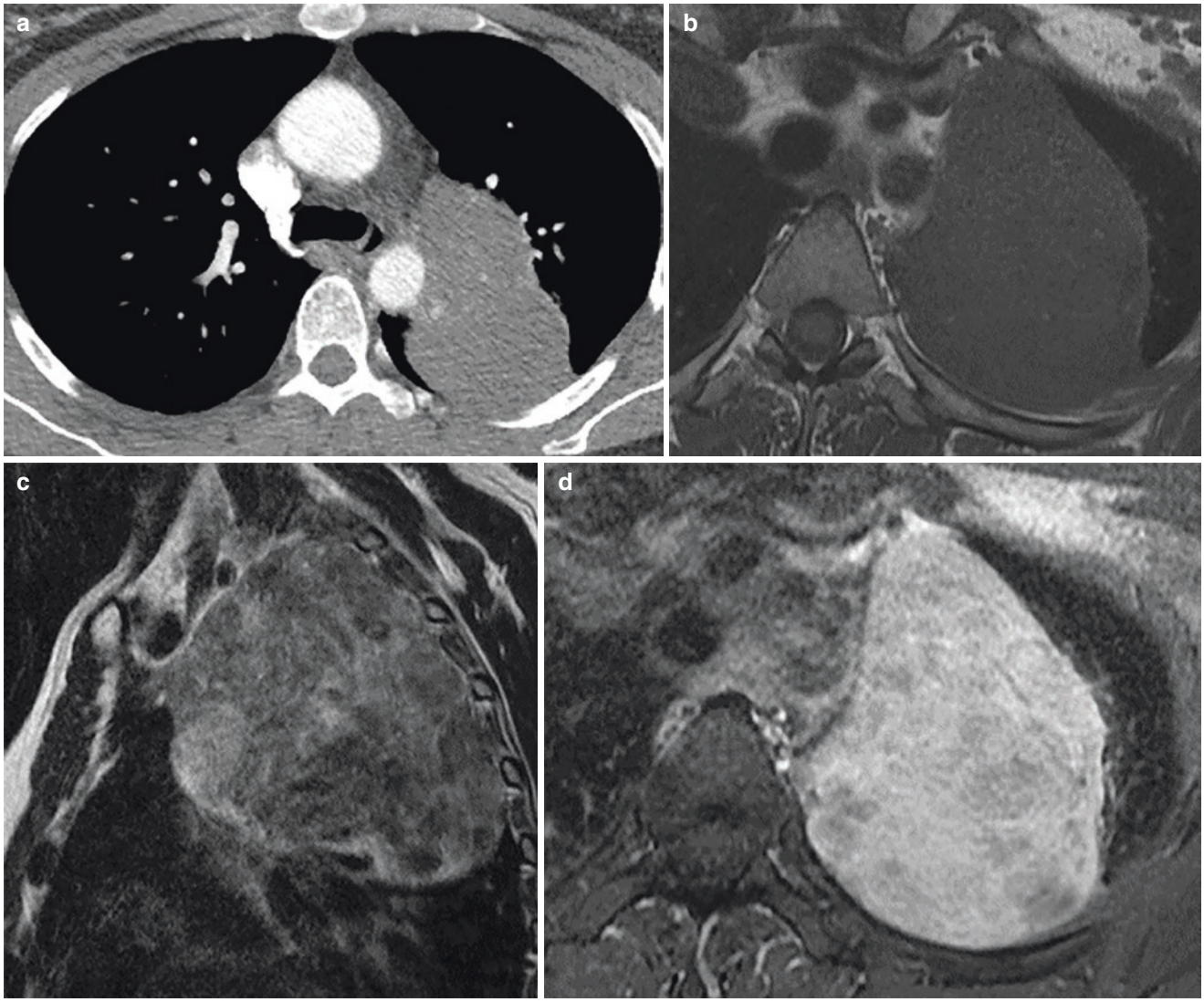


**Fig. 1.59** (**a**) Axial CT shows homogeneous soft tissue mass in the posterior left upper hemithorax along the oblique fissure, (**b**) axial T1-weighted MRI shows the mass has low signal intensity, (**c**) sagittal T2-weighted MRI shows the mass has heterogeneous high signal intensity, (**d**) contrast-enhanced axial T1-weighted MRI shows intense homogeneous enhancement of the tumor

on the adjacent lung parenchyma or mediastinal structures rather than invasion of these structures. Usually, no locoregional lymphadenopathy is seen. Calcification is uncommon, occurring in less than 10% of cases and more frequently seen in larger tumors. Associated pleural effusions are seen in up to 20% of cases [248, 249]. On MR imaging, these tumors demonstrate low to intermediate signal intensity on both T1-weighted and T2-weighted images due to the presence of fibrous tissue [250, 251]. Heterogeneous T2 hyperintensity is often present and likely due to necrosis and cystic or myxoid degeneration [252]. Low signal intensity internal septations can also be visualized on T2-weighted images. Intense homogeneous or heterogeneous enhancement is seen with administration of intravenous gadolinium depending upon the size of the tumors [249, 253] (Fig. 1.59a–d). Several studies have attempted to distinguish benign and malignant SFT on the basis of radiological appearance. The imaging findings that favor malignant SFT include large tumor size, heterogeneous density, abundant intratumoral blood vessels, presence of internal calcification, and ipsilateral pleural effusion [254, 255]. On FDG-PET/CT, the SUV of the malignant SFT is higher than that of benign SFT but relatively low compared to other malignancies, such as metastasis from primary lung cancer or primary pleural sarcoma (Fig. 1.60a–c). FDG-PET can be a valuable diagnostic tool in differentiating SFT from other malignant conditions [233, 241, 242, 256].

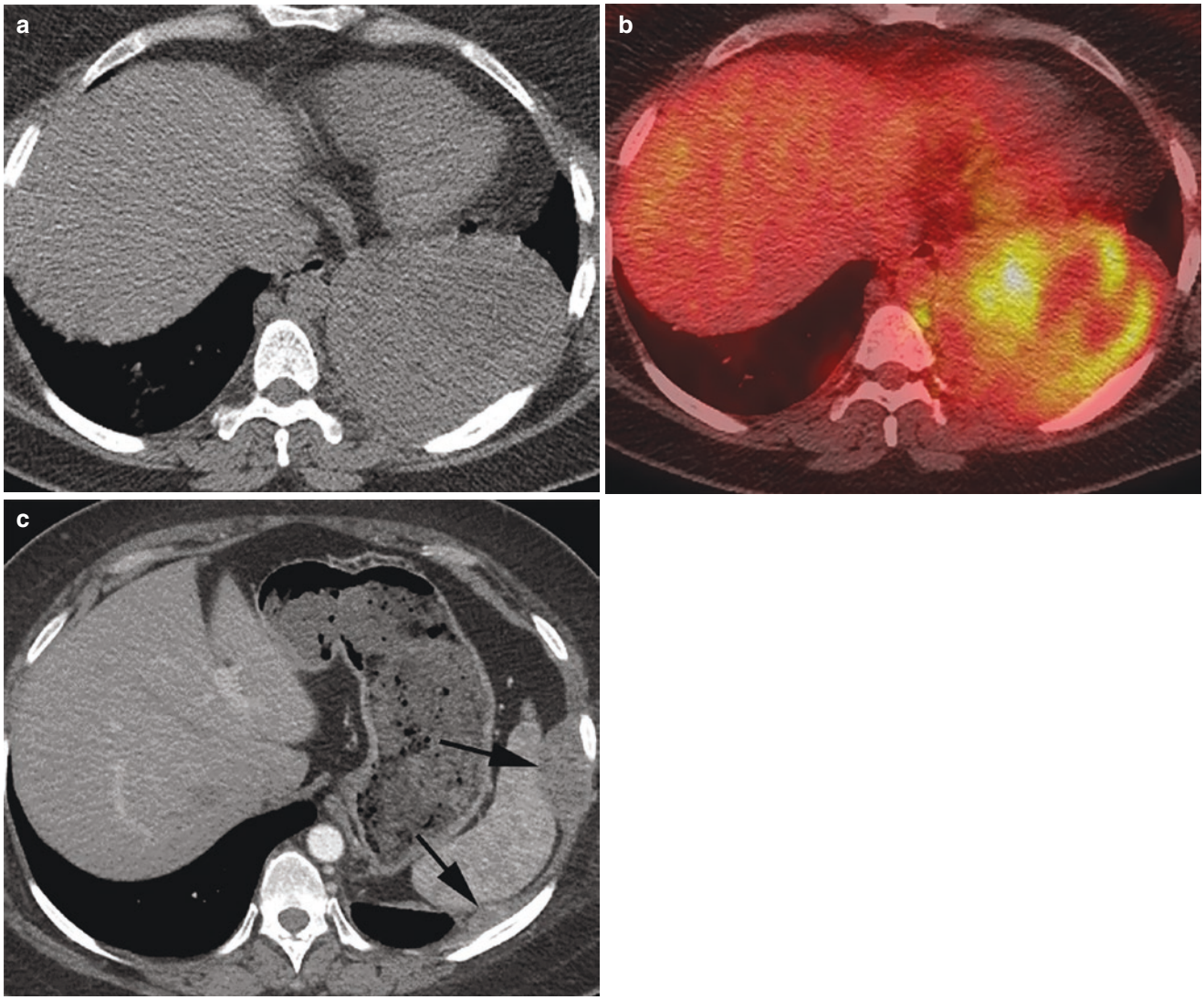


**Fig. 1.60** (**a**) Axial CT shows soft tissue mass in the left lower hemithorax, (**b**) axial FDG PET/CT shows FDG avidity within the mass, (**c**) contrast-enhanced CT 1 year after resection shows new nodules along the left diaphragmatic pleura arrows) consistent with tumor recurrence. One left pleural tumor indents the lateral border of the spleen

## Pathological Features

### Macroscopic Features

The tumors are commonly well circumscribed but not encapsulated (Fig. 1.61). At cut surface the tumors are usually light tan in color with a whorled appearance and rubbery consistency. If areas of hemorrhage and necrosis are present in these tumors, those are considered to represent features associated with malignancy or aggressiveness. These tumors may reach larger size of over 20 cm in greatest diameter. Generally they are solid but in rare occasions the tumor may also show cystic changes.


**Fig. 1.61** SFT attached to the visceral pleura with a wedge of lung parenchyma

### Histological Features

The versatility of growth pattern in SFT is well known and has been described in detail [257]. Essentially, the tumor may

show features similar to those described in other spindle cell tumors such as hemangiopericytoma, angiofibroma, synovial sarcoma, neural type of tumors, and fibrosarcoma, among others (Fig. 1.62a–i) [257]. However, one of the most common growth patterns is characterized by a bland spindle cell proliferation in which the tumor may show hypo and hyper cellular areas admixed with extensive collagenization. The spindle cell component appears to be dissecting fibrocollagen given the appearance of the so-called "ropy collage." Also, an important component of these tumors is the presence of dilated vascular spaces alternating with the spindle cell proliferation, similar to that described in vascular tumors such as hemagiopericytoma. In the description of 223 cases by England and Hochholzer [234], the authors separated these tumors into benign and malignant based on the presence of hemorrhage, necrosis, cellular pleomorphism, and mitotic

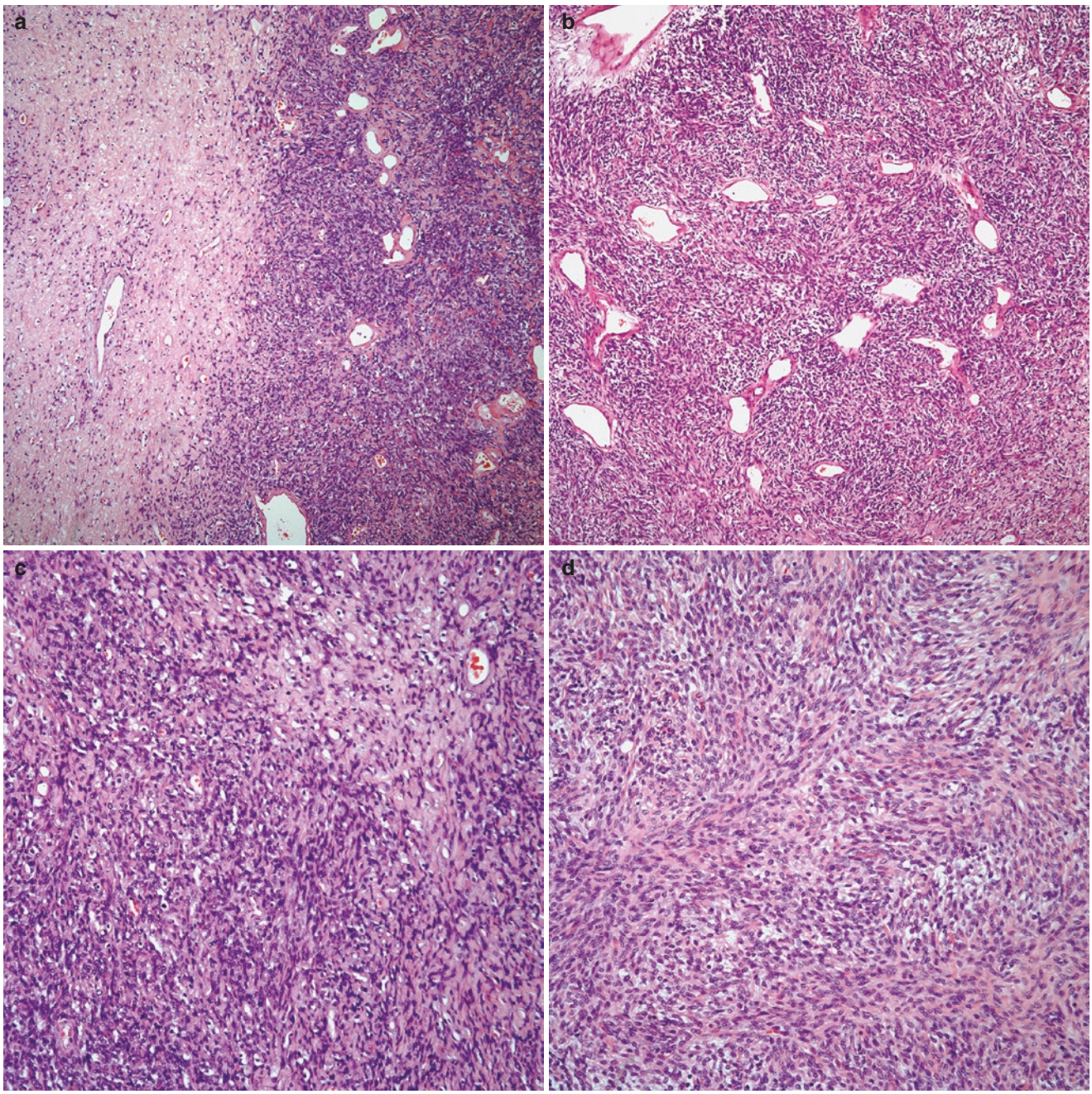


**Fig. 1.62** (**a**) SFT showing hypo- and hypercellular areas, (**b**) SFT showing a hemangiopericytic growth pattern; (**c**) SFT with solid spindle cell proliferation, (**d**) SFT with fibrosarcoma-like pattern, (**e**) SFT with solid epithelioid-like growth pattern, (**f**) SFT showing mitotic activity, (**g**) SFT with more subtle spindle cell proliferation and fibrocollagen (**h**) SFT with more angiofibromatous areas, (**i**) SFT showing the characteristic ropy collagen

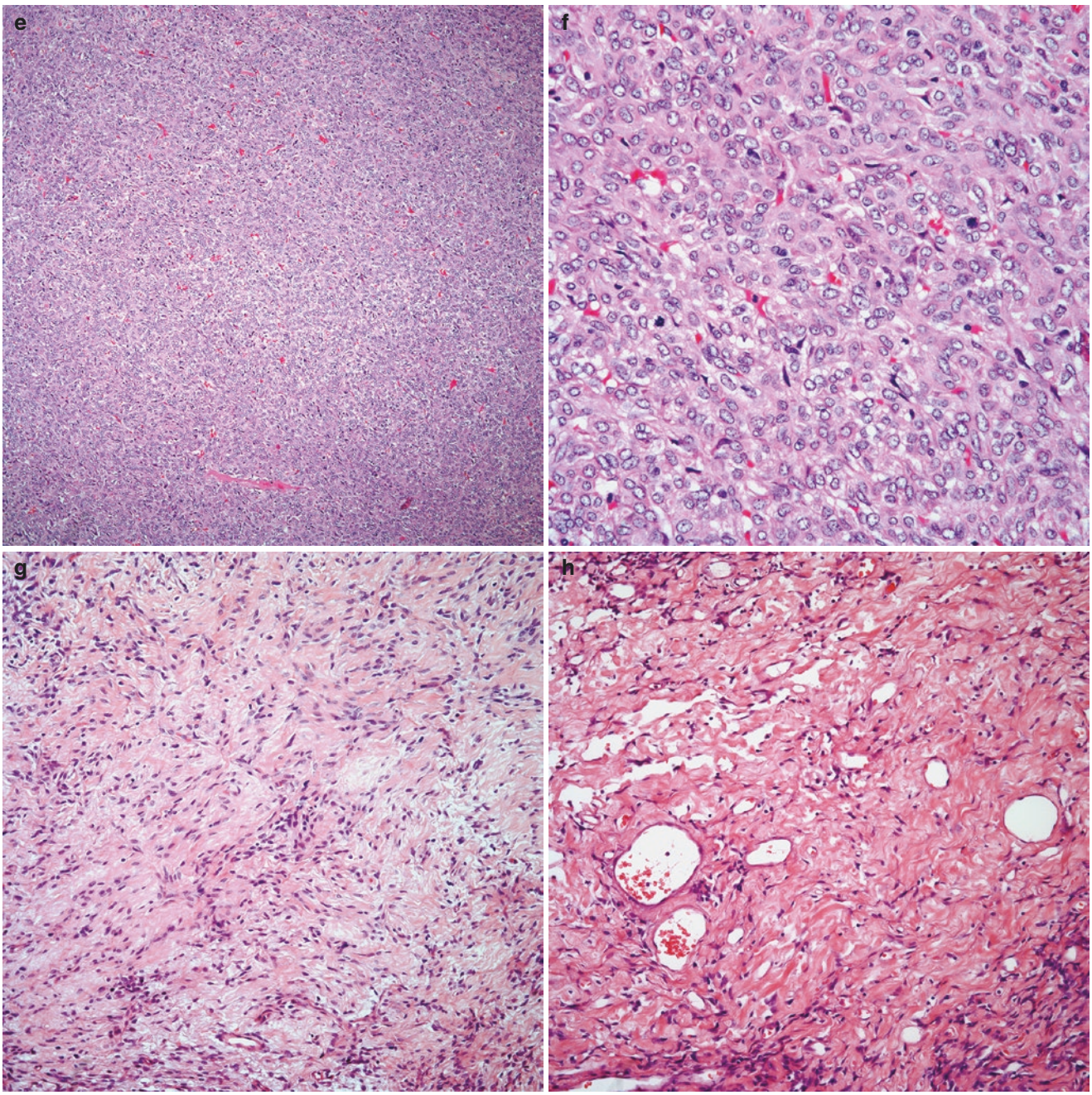


**Fig. 1.62** (continued)

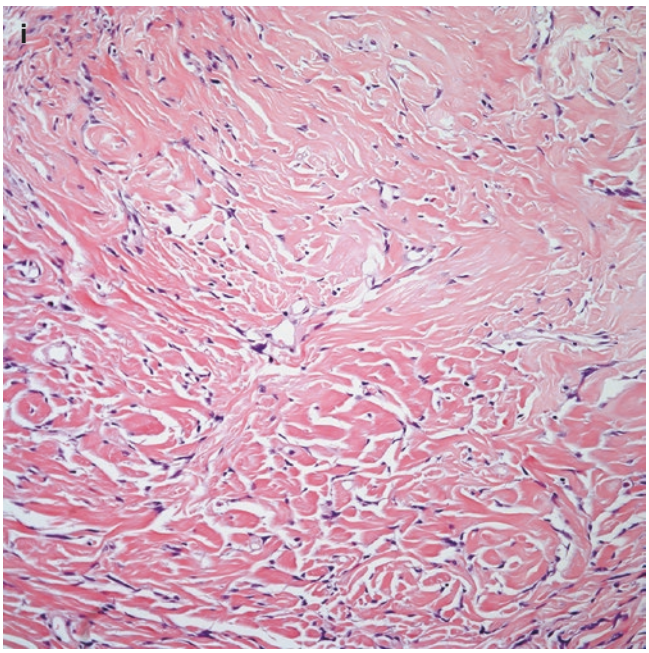


**Fig. 1.62** (continued)

activity [234]. This latter feature was established as >4 mitotic figures per 10 high power fields in cases that were considered malignant. Of the 223 cases described 82 were classified as malignant. Even though there has been mentioned that size of the tumor is an important factor in clinical behavior of these tumors, the problem is that size of the tumor and histological features do not necessarily correlate; therefore, the histological parameters are the ones more commonly associated with clinical outcome. Nevertheless, larger tumors are likely to invade adjacent organs and become locally aggressive.

### Immunohistochemical Features

More recently the use of immunohistochemical stains has become an important tool in the diagnosis of SFT mainly in those cases that do not show the conventional features of the tumor. In that regard, the most reliable stain appears to be STAT-6 [258–260], which shows nuclear staining in tumor cells. This immunostain appears to consistently stain more than 90% of these tumors. However, it is also important to highlight that SFT may also show positive staining for vimentin, Bcl-2, CD-34, and CD99 (Fig. 1.63a–d), while in general SFT is negative for epithelial markers such as keratin and EMA, even though in some cases weak focal staining may be present.

## Desmoid Tumor

Desmoid tumors are unusual, locally aggressive fibrous neoplasms that arise from fascia at any anatomical site in the body. Intra-abdominal sites comprise 50% of desmoid tumors. The most common extra-abdominal sites include the chest wall, shoulder girdle, inguinal region, and head and neck [261]. Desmoid tumors in the chest wall usually present as a palpable mass with occasional extension into the pleura. The estimated incidence of desmoid tumors in the general population is 2–4 cases per million per year. These tumors most commonly occur in the third and fourth decades, but may occur at any age. Racial and ethnic groups are not disproportionally affected [262, 263]. There is no gender predilection [264]. The etiology of desmoid tumors is unclear but several commonly associated factors have been identified. There is a significant association with previous trauma in up to 25% of patients [265]. Desmoid tumor occurs frequently in patients with familial adenomatous polyposis, especially Gardner syndrome [266].

The majority of desmoid tumors are asymptomatic masses detected as incidental finding on imaging. Symptoms vary with the location of the tumor. Chest pain owing to nerve involvement, dyspnea, and pleural effusion are common presenting symptoms [264].

Incisional biopsies offer larger tissue samples and are preferred over core needle biopsies. Wide surgical resection is the treatment of choice with radiotherapy reserved for patients in whom wide local excision cannot be accomplished or surgical resection is not feasible. Local recurrence despite aggressive surgical intervention occurs in 29% of patients. The overall prognosis is good, with a 5-year survival rate of 93% [267].

Most desmoid tumors of the thorax originate from the chest wall and imaging shows a soft tissue mass (Fig. 1.64a–d). True intrathoracic desmoid tumors originating within the pleura or mediastinum with minimal chest wall involvement are exceedingly rare [268]. Intrapleural tumors are often significantly larger at the time of diagnosis due to the lack of symptoms. The most common intrathoracic tumors resembling desmoid tumors are solitary fibrous tumors. They are indistinguishable on preoperative radiologic imaging. Solitary fibrous tumors generally are not as invasive as desmoid tumors and are differentiated on histopathologic criteria [267–269].

### Pathological Features

#### Macroscopic Features

These tumors have been described as white in color and firm consistency. Based on the cases that have been reported in the pleura, the tumor may involve the visceral and parietal pleura and the size of the tumor may range from a few centimeters to more than 10 cm in greatest diameter. The presence of marked areas of necrosis and hemorrhage is not common in these tumors. The tumors are not encapsulated but rather show infiltrative features.

#### Histological Features

The same as desmoid tumors in other locations, those described in the pleura share similar histological features.

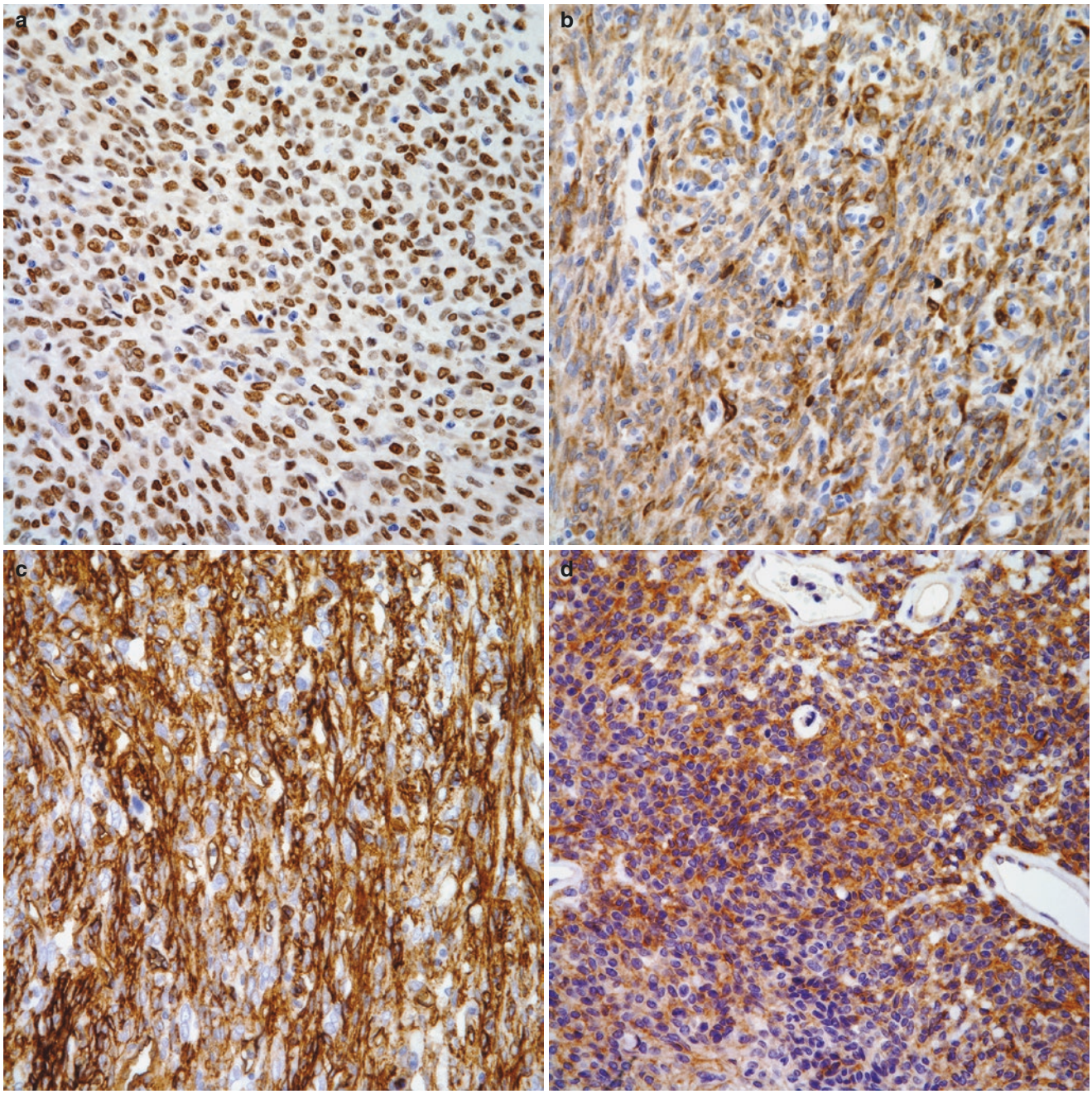


**Fig. 1.63** (**a**) Immunohistochemical stain for STAT-6 showing positive nuclear staining, (**b**) immunohistochemical stain for Bcl-2 showing positive staining in tumor cells, (**c**) immunohistochemical stain for CD-34 showing positive staining in tumor cells, (**d**) Immunohistochemical stain for CD-99 showing positive staining in tumor cells

The tumor characteristically shows fascicles of spindle cells with tapered, wavy to elongated nuclei, embedded in finely fibrillary matrix with numerous vessels. Nuclear atypia and mitotic activity are not common in these tumors (Fig. 1.65a–c).

### Immunohistochemical Features

In cases reported in the pleura or in other locations, desmoid tumor may show positive staining for vimentin, desmin smooth muscle actin, cyclin D1, and beta-catenin, but negative for S-100 protein [269, 270]. More importantly, the use of STAT-6 becomes very important in separating desmoid tumors from SFT.

## Calcifying Fibrous Tumor

Calcifying fibrous tumors (CFT) are rare benign tumors of mesenchymal origin, which ubiquitously localize to the soft tissues, extremities and, rarely, the pleura. The stomach is

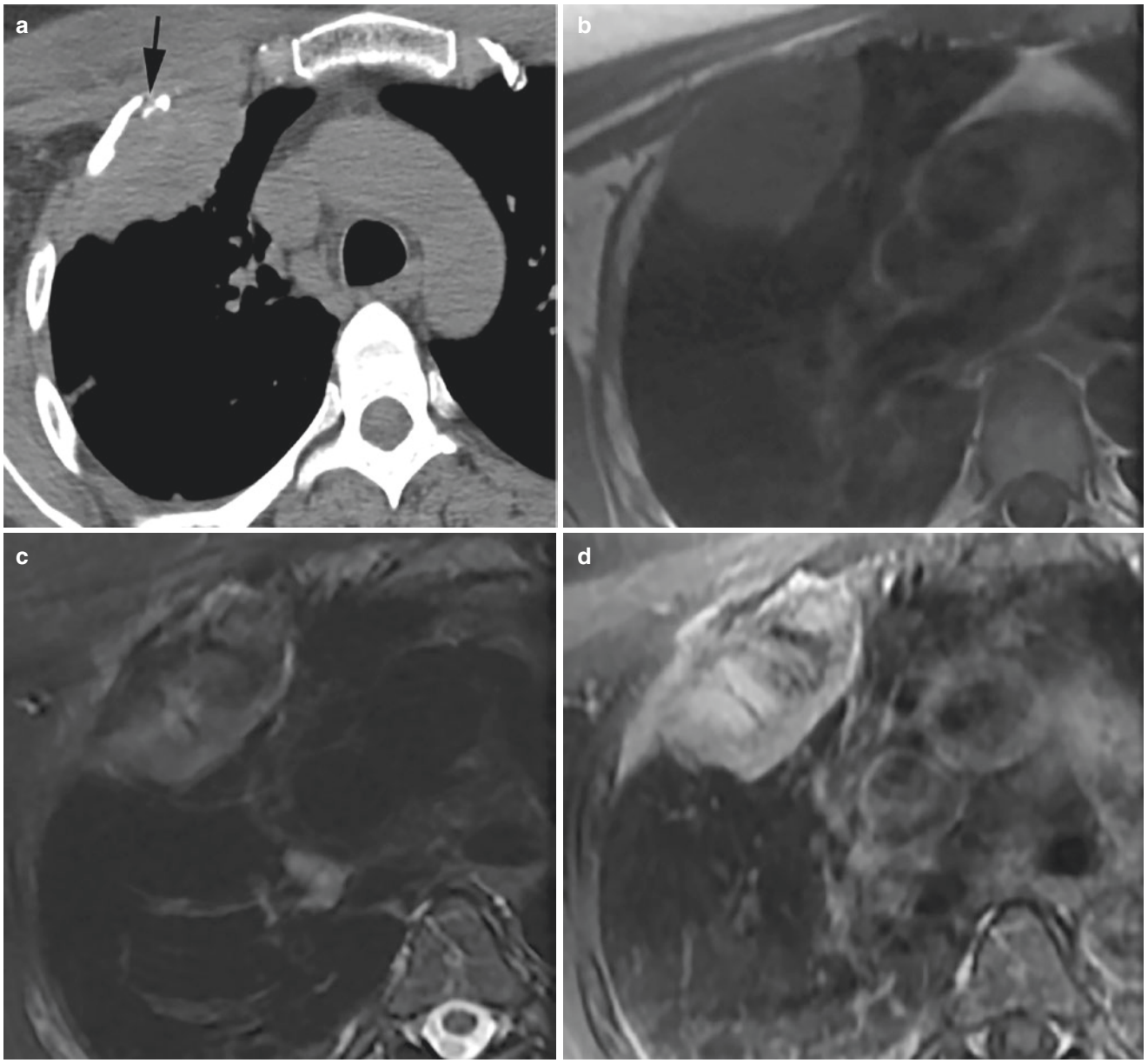


**Fig. 1.64** Desmoid tumor. (**a**) Axial CT shows peripheral soft tissue mass in the right anterior pleura with adjacent rib erosion (arrow), (**b**) axial T1-weighted MRI shows the mass has low signal intensity, (**c**) axial T2-weighted MRI shows the mass has heterogeneous high signal intensity, (**d**) contrast-enhanced axial T1-weighted MRI shows heterogeneous enhancement of the tumor

the most common soft tissue site. Pleural tumors are seen in 10% of cases [271].

There are no known etiologic factors [271]. A slight female predilection (ratio 1:1.27), and trimodal age distribution, with the first peak at 0–4 years, and a second and third peak in the mid second and third decades of life have been reported [271]. Each age distribution may reflect different pathogenic phenotypes, with the third spike representing a form of late sclerosing myofibroblastic tumor [272–274]. Genetic and/or embryologic factors are postulated in the pathogenesis of childhood calcifying fibrous tumors, while trauma may underlie the development of early adulthood tumors [275–277].

In the majority of patients, calcifying fibrous tumors are identified as an incidental finding on imaging studies in asymptomatic patients. Occasionally, chest pain and nonproductive cough are presenting symptoms. The differential diagnosis varies with the location. An extensive list of benign and malignant disorders share clinical and/or morphologic features with calcifying fibrous tumors and include fibromatosis, solitary fibrous tumor (SFT), chronic fibrous pleuritis, calcified granulomas, calcified pleural plaques, dendrocytoma, desmoplastic mesothelioma, inflammatory myofibroblastic tumor (IMT), intermediate fibrous histiocytoma, and amyloid tumor. Biopsy is needed to confirm the diagnosis. Surgical resection is the treatment of choice and is usually curative. Recurrent disease is unusual but has been reported in non-pleural CFT and overall prognosis is excellent [271].

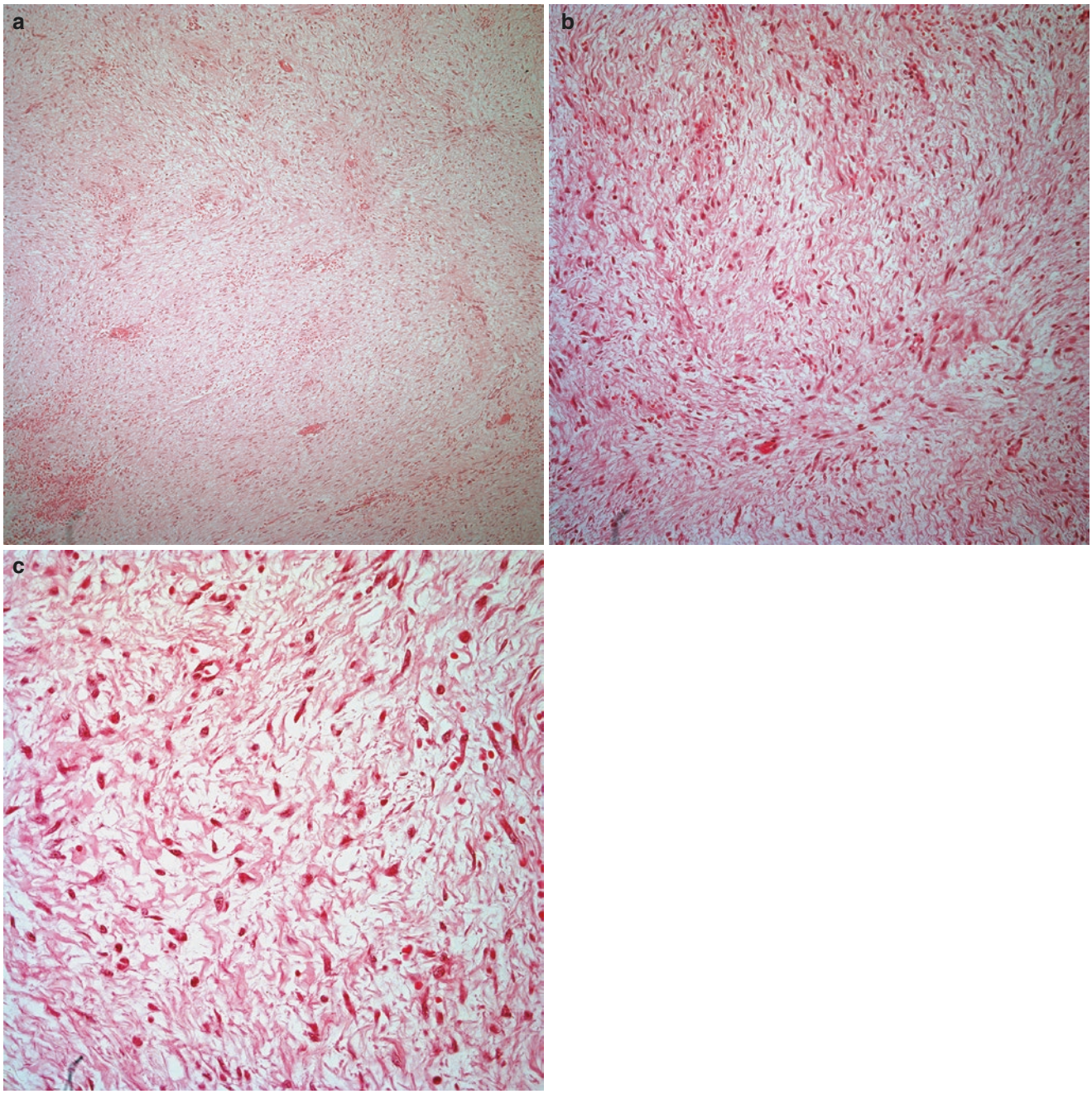


**Fig. 1.65** (**a**) Desmoid tumor of the pleura showing a spindle cell proliferation embedded in a loose stroma, (**b**) haphazard distribution of the spindle cell proliferation in a fibrillary matrix, (**c**) higher magnification of the spindle cell proliferation lacking nuclear atypia and mitotic activity

## Pathological Features

### Macroscopic Features

Up to 10% of all CFTs have been reported in the pleura [271]. Calcifying fibrous tumor of the pleura is generally a solitary nonencapsulated, well-circumscribed, solid mass but it may present with multiple nodules [278].

### Histological Features

The hallmark of these tumors is the presence of extensive areas of collagenization with an associated bland spindle cell proliferation and the presence of scattered calcifications of different sizes (Fig. 1.66a–d). Inflammatory reaction composed of lymphocytes and plasma cells may be seen but it is not marked. Nuclear atypia, increased mitotic activity, areas

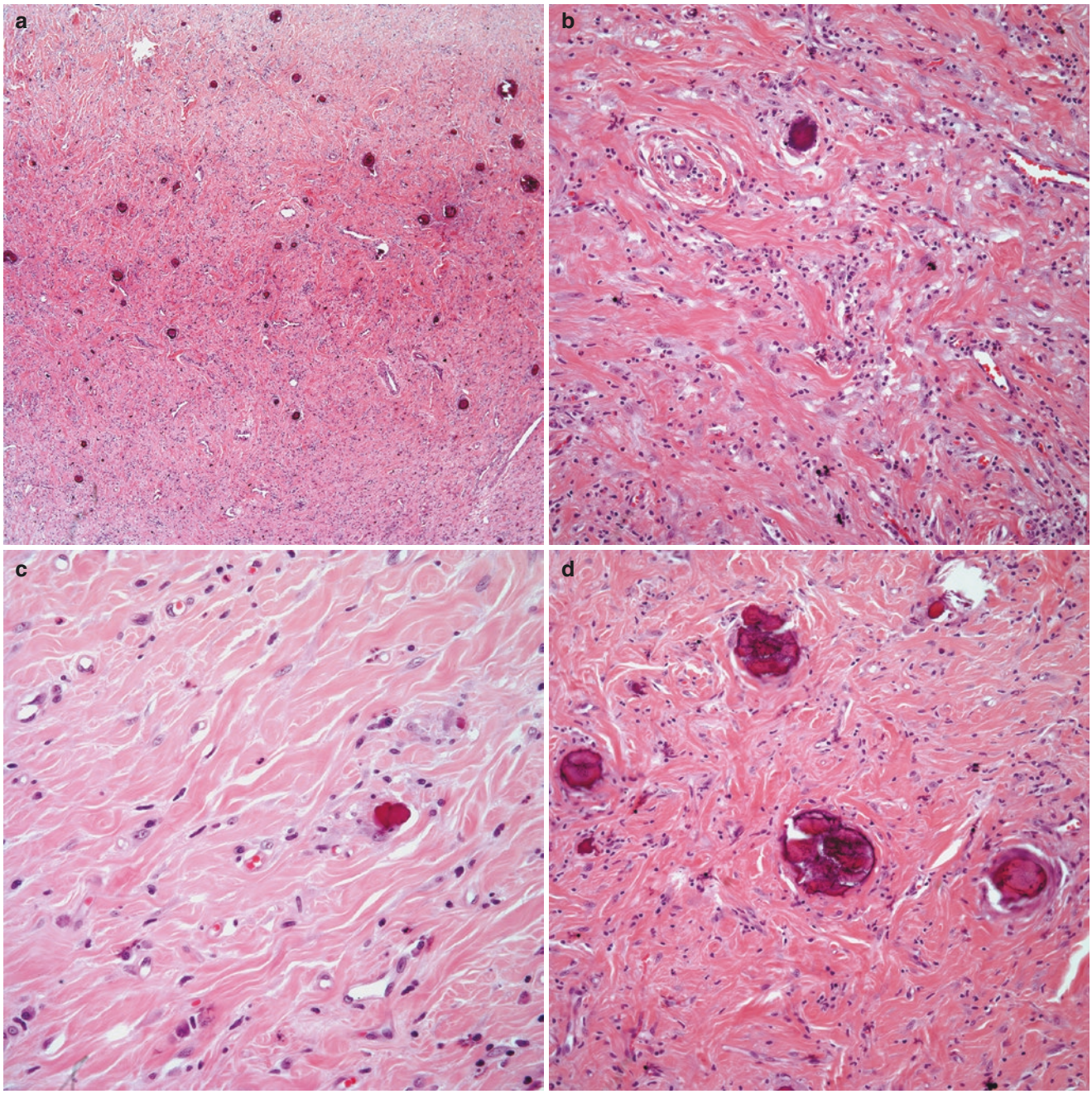


**Fig. 1.66** (**a**) Low power view of a pleural Calcifying Fibrous Tumor (CFT) showing numerous calcifications, (**b**) the tumor may show focal calcifications and inflammatory reaction, (**c**) focal calcifications with areas resembling SFT, (**d**) conventional areas of CFT showing collagenization and numerous calcifications

of necrosis and hemorrhage are generally absent in these tumors. In general terms, without the presence of calcification, the histological features of this tumor mimic closely those of SFT. Therefore, the need for immunohistochemical stains properly categorized the tumor.

### Immunohistochemical Features

Because the histological features of this tumor mimic those of SFT, the main goal is to separate both neoplasms. In that regard, calcifying fibrous tumors should show negative staining for CD-34 and for STAT-6 that are commonly associated with SFT. In general, calcifying fibrous tumor is also negative for epithelial markers such keratin and EMA and also has been found negative for muscle markers such as smooth muscle actin, desmin, and h-caldesmon. D2–40, which is a vascular marker has also been reported as negative. However, it is important to highlight that the majority of these tumors have been reported prior to the discovery of STAT-6; therefore, even though one would expect negative results for calcifying fibrous tumor, it is uncertain at this point.

## Vascular Neoplasms

Vascular tumors that have been most frequently identified as primary pleural neoplasms are epithelioid hemangioendothelioma and angiosarcoma. These two neoplasms share similar morphohistologic and immunohistochemical phenotypes and are distinguished by the presence of necrosis, nuclear atypia, and increased mitotic activity on resected tissue. Molecular tools can also aid in the final classification of these tumors. Because of the similarities between these two tumors, histology, immunohistochemistry, and molecular diagnosis will be presented together.

### Epithelioid Hemangioendothelioma

Epithelioid hemangioendothelioma (EHE) is a rare vascular tumor that may arise in soft tissue, bone, and other organs throughout the body. Intrathoracic tumors involving the lung, pleura, and mediastinum have been described. Primary pleural epithelioid hemangioendothelioma (PEH) appears to be more aggressive than EHE tumors at other locations (including pulmonary EHE) with poor clinical outcomes [279, 280]. Epidemiologic data for these rare tumors are limited to case reports and case series and risk factors have not been well defined. However, limited information suggests a male predominance with an average age of 52 years at diagnosis. Loose associations with asbestos and radiation exposure have been suggested [279, 281–284]. Nonspecific symptoms of dyspnea, chest pain, cough, and fever are the most common at presentation. Back pain associated with extensive pleural disease has also been reported. These tumors may be widely metastatic at diagnosis, resulting in a variety of clinical symptoms. The diagnosis of PEH requires histopathological examination of specimens derived preferably from thoracoscopic pleural biopsies. Poor prognosticators include the presence of respiratory symptoms or pleural effusion at presentation, fibrous/fibrinous pleuritis with extrapleural extensive intravascular, endobronchial, or interstitial tumor spread, distant metastases to the liver and peripheral lymph nodes, and the presence of spindle cells in the tumor.

For the rare case of localized pleural disease, surgical resection is recommended, although the tumor may quickly recur postoperatively in up to 20% of patients. A variety of conventional chemotherapeutic agents as well as targeted therapies (mTOR kinase inhibitors), and taxane-based chemotherapy regimens have been used. In one report, combination therapy with etoposide and carboplatin resulted in complete remission 18 months after the diagnosis [285]. However, no treatment strategy has demonstrated consistent and durable benefit, which underscores the critical need for new therapeutic strategies.

Diffuse pleural thickening, associated with pleural EHE, is an unusual manifestation of this tumor [286]. Imaging characteristics of pleural EHE are nonspecific and overlap with other pleural pathology. Pleural effusions, pleural thickening, and pleural nodules are common findings on chest imaging studies. Pleural disease is frequently unilateral and right-sided. Routine radiographs generally demonstrate unilateral effusion that can vary from small to large, with complete opacification of the hemithorax. Depending on the degree of solid soft tissue pleural disease, pleural thickening or nodularity can sometimes be visualized. CT scans are superior to chest radiographs in identifying loculated effusions, which are occasionally seen. Pleural thickening and nodularity are generally seen with variable extension into the hemithorax (Fig. 1.67). Mediastinal adenopathy, mediastinal invasion, interlobular septal thickening suggesting lymphangitic spread, and pulmonary metastases are variably demonstrated. Limited data on MRI of pleural EHE showed circumferential pleural thickening, nodularity, and loculated effusion [282]. FDG-avid lesions on PET/CT imaging help to distinguish PEH from benign pleural lesions and also to guide pleural biopsies [286, 287].


**Fig. 1.67** Epithelioid Hemangioendothelioma (EHE). Contrast-enhanced axial CT of a pleural EH, which demonstrates pleural-based masses (M), which extend into ill-defined lung parenchymal opacities. The tumor is often associated with simple and complex pleural fluid collections

## Pleural Angiosarcoma

Primary pleural angiosarcoma (PPA) is a subtype of sarcoma of vascular origin [288]. Skin and subcutaneous soft tissues are the most common sites for angiosarcomas with metastasis accounting for the majority of angiosarcoma cases involving the lungs and pleura. Primary pleural angiosarcoma (PPA) is exceedingly rare with only a few dozen cases reported in the English literature [289]. Primary angiosarcomas of the pleura account for less than 1% of all soft tissue sarcomas [290]. Information derived from case series suggests associations with chest irradiation, chronic tuberculous pyothorax, anabolic steroid therapy, and exposure to minerals and gases, including asbestos, arsenic, and vinyl chloride. However, these associations are primarily anecdotal and have not been well studied [290–298].

The age at diagnosis ranges from 22 to 79 years, with peak incidence in the seventh decade of life. Men are more commonly affected than women [299]. Pleuritic chest pain, dyspnea, hemoptysis, and weight loss are the most common presenting symptoms. The disease is rapidly progressive in most cases and commonly fatal within the first few months of presentation [291, 295, 300]. Histological and immunohistochemical studies of the pleural samples are required for definitive diagnosis. Pleural fluid cytology is often negative. Exploration of the pleural cavity with VATS allows direct visualization and biopsies of the involved pleura and is the preferred diagnostic approach. Hilar lymph node dissection during VATS exploration has been suggested, although the prognostic significance of lymph node invasion remains uncertain, due to the small number of reported cases. Complete surgical resection is often difficult due to multifocal disease. Chemotherapy and chemoradiation therapy combinations have been attempted with variable success. No specific treatment modality has been established. The prognosis remains poor despite aggressive therapy.

Imaging findings are nonspecific and cannot differentiate PPA from other primary or metastatic processes of the pleura. Routine radiographs generally demonstrate unilateral or bilateral pleural effusions, pleural thickening, or pleural mass lesions. Non-enhanced and contrast-enhanced CT can detect the often bloody effusions, based on elevated attenuation of the fluid and/or hematocrit layer. CT additionally shows heterogeneous enhancing lobulated pleural masses with hemorrhagic cystic components (Fig. 1.68). PET/CT generally demonstrates FDG avid pleural nodules or thickening [289]. Surgical resection is the preferred treatment option followed by radiotherapy.


**Fig. 1.68** Pleural angiosarcoma. Contrast-enhanced axial CT demonstrates a heterogeneously enhancing pleural mass (M) in the medial left lower hemithorax and a small malignant pleural effusion (*)

## Histopathological Features

### Epithelioid Hemangioendothelioma (EH)

P-EH shows similar histological features as its counterparts in the lung, liver, and soft tissues. The tumor characteristically shows the cords, strands of a solid proliferation of medium size cells with round to oval nuclei, prominent nucleoli embedded in a myxoid or chondromyxoid stroma (Fig. 1.69a–g). In some cases, the tumor cells may show "rhabdoid" features. Often these epithelioid cells appear to be engulfing red cells or forming intracellular lumens. Similarly as cases of epithelioid mesothelioma, the tumor cells in EH may also extend into the adipose tissue. In general, increased mitotic activity or necrosis are not part of EH and its presence should alert the possibility of a higher-grade neoplasm.

### Pleural Angiosarcoma

Also the tumor shares similar histological features as its counterparts in soft tissues. The tumor may show sheets of neoplastic cells or the tumor may show cords or strands of neoplastic cells embedded in a collagenous stroma. The neoplastic cells may show different morphological features ranging from spindle to epithelioid with eosinophilic cytoplasm, and prominent nucleoli, more often seen in the epithelioid variant of angiosarcoma (Fig. 1.70a–e). Necrosis and hemorrhage are common features, while mitotic activity is easily identified.

### Immunohistochemical Features

Both tumors shared similar immunohistochemical profile, namely, positive staining for vascular markers including CD-34, CD-31 (Fig. 1.71a, b), Factor VIII-related antigen, Erg, and in some cases D2–40. In addition, it has been stated that nuclear staining for CAMTA1 is a feature of epithelioid

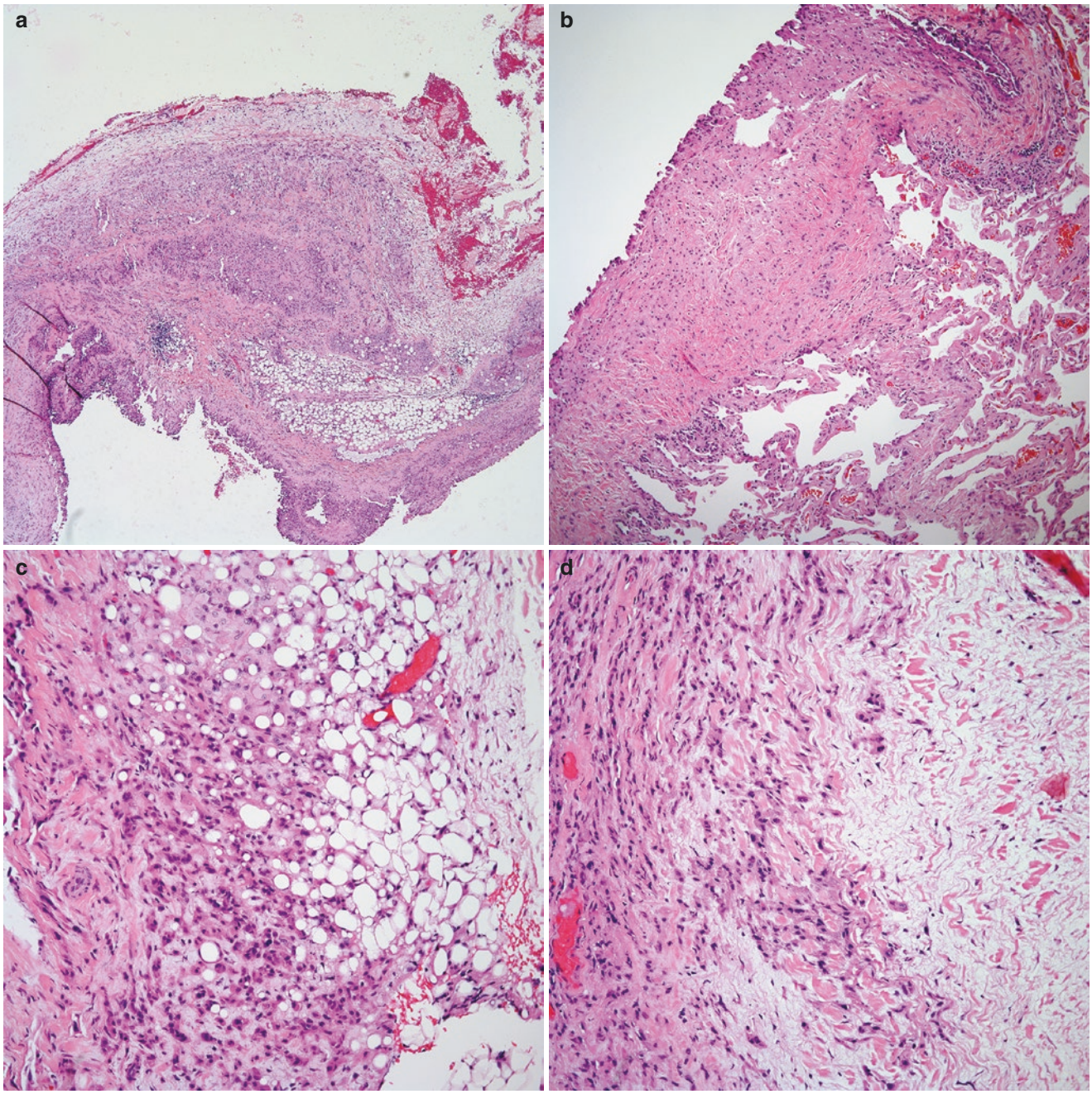


**Fig. 1.69** (**a**) Pleural biopsy of an EHE showing an epithelioid neoplasm infiltrating adipose tissue, (**b**) wedge biopsy of lung showing an epithelioid neoplasm along the pleural surface, (**c**) epithelioid neoplasm infiltrating adipose tissue, (**d**) Strands of neoplastic cells infiltrating fibroconnective tissue, (**e**) epithelioid cells embedded in a myxoid stroma, (**f**) spindle and epithelioid components of a pleural EHE mimicing biphasic mesothelioma, (**g**) EHE showing spindle cells engulfing red cells with lumen formation

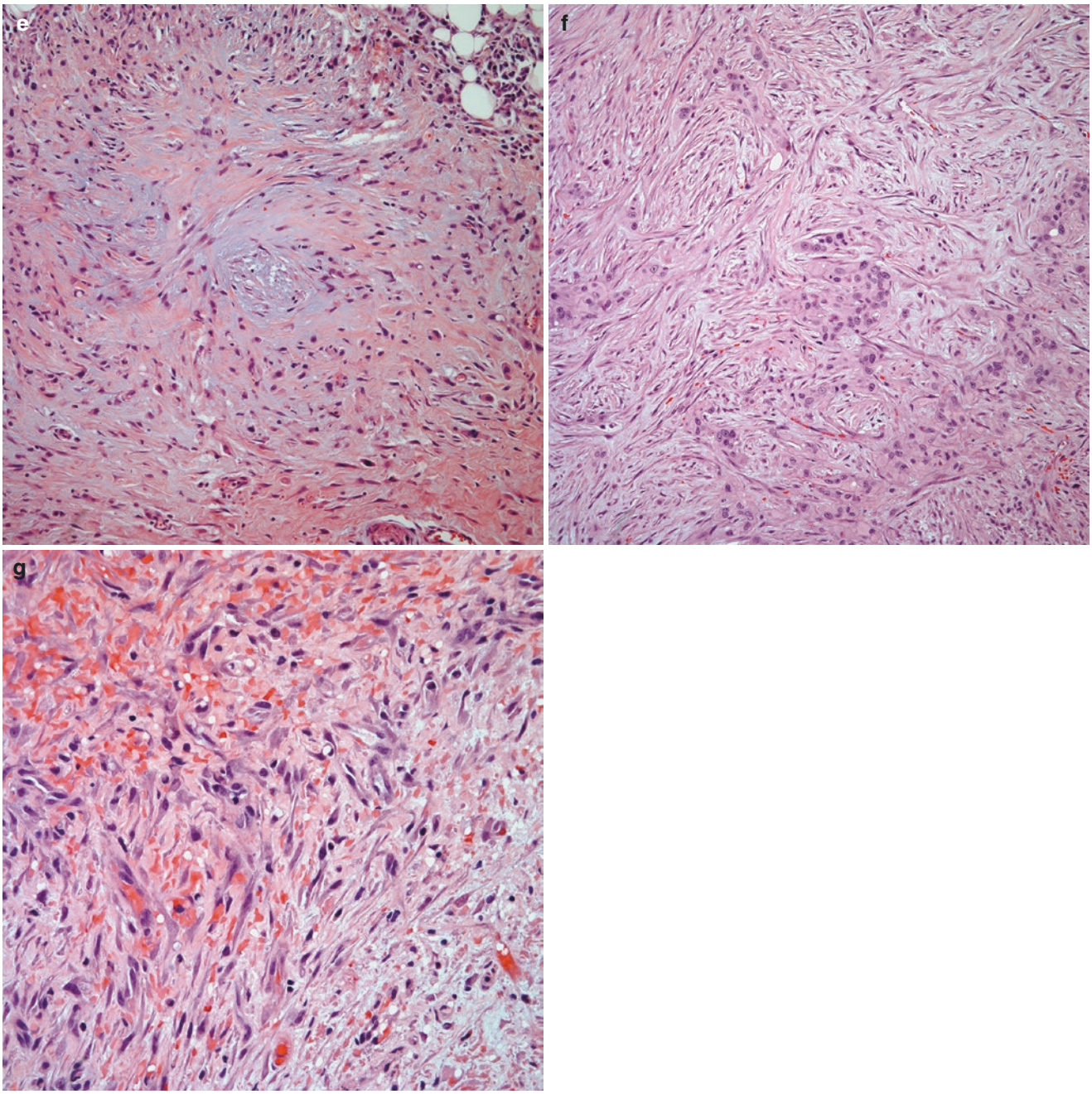


**Fig. 1.69** (continued)

hemangioendothelioma [299]. It is also important to highlight that these tumors may also show positive staining for epithelial markers, namely, keratin and CEA.

### Molecular Features

The presence of reciprocal translocations t(1:3)(p36q25), WWTR1-CAMTA1 fusion gene, and YAP1-TFE fusion gene have been associated with epithelioid hemangioendothelioma and may be of aid in cases in which minimal tissue is available for diagnosis or in difficult cases [301].

## Neuroectodermal Tumors

Primitive neuroectodermal tumors (PNET) comprise several subclasses of small round tumors that occur in the brain and peripheral sites, including bone, soft tissues, and chest wall. These highly malignant neoplasms must be distinguished from other tumors with small round cells, such as non-Hodgkin lymphoma, neuroblastoma, rhabdomyosarcoma, retinoblastoma, mesenchymal chrondrosarcoma, malignant peripheral sheath tumor, and melanoma. Peripheral PNETs are histologically and molecularly similar to Ewing's sar-

coma. Those growing outside of bone are known as extraosseous Ewing sarcomas and those of thoracopulmonary origin are designated as Askin tumors. Askin tumors are highly aggressive neoplasms of the chest wall or perihilar region. Primary pleural PNETs are extremely rare (Fig. 1.72a, b) [302]. These tumors are most frequently encountered in the pediatric population and in young adults under the age of 35 and should be included in the differential diagnosis of chest wall tumors in this age group, although isolated cases have been described in patients of all ages. A slight male predominance has been observed. PNETs may develop de novo in association with a genomic alteration that involves translocation between the long arms of chromosomes 11 and 22 (t11:22) [303]. Radiation-induced PNET has also been reported [304–306]. Patients may present with nonspecific symptoms of cough, fever, dyspnea, hemoptysis, or chest pain. Multimodality treatment strategies that include early surgical resection and chemoradiation therapy are generally

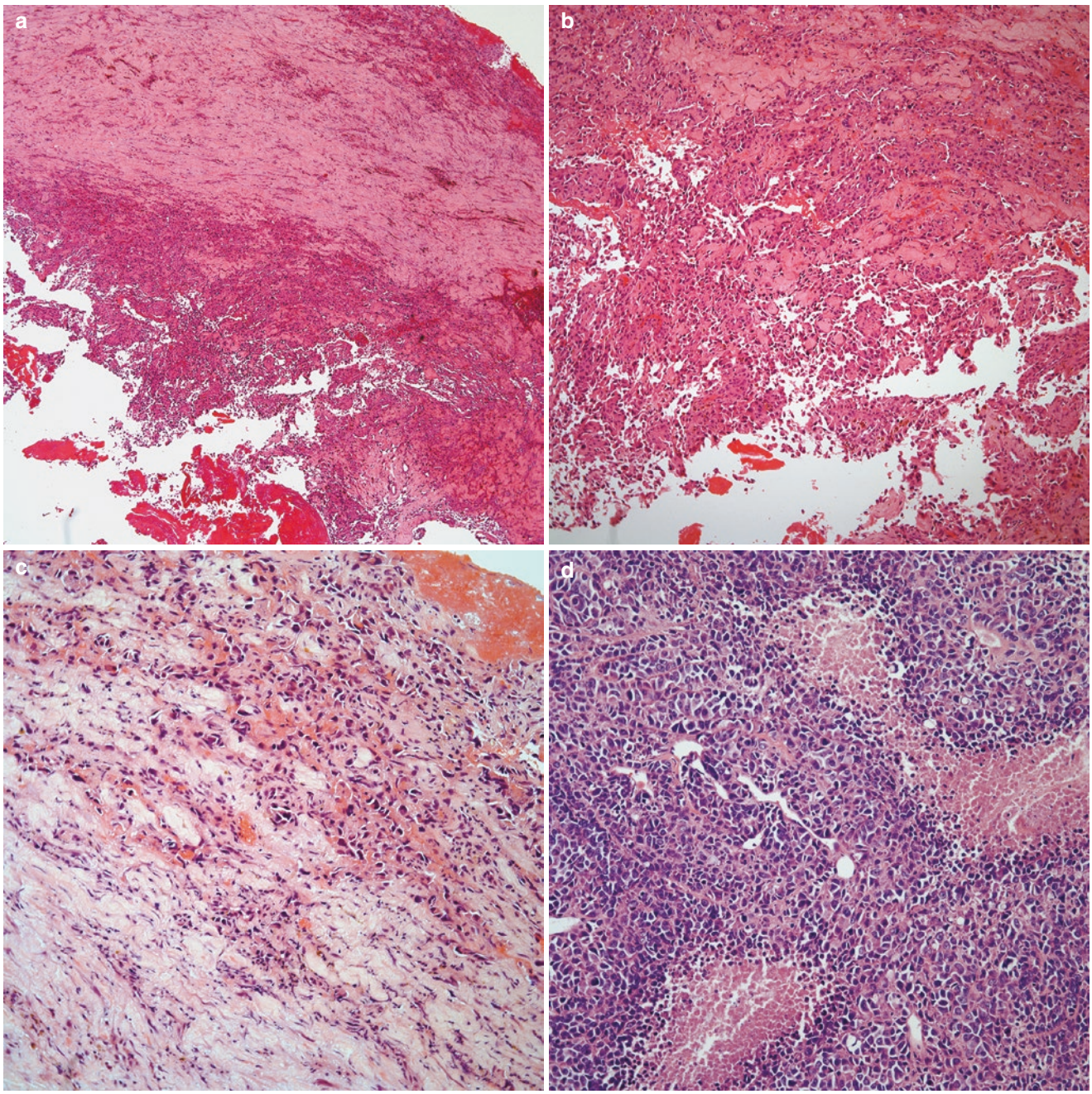


**Fig. 1.70** (**a**) Pleural biopsy of a primary angiosarcoma of the pleura, (**b**) angiosarcoma showing more cellular atypia and a pseudopapillary growth pattern, (**c**) strands of tumor cells dissecting fibroconnective tissue, (**d**) epithelioid angiosarcoma with areas of necrosis; (**e**) easily identifiable mitotic figures

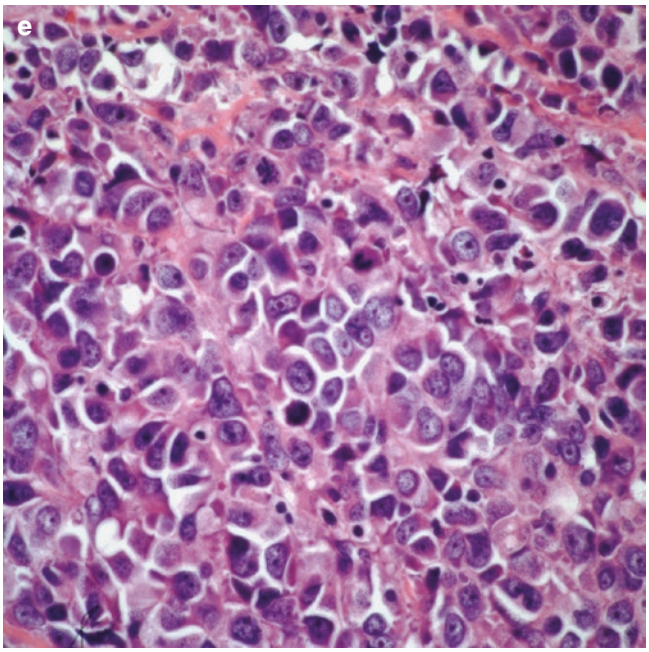


**Fig. 1.70** (continued)

recommended. This aggressive approach coupled with better understanding of the pathobiology of PNET/Ewing sarcoma has resulted in an improved 1-year survival, however, the 5 year survival remains poor at 25% [302–309].

Primary pleural PNETs often present with nonspecific imaging findings, including chest wall soft tissue mass evidence of rib invasion, and pleural effusions [302]. Routine radiographs show a pleural mass with or without associated pleural effusion. Contrast-enhanced CT demonstrates heterogeneously enhancing pleural masses with areas of central cystic change or necrosis with rare calcification (Fig. 1.73). Evidence of chest wall invasion and distal metastases, which commonly involve the lungs, bones, marrow, liver, and brain are best seen of CT. Tumor localization and extent of chest wall invasion are better determined with MRI. Masses are hyperintense on T1-weighted images and intermediate to hyperintense on T2-weighted sequences and mild to intense avidity with intravenous contrast enhancement [303]. PET/CT demonstrates increased uptake in the region of the pleural tumor and in areas of chest wall invasion.

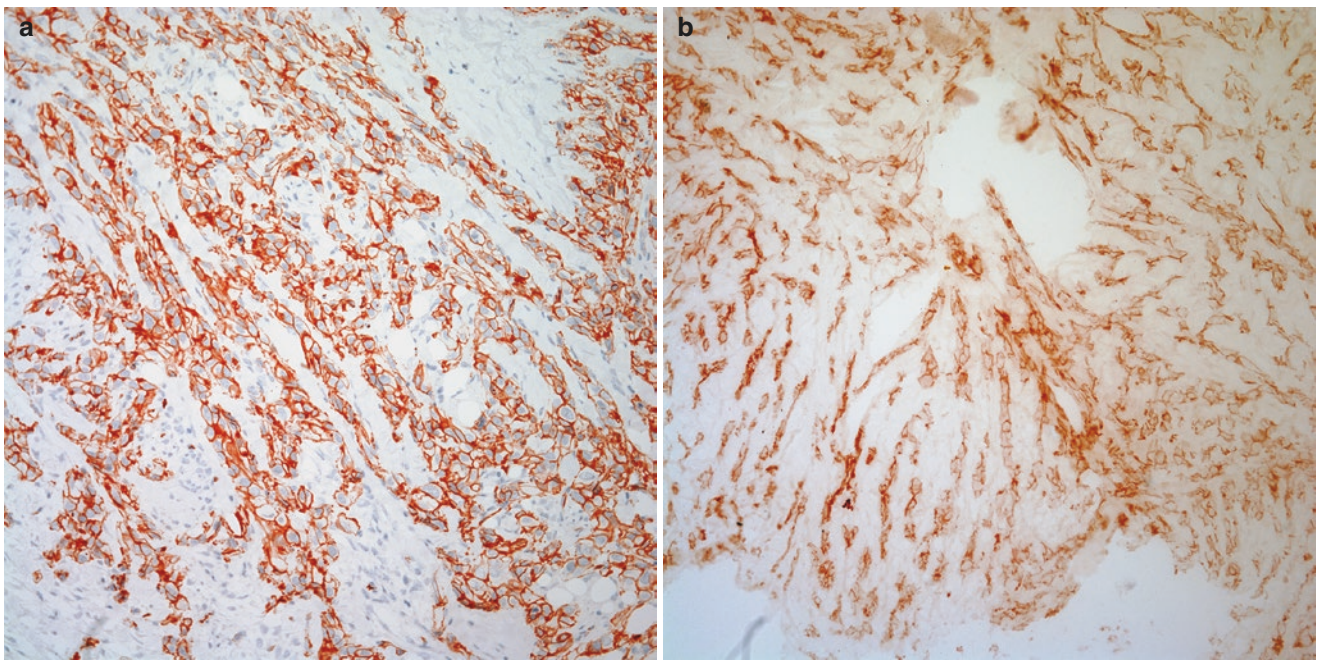


**Fig. 1.71** (**a**) Immunohistochemical stain for CD34 (vascular marker showing positive staining in tumor cells, (**b**) immunohistochemical stain for CD = 31 (vascular marker) showing positive staining in tumor cells

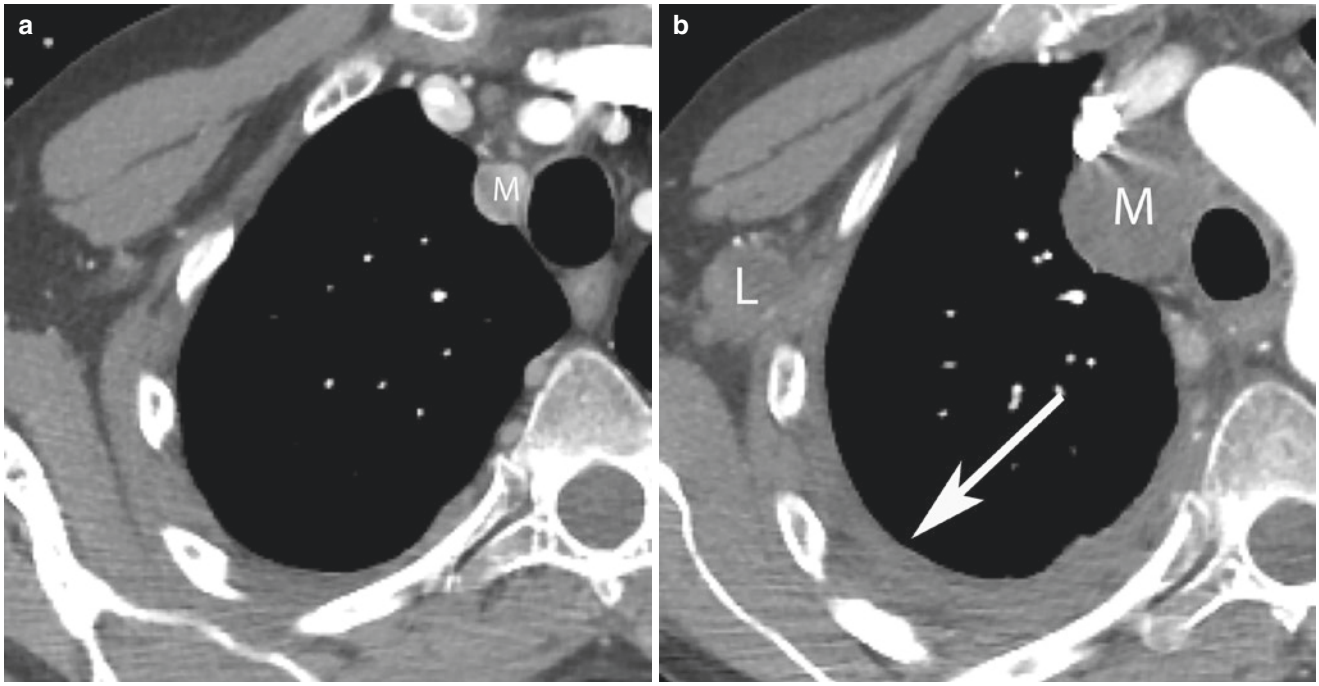


**Fig. 1.72** Primitive neuroectodermal tumor (PNET). (**a**) Contrast-enhanced axial CT shows a small heterogeneously enhancing right paratracheal pleural nodule (M), (**b**) contrast-enhanced axial CT 2 months later shows marked growth of pleural tumor (M) and interval development of a small malignant pleural effusion (arrow) and a metastatic right axillary lymph node (L)


**Fig. 1.73** Primitive neuroectodermal tumor (PNET). Contrast-enhanced axial CT shows a heterogeneous mass (M) with subtle areas of decreased attenuation (*) consistent with cystic components and small pleural effusion (arrow). Rarely, calcifications can be seen

Multimodality treatment strategies that include early surgical resection and chemoradiation therapy are generally recommended. This aggressive approach coupled with better understanding of the pathobiology of PNET/Ewing sarcoma has resulted in an improved 1-year survival, however, the 5-year survival remains poor at 25%.

## Pathological Features

### Macroscopic Features

In general these tumors may range in size from a few centimeters to larger than 10 cm in greatest diameter. They are commonly hemorrhagic and necrotic, not encapsulated but with infiltrative borders.

### Microscopic Features

In the original description by Angerval and Enzinger, the authors noted the similitude of primary tumors of the bone and those of the soft tissues; therefore, the original designation was extraskeletal Ewing sarcoma. However, it was Askin who later on reported 20 additional cases in the thorax and designated those tumors as small round cell tumors of the thoracopulmonary region (Askin tumor) [310]. Essentially those tumors shared similar characteristics as those in the soft tissues described by Enzinger [311]. Currently, all those tumors have been designated under the name of PNET.

These tumors essentially show the presence of a neoplastic cellular proliferation composed of small cells with scant cytoplasm, round to oval nuclei and inconspicuous nucleoli, rosettes, increased mitotic activity, necrosis, and hemorrhage (Fig. 1.74a–c). However, those features may be present in different proportion in each tumor.

### Immunohistochemical Features

By immunohistochemistry, there is not one single immunostain that is specific for PNET. However, these tumors are often positive for CD99 (Fig. 1.75) and NSE. Keratin, S-100 protein, and Synaptophysin may be seen focally positive in these tumors. Other stains that may be positive include NB84 and WT1 [312].

### Molecular Features

Because there is not a single immunostain that is diagnostic of PNET, often the use of molecular techniques aids in the final interpretation of these tumors. Common translocations that have been associated with PNET include: t(11;22)(q24;q12) and t(21;22)(q22;1q12).

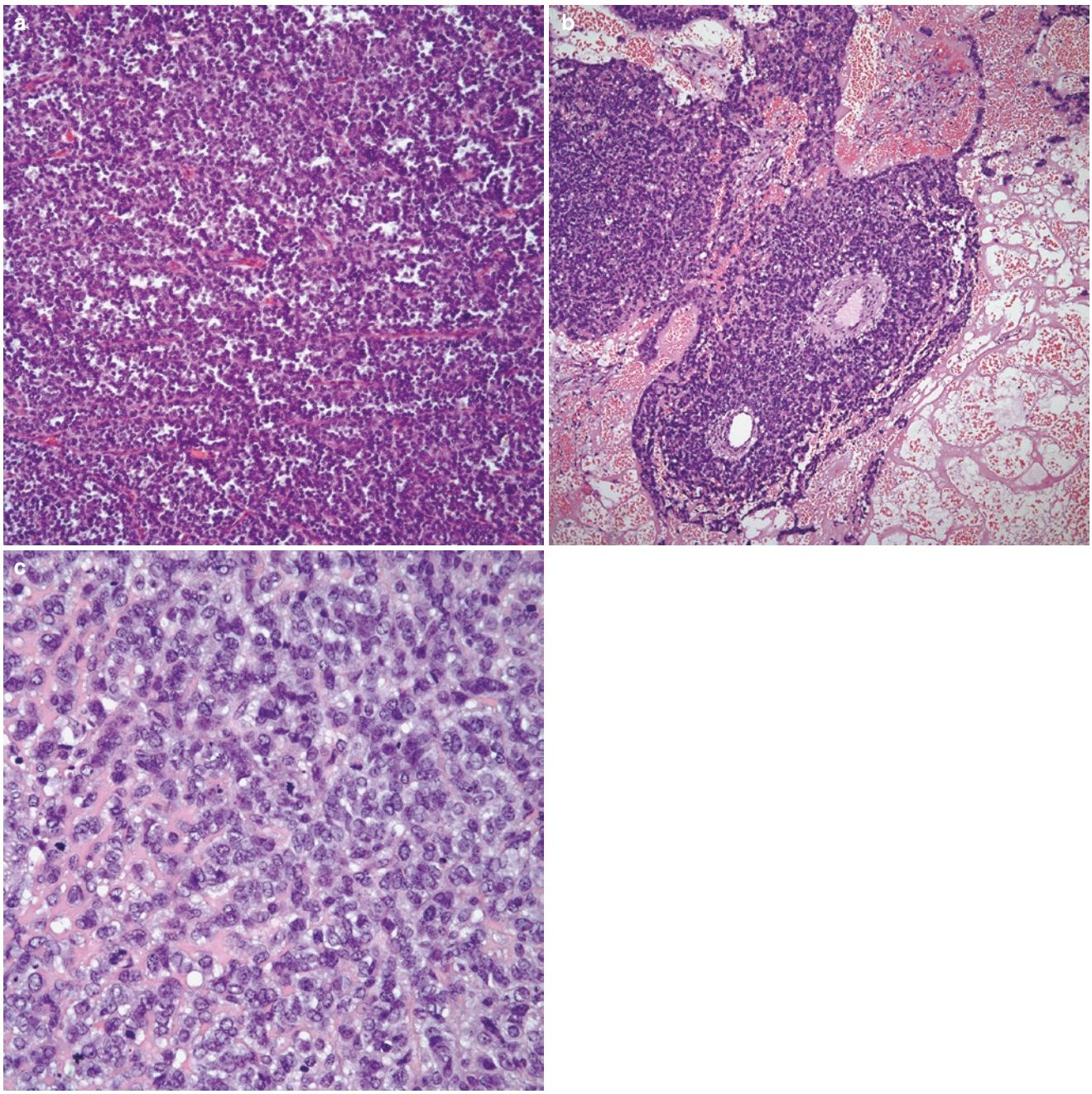


**Fig. 1.74** (**a**) Low power view of a PNET showing sheets of small cell malignant cells, (**b**) PNET with areas of fibrinoid necrosis and hemorrhage, (**c**) higher magnification showing cellular atypia and mitotic activity

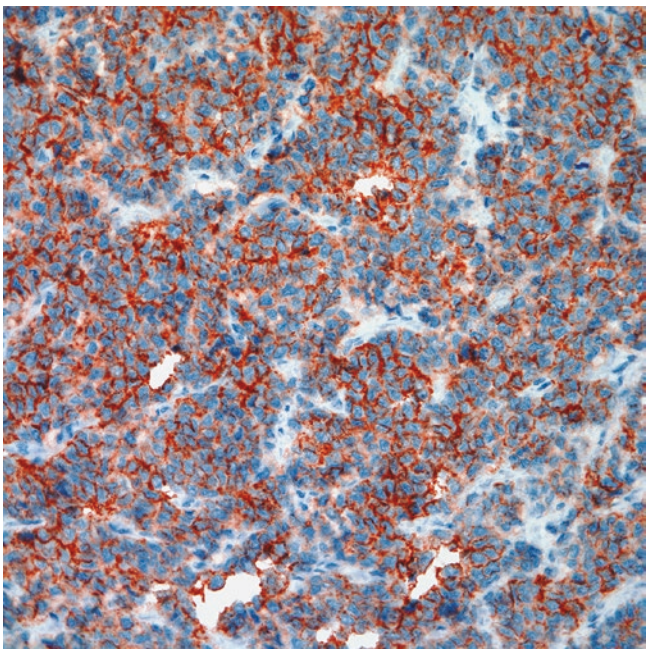

**Fig. 1.75** Immunohistochemical stain for CD-99 positive in PNET

## Other Pleural Sarcomas

Other sarcomas arising from the pleura have been rarely described. Among these, smooth muscle tumors and synovial sarcomas are the most commonly mentioned.

### Primary Smooth Muscle Tumors of the Pleura

Primary smooth muscle tumors of the pleura are exceptionally rare pleural sarcomas. Information has been limited to case reports and case series, which describe nonspecific symptoms of cough and chest pain in predominantly male adults. Tumors of variable sizes may present as solitary pleural-based neoplasms or rarely, diffuse pleural thickening that mimics mesothelioma [313–315]. The clinical behavior of smooth muscle tumors of the pleura may mimic the behavior of smooth muscle tumors originating in soft tissues. Treatment options including surgery, radiation, and chemotherapy are guided by the grade of tumor.

Histologically, a spectrum of behaviors have been reported, ranging from aggressive tumors that mimic leiomyosarcoma with characteristic spindle cell proliferation, cellular pleomorphism, necrosis, and mitotic activity (Fig. 1.76a–c) to tumors of uncertain malignant potential that display minimal cellular atypia and mitotic activity [313–315].

### Synovial Sarcoma

Primary pleuroparenchymal synovial sarcomas (PPSS) are rare tumors. Only a few small case series and single case reports have been reported [316, 317]. Originally thought to arise from synovial cells, these tumors are now known to originate from pluripotential mesenchymal cells that are capable of partial or aberrant epithelial differentiation [318]. Synovial sarcomas are most frequently seen in soft tissues of the extremities and head and neck regions, but have also been recognized in other locations, including the esophagus, heart, retroperitoneum, chest wall, mediastinum, lung, and pleura. The median age at diagnosis is 40 years, but may appear at any age. A 2:1 male predominance has been observed [119]. Chest pain, pleural effusion, hemoptysis, and dyspnea are common presenting symptoms, although occasionally patients are asymptomatic with incidental findings on chest CT. Pneumothorax is a frequent finding in patients with cystic variants of synovial sarcoma. In those reports, the age of the patients has varied from childhood to adulthood.

Surgical resection in combination with radiotherapy and/or chemotherapy is the preferred treatment strategy. Prognostic factors, including younger age, tumor size <5 cm, mitotic rate of <10/10 HPF, negative surgical margins, and SS18-SSX type (SS18-SSX2) favorably impact survival. However with a 5-year survival rate of only 30%, the prognosis remains dismal.

On routine radiographs, PPSS generally presents as a peripheral pleural based mass defined by well-circumscribed borders with round, ovoid, or lobulated contours, which can contain calcifications. Contrast-enhanced CT demonstrates peripheral pleural or fissural soft tissue masses with areas of low attenuation, possible septations, heterogeneous enhancement, and possible thin rim enhancement (Fig. 1.77a, b) [319]. MRI demonstrates heterogeneous signal on T1-weighted and T2-weighted images with fluid-fluid levels due to areas of hemorrhage and necrosis [303]. PET/CT studies show increased FDG uptake within the tumor.

Only a few small series of cases or single case reports have been presented in the literature [316, 317]. In those reports, the age of the patients has varied from childhood to adulthood.

Surgical resection in combination with radiotherapy and/or chemotherapy is the preferred treatment strategy. Prognostic factors, including age (better in young patients), tumor size <5 cm, mitotic rate of <10/10 HPF, negative surgical margins and SS18-SSX type (SS18-SSX2) favorably impact survival. However with a 5-year survival rate of only 30%, the prognosis remains dismal.

## Pathological Features

### Macrocopic Features

The tumors generally present as a pleural-based mass that can reach more than 10 cm in greatest dimension. These tumor masses are solid, light tan in color. Extensive necrosis and hemorrhage are usually not present.

### Microscopic Features

As in synovial sarcomas of the soft tissue, the tumors may present a monophasic or a biphasic growth pattern. In cases of monophasic synovial sarcoma, the tumors show a neoplas-

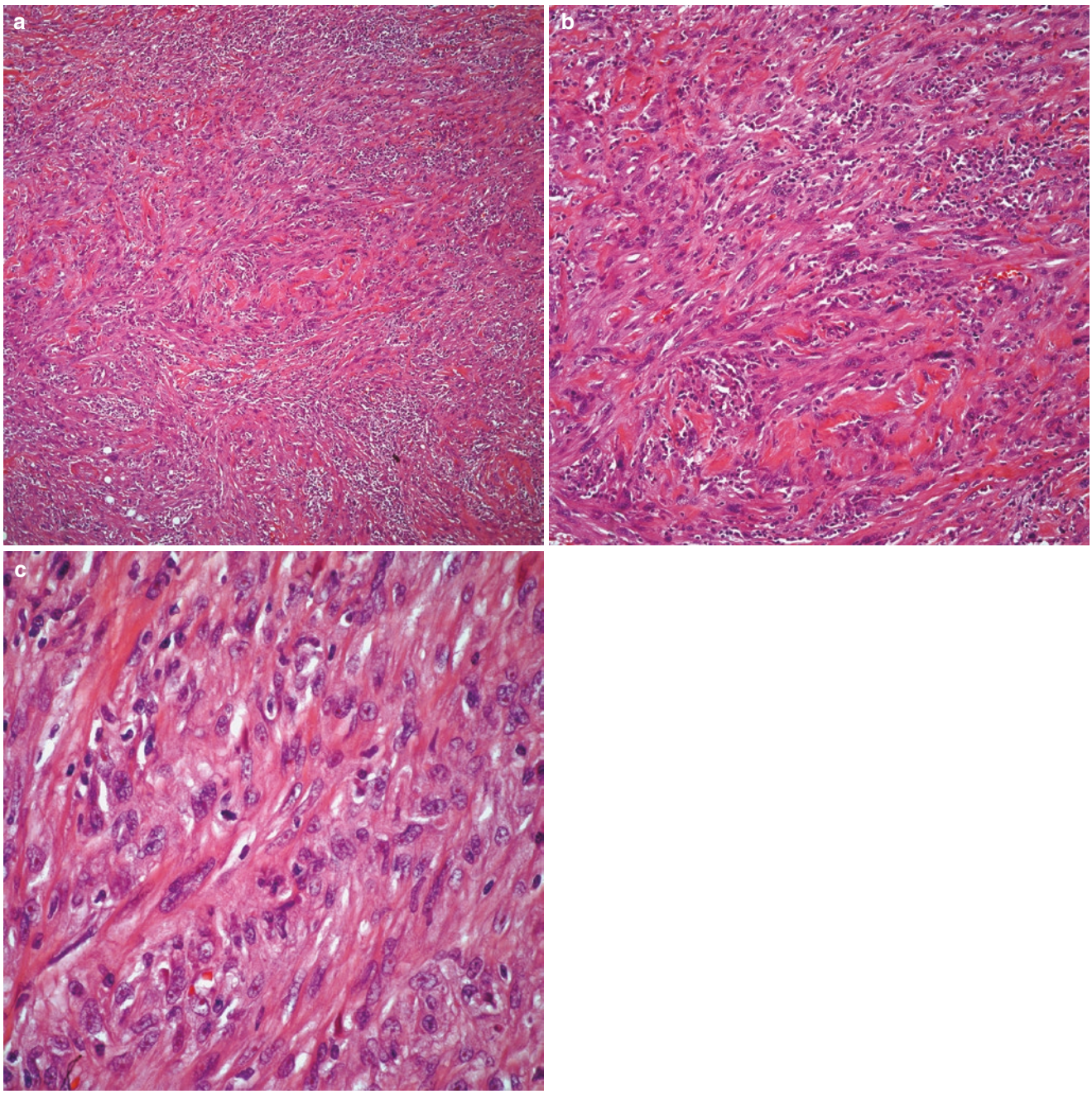


**Fig. 1.76** (**a**) Low power of a leiomyosarcoma showing a malignant spindle cell proliferation, (**b**) marked nuclear atypia, (**c**) mitotic activity

tic cellular proliferation composed of spindle cells with elongated nuclei and inconspicuous nucleoli. The tumor may show a fibrosarcoma-like growth pattern or a hemangiopericytic-like growth pattern (Fig. 1.78a, b). Nuclear atypia is present and the mitotic activity varies from a few mitotic figures per 10 high power fields to more than 10 mitoses per 10 high power fields. Focal areas of necrosis and hemorrhage can be present. In cases of biphasic synovial sarcoma, the spindle cell component shares similar features as those seen in the monophasic variant; however, this spindle cellular proliferation is admixed with a glandular component that is commonly lined by low or tall columnar epithelium (Fig. 1.79a, b). Mitotic activity in the glandular component is not easily identifiable.

### Immunohistochemical Features

Synovial sarcomas characteristically show focal positive staining for keratin and for EMA. In addition, the tumor may also show positive staining for FLI1, TLE (Fig. 1.80a, b), Bcl-2, and CD-99. In some case S-100 protein and calponin, calretinin, and CD-117 may show positive staining in tumor cells.

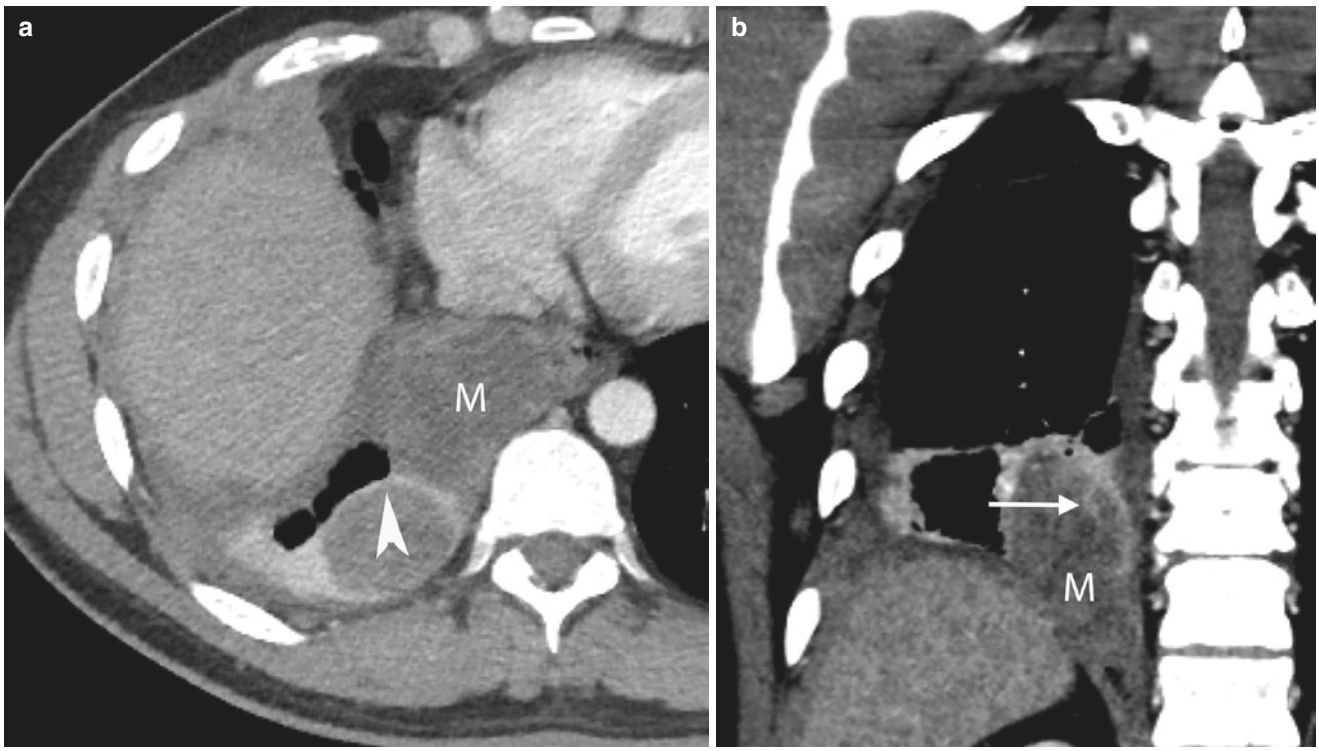


**Fig. 1.77** Pleural synovial angiosarcoma. (**a**, **b**) Contrast-enhanced axial and coronal CT shows a heterogeneous mass (M) in the right lower hemithorax with areas demonstrating peripheral enhancement (arrowhead) and thin internal enhancing septation (arrow)

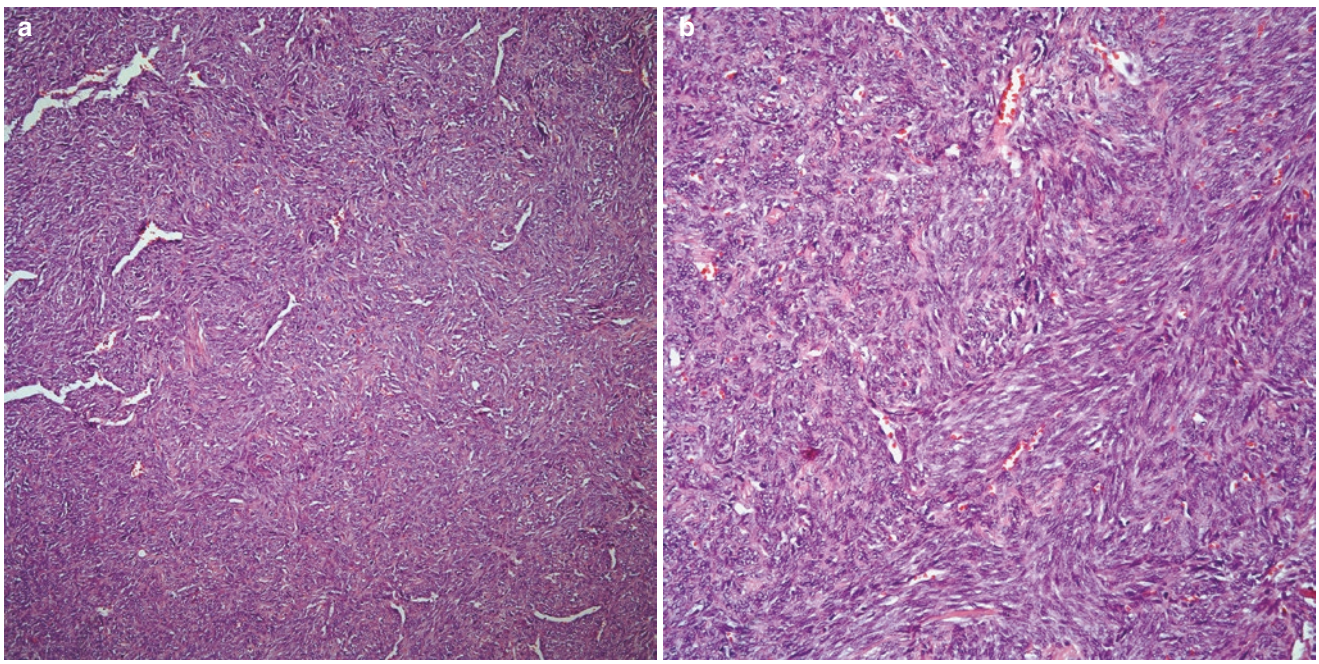


**Fig. 1.78** (**a**) Low power view of a monophasic synovial sarcoma showing a hemangiopericytic growth pattern, (**b**) monophasic synovial sarcoma composed of only a malignant spindle cell proliferation

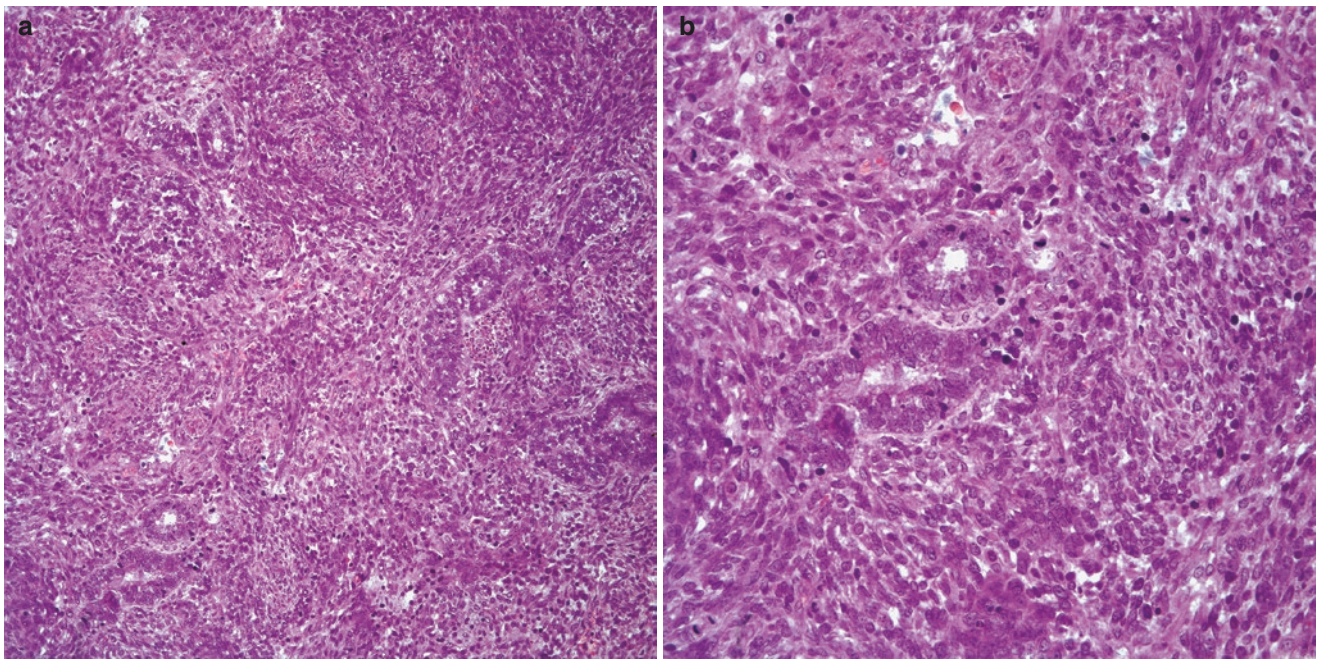


**Fig. 1.79** (**a**) Biphasic synovial sarcoma showing spindle cell component and glandular component, (**b**) closer view at the two different components of a biphasic synovial sarcoma. Note the presence of mitotic activity

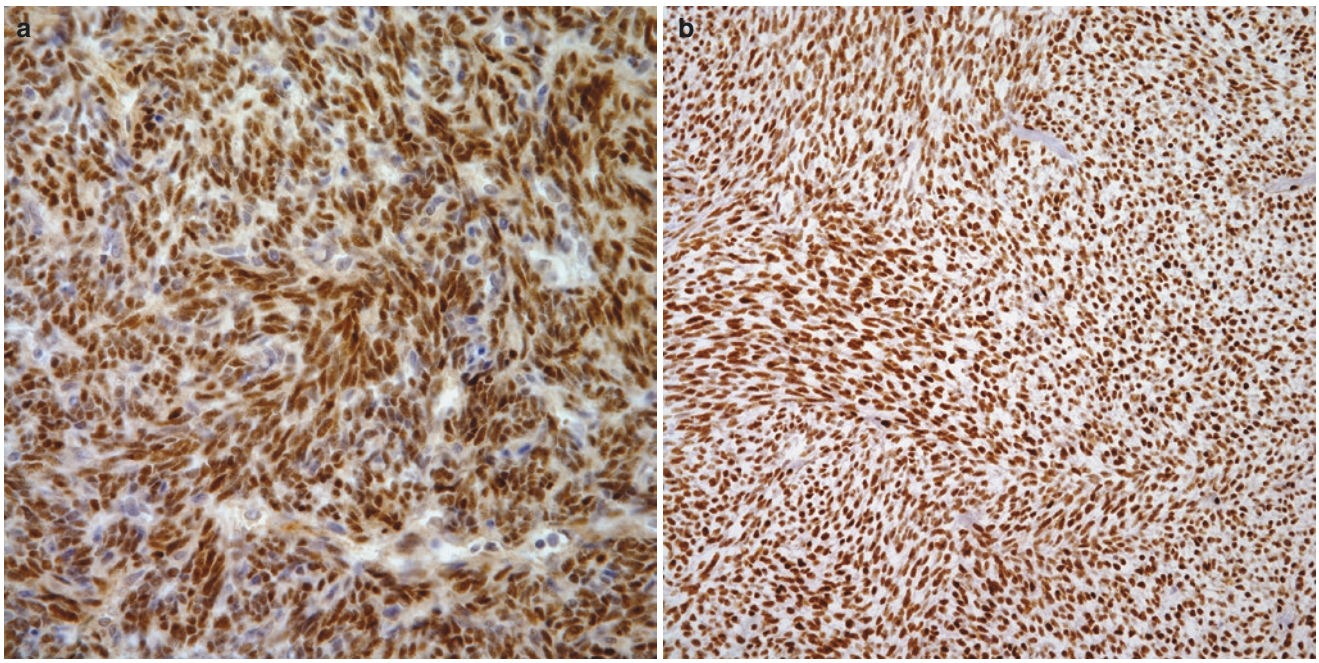


**Fig. 1.80** (**a**) Immunohistochemical stain for TLE-1 showing positive nuclear staining in synovial sarcoma, (**b**) immunohistochemical stain for FLI-1 showing positive nuclear staining in synovial sarcoma

### Molecular Features

Synovial sarcoma is characterized by the nonrandom t(X;18)(p11.2;q11.2) translocation involving the SS18 gene on chromosome 18 and one of the SSX genes on the X chromosome. This translocation generates an oncogenic SS18-SSX fusion transcript in more than 90% of the cases [320, 321]. Identification of this genetic abnormality coupled with consistent histology and immunophenotype, establishes the diagnosis [321].

## Body Cavity Lymphoma

Body cavity lymphoma is a term used to describe a heterogeneous group of primary intracavitary non-Hodgkin's lymphomas (NHL). They originate within potential spaces including pleural, peritoneal, or pericardial cavities that contain transudative, acellular fluid and, under normal conditions are devoid of lymphoid tissue. These are rare clinical entities and are distinct from the more common pleural diseases caused by lymphomatous spread in typical NHLs. The two most common types of body cavity lymphomas encountered are primary effusion lymphoma (PEL) and pyothorax-associated lymphoma (PAL) [322].

### Primary Effusion Lymphoma

Primary effusion lymphoma is a rare, large non-Hodgkin's B cell lymphoma with an aggressive phenotype, which was first recognized as a distinct malignancy in the WHO classification of neoplasms of hematopoietic and lymphoid tissues in 2001 [323]. These tumors predominantly arise in body cavities and occasionally in extracavitary regions. PEL is characterized by lymphomatous effusions on serosal surfaces without an identifiable solid component [324]. The disease is associated with human herpes virus 8 (HHV8) [322]. Epstein-Barr virus (EBV) coinfection occurs in 60–90% [325]. These viruses infect the B cell during its latent phase and stimulate oncogenesis through a variety of mechanisms.

PEL was originally described as an Acquired Immunodeficiency Syndrome (AIDS)-related malignancy, but it is now known to occur in other immunocompromised states, such as recipients of solid organ transplant, cirrhosis, and also in the elderly. This tumor constitutes 1–4% of Human Immunodeficiency Virus (HIV)-related lymphomas and <1% of lymphomas in non-HIV populations [326]. The disease tends to occur much later in those without HIV, with a median age of 73 [327]. Specific risk factors in HIV-positive patients include low CD4, T cell count, male homosexuality and drug use [327].

Patients typically present with effusions involving the serosal surfaces of the pleura (60–90%), peritoneum (30–60%), pericardium (up to 30%), joint spaces, and rarely the meninges (Fig. 1.81a, b). Symptoms result from the mass effect of fluid accumulation and vary by the site affected. Patients with pleural or pericardial disease may present with dyspnea. Additionally, dizziness, syncope, and hypotension may be prominent symptoms as pericardial fluid accumulates, whereas abdominal distention and ascites are primary symptoms among patients with peritoneal disease. In addition to these site-specific symptoms, PEL can present with typical B symptoms [326]. The diagnosis requires cytologic examination of the malignant fluid, immunophenotypic studies, as well as molecular identification of HHV8 [327]. Other subtypes of non-Hodgkin lymphoma may rarely present with lymphomatous effusions that mimic PEL. For example, plasmacytoid lymphoma and Burkitt lymphoma with plasmacytoid differentiation are two HIV-associated variants of diffuse large B cell lymphoma that may present as large lymphomatous effusions. Anaplastic lymphoma, pyothorax-associated lymphoma, and plasma cell myeloma share morphologic features with PEL and are in the differential diagnosis. In addition, HHV8-associated post-transplant lymphoproliferative effusions may mimic PEL. These disorders may be distinguished from PEL on the basis of clinical presentation, tumor morphology, and immunophenotype profiles. No specific treatment exists. Thoracentesis, indwelling pleural

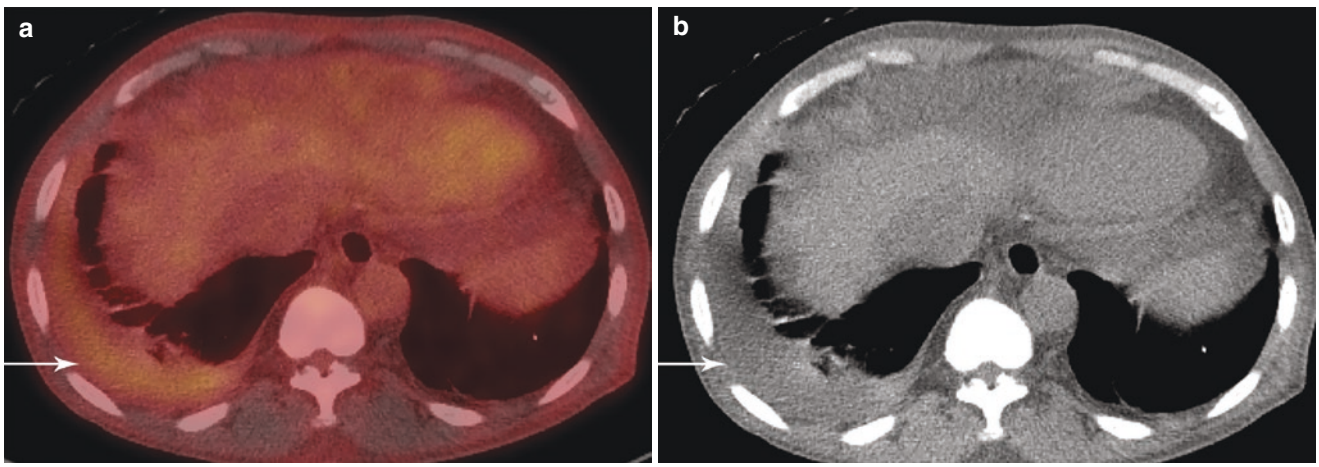


**Fig. 1.81** Primary effusion lymphoma in a patient with human herpes virus 8 infection. (**a**, **b**) Axial FDG PET/CT and non-contrast axial CT show a small right pleural effusion with FDG uptake similar to that of the liver with SUV of 2.6. There was no evidence of peritoneal involvement

catheter placement and talc pleurodesis are reasonable palliative approaches to decrease symptoms associated with accumulation of pleural fluid. Standard chemotherapy for other types of non-Hodgkin lymphoma is typically given; however, the prognosis remains poor, with a median survival of only 6 months [326].

Typical radiological features of primary effusion lymphoma are the presence of pleural effusion and liver and/or splenic enlargement in the absence of lymphadenopathy [328, 329]. CT findings are nonspecific, including unilateral pleural effusion that may be associated with loss of volume of the involved hemithorax and pleural thickening [326, 330].

### Pyothorax-Associated Lymphoma

Pyothorax-associated lymphoma (PAL) is a pleural-based Ebstein-Barr virus-associated B-cell non-Hodgkin's lymphoma. Like primary effusion lymphoma, PAL presents as a lymphomatous effusion, but often has a local solid component and is HHV8-negative [322]. Most of the information comes from Japanese reports, which suggest a male predominance with a median age of 65–70 years at presentation [331]. PAL has been reported in 2% of patients with a history of longstanding pleural inflammation [332]. The disease has been reported 20 or more years following artificial pneumothorax for the management of pleuropulmonary tuberculosis. Chest pain, dyspnea, and fever are presenting signs and symptoms in 50% of patients [332].

Benign complications of empyema, such as empyema necessitans, and malignant pleural tumors with coincident empyema should be excluded. Thoracostomy has been recommended for management of the pyothorax prior to and during chemotherapy. Chemotherapy, adjuvant radiation therapy, and surgery have been used to treat PAL, however, the overall prognosis remains poor, with a 5-year survival of 21% [332–335].

## Pleural Manifestations of Hematologic Malignancy

Pleural disease in hematologic malignancy largely consists of pleural effusions. In contrast to primary pleural lymphoma, secondary pleural involvement in systemic hematologic malignancies is relatively common.

Pleural involvement can be seen in 30% of patients with Hodgkin's lymphoma (HL). In addition, approximately 20% of patients with non-Hodgkin's have pleural involvement during their disease course [336]. Diffuse large B-Cell lymphoma (DLBCL) is the most common subtype, followed by follicular lymphoma [337]. Rare reports of primary pleural lymphoma unassociated with risk factors for PEL/PAL have also been described [338].

Malignant pleural effusions are uncommon in acute and chronic leukemias, myelodysplastic syndrome (MDS), and myeloproliferative neoplasms (MPN). The most common presentations occur in relapse states in which the pleura may serve as an extramedullary site of involvement. Pleural disease typically accompanies marrow involvement [339].

Myeloid sarcoma (MS) is an extramedullary infiltrating tumor composed of immature myeloid cells (Fig. 1.82a, b). MS may occur in 2–7% of patients with acute myelogenous leukemia (AML) and has been reported with multiple other hematologic malignancies, including chronic myelogenous leukemia, MDS, and MPN during blast transformation or disease relapse [340]. Malignant pleural effusions occur in

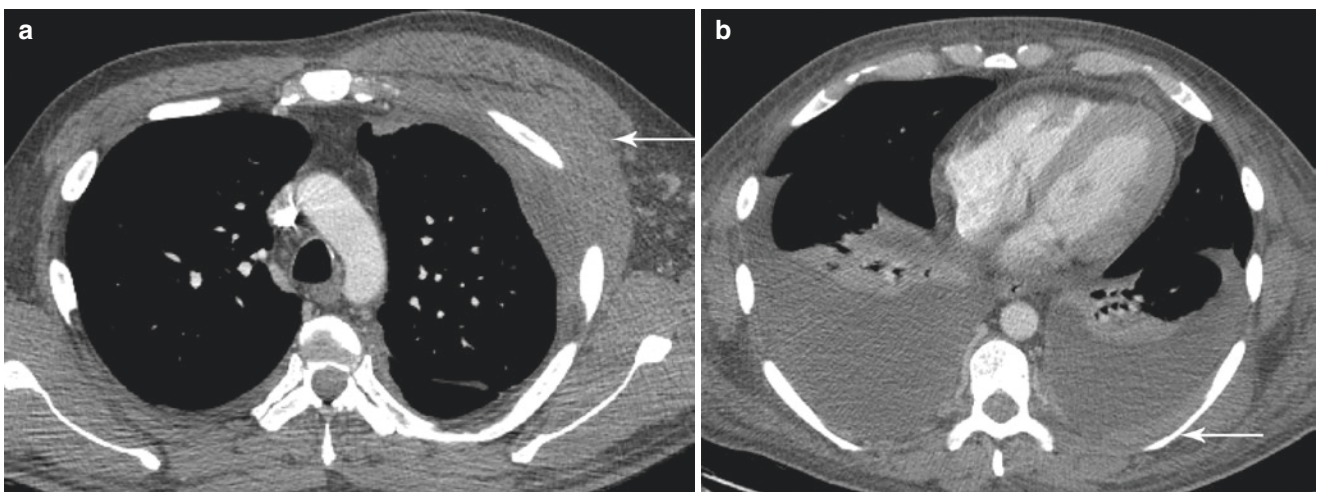


**Fig. 1.82** Myeloid sarcoma in a patient with chronic myelogenous leukemia. (**a**) Contrast-enhanced axial chest CT shows left anterior chest wall soft tissue infiltration (arrow). There are bilateral pleural effusions, (**b**) contrast-enhanced axial chest CT shows left posterior pleural thickening (arrow)

association with MS most often in the setting of coexisting medullary disease. Mediastinal or lung involvement is also common [340, 341].

In chronic lymphocytic leukemia, pleural involvement may be associated with the development of Richter syndrome or synchronous secondary malignancy. Pleural disease is rarely associated with MPNs, such as systemic mastocytosis, chronic eosinophilic leukemia, myelofibrosis, and polycythemia vera and, when present, is often a manifestation of systemic disease or, rarely, extramedullary hematopoiesis [340].

Pleural effusions are reported in approximately 6% of patients with multiple myeloma. Approximately 80% of these effusions are associated with IgA multiple myeloma [342]. Effusions are typically caused by direct implantation of myeloma cells on the pleura or extension of myeloma from local sources. Mediastinal involvement with subsequent lymphatic obstruction is rare, occurring in <1% of cases [343]. Plasmacytomas occur in 6–20% of multiple myeloma cases and uncommonly affect the pleura [344]. Secondary extramedullary multiple myeloma refers to plasmacytomas found in association with bone marrow involvement by myeloma. Primary tumors presenting as solitary extramedullary plasmacytoma (SEP) that are unassociated with marrow involvement have also been rarely reported. SEP has a male predominance with a median age of 55 years. Less than 25% of patients with SEP have coexisting monoclonal gammopathy [345, 346]. The majority of effusions encountered in multiple myeloma are secondary to systemic sequelae, including renal insufficiency, nephrotic syndrome, congestive heart failure, pulmonary embolus, or secondary neoplasms. Other gammopathies, including amyloidosis and Waldenstrom macroglobulinemia rarely affect the pleura [336].

Secondary pleural involvement in hematologic malignancies is often due to direct disease infiltration of the pleural space. Widespread disease, in particular, disease that involves the mediastinum, may cause pleural effusions as a result of lymphatic or thoracic duct obstruction. Several therapeutic agents used in hematologic malignancies, such as dasatinib or gemcitabine, are known to cause pleural effusions [336].

Many patients with malignant pleural disease are asymptomatic. In patients with symptoms, typical findings include cough, dyspnea, chest pain, and pleurisy. Pleural fluid often appears serous or serosanguinous and is typically exudative. Transudative effusions may occur as the result of manifestations of systemic disease unrelated to direct malignant involvement. Chylous effusions are found in 19% of non-Hodgkin's lymphoma and 3% of Hodkin's lymphoma [336].

Immunocompromised states are extremely common among patients with hematologic malignancies. Consequently, approximately 50% of pleural effusions in this setting are unrelated to direct malignant infiltration of the pleura, but rather due to infection or parapneumonic etiologies. Other causes include cardiomyopathy, liver dysfunction, renal insufficiency, or thrombosis. Therefore, thoracentesis for sampling of pleural fluid and analysis for microscopic, chemical, and cellular content represents the first step in the diagnostic workup. Chemical analysis typically suggests exudative effusions, although transudative pleural fluid is reported in a small percentage of patients with malignant effusions. Cytologic evaluation and flow cytometry should be included in the initial pleural fluid assessment to exclude malignancy. The diagnostic yield of pleural cytology is estimated at 61–75% in patients with lymphoma and leukemia [336]. Clinical correlation is also important, as pleural fluid may be contaminated with peripheral blood. Thoracoscopy with pleural biopsy may also be considered, particularly when exclusion of malignancy or diagnosis of a secondary process may change management. Pleural fluid protein electrophoresis and histologic exam of specimens obtained by pleural biopsy are important adjunctive tests for patients with suspected myelomatous pleural effusions [347]. In addition to bone marrow aspiration and biopsy, immunohistologic examination of core or surgical biopsies along with flow cytometry, cytogenetic, and molecular studies may assist in establishing the diagnosis of pleural effusions associated with myeloid sarcoma [340].

## Pleural Metastasis

While MPM is the most common primary pleural malignancy, pleural metastasis is the overall most common pleural tumor. Adenocarcinomas more commonly metastasize to the pleura than other histological subtypes [1]. Lung carcinoma accounts for 40% of pleural metastases (Fig. 1.83a, b), followed by breast carcinoma at 20%, lymphoma at 10%, and unknown primary at 10% [348]. Invasive thymoma and ovarian cancer can also metastasize to the pleura (Fig. 1.84). Of note, pleural metastases are second only to left heart failure as the most common cause of pleural effusions in adults (Fig. 1.85) [348].

Radiographic findings are nonspecific, including unilateral or bilateral pleural effusions and focal or diffuse pleural thickening. Contrast-enhanced CT and MRI can better evaluate effusions for evidence of complex fluid, associated pleural thickening or nodularity, discrete soft tissue mass, circumferential pleural thickening, or infiltration into the adjacent lung parenchyma (Fig. 1.86) [348]. As expected, pleural metastases generally demonstrate heterogeneous enhancement with administration of intravenous contrast. PET/CT can be utilized to distinguish between benign and malignant pleural processes with the latter demonstrating increased FDG uptake [1].While not a part of staging

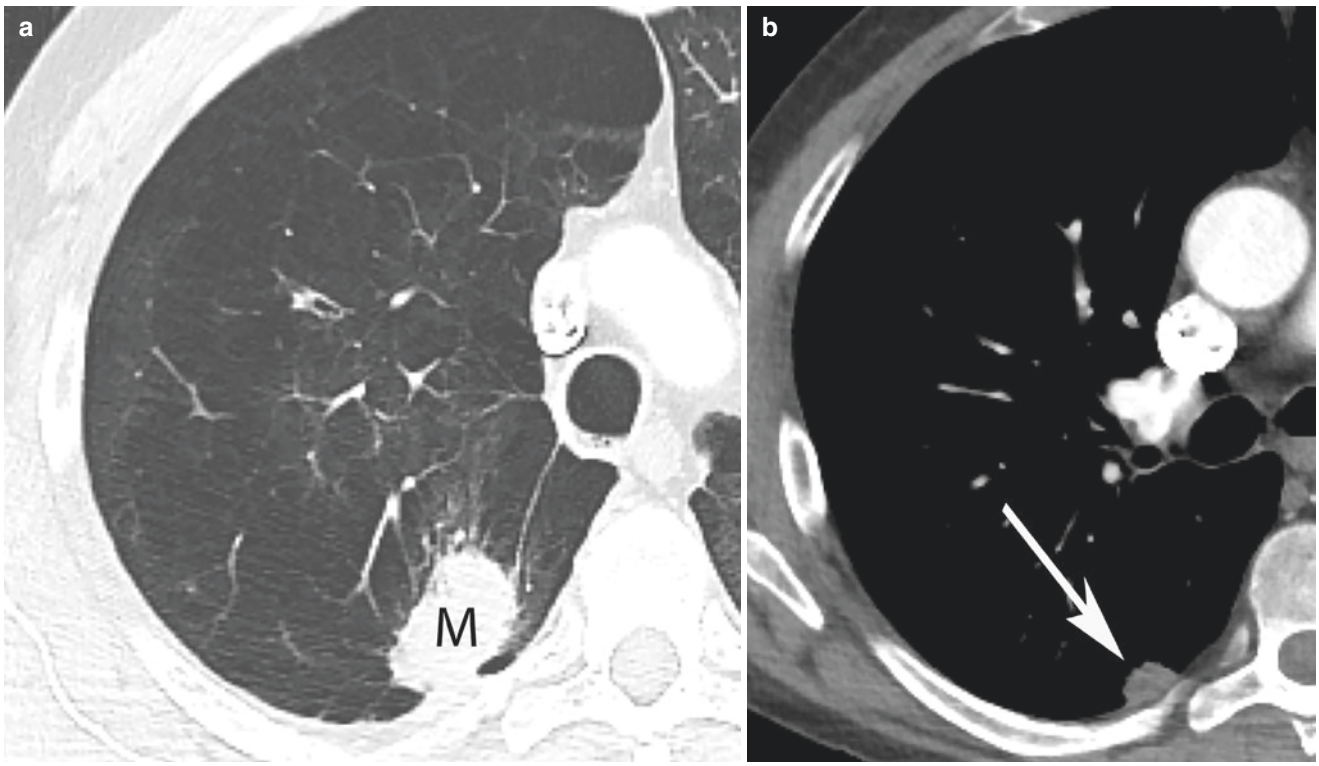


**Fig. 1.83** Pleural metastasis from lung adenocarcinoma. (**a**, **b**) Contrast-enhanced axial CT in lung and soft tissue windows demonstrates a spiculated soft tissue mass (M) in the posterior segment of the right upper lobe consistent with biopsy proven primary lung adenocarcinoma, with a small heterogeneously enhancing pleural nodule in the right lower hemithorax (arrow) representing a pleural metastasis. Lung carcinoma represents the most common primary tumor with pleural metastasis

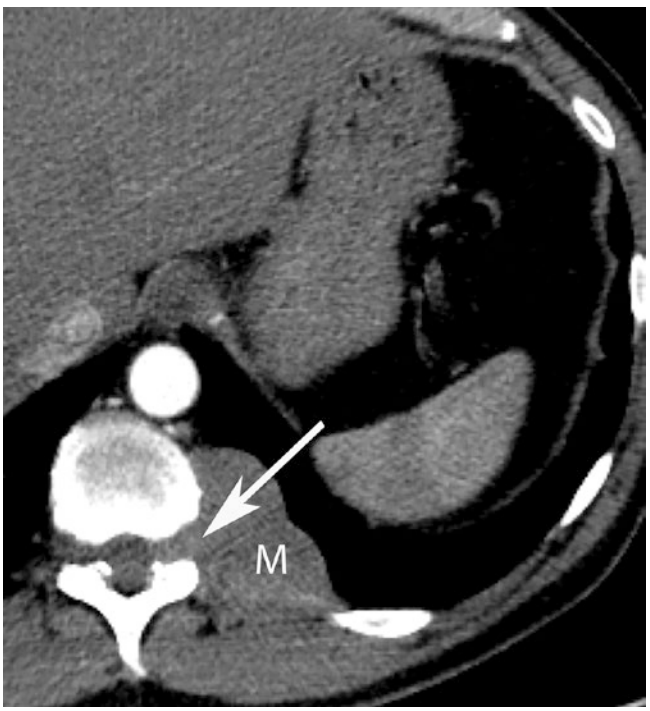


**Fig. 1.84** Pleural metastasis from thymoma. Contrast-enhanced axial CT with invasive thymoma demonstrates a lobular left pleural metastasis (M) in the lower hemithorax invading the adjacent neural foramen (arrow)

evaluation, as previously discussed, ultrasound can aid in image-guided thoracentesis for fluid analysis and pleural biopsy.

## Pleural Effusions

### Epidemiology and Associated Conditions

Under normal circumstances, the volume of fluid within the pleural space is small, roughly is 0.1–0.2 mL/kg of body weight [3]. Substantial increases in fluid volume occur in disease states, which may cause complete collapse of the ipsilateral lung and contralateral shift of the mediastinum. Estimates of pleural effusions in the United States are in excess of 1.5 million patients per year, with most cases resulting from congestive heart failure, cancer, and pneumonia [349]. Pleural fluid accumulation does not presage any specific disease, but rather is a reflection of underlying pathology arising from a wide variety of lung, pleural, and systemic disorders. Thus, a thorough history and physical examination may glean important clues to the etiologic diagnosis. For example, fever and pulmonary infiltrates may suggest an infective etiology. Postcardiotomy syndrome should be considered among patients with recent cardiac surgery who present with fever and pleuritic chest pain. A history of

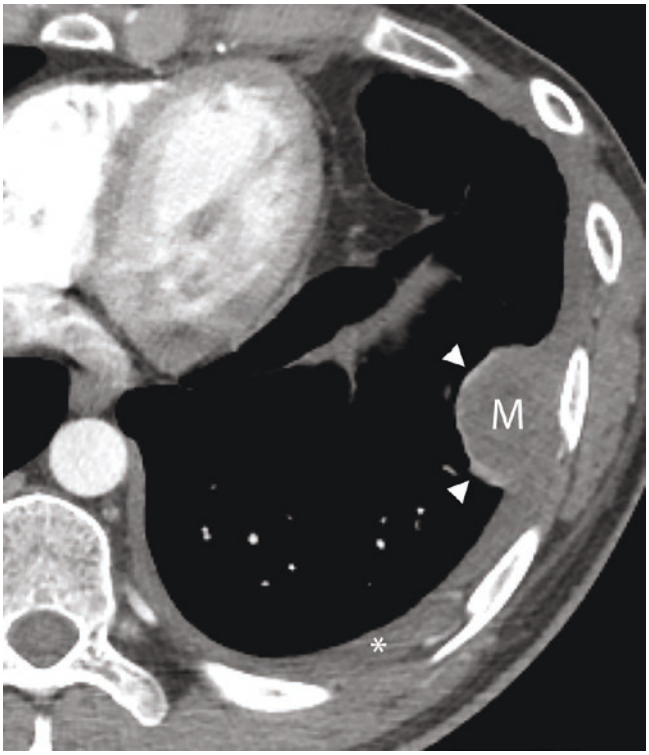


**Fig. 1.85** Pleural metastasis from germ cell tumor. Contrast-enhanced axial CT with mixed germ cell tumor of the prevascular mediastinum demonstrates a pleural metastasis (M) with mild rim enhancement (arrowheads) and a small left pleural effusion (*). Pleural metastasis is the second most common etiology of pleural effusion in adults after left heart failure

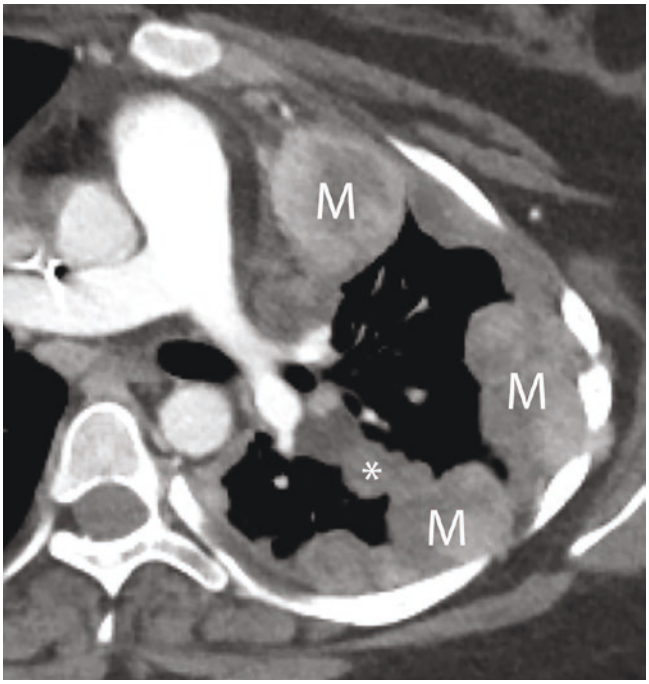


**Fig. 1.86** Pleural metastasis from synovial sarcoma. Contrast-enhanced axial CT with gluteal synovial sarcoma with multiple large heterogeneously enhancing pleural metastases (M) with additional fissural metastasis (*)

trauma or thoracic surgery raises concerns for hemothorax or chylothorax. Acute pleurtic chest pain in the setting of unilateral leg swelling and a right ventricular heave may imply pulmonary thromboembolic disease. A history of occupational exposure to asbestos or chronic exposure to specific prescription medications may strongly indicate asbestos-related and drug-related pleural effusions, respectively. Findings of bilateral leg swelling and/or generalized edema may suggest pleural effusions associated with transudates, such as those caused by renal, cardiac, or liver impairment. More specifically, distended neck veins and an S3 gallop coupled with peripheral edema and an elevated NTpro bone natriuretic peptide (NTproBNP) suggests congestive heart failure. Lymphadenopathy or hepatosplenomegaly may signal a malignant cause [350]. Caudal displacement of the diaphragm is another important factor, which places the length–tension relationship of this muscle at a disadvantage, and contributes to symptoms of dyspnea and increased work of breathing [350, 351].

Standard chest radiographs (CXRs) and ultrasonography are critical components of the initial work-up that provide valuable information regarding effusion size, and position of the mediastinum and diaphragms. CXRs are the initial imaging of choice in the diagnosis of pleural effusions. Fluid volumes of 200 mL or greater are radiographically apparent on posteroanterior views, and blunting of the costophrenic angles with fluid volumes as little as 50 mL can be appreciated on lateral films. Computed tomography (CT) offers additional information. The presence of loculations and air fluid levels within the pleural space and characteristics of the underlying lung parenchyma are better delineated by chest computed tomography (CT). In addition, detailed anatomical information provided by CT imaging, including descriptions of the lung parenchyma, chest wall, parietal and visceral pleural surfaces, and mediastinum offer important clues to the differential diagnosis. Point-of-care imaging with ultrasonography has been associated with more accurate quantitation of pleural fluid volume, resulting in higher rates of successful pleural fluid aspiration. Pleural ultrasonography has been shown to be superior to chest CT in detecting septations within the pleural fluid. Perhaps most importantly, fewer complications have been reported with pleural interventions guided by ultrasound compared to those in which ultrasonography is not used [352–355]. The British Thoracic Society, American Thoracic Society, Society of Thoracic Radiology, and the Society of Thoracic Surgeons now recommend ultrasound imaging to guide thoracentesis and other pleural interventions [355, 356]. Pleural pressure measurements by manometry have been shown to facilitate larger-volume thoracentesis and support the preliminary diagnosis

of trapped lung but do not lessen procedure-related discomfort [357]. The volume of pleural fluid that is considered safe for evacuation in one setting is a matter for ongoing debate. Consensus statements from several national and international thoracic societies, including the American Thoracic Society and the European Respiratory Society suggest limiting the volume of pleural fluid evacuation to 1.0–1.5 L and discontinuing drainage if the patient develops symptoms of dyspnea, cough, or chest discomfort [358]. However, in our experience in the absence of procedure-related symptoms of chest pain, cough, or dyspnea, careful removal of larger pleural fluid volumes may be tolerated. Moreover, we have observed that symptom-limited, large-volume thoracentesis appears to be safe in patients with ipsilateral mediastinal shift on preprocedure chest imaging studies [359].

Analysis of pleural fluid protein content and cellular components may help to inform disease etiology. Thus, sampling of pleural fluid with thoracentesis is recommended whenever possible for all patients with unexplained pleural effusions. Free-flowing effusions that are 10 mm or more in diameter on untrasonography or lateral decubitus radiography are typically of sufficient size for thoracentesis. In patients with clear stigmata of congestive heart failure and bilateral pleural effusions, reassessment for the need for thoracentesis following a trial of diuresis is reasonable. Resolution of pleural effusions due to congestive heart failure typically occurs with 48 h after initiation of diuresis in 75% of patients [6]. Thus, in patients with clear clinical stigmata of congestive heart failure and bilateral pleural effusions, reassessment for the need for thoracentesis following a trial of diuresis is reasonable.

Routine pleural fluid analyses typically include cytological examination and determination of LDH, protein, glucose, albumin, pH, and cell count and differential. Fluid characteristics are divided into exudates and transudates according to Light's criteria, which were initially described in 1972 (Table 1.3) [7, 8]. Increased lactate dehydrogenase (LDH) or protein in pleural fluid relative to serum is characteristic of exudative effusions, which typically occur as a result of inflammatory or infiltrative neoplastic disorders causing increased vascular permeability along the pleural surface or adjacent lung. Specifically, effusions are considered exudative if at least one of the following criteria is present: pleural fluid LDH to serum LDH ratio of greater than 0.6; pleural fluid LDH level greater than 200 IU per liter (or >67% of the upper limit of the normal range for serum LDH); or a ratio of pleural fluid protein to serum protein higher than 0.5 [7]. Transudative effusions, by contrast, result from an imbalance in hydrostatic and oncotic pressures caused by systemic factors. Using Light's criteria, exudative effusions are correctly identified in 70–80% of patients. However, approximately 25–30% of cardiac effusions and 20% of hepatic hydrothoraces are misclassified as exudates. This classification error is most often seen among patients undergoing diuretic therapy [360, 361]. Calculation of the difference between serum versus pleural albumin levels of greater than 1.2 g/dL favors a transudative effusion, although the reliability of this observation remains uncertain. Urinothorax represents another condition in which classification of the pleural fluid has not been clearly delineated. This rare, male-dominant disorder is suggested by findings of urine in the pleural space in association with obstructive or traumatic uropathy [362]. Urinary fluid migrates into the pleural space, presumably through diaphragmatic lymphatics. Dyspnea in association with moderate unilateral pleural effusions has been documented in case reports. The urine commonly maintains its color and smell in the pleural space. Low pleural fluid glucose (<60 mg/dL), acidic urine (pH < 7.30), and pleural/serum creatinine ratio of >1 are characteristic features of urinothorax. Both transudates and exudates have been described, with the latter more often occurring in cases of traumatic urinothorax with associated infection in the urine [363–365].

Although the frequency of each type of effusion varies with the clinical setting, cancer, heart failure, and parapneumonic infections are the predominant overall causes in most large series [9]. Congestive heart failure, cirrhosis, and nephrotic syndrome, which underlie most transudative effusions are often considered benign conditions; however associated 1-year mortality rates of 46–50% suggest a more dismal prognosis [366]. In addition to transudative versus exudative classifications, pleural effusions may be subcategorized into lymphocytic versus neutrophilic, and malignant versus nonmalignant domains. This binary approach fails to recognize that pleural effusions may be triggered by multiple factors in up to 30% of patients [367]. Moreover, multiple causative factors may be interrelated, with one exacerbating the other (i.e., malignancy and hypoalbuminemia; infection, and hypoalbuminemia). Nonetheless, subtyping effusions into these various categories offers useful information regarding the predominant drivers of fluid accumulation. For example, the predominance of neutrophils in the cell differential suggests an acute inflammatory process while a lymphocyte-predominant effusion indicates a more chronic process, such as tuberculosis or malignancy. Lymphocyte subset analysis using flow cytometry may aid in the diagnosis of hematological malignancies [368]. Eosinophilic effusions, defined as greater than 10% eosinophils in the pleural fluid commonly results from blood or air in the pleural cavity. However, a variety of conditions may drive eosinophilic effusions, including pulmonary infarction, malignancy, parapneumonic effusions, tuberculosis, parasitic disease, drug-induced pleurisy, benign asbestos pleural effusion, and eosinophilic granulomatosis with polyangiitis. A low pleural to serum glucose ratio of <0.5 may be seen in malignancy, esophageal rupture, systemic lupus erythematosus, tuberculosis, empyema, and rheumatoid arthritis. Esophageal rupture, malignancy, and

pancreatis are also associated with elevations in pleural fluid amylase [369]. Notably, pleural fluid cytology is positive for malignant cells in only 60% of cases. Other findings in MPE include low pleural fluid glucose (<60 mg/dL), and a low pH < 7.30.

A careful clinical evaluation coupled with clinical imaging and fluid analysis yields a diagnosis in approximately 75–80% of patients. However, 20–25% of pleural effusions remain of uncertain etiology despite a standard workup [370]. Confirmation of disease, therefore, often requires histologic confirmation from tissue obtained from blind-closed needle biopsy, image-guided needle biopsy, pleuroscopy with biopies, and video-assisted thoracoscopic surgery (VATs). Thoracoscopy facilitates direct assessment of the tumor burden within the pleural cavity and allows for large biopsy samples with direct visual control of the pleural surfaces. With a diagnostic yield of 95%, and a relatively good safety profile, it is a preferred approach for unexplained effusions in selected patients.

Infectious etiologies, including empyema and parapneumonic effusions, are the most common cause of exudative effusions and are discussed elsewhere in this chapter. Malignant pleural effusions (MPEs), the second leading cause of exudative effusions, account for more than 125,000 hospitalizations and a leading indication for thoracentesis [371]. MPEs have been reported in association with a wide variety of neoplasms. Lung cancers account for nearly 50% of all MPEs, followed by breast carcinoma and lymphoma [10]. The primary pathogenic mechanism of MPE is increased vascular permeability and direct tumor involvement of the pleura, often with concomitant obstruction of lymphatic drainage. Elevation in the local expression of vascular endothelial growth factor (VEGF), a potent mediator of vascular permeability, has been reported in this setting [11]. Paramalignant effusions resulting from local or systemic effects of the tumor rather than direct malignant pleural involvement have been reported in 17% of patients with cancer. Obstructive pneumonitis, atelectasis, bronchial obstruction, pulmonary embolism, radiochemotherapy-induced toxicity, hypoalbuminemia, and trapped lung are common causes of paramalignant effusions. Paraneoplastic obstruction of lymphatics may result in a triglyceride-rich pleural effusion known as chylothorax. Pleural fluid triglycerides greater than 110 mg/dL and the presence of chylomicrons in the fluid as demonstrated by lipoprotein electrophoresis establishes the diagnosis. The fluid associated with chylothoraces is characteristically milky in appearance, however serosanguinous and sanguinous have also been described [372]. In the absence of a trauma history, large bloody pleural effusions are highly suggestive of malignancy. Malignant pleural effusions may appear grossly bloody without meeting the criteria for hemothorax, defined as a pleural fluid hematocrit that is 50% or greater than the hematocrit of peripheral blood. Leukemic infiltration of the pleura may also cause pleural effusions, however pleural fluid accumulation in the setting of hematologic malignancies more often occurs in association with infection. MPE along with accompanying symptoms of malaise, anorexia, and weight loss signal advanced disease and portend a poor prognosis. Among patients with lung cancer, median survival is reduced regardless of effusion size compared to patients with lung cancer and no effusion [373, 374]. A median survival of 4–7 months has been reported among patients with MPE and is influenced by tumor subtype. Lung and gastric cancers confer the worse outcomes (2–3 months) compared to mesothelioma and hematologic cancers (approximately 1 year) [375].

## Management

Rates of malignant pleural fluid reaccumulation is high (97%), with most effusions recurring within 1–3 days following fluid evacuation. Knowledge of lung re-expansion following large-volume thoracentesis and whether the procedure resulted in improvement in dyspnea are critical pieces of information in considering further palliative treatment strategies. If symptoms are not alleviated after large-volume thoracentesis, further diagnostic testing to investigate alternative causes of dyspnea should be pursued. Patients with CXR evidence of lung re-expansion and who report amelioration in symptoms post thoracentesis may be candidates for intrapleural catheter placement, chemical pleurodesis, or combination procedures, whereas among individuals with a nonexpendable (trapped) lung, a tunneled pleural catheter is the treatment of choice for recurrent MPE. Tunneled or indwelling pleural catheter (IPC) placement is a minimally invasive procedure that can be performed as an outpatient. These small-bore flexible catheters are tunneled under the skin, and can be managed at home. Several randomized trials and one meta-analysis suggest durable symptom palliation. Spontaneous pleurodesis occurs in 40–50% of patients with regular drainage, at a mean of 60 days after catheter insertion [355, 376, 377]. Trials have suggested that daily drainage and the use of sclerosing agents may promote earlier pleurodesis and substantially fewer days with the catheter [377–379]. Catheter infection has been reported in 5% of patients. In the absence of empyema, the infection may be treated successfully with antibiotics without the need for catheter removal in most cases [380]. Other reported complications of IPC include the formation of catheter- or disease-related loculations and catheter fracture. Loculations are frequently associated with nonreexpandable lung and may be amenable to fibrinolytic therapy. Retained intrapleural cathether fragments caused by catheter fracture have been anecdotally reported [381–383].

Pleurodesis is a viable alternative to IPC, particularly among patients with rapidly recurrent MPE (within 1 month), evidence of lung reexpansion on a post thoracentesis CXR, and an anticipated survival of >2 months. Pleural symphysis is achieved by the introduction of a sclerosant, which triggers inflammation and fibrosis within the pleural space. In carefully selected patients, successful outcomes with talc pleurodesis is much higher (70–90%) than the reported rates of pleurodesis achieved with IPC catheters [384, 385]. The approach to pleurodesis broadly varies in terms of the sclerosing agent and formulation (insufflation versus slurry), pleurodesis type (chemical versus mechanical), and method of delivery (direct application during pleuroscopy versus large bore chest tube versus IPC). Specific choices are institution-driven and operator-dependent. Chemical pleurodesis using sterile talc is the most consistently preferred method of pleurodesis. Rates of symptom palliation appear similar in IPC versus chemical pleurodesis, however compared to IPC, chemical pleurodesis offers a shorter time to symptom palliation without the need for a long-term catheter. Talc pleurodesis requires a 3–5 day hospitalization. Pain, transient hypoxemia, and fever are common during or immediately after the procedure. Rarely hypoxic respiratory failure associated with ARDS following talc-instillation has been reported and is felt to correlate with talc partical size of <5–10 μm [376].

## References


1. Sureka B, et al. Radiological review of pleural tumors. Indian J Radiol Imaging. 2013;23(4):313–20.
2. Finley DJ, Rusch VW. Anatomy of the pleura. Thorac Surg Clin. 2011;21(2):157–63, vii.
3. Noppen M. Normal volume and cellular contents of pleural fluid. Curr Opin Pulm Med. 2001;7(4):180–2.
4. Negrini D, Moriondo A. Pleural function and lymphatics. Acta Physiol (Oxf). 2013;207(2):244–59.
5. Charalampidis C, et al. Pleura space anatomy. J Thorac Dis. 2015;7(Suppl 1):S27–32.
6. Shinto RA, Light RW. Effects of diuresis on the characteristics of pleural fluid in patients with congestive heart failure. Am J Med. 1990;88(3):230–4.
7. Light RW, et al. Pleural effusions: the diagnostic separation of transudates and exudates. Ann Intern Med. 1972;77(4):507–13.
8. Broaddus VC, Light RW. What is the origin of pleural transudates and exudates? Chest. 1992;102(3):658–9.
9. Porcel JM, et al. Etiology of pleural effusions: analysis of more than 3,000 consecutive thoracenteses. Arch Bronconeumol. 2014;50(5):161–5.
10. Johnston WW. The malignant pleural effusion. A review of cytopathologic diagnoses of 584 specimens from 472 consecutive patients. Cancer. 1985;56(4):905–9.
11. Zebrowski BK, et al. Vascular endothelial growth factor levels and induction of permeability in malignant pleural effusions. Clin Cancer Res. 1999;5(11):3364–8.
12. Ryu JH, Yi ES. Immunoglobulin G4-related disease and the lung. Clin Chest Med. 2016;37(3):569–78.
13. Huggins JT, Sahn SA. Causes and management of pleural fibrosis. Respirology. 2004;9(4):441–7.
14. Batra H, Antony VB. Pleural mesothelial cells in pleural and lung diseases. J Thorac Dis. 2015;7(6):964–80.
15. Maldonado F, Feller-Kopman D. Should manometry be routinely used during thoracentesis? Yes, but not without some basic physiologic understanding! Expert Rev Respir Med. 2016;10(10):1035–7.
16. Lentz RJ, et al. The impact of gravity vs suction-driven therapeutic thoracentesis on pressure-related complications: the GRAVITAS Multicenter Randomized Controlled Trial. Chest. 2019;156:A1102.
17. Feller-Kopman D. Point: should pleural manometry be performed routinely during thoracentesis? Yes. Chest. 2012;141(4):844–5.
18. Chopra A, et al. The relationship of pleural manometry with Post-thoracentesis chest radiographic findings in malignant pleural effusion. Chest. 2020;157(2):421–6.
19. Singh RK, Pattari S. *Xanthomatous pleuritis.* Respir Med Case Rep. 2018;23:143–4.
20. Askin FB, McCann BG, Kuhn C. Reactive eosinophilic pleuritis: a lesion to be distinguished from pulmonary eosinophilic granuloma. Arch Pathol Lab Med. 1977;101(4):187–91.
21. Fang L, et al. Recurrent eosinophilic pleuritis caused by sparganum infection: a case report and review of the literature. Medicine (Baltimore). 2020;99(22):e20226.
22. Evison M, et al. Olanzapine-induced eosinophilic pleuritis. Respir Med Case Rep. 2015;14:24–6.
23. Bartlett JG. Anaerobic bacterial infections of the lung and pleural space. Clin Infect Dis. 1993;16(Suppl 4):S248–55.
24. Antony VB, Mohammed KA. Pathophysiology of pleural space infections. Semin Respir Infect. 1999;14(1):9–17.
25. Yew WW, et al. Diagnosis of tuberculous pleural effusion by the detection of tuberculostearic acid in pleural aspirates. Chest. 1991;100(5):1261–3.
26. Cohen LA, Light RW. Tuberculous pleural effusion. Turk Thorac J. 2015;16(1):1–9.
27. Seibert AF, et al. Tuberculous pleural effusion - 20-year experience. Chest. 1991;99(4):883–6.
28. Valdes L, et al. Tuberculous pleural effusions. Eur J Intern Med. 2003;14(2):77–88.
29. Chan CH, et al. Clinical and pathological features of tuberculous pleural effusion and its long-term consequences. Respiration. 1991;58(3–4):171–5.
30. Barbas CS, et al. The relationship between pleural fluid findings and the development of pleural thickening in patients with pleural tuberculosis. Chest. 1991;100(5):1264–7.
31. de Pablo A, et al. Are pleural fluid parameters related to the development of residual pleural thickening in tuberculosis? Chest. 1997;112(5):1293–7.
32. Candela A, et al. Functional sequelae of tuberculous pleurisy in patients correctly treated. Chest. 2003;123(6):1996–2000.
33. Baumann MH, et al. Pleural tuberculosis in the United States: incidence and drug resistance. Chest. 2007;131(4):1125–32.
34. Light RW. Update on tuberculous pleural effusion. Respirology. 2010;15(3):451–8.
35. Bhuniya S, et al. Role of therapeutic thoracentesis in tuberculous pleural effusion. Ann Thorac Med. 2012;7(4):215–9.
36. Dawood W, et al. Pleural tuberculosis mimicking malignant mesothelioma. Respir Med Case Rep. 2020;29:100964.
37. Isoda K, Hamamoto Y. Uremic pleuritis--clinicopathological analysis of 26 autopsy cases. Bull Osaka Med Sch. 1984;30(2):73–80.
38. Nidus BD, et al. Uremic pleuritis--a clinicopathological entity. N Engl J Med. 1969;281(5):255–6.
39. Rashid-Farokhi F, et al. Uremic pleuritis in chronic hemodialysis patients. Hemodial Int. 2013;17(1):94–100.

40. Broderick SR. Hemothorax etiology, diagnosis and management. Thorac Surg Clin. 2013;23(1):89.
41. Demetri L, et al. Is observation for traumatic hemothorax safe? J Trauma Acute Care Surg. 2018;84(3):454–8.
42. Heidecker J, Sahn SA. The spectrum of pleural effusions after coronary artery bypass grafting surgery. Clin Chest Med. 2006;27(2):267–83.
43. Light RW. Pleural effusions after coronary artery bypass graft surgery. Curr Opin Pulm Med. 2002;8(4):308–11.
44. Schuller D, Morrow LE. Pulmonary complications after coronary revascularization. Curr Opin Cardiol. 2000;15(5):309–15.
45. Lee YC, et al. Symptomatic persistent post-coronary artery bypass graft pleural effusions requiring operative treatment: clinical and histologic features. Chest. 2001;119(3):795–800.
46. Kerper LE, et al. Systematic review of pleural plaques and lung function. Inhal Toxicol. 2015;27(1):15–44.
47. Maxim LD, Utell MJ. Review of refractory ceramic fiber (RCF) toxicity, epidemiology and occupational exposure. Inhal Toxicol. 2018;30(2):49–71.
48. Norbet C, et al. Asbestos-related lung disease: a pictorial review. Curr Probl Diagn Radiol. 2015;44(4):371–82.
49. Sprince NL, et al. Asbestos exposure and asbestos-related pleural and parenchymal disease. Associations with immune imbalance. Am Rev Respir Dis. 1991;143(4 Pt 1):822–8.
50. Weill D, Weill H. Diagnosis and initial management of nonmalignant diseases related to asbestos. Am J Respir Crit Care Med. 2005;171(5):527–8, author reply 528–30.
51. Weill H. Biological effects: asbestos-cement manufacturing. Ann Occup Hyg. 1994;38(4):533–8, 413.
52. Cox CW, Rose CS, Lynch DA. State of the art: imaging of occupational lung disease. Radiology. 2014;270(3):681–96.
53. Barnes H, et al. Silica-associated lung disease: an old-world exposure in modern industries. Respirology. 2019;24(12):1165–75.
54. Ding M, et al. Diseases caused by silica: mechanisms of injury and disease development. Int Immunopharmacol. 2002;2(2–3):173–82.
55. Stafford M, et al. Treatment of acute silicoproteinosis by whole-lung lavage. Semin Cardiothorac Vasc Anesth. 2013;17(2):152–9.
56. Karnak D, et al. Acute silicoproteinosis: therapy success. Respiration. 2011;82(6):550–1.
57. Lake F, Proudman S. Rheumatoid arthritis and lung disease: from mechanisms to a practical approach. Semin Respir Crit Care Med. 2014;35(2):222–38.
58. Kelly C, et al. Lung involvement in inflammatory rheumatic diseases. Best Pract Res Clin Rheumatol. 2016;30(5):870–88.
59. Antony VB. Drug-induced pleural disease. Clin Chest Med. 1998;19(2):331–40.
60. Tintner R, et al. Pleuropulmonary fibrosis after long-term treatment with the dopamine agonist pergolide for Parkinson disease. Arch Neurol. 2005;62(8):1290–5.
61. Tornling G, et al. Pleuropulmonary reactions in patients on bromocriptine treatment. Eur J Respir Dis. 1986;68(1):35–8.
62. Shaunak S, et al. Pericardial, retroperitoneal, and pleural fibrosis induced by pergolide. J Neurol Neurosurg Psychiatry. 1999;66(1):79–81.
63. Kok-Jensen A, Lindeneg O. Pleurisy and fibrosis of the pleura during methysergide treatment of hemicrania. Scand J Respir Dis. 1970;51(3):218–22.
64. Belmonte Y, et al. Pleuropulmonary toxicity of another anti-Parkinson's drug: Cabergoline. Open Respir Med J. 2009;3:90–3.
65. Hamada K, et al. Cyclophosphamide-induced late-onset lung disease. Intern Med. 2003;42(1):82–7.
66. Malik SW, et al. Lung toxicity associated with cyclophosphamide use. Two distinct patterns. Am J Respir Crit Care Med. 1996;154(6 Pt 1):1851–6.
67. Papiris SA, et al. Amiodarone: review of pulmonary effects and toxicity. Drug Saf. 2010;33(7):539–58.
68. Standertskjold-Nordenstam CG, et al. Amiodarone pulmonary toxicity. Chest radiography and CT in asymptomatic patients. Chest. 1985;88(1):143–5.
69. Sweidan AJ, et al. Amiodarone-induced pulmonary toxicity - a frequently missed complication. Clin Med Insights Case Rep. 2016;9:91–4.
70. Fernandez Garcia D, et al. IgG4-related disease with lung involvement. Arch Bronconeumol. 2019;55(3):165–6.
71. Morales AT, et al. An update on IgG4-related lung disease. Eur J Intern Med. 2019;66:18–24.
72. Pandita A, Wong J. IgG4-related disease in lung: a diagnostic challenge. Pathology. 2020;52:390.
73. Kinoshita Y, et al. Pleuroparenchymal fibroelastosis as a histological background of autoimmune diseases. Virchows Arch. 2019;474(1):97–104.
74. Zhang S, et al. Pleuroparenchymal fibroelastosis secondary to autologous hematopoietic stem cell transplantation: a case report. Exp Ther Med. 2019;17(4):2557–60.
75. Chua F, et al. Pleuroparenchymal fibroelastosis. A review of clinical, radiological, and pathological characteristics. Ann Am Thorac Soc. 2019;16(11):1351–9.
76. Cheng SK, Chuah KL. Pleuroparenchymal fibroelastosis of the lung: a review. Arch Pathol Lab Med. 2016;140(8):849–53.
77. Enomoto Y, et al. Clinical diagnosis of idiopathic pleuroparenchymal fibroelastosis: a retrospective multicenter study. Respir Med. 2017;133:1–5.
78. Kono M, et al. Clinical significance of lower-lobe interstitial lung disease on high-resolution computed tomography in patients with idiopathic pleuroparenchymal fibroelastosis. Respir Med. 2019;154:122–6.
79. Lynch DA, Gamsu G, Aberle DR. Conventional and high resolution computed tomography in the diagnosis of asbestos-related diseases. Radiographics. 1989;9(3):523–51.
80. Murray JG, et al. CT appearance of the pleural space after talc pleurodesis. AJR Am J Roentgenol. 1997;169(1):89–91.
81. Karpathiou G, Stefanou D, Froudarakis ME. Pleural neoplastic pathology. Respir Med. 2015;109(8):931–43.
82. Cagle PT, Churg A. Differential diagnosis of benign and malignant mesothelial proliferations on pleural biopsies. Arch Pathol Lab Med. 2005;129(11):1421–7.
83. Churg A, Galateau-Salle F. The separation of benign and malignant mesothelial proliferations. Arch Pathol Lab Med. 2012;136(10):1217–26.
84. Henderson DW, Shilkin KB, Whitaker D. Reactive mesothelial hyperplasia vs mesothelioma, including mesothelioma in situ: a brief review. Am J Clin Pathol. 1998;110(3):397–404.
85. Kradin RL, Mark EJ. Distinguishing benign mesothelial hyperplasia from neoplasia: a practical approach. Semin Diagn Pathol. 2006;23(1):4–14.
86. Zeren EH, Demirag F. Benign and malignant mesothelial proliferation. Surg Pathol Clin. 2010;3(1):83–107.
87. Churg A, et al. Malignant mesothelioma in situ: morphologic features and clinical outcome. Mod Pathol. 2020;33(2):297–302.
88. Holoch KJ, Lessey BA. Endometriosis and infertility. Clin Obstet Gynecol. 2010;53(2):429–38.
89. Visouli AN, et al. Catamenial pneumothorax. J Thorac Dis. 2014;6(Suppl 4):S448–60.
90. Riley L, et al. Obstetric and gynecologic causes of pleural effusions. Dis Mon. 2019;65(4):109–14.
91. Nair SS, Nayar J. Thoracic endometriosis syndrome: a veritable Pandora's box. J Clin Diagn Res. 2016;10(4):QR04-8.
92. Channabasavaiah AD, Joseph JV. Thoracic endometriosis: revisiting the association between clinical presentation and thoracic

pathology based on thoracoscopic findings in 110 patients. Medicine (Baltimore). 2010;89(3):183–8.
93. Picozzi G, et al. MRI features of pleural endometriosis after catamenial haemothorax. BMJ Case Rep. 2009;2009:bcr2006071415.
94. Alifano M, et al. Thoracic endometriosis: current knowledge. Ann Thorac Surg. 2006;81(2):761–9.
95. Alwadhi S, et al. Thoracic endometriosis-a rare cause of haemoptysis. J Clin Diagn Res. 2016;10(4):TD01-2.
96. Chung SY, et al. Computed tomography findings of pathologically confirmed pulmonary parenchymal endometriosis. J Comput Assist Tomogr. 2005;29(6):815–8.
97. Rousset P, et al. Thoracic endometriosis syndrome: CT and MRI features. Clin Radiol. 2014;69(3):323–30.
98. Augoulea A, Lambrinoudaki I, Christodoulakos G. Thoracic endometriosis syndrome. Respiration. 2008;75(1):113–9.
99. Flieder DB, et al. Pleuro-pulmonary endometriosis and pulmonary ectopic deciduosis: a clinicopathologic and immunohistochemical study of 10 cases with emphasis on diagnostic pitfalls. Hum Pathol. 1998;29(12):1495–503.
100. Karpel JP, Appel D, Merav A. Pulmonary endometriosis. Lung. 1985;163(3):151–9.
101. Lattes R, et al. A clinical and pathologic study of endometriosis of the lung. Surg Gynecol Obstet. 1956;103(5):552–8.
102. Foster DC, et al. Pleural and parenchymal pulmonary endometriosis. Obstet Gynecol. 1981;58(5):552–6.
103. Handra-Luca A, et al. [Adenomatoid tumor of the pleura. Case report]. Ann Pathol. 2000;20(4):369–72.
104. Kaplan MA, et al. Adenomatoid tumors of the pleura. Am J Surg Pathol. 1996;20(10):1219–23.
105. Minato H, et al. Adenomatoid tumor of the pleura. Pathol Int. 2009;59(8):567–71.
106. Weissferdt A, Kalhor N, Suster S. Malignant mesothelioma with prominent adenomatoid features: a clinicopathologic and immunohistochemical study of 10 cases. Ann Diagn Pathol. 2011;15(1):25–9.
107. Gordon GJ, et al. Using gene expression ratios to predict outcome among patients with mesothelioma. J Natl Cancer Inst. 2003;95(8):598–605.
108. Gordon GJ, et al. Expression patterns of inhibitor of apoptosis proteins in malignant pleural mesothelioma. J Pathol. 2007;211(4):447–54.
109. Hirao T, et al. Alterations of the p16(INK4) locus in human malignant mesothelial tumors. Carcinogenesis. 2002;23(7):1127–30.
110. Wald O, Sugarbaker DJ. New concepts in the treatment of malignant pleural mesothelioma. Annu Rev Med. 2018;69:365–77.
111. Baas P, et al. Malignant pleural mesothelioma: ESMO clinical practice guidelines for diagnosis, treatment and follow-up. Ann Oncol. 2015;26(Suppl 5):v31–9.
112. Wolf AS, Flores RM. Current treatment of mesothelioma: extrapleural pneumonectomy versus pleurectomy/decortication. Thorac Surg Clin. 2016;26(3):359–75.
113. Wolf AS, Flores RM. Updates in staging and management of malignant pleural mesothelioma. Surg Oncol Clin N Am. 2020;29(4):603–12.
114. Wu L, de Perrot M. Radio-immunotherapy and chemo-immunotherapy as a novel treatment paradigm in malignant pleural mesothelioma. Transl Lung Cancer Res. 2017;6(3):325–34.
115. Zeltsman M, et al. CAR T-cell therapy for lung cancer and malignant pleural mesothelioma. Transl Res. 2017;187:1–10.
116. Hiriart E, Deepe R, Wessels A. Mesothelium and malignant mesothelioma. J Dev Biol. 2019;7(2):7.
117. Marsh GM, et al. Non-occupational exposure to asbestos and risk of pleural mesothelioma: review and meta-analysis. Occup Environ Med. 2017;74(11):838–46.
118. Price B, Ware A. Time trend of mesothelioma incidence in the United States and projection of future cases: an update based on SEER data for 1973 through 2005. Crit Rev Toxicol. 2009;39(7):576–88.
119. Attanoos RL, Pugh MR. The diagnosis of pleural tumors other than mesothelioma. Arch Pathol Lab Med. 2018;142(8):902–13.
120. Kliment CR, Clemens K, Oury TD. North American erionite-associated mesothelioma with pleural plaques and pulmonary fibrosis: a case report. Int J Clin Exp Pathol. 2009;2(4):407–10.
121. Paoletti L, et al. Unusually high incidence of malignant pleural mesothelioma in a town of eastern Sicily: an epidemiological and environmental study. Arch Environ Health. 2000;55(6):392–8.
122. Teta MJ, et al. Therapeutic radiation for lymphoma: risk of malignant mesothelioma. Cancer. 2007;109(7):1432–8.
123. Shannon VR, Nesbitt JC, Libshitz HI. Malignant pleural mesothelioma after radiation therapy for breast cancer. A report of two additional patients. Cancer. 1995;76(3):437–41.
124. Farioli A, et al. Radiation-induced mesothelioma among long-term solid cancer survivors: a longitudinal analysis of SEER database. Cancer Med. 2016;5(5):950–9.
125. Antman KH, et al. Malignant mesothelioma following radiation exposure. J Clin Oncol. 1983;1(11):695–700.
126. Testa JR, et al. Germline BAP1 mutations predispose to malignant mesothelioma. Nat Genet. 2011;43(10):1022–5.
127. Bianchi C, Bianchi T. Malignant mesothelioma: global incidence and relationship with asbestos. Ind Health. 2007;45(3):379–87.
128. Delgermaa V, et al. Global mesothelioma deaths reported to the World Health Organization between 1994 and 2008. Bull World Health Organ. 2011;89(10):716–24, 724A–C.
129. Rusch VW, et al. Initial analysis of the International Association for the Study of Lung Cancer Mesothelioma Database. J Thorac Oncol. 2012;7(11):1631–9.
130. Craighead JE. Epidemiology of mesothelioma and historical background. Recent Results Cancer Res. 2011;189:13–25.
131. Finn RS, et al. Postmortem findings of malignant pleural mesothelioma: a two-center study of 318 patients. Chest. 2012;142(5):1267–73.
132. Gill RR, et al. Radiologic considerations and standardization of malignant pleural mesothelioma imaging within clinical trials: consensus statement from the NCI thoracic malignancy steering committee - International Association for the Study of Lung Cancer - Mesothelioma Applied Research Foundation clinical trials planning meeting. J Thorac Oncol. 2019;14(10):1718–31.
133. Armato SG III, et al. Imaging in pleural mesothelioma: a review of the 14th international conference of the International Mesothelioma Interest Group. Lung Cancer. 2019;130:108–14.
134. Rusch VW, Giroux D. Do we need a revised staging system for malignant pleural mesothelioma? Analysis of the IASLC database. Ann Cardiothorac Surg. 2012;1(4):438–48.
135. Byrne MJ, Nowak AK. Modified RECIST criteria for assessment of response in malignant pleural mesothelioma. Ann Oncol. 2004;15(2):257–60.
136. Opitz I, et al. A new prognostic score supporting treatment allocation for multimodality therapy for malignant pleural mesothelioma: a review of 12 years' experience. J Thorac Oncol. 2015;10(11):1634–41.
137. Walker S, Bibby AC, Maskell NA. Current best practice in the evaluation and management of malignant pleural effusions. Ther Adv Respir Dis. 2017;11(2):105–14.
138. Flores RM, et al. Extrapleural pneumonectomy versus pleurectomy/decortication in the surgical management of malignant pleural mesothelioma: results in 663 patients. J Thorac Cardiovasc Surg. 2008;135(3):620–6, 626.e1–3.
139. van Zandwijk N, et al. Guidelines for the diagnosis and treatment of malignant pleural mesothelioma. J Thorac Dis. 2013;5(6):E254–307.

140. Ye L, et al. Immunotherapy strategies for mesothelioma - the role of tumor specific neoantigens in a new era of precision medicine. Expert Rev Respir Med. 2019;13(2):181–92.
141. Cantó A, et al. Videothoracoscopy in the diagnosis and treatment of malignant pleural mesothelioma with associated pleural effusions. Thorac Cardiovasc Surg. 1997;45(1):16–9.
142. Xia H, et al. Efficacy and safety of talc pleurodesis for malignant pleural effusion: a meta-analysis. PLoS One. 2014;9(1):e87060.
143. Miller BH, et al. From the archives of the AFIP. Malignant pleural mesothelioma: radiologic-pathologic correlation. Radiographics. 1996;16(3):613–44.
144. Bayman N, et al. Protocol for PIT: a phase III trial of prophylactic irradiation of tracts in patients with malignant pleural mesothelioma following invasive chest wall intervention. BMJ Open. 2016;6(1):e010589.
145. Halford P, Clive AO. Is there a role for prophylactic radiotherapy to intervention tract sites in patients with malignant pleural mesothelioma? Transl Lung Cancer Res. 2018;7(5):584–92.
146. O'Rourke N, et al. A randomised controlled trial of intervention site radiotherapy in malignant pleural mesothelioma. Radiother Oncol. 2007;84(1):18–22.
147. Bydder S, et al. A randomised trial of single-dose radiotherapy to prevent procedure tract metastasis by malignant mesothelioma. Br J Cancer. 2004;91(1):9–10.
148. Wechsler RJ, Rao VM, Steiner RM. The radiology of thoracic malignant mesothelioma. Crit Rev Diagn Imaging. 1984;20(4):283–310.
149. Nickell LT Jr, et al. Multimodality imaging for characterization, classification, and staging of malignant pleural mesothelioma. Radiographics. 2014;34(6):1692–706.
150. Kawashima A, Libshitz HI. Malignant pleural mesothelioma: CT manifestations in 50 cases. AJR Am J Roentgenol. 1990;155(5):965–9.
151. Leung AN, Muller NL, Miller RR. CT in differential diagnosis of diffuse pleural disease. AJR Am J Roentgenol. 1990;154(3):487–92.
152. Shiba N, et al. A case of malignant pleural mesothelioma with osseous and cartilaginous differentiation. J Thorac Imaging. 2011;26(1):W30–2.
153. Patz EF Jr, et al. Malignant pleural mesothelioma: value of CT and MR imaging in predicting resectability. AJR Am J Roentgenol. 1992;159(5):961–6.
154. Sharma A, et al. Patterns of lymphadenopathy in thoracic malignancies. Radiographics. 2004;24(2):419–34.
155. Kim SB, Varkey B, Choi H. Diagnosis of malignant pleural mesothelioma by axillary lymph node biopsy. Chest. 1987;91(2):279–81.
156. Eibel R, Tuengerthal S, Schoenberg SO. The role of new imaging techniques in diagnosis and staging of malignant pleural mesothelioma. Curr Opin Oncol. 2003;15(2):131–8.
157. Plathow C, et al. Quantification of lung tumor volume and rotation at 3D dynamic parallel MR imaging with view sharing: preliminary results. Radiology. 2006;240(2):537–45.
158. Giesel FL, et al. Dynamic contrast-enhanced MRI of malignant pleural mesothelioma: a feasibility study of noninvasive assessment, therapeutic follow-up, and possible predictor of improved outcome. Chest. 2006;129(6):1570–6.
159. Gill RR, et al. Diffusion-weighted MRI of malignant pleural mesothelioma: preliminary assessment of apparent diffusion coefficient in histologic subtypes. AJR Am J Roentgenol. 2010;195(2):W125–30.
160. Coolen J, et al. Malignant pleural mesothelioma: visual assessment by using pleural pointillism at diffusion-weighted MR imaging. Radiology. 2015;274(2):576–84.
161. Yildirim H, et al. Clinical value of fluorodeoxyglucose-positron emission tomography/computed tomography in differentiation of malignant mesothelioma from asbestos-related benign pleural disease: an observational pilot study. J Thorac Oncol. 2009;4(12):1480–4.
162. Plathow C, et al. Computed tomography, positron emission tomography, positron emission tomography/computed tomography, and magnetic resonance imaging for staging of limited pleural mesothelioma: initial results. Investig Radiol. 2008;43(10):737–44.
163. Nowak AK, et al. The IASLC Mesothelioma Staging Project: proposals for revisions of the T descriptors in the forthcoming eighth edition of the TNM classification for pleural mesothelioma. J Thorac Oncol. 2016;11(12):2089–99.
164. Therasse P, et al. New guidelines to evaluate the response to treatment in solid tumors. European Organization for Research and Treatment of Cancer, National Cancer Institute of the United States, National Cancer Institute of Canada. J Natl Cancer Inst. 2000;92(3):205–16.
165. van Klaveren RJ, et al. Inadequacy of the RECIST criteria for response evaluation in patients with malignant pleural mesothelioma. Lung Cancer. 2004;43(1):63–9.
166. Eisenhauer EA, et al. New response evaluation criteria in solid tumours: revised RECIST guideline (version 1.1). Eur J Cancer. 2009;45(2):228–47.
167. Armato SG III, Nowak AK. Revised modified response evaluation criteria in solid tumors for assessment of response in malignant pleural mesothelioma (version 1.1). J Thorac Oncol. 2018;13(7):1012–21.
168. Pass HI, et al. Preoperative tumor volume is associated with outcome in malignant pleural mesothelioma. J Thorac Cardiovasc Surg. 1998;115(2):310–7, discussion 317–8.
169. Frauenfelder T, et al. Volumetry: an alternative to assess therapy response for malignant pleural mesothelioma? Eur Respir J. 2011;38(1):162–8.
170. Gill RR, et al. Epithelial malignant pleural mesothelioma after extrapleural pneumonectomy: stratification of survival with CT-derived tumor volume. AJR Am J Roentgenol. 2012;198(2):359–63.
171. Gill RR, et al. North American multicenter volumetric CT study for clinical staging of malignant pleural mesothelioma: feasibility and logistics of setting up a quantitative imaging study. J Thorac Oncol. 2016;11(8):1335–44.
172. Francis RJ, et al. Early prediction of response to chemotherapy and survival in malignant pleural mesothelioma using a novel semiautomated 3-dimensional volume-based analysis of serial 18F-FDG PET scans. J Nucl Med. 2007;48(9):1449–58.
173. Nowak AK, et al. A novel prognostic model for malignant mesothelioma incorporating quantitative FDG-PET imaging with clinical parameters. Clin Cancer Res. 2010;16(8):2409–17.
174. Berzenji L, Van Schil PE, Carp L. The eighth TNM classification for malignant pleural mesothelioma. Transl Lung Cancer Res. 2018;7(5):543–9.
175. Arrossi AV, et al. Histologic assessment and prognostic factors of malignant pleural mesothelioma treated with extrapleural pneumonectomy. Am J Clin Pathol. 2008;130(5):754–64.
176. Moran CA, Wick MR, Suster S. The role of immunohistochemistry in the diagnosis of malignant mesothelioma. Semin Diagn Pathol. 2000;17(3):178–83.
177. Mann S, et al. Revisiting localized malignant mesothelioma. Ann Diagn Pathol. 2019;39:74–7.
178. Churg A, et al. Malignant mesothelioma in situ. Histopathology. 2018;72(6):1033–8.
179. Wick MR, et al. Immunohistochemical differential diagnosis of pleural effusions, with emphasis on malignant mesothelioma. Curr Opin Pulm Med. 2001;7(4):187–92.
180. Suster S, Moran CA. Applications and limitations of immunohistochemistry in the diagnosis of malignant mesothelioma. Adv Anat Pathol. 2006;13(6):316–29.

181. Yousem SA, Hochholzer L. Malignant mesotheliomas with osseous and cartilaginous differentiation. Arch Pathol Lab Med. 1987;111(1):62–6.
182. Henderson DW, et al. Lymphohistiocytoid mesothelioma: a rare lymphomatoid variant of predominantly sarcomatoid mesothelioma. Ultrastruct Pathol. 1988;12(4):367–84.
183. Ordonez NG, Myhre M, Mackay B. Clear cell mesothelioma. Ultrastruct Pathol. 1996;20(4):331–6.
184. Ordonez NG. Epithelial mesothelioma with deciduoid features: report of four cases. Am J Surg Pathol. 2000;24(6):816–23.
185. Peterson JT Jr, Greenberg SD, Buffler PA. Non-asbestos-related malignant mesothelioma. A review. Cancer. 1984;54(5):951–60.
186. Ordonez NG. Value of cytokeratin 5/6 immunostaining in distinguishing epithelial mesothelioma of the pleura from lung adenocarcinoma. Am J Surg Pathol. 1998;22(10):1215–21.
187. Dei Tos AP, Doglioni C. Calretinin: a novel tool for diagnostic immunohistochemistry. Adv Anat Pathol. 1998;5(1):61–6.
188. Oates J, Edwards C. HBME-1, MOC-31, WT1 and calretinin: an assessment of recently described markers for mesothelioma and adenocarcinoma. Histopathology. 2000;36(4):341–7.
189. Ordonez NG. Value of thyroid transcription factor-1, E-cadherin, BG8, WT1, and CD44S immunostaining in distinguishing epithelial pleural mesothelioma from pulmonary and nonpulmonary adenocarcinoma. Am J Surg Pathol. 2000;24(4):598–606.
190. Collins CL, et al. Thrombomodulin expression in malignant pleural mesothelioma and pulmonary adenocarcinoma. Am J Pathol. 1992;141(4):827–33.
191. Ordonez NG. Application of mesothelin immunostaining in tumor diagnosis. Am J Surg Pathol. 2003;27(11):1418–28.
192. Mangano WE, et al. The diagnosis of desmoplastic malignant mesothelioma and its distinction from fibrous pleurisy: a histologic and immunohistochemical analysis of 31 cases including p53 immunostaining. Am J Clin Pathol. 1998;110(2):191–9.
193. Colby TV. The diagnosis of desmoplastic malignant mesothelioma. Am J Clin Pathol. 1998;110(2):135–6.
194. Chiosea S, et al. Diagnostic importance of 9p21 homozygous deletion in malignant mesotheliomas. Mod Pathol. 2008;21(6):742–7.
195. Hida T, et al. BAP1 immunohistochemistry and p16 FISH results in combination provide higher confidence in malignant pleural mesothelioma diagnosis: ROC analysis of the two tests. Pathol Int. 2016;66(10):563–70.
196. Hwang HC, et al. BAP1 immunohistochemistry and p16 FISH in the diagnosis of sarcomatous and desmoplastic mesotheliomas. Am J Surg Pathol. 2016;40(5):714–8.
197. Kulduk G, et al. The importance of FISH signal cut-off values for 9p21 deletion in malignant pleural mesothelioma: is it underestimated? Pathol Res Pract. 2019;215(6):152377.
198. Takeda M, et al. 9p21 deletion in the diagnosis of malignant mesothelioma, using fluorescence in situ hybridization analysis. Pathol Int. 2010;60(5):395–9.
199. Chung CT, et al. FISH assay development for the detection of p16/CDKN2A deletion in malignant pleural mesothelioma. J Clin Pathol. 2010;63(7):630–4.
200. Dacic S, et al. Prognostic significance of p16/cdkn2a loss in pleural malignant mesotheliomas. Virchows Arch. 2008;453(6):627–35.
201. McGregor SM, et al. BAP1 immunohistochemistry has limited prognostic utility as a complement of CDKN2A (p16) fluorescence in situ hybridization in malignant pleural mesothelioma. Hum Pathol. 2017;60:86–94.
202. Sheffield BS, et al. BAP1 immunohistochemistry and p16 FISH to separate benign from malignant mesothelial proliferations. Am J Surg Pathol. 2015;39(7):977–82.
203. Wu D, et al. Usefulness of p16/CDKN2A fluorescence in situ hybridization and BAP1 immunohistochemistry for the diagnosis of biphasic mesothelioma. Ann Diagn Pathol. 2017;26:31–7.
204. Wu D, et al. Diagnostic usefulness of p16/CDKN2A FISH in distinguishing between sarcomatoid mesothelioma and fibrous pleuritis. Am J Clin Pathol. 2013;139(1):39–46.
205. Oramas DM, Zaleski M, Moran CA. Sarcomatoid mesothelioma: a cliniocopathological and immunohistochemical study of 64 cases. Int J Surg Pathol. 2021;29:820–5.
206. Zaleski M, Kalhor N, Fujimoto J, Wistuba I, Moran CA. Sarcomatoid mesothelioma: a CDKN2A molecular analysis of 53 cases with immunohistochemical correlation with BAP1. Pathol Res Pract. 2020;216(12):153267. PMID: 33176261.
207. Harwood TR, Gracey DR, Yokoo H. Pseudomesotheliomatous carcinoma of the lung. A variant of peripheral lung cancer. Am J Clin Pathol. 1976;65(2):159–67.
208. Koss M, et al. Pseudomesotheliomatous adenocarcinoma: a reappraisal. Semin Diagn Pathol. 1992;9(2):117–23.
209. Attanoos RL, Gibbs AR. 'Pseudomesotheliomatous' carcinomas of the pleura: a 10-year analysis of cases from the Environmental Lung Disease Research Group, Cardiff. Histopathology. 2003;43(5):444–52.
210. Dodson RF, Hammar SP. Analysis of asbestos concentration in 20 cases of pseudomesotheliomatous lung cancer. Ultrastruct Pathol. 2015;39(1):13–22.
211. An AR, et al. Pseudomesotheliomatous carcinoma of the lung in the parietal pleura. J Pathol Transl Med. 2020;54(2):192–5.
212. Hattori Y, et al. Pseudomesotheliomatous carcinoma of the pleura: an autopsy case of metastasis from a G-CSF-producing anaplastic carcinoma of the pancreas. APMIS. 2018;126(2):166–70.
213. Pardo J, et al. Pseudomesotheliomatous carcinoma of the lung with a distinct morphology, immunohistochemistry, and comparative genomic hybridization profile. Ann Diagn Pathol. 2007;11(4):241–51.
214. Shah IA, et al. Pseudomesotheliomatous carcinoma involving pleura and peritoneum: a clinicopathologic and immunohistochemical study of three cases. Ann Diagn Pathol. 1999;3(3):148–59.
215. Simonsen J. Pseudomesotheliomatous carcinoma of the lung with asbestos exposure. Am J Forensic Med Pathol. 1986;7(1):49–51.
216. Vukovic J, et al. Pseudomesotheliomatous carcinoma of the lung. Vojnosanit Pregl. 2016;73(12):1168–72.
217. Detterbeck FC, Parsons AM. Thymic tumors. Ann Thorac Surg. 2004;77(5):1860–9.
218. Weissferdt A, Moran CA. The spectrum of ectopic thymomas. Virchows Arch. 2016;469(3):245–54.
219. Filosso PL, et al. Ectopic pleural thymoma mimicking a giant solitary fibrous tumour of the pleura. Interact Cardiovasc Thorac Surg. 2012;15(5):930–2.
220. Moran CA, et al. Thymomas presenting as pleural tumors. Report of eight cases. Am J Surg Pathol. 1992;16(2):138–44.
221. Kim HS, et al. Myasthenia gravis in ectopic thymoma presenting as pleural masses. Lung Cancer. 2007;57(1):115–7.
222. Kitada M, et al. Ectopic thymoma presenting as a giant intrathoracic tumor: a case report. World J Surg Oncol. 2011;9:66.
223. Moran CA, Suster S. Primary mucoepidermoid carcinoma of the pleura. A clinicopathologic study of two cases. Am J Clin Pathol. 2003;120(3):381–5.
224. Moran CA, Suster S. Mucoepidermoid carcinomas of the thymus. A clinicopathologic study of six cases. Am J Surg Pathol. 1995;19(7):826–34.
225. Weissferdt A, Kalhor N, Moran CA. Pleuromediastinal epithelial-myoepithelial carcinomas: a Clinicopathologic and immunohistochemical study of two cases. Am J Clin Pathol. 2016;146(6):736–40.
226. Yalcin CE, Tihan T. Solitary fibrous tumor/hemangiopericytoma dichotomy revisited: a restless family of neoplasms in the CNS. Adv Anat Pathol. 2016;23(2):104–11.

227. Chang ED, et al. Malignant solitary fibrous tumor of the pleura causing recurrent hypoglycemia; immunohistochemical stain of insulin-like growth factor i receptor in three cases. J Korean Med Sci. 2001;16(2):220–4.
228. Chick JF, Chauhan NR, Madan R. Solitary fibrous tumors of the thorax: nomenclature, epidemiology, radiologic and pathologic findings, differential diagnoses, and management. AJR Am J Roentgenol. 2013;200(3):W238–48.
229. Sung SH, et al. Solitary fibrous tumors of the pleura: surgical outcome and clinical course. Ann Thorac Surg. 2005;79(1):303–7.
230. Briselli M, Mark EJ, Dickersin GR. Solitary fibrous tumors of the pleura: eight new cases and review of 360 cases in the literature. Cancer. 1981;47(11):2678–89.
231. Lu C, et al. Solitary fibrous tumor of the pleura: an analysis of 13 cases. World J Surg. 2008;32(8):1663–8.
232. Cardillo G, et al. Solitary fibrous tumors of the pleura. Curr Opin Pulm Med. 2012;18(4):339–46.
233. de Perrot M, et al. Solitary fibrous tumors of the pleura. Ann Thorac Surg. 2002;74(1):285–93.
234. England DM, Hochholzer L, McCarthy MJ. Localized benign and malignant fibrous tumors of the pleura. A clinicopathologic review of 223 cases. Am J Surg Pathol. 1989;13(8):640–58.
235. Robinson LA, Reilly RB. Localized pleural mesothelioma. The clinical spectrum. Chest. 1994;106(5):1611–5.
236. Moat NE, et al. Spontaneous hypoglycaemia and pleural fibroma: role of insulin like growth factors. Thorax. 1991;46(12):932–3.
237. Antonella D, et al. Doege-potter syndrome by malignant solitary fibrous tumor of the liver: a case report and review of literature. World J Gastrointest Surg. 2019;11(8):348–57.
238. Suter M, et al. Localized fibrous tumours of the pleura: 15 new cases and review of the literature. Eur J Cardiothorac Surg. 1998;14(5):453–9.
239. Rena O, et al. Solitary fibrous tumour of the pleura: surgical treatment. Eur J Cardiothorac Surg. 2001;19(2):185–9.
240. Cardillo G, et al. Localized (solitary) fibrous tumors of the pleura: an analysis of 55 patients. Ann Thorac Surg. 2000;70(6):1808–12.
241. Takahama M, et al. Video-assisted thoracoscopic surgery is a promising treatment for solitary fibrous tumor of the pleura. Chest. 2004;125(3):1144–7.
242. Kohler M, et al. Diagnosis, treatment and long-term outcome of solitary fibrous tumours of the pleura. Eur J Cardiothorac Surg. 2007;32(3):403–8.
243. Desser TS, Stark P. Pictorial essay: solitary fibrous tumor of the pleura. J Thorac Imaging. 1998;13(1):27–35.
244. Chong S, et al. Benign localized fibrous tumour of the pleura: CT features with histopathological correlations. Clin Radiol. 2006;61(10):875–82.
245. Cardinale L, et al. CT features of solitary fibrous tumour of the pleura: experience in 26 patients. Radiol Med. 2006;111(5):640–50.
246. Lee KS, et al. CT findings in benign fibrous mesothelioma of the pleura: pathologic correlation in nine patients. AJR Am J Roentgenol. 1992;158(5):983–6.
247. Saifuddin A, et al. Primary malignant localized fibrous tumours of the pleura: clinical, radiological and pathological features. Clin Radiol. 1992;45(1):13–7.
248. Bilbey JH, et al. Localized fibrous mesothelioma of pleura following external ionizing radiation therapy. Chest. 1988;94(6):1291–2.
249. Ferretti GR, et al. Localized benign fibrous tumors of the pleura. AJR Am J Roentgenol. 1997;169(3):683–6.
250. Tateishi U, et al. Solitary fibrous tumor of the pleura: MR appearance and enhancement pattern. J Comput Assist Tomogr. 2002;26(2):174–9.
251. Harris GN, Rozenshtein A, Schiff MJ. Benign fibrous mesothelioma of the pleura: MR imaging findings. AJR Am J Roentgenol. 1995;165(5):1143–4.
252. Rosado-de-Christenson ML, et al. From the archives of the AFIP: localized fibrous tumor of the pleura. Radiographics. 2003;23(3):759–83.
253. George JC. Benign fibrous mesothelioma of the pleura: MR findings. AJR Am J Roentgenol. 1993;160(1):204–5.
254. You X, et al. CT diagnosis and differentiation of benign and malignant varieties of solitary fibrous tumor of the pleura. Medicine (Baltimore). 2017;96(49):e9058.
255. Gupta A, et al. Solitary fibrous tumour of pleura: CT differentiation of benign and malignant types. Clin Radiol. 2017;72(9):796 e9–796 e17.
256. Yeom YK, et al. Solitary fibrous tumors of the pleura of the thorax: CT and FDG PET characteristics in a tertiary referral center. Medicine (Baltimore). 2015;94(38):e1548.
257. Moran CA, Suster S, Koss MN. The spectrum of histologic growth patterns in benign and malignant fibrous tumors of the pleura. Semin Diagn Pathol. 1992;9(2):169–80.
258. Fusco N, et al. Recurrent NAB2-STAT6 gene fusions and oestrogen receptor-alpha expression in pulmonary adenofibromas. Histopathology. 2017;70(6):906–17.
259. Doyle LA, et al. Nuclear expression of STAT6 distinguishes solitary fibrous tumor from histologic mimics. Mod Pathol. 2014;27(3):390–5.
260. Demicco EG, et al. Extensive survey of STAT6 expression in a large series of mesenchymal tumors. Am J Clin Pathol. 2015;143(5):672–82.
261. Dalen BP, Bergh PM, Gunterberg BU. Desmoid tumors: a clinical review of 30 patients with more than 20 years' follow-up. Acta Orthop Scand. 2003;74(4):455–9.
262. Escobar C, et al. Update on desmoid tumors. Ann Oncol. 2012;23(3):562–9.
263. Tokarek T, et al. Desmoid tumor of lung with pleural involvement - the case of unique location of aggressive fibromatosis. Folia Med Cracov. 2015;55(1):53–9.
264. Shinagare AB, et al. A to Z of desmoid tumors. AJR Am J Roentgenol. 2011;197(6):W1008–14.
265. Lopez R, et al. Problems in diagnosis and management of desmoid tumors. Am J Surg. 1990;159(5):450–3.
266. Meyerson SL, D'Amico TA. Intrathoracic desmoid tumor: brief report and review of literature. J Thorac Oncol. 2008;3(6):656–9.
267. Brodsky JT, et al. Desmoid tumors of the chest wall. A locally recurrent problem. J Thorac Cardiovasc Surg. 1992;104(4):900–3.
268. Winer-Muram HT, Bowman LC, Parham D. Intrathoracic desmoid tumor: CT and MRI appearance. South Med J. 1994;87(10):1007–9.
269. Wilson RW, Gallateau-Salle F, Moran CA. Desmoid tumors of the pleura: a clinicopathologic mimic of localized fibrous tumor. Mod Pathol. 1999;12(1):9–14.
270. Andino L, et al. Pleuropulmonary desmoid tumors: immunohistochemical comparison with solitary fibrous tumors and assessment of beta-catenin and cyclin D1 expression. Arch Pathol Lab Med. 2006;130(10):1503–9.
271. Chorti A, Papavramidis TS, Michalopoulos A. Calcifying fibrous tumor: review of 157 patients reported in international literature. Medicine (Baltimore). 2016;95(20):e3690.
272. Van Dorpe J, et al. Is calcifying fibrous pseudotumor a late sclerosing stage of inflammatory myofibroblastic tumor? Am J Surg Pathol. 1999;23(3):329–35.
273. Chen KT. Familial peritoneal multifocal calcifying fibrous tumor. Am J Clin Pathol. 2003;119(6):811–5.

274. Lee D, Suh YL, Lee SK. Calcifying fibrous pseudotumour arising in a gastric inflammatory myofibroblastic tumour. Pathology. 2006;38(6):588–91.
275. Kocova L, et al. Calcifying fibrous pseudotumour of visceral peritoneum. Histopathology. 1997;31(2):182–4.
276. Valladolid G, et al. Calcifying fibrous tumor of the small intestine associated with Castleman-like lymphadenopathy. J Gastrointest Surg. 2014;18(6):1205–8.
277. Fukunaga M, et al. Calcifying fibrous pseudotumor. Pathol Int. 1997;47(1):60–3.
278. Ishida M, Okabe H. Disseminated calcifying tumor of the pleura. Pathol Int. 2013;63(6):333–5.
279. Sanxi A, et al. [Pleural epithelioid hemangioendothelioma: a case report and review of the literature]. Zhonghua Jie He He Hu Xi Za Zhi. 2015;38(3):174–8.
280. Fan Y, et al. Pleural epithelioid hemangioendothelioma: a case report and literature review. J Natl Med Assoc. 2016;108(2):124–9.
281. Oliveira A, Carvalho L. [Epithelioid haemangioendothelioma of the pleura: 29 months survival]. Rev Port Pneumol. 2006;12(4):455–61.
282. Crotty EJ, et al. Epithelioid hemangioendothelioma of the pleura: clinical and radiologic features. AJR Am J Roentgenol. 2000;175(6):1545–9.
283. Saqi A, et al. Primary pleural epithelioid hemangioendothelioma with rhabdoid phenotype: report and review of the literature. Diagn Cytopathol. 2007;35(4):203–8.
284. Lau K, et al. Clinical patterns and outcome in epithelioid hemangioendothelioma with or without pulmonary involvement: insights from an internet registry in the study of a rare cancer. Chest. 2011;140(5):1312–8.
285. Pinet C, et al. Aggressive form of pleural epithelioid haemangioendothelioma: complete response after chemotherapy. Eur Respir J. 1999;14(1):237–8.
286. Woo JH, et al. Epithelioid hemangioendothelioma in the thorax: clinicopathologic, CT, PET, and prognostic features. Medicine (Baltimore). 2016;95(30):e4348.
287. Salahudeen HM, et al. CT appearances of pleural tumours. Clin Radiol. 2009;64(9):918–30.
288. Young RJ, et al. Angiosarcoma. Lancet Oncol. 2010;11(10):983–91.
289. Abu-Zaid A, Mohammed S. Primary pleural angiosarcoma in a 63-year-old gentleman. Case Rep Pulmonol. 2013;2013:974567.
290. Lin BT, et al. Malignant vascular tumors of the serous membranes mimicking mesothelioma. A report of 14 cases. Am J Surg Pathol. 1996;20(12):1431–9.
291. Alexiou C, et al. Primary angiosarcomas of the chest wall and pleura. Eur J Cardiothorac Surg. 1998;14(5):523–6.
292. Miller R, et al. Radiation-induced angiosarcoma as a cause of pleural effusion. Am J Respir Crit Care Med. 2017;196(4):e10–1.
293. Baisi A, et al. Primary multifocal angiosarcoma of the pleura. Interact Cardiovasc Thorac Surg. 2011;12(6):1069–70.
294. Naka N, et al. Angiosarcoma in Japan. A review of 99 cases. Cancer. 1995;75(4):989–96.
295. Pramesh CS, et al. Angiosarcoma of the pleura. Ann Thorac Cardiovasc Surg. 2004;10(3):187–90.
296. Zhang S, et al. Primary epithelioid angiosarcoma of the pleura: a case report and review of literature. Int J Clin Exp Pathol. 2015;8(2):2153–8.
297. Attanoos RL, et al. Malignant vascular tumours of the pleura in "asbestos" workers and endothelial differentiation in malignant mesothelioma. Thorax. 2000;55(10):860–3.
298. Zhang PJ, Livolsi VA, Brooks JJ. Malignant epithelioid vascular tumors of the pleura: report of a series and literature review. Hum Pathol. 2000;31(1):29–34.
299. Doyle LA, Fletcher CD, Hornick JL. Nuclear expression of CAMTA1 distinguishes epithelioid hemangioendothelioma from histologic mimics. Am J Surg Pathol. 2016;40(1):94–102.
300. Sedhai YR, et al. Primary pleural angiosarcoma: case report and literature review. SAGE Open Med Case Rep. 2020;8:2050313X20904595.
301. Lee SJ, et al. Epithelioid hemangioendotheliomas with TFE3 gene translocations are compossible with CAMTA1 gene rearrangements. Oncotarget. 2016;7(7):7480–8.
302. Xia T, et al. Askin tumor: CT and FDG-PET/CT imaging findings and follow-up. Medicine (Baltimore). 2014;93(6):e42.
303. Gladish GW, et al. Primary thoracic sarcomas. Radiographics. 2002;22(3):621–37.
304. Zhang KE, et al. Askin's tumor: 11 cases and a review of the literature. Oncol Lett. 2016;11(1):253–6.
305. Manshani N, et al. Peripheral primitive neuroectodermal tumour of the pleura: case report and literature review. Int J Clin Pract. 2010;64(1):133–4.
306. Gao L, et al. Peripheral primitive neuroectodermal tumors: a retrospective analysis of 89 cases and literature review. Oncol Lett. 2019;18(6):6885–90.
307. Zimmermann T, et al. Peripheral primitive neuroectodermal tumor: challenge for multimodal treatment. World J Surg. 2001;25(11):1367–72.
308. Grier HE, et al. Addition of ifosfamide and etoposide to standard chemotherapy for Ewing's sarcoma and primitive neuroectodermal tumor of bone. N Engl J Med. 2003;348(8):694–701.
309. Subbiah V, et al. Ewing's sarcoma: standard and experimental treatment options. Curr Treat Options in Oncol. 2009;10(1–2):126–40.
310. Askin FB, et al. Malignant small cell tumor of the thoracopulmonary region in childhood: a distinctive clinicopathologic entity of uncertain histogenesis. Cancer. 1979;43(6):2438–51.
311. Angervall L, Enzinger FM. Extraskeletal neoplasm resembling Ewing's sarcoma. Cancer. 1975;36(1):240–51.
312. Miettinen M, et al. Monoclonal antibody NB84 in the differential diagnosis of neuroblastoma and other small round cell tumors. Am J Surg Pathol. 1998;22(3):327–32.
313. Al-Daraji WI, et al. Primary smooth muscle tumor of the pleura: a clinicopathological case report with ultrastructural observations and a review of the literature. Ultrastruct Pathol. 2005;29(5):389–98.
314. Proca DM, et al. Smooth muscle tumor of the pleura. A case report and review of the literature. Arch Pathol Lab Med. 2000;124(11):1688–92.
315. Moran CA, Suster S, Koss MN. Smooth muscle tumours presenting as pleural neoplasms. Histopathology. 1995;27(3):227–34.
316. Silva RG, et al. Primary monophasic synovial sarcoma of the pleura: neoadjuvant chemotherapy followed by complete resection. Thorac Cancer. 2010;1(3):95–101.
317. Gaertner E, et al. Biphasic synovial sarcomas arising in the pleural cavity. A clinicopathologic study of five cases. Am J Surg Pathol. 1996;20(1):36–45.
318. Leader M, et al. Synovial sarcomas. True carcinosarcomas? Cancer. 1987;59(12):2096–8.
319. Frazier AA, et al. From the archives of the AFIP: pleuropulmonary synovial sarcoma. Radiographics. 2006;26(3):923–40.
320. Przybyl J, et al. Recurrent and novel SS18-SSX fusion transcripts in synovial sarcoma: description of three new cases. Tumour Biol. 2012;33(6):2245–53.
321. Panigrahi MK, et al. Primary pulmonary synovial sarcoma: a reappraisal. J Cancer Res Ther. 2018;14(3):481–9.
322. Ascoli V, Lo-Coco F. Body cavity lymphoma. Curr Opin Pulm Med. 2002;8(4):317–22.
323. Harris NL, et al. World Health Organization classification of neoplastic diseases of the hematopoietic and lymphoid tissues: report

of the Clinical Advisory Committee meeting-Airlie House, Virginia, November 1997. J Clin Oncol. 1999;17(12):3835–49.
324. Said J, Cesarman E. Primary effusion lymphoma. In: Swerdlow SH, Harris NL, et al., editors. WHO classification of tumours of haematopoietic and lymphoid tissues. Lyon: IARC Press; 2017.
325. Dunleavy K, Wilson WH. How I treat HIV-associated lymphoma. Blood. 2012;119(14):3245–55.
326. Narkhede M, Arora S, Ujjani C. Primary effusion lymphoma: current perspectives. Onco Targets Ther. 2018;11:3747–54.
327. Shimada K, Hayakawa F, Kiyoi H. Biology and management of primary effusion lymphoma. Blood. 2018;132(18):1879–88.
328. Simonelli C, et al. Clinical features and outcome of primary effusion lymphoma in HIV-infected patients: a single-institution study. J Clin Oncol. 2003;21(21):3948–54.
329. Chen YB, Rahemtullah A, Hochberg E. Primary effusion lymphoma. Oncologist. 2007;12(5):569–76.
330. Jeong YJ, et al. Neoplastic and nonneoplastic conditions of serosal membrane origin: CT findings. Radiographics. 2008;28(3):801–17, discussion 817–8, quiz 912.
331. Shannon-Lowe C, Rickinson AB, Bell AI. Epstein-Barr virus-associated lymphomas. Philos Trans R Soc Lond Ser B Biol Sci. 2017;372(1732):20160271.
332. Nakatsuka S, et al. Pyothorax-associated lymphoma: a review of 106 cases. J Clin Oncol. 2002;20(20):4255–60.
333. Welcker K, et al. Pyothorax-associated lymphoma (PAL): report and review of a rare entity. Thorac Surg Sci. 2004;1:Doc03.
334. Yoshitomi A, et al. [Pyothorax associated lymphoma treated by chemotherapy after thoracostomy]. Nihon Kokyuki Gakkai Zasshi. 1999;37(8):619–22.
335. Yoshida A, et al. [A case of chronic tuberculous pyothorax associated malignant lymphoma]. Kekkaku. 1996;71(6):415–21.
336. Bashoura L, Eapen GA, Faiz SA. Pulmonary manifestations of lymphoma and leukemia. Clin Chest Med. 2017;38(2):187–200.
337. Vega F, et al. Lymphomas involving the pleura: a clinicopathologic study of 34 cases diagnosed by pleural biopsy. Arch Pathol Lab Med. 2006;130(10):1497–502.
338. Ahmad H, et al. Primary pleural lymphomas. Thorax. 2003;58(10):908–9.
339. Alexandrakis MG, et al. Pleural effusions in hematologic malignancies. Chest. 2004;125(4):1546–55.
340. Kaur V, et al. Clinical characteristics, molecular profile and outcomes of myeloid sarcoma: a single institution experience over 13 years. Hematology. 2018;23(1):17–24.
341. Sahu KK, et al. Myeloid sarcoma: an unusual case of mediastinal mass and malignant pleural effusion with review of literature. Indian J Hematol Blood Transfus. 2015;31(4):466–71.
342. Rodriguez JN, et al. Pleural effusion in multiple myeloma. Chest. 1994;105(2):622–4.
343. Kintzer JS Jr, Rosenow EC 3rd, Kyle RA. Thoracic and pulmonary abnormalities in multiple myeloma. A review of 958 cases. Arch Intern Med. 1978;138(5):727–30.
344. Oriol A. Multiple myeloma with extramedullary disease. Adv Ther. 2011;28(Suppl 7):1–6.
345. Galieni P, et al. Clinical outcome of extramedullary plasmacytoma. Haematologica. 2000;85(1):47–51.
346. Dimopoulos MA, Kiamouris C, Moulopoulos LA. Solitary plasmacytoma of bone and extramedullary plasmacytoma. Hematol Oncol Clin North Am. 1999;13(6):1249–57.
347. Palmer HE, Wilson CS, Bardales RH. Cytology and flow cytometry of malignant effusions of multiple myeloma. Diagn Cytopathol. 2000;22(3):147–51.
348. Hussein-Jelen T, Bankier AA, Eisenberg RL. Solid pleural lesions. AJR Am J Roentgenol. 2012;198(6):W512–20.
349. Light RW. Clinical practice. Pleural effusion. N Engl J Med. 2002;346(25):1971–7.
350. Agustí AG, et al. Ventilation-perfusion mismatch in patients with pleural effusion: effects of thoracentesis. Am J Respir Crit Care Med. 1997;156(4 Pt 1):1205–9.
351. Estenne M, Yernault JC, De Troyer A. Mechanism of relief of dyspnea after thoracocentesis in patients with large pleural effusions. Am J Med. 1983;74(5):813–9.
352. Koegelenberg CF, et al. The utility of ultrasound-guided thoracentesis and pleural biopsy in undiagnosed pleural exudates. Thorax. 2015;70(10):995–7.
353. Eibenberger KL, et al. Quantification of pleural effusions: sonography versus radiography. Radiology. 1994;191(3):681–4.
354. Qureshi NR, Rahman NM, Gleeson FV. Thoracic ultrasound in the diagnosis of malignant pleural effusion. Thorax. 2009;64(2):139–43.
355. Feller-Kopman DJ, et al. Management of malignant pleural effusions. An official ATS/STS/STR clinical practice guideline. Am J Respir Crit Care Med. 2018;198(7):839–49.
356. Havelock T, et al. Pleural procedures and thoracic ultrasound: British Thoracic Society pleural disease guideline 2010. Thorax. 2010;65 Suppl 2:ii61–76.
357. Villena V, et al. Measurement of pleural pressure during therapeutic thoracentesis. Am J Respir Crit Care Med. 2000;162(4 Pt 1):1534–8.
358. Antony VB, et al. Management of malignant pleural effusions. Eur Respir J. 2001;18(2):402–19.
359. Sagar AES, et al. Complications following symptom limited thoracentesis using suction. Eur Respir J. 2020;56:1902356.
360. Romero-Candeira S, et al. Influence of diuretics on the concentration of proteins and other components of pleural transudates in patients with heart failure. Am J Med. 2001;110(9):681–6.
361. Romero-Candeira S, et al. Is it meaningful to use biochemical parameters to discriminate between transudative and exudative pleural effusions? Chest. 2002;122(5):1524–9.
362. Casallas A, Castañeda-Cardona C, Rosselli D. Urinothorax: case report and systematic review of the literature. Urol Ann. 2016;8(1):91–4.
363. Garcia-Simon R, et al. Urinothorax: an unusual complication of an oncologic gynecological surgery. Taiwan J Obstet Gynecol. 2015;54(3):336–8.
364. Ferreira PG, Furriel F, Ferreira AJ. Urinothorax as an unusual type of pleural effusion - clinical report and review. Rev Port Pneumol. 2013;19(2):80–3.
365. Toubes ME, et al. Urinothorax: a systematic review. J Thorac Dis. 2017;9(5):1209.
366. Walker SP, et al. Nonmalignant pleural effusions: a prospective study of 356 consecutive unselected patients. Chest. 2017;151(5):1099–105.
367. Bintcliffe OJ, et al. Unilateral pleural effusions with more than one apparent etiology. A prospective observational study. Ann Am Thorac Soc. 2016;13(7):1050–6.
368. Hooper C, Lee YC, Maskell N. Investigation of a unilateral pleural effusion in adults: British Thoracic Society pleural disease guideline 2010. Thorax. 2010;65 Suppl 2:ii4–17.
369. Sahn SA. The value of pleural fluid analysis. Am J Med Sci. 2008;335(1):7–15.
370. Porcel JM, et al. The diagnosis of pleural effusions. Expert Rev Respir Med. 2015;9(6):801–15.
371. Taghizadeh N, Fortin M, Tremblay A. US hospitalizations for malignant pleural effusions: data from the 2012 National Inpatient Sample. Chest. 2017;151(4):845–54.
372. Maldonado F, et al. Pleural fluid characteristics of chylothorax. Mayo Clin Proc. 2009;84(2):129–33.

373. Porcel JM. Malignant pleural effusions because of lung cancer. Curr Opin Pulm Med. 2016;22(4):356–61.
374. Porcel JM, et al. Clinical features and survival of lung cancer patients with pleural effusions. Respirology. 2015;20(4):654–9.
375. Clive AO, et al. Predicting survival in malignant pleural effusion: development and validation of the LENT prognostic score. Thorax. 2014;69(12):1098–104.
376. Iyer NP, et al. Indwelling pleural catheter versus pleurodesis for malignant pleural effusions. A systematic review and meta-analysis. Ann Am Thorac Soc. 2019;16(1):124–31.
377. Wahidi MM, et al. Randomized trial of pleural fluid drainage frequency in patients with malignant pleural effusions. The ASAP trial. Am J Respir Crit Care Med. 2017;195(8):1050–7.
378. Krochmal R, et al. Patient evaluation for rapid pleurodesis of malignant pleural effusions. J Thorac Dis. 2016;8(9):2538–43.
379. Reddy C, et al. Rapid pleurodesis for malignant pleural effusions: a pilot study. Chest. 2011;139(6):1419–23.
380. Fysh ETH, et al. Clinical outcomes of indwelling pleural catheter-related pleural infections: an international multicenter study. Chest. 2013;144(5):1597–602.
381. Gilbert CR, et al. Management of indwelling tunneled pleural catheters: a modified Delphi Consensus statement. Chest. 2020;158(5):2221–8.
382. Grosu HB, et al. Complications of removal of indwelling pleural catheters. Chest. 2012;142(4):1071.
383. Vial MR, et al. Intrapleural fibrinolytic therapy in patients with nondraining indwelling pleural catheters. J Bronchol Interv Pulmonol. 2016;23(2):98–105.
384. Steger V, et al. Who gains most? A 10-year experience with 611 thoracoscopic talc pleurodeses. Ann Thorac Surg. 2007;83(6):1940–5.
385. Steger V, et al. Long-term follow-up of thoracoscopic talc pleurodesis for primary spontaneous pneumothorax. Eur Respir J. 2007;30(3):598–9, author reply 599–600.